University of Cape Town

DEPARTMENT OF MECHANICAL ENGINEERING
RONDEBOSCH, CAPE TOWN, SOUTH AFRICA

Deformation and tearing of uniformly blast-loaded quadrangular stiffened plates

Steeve Chung Kim Yuen

OCTOBER 2000

Thesis submitted in partial fulfillment of the requirements for Master's Degree in Engineering

Declaration

I, Steeve Chung Kim Yuen, declare that this dissertation is essentially my own work. It is being submitted in partial fulfilment of the requirements for Master of Science in Engineering degree at the University of Cape Town and has not been submitted in this or any other form for a degree at any other university.

Signed by candidate

.....

Steeve Chung Kim Yuen

October 2000

Abstract

An investigation into the deformation and tearing of stiffened quadrangular plates subjected to a uniform blast load is presented. A series of experimental results and numerical modelling using the finite element package; ABAQUS, on built-in quadrangular mild steel plates of different stiffener configurations and sizes subjected to a uniform blast load are reported.

The main objectives of this investigation are to determine the dynamic response of stiffened quadrangular plates subjected to uniform blast loads, to assess the effect of the stiffener configuration and size on plate failure and to use a new approach that uses material properties that include temperature dependency to model the plate response.

The experimental procedure consists of creating an impulsive load with the use of plastic explosive and measuring the resulting impulse using a ballistic pendulum. Explosive is centrally laid out in two concentric rectangular annuli on quadrangular plates of thickness 1.6mm with stiffeners of sizes; 3x3mm, 3x7mm, 4x3mm and 4x7mm; and configurations; none, single, double, cross and double cross; to provide the impulse required to give deformations up to plate tearing.

In all the tests of Mode I category of large inelastic deformation, the plate profiles are characterised by a uniform global dome. The results of mid-point deflection versus impulse for the various stiffener sizes and configurations for Mode I show a generally linear relationship.

In all the experiments, thinning mechanisms at the boundary are observed for all plates despite different stiffener sizes and configurations. Thinning, however, is not consistent all around the boundary. Thinning is also observed at the stiffener side closest to the boundary for double and double cross stiffened plates. There is, furthermore, a reduction in the stiffener width where two stiffeners cross each other perpendicularly.

With increasing impulse the plate deformation increases to a point where tearing occurs. Tearing first occurs at the middle of the sides of the quadrangular plates and then progresses towards the corners as the impulse increases. No sign of tearing along the stiffener is observed. In all cases tearing occurs across the stiffener. Tearing is also found to be a function of maximum displacement of the plate irrespective of the stiffener sizes and configurations. The maximum central displacement associated with these failures decreases as the stiffness of the plate increases.

A numerical analysis is carried out using the general-purpose finite element code; ABAQUS/Explicit which incorporates non-linear geometry, material effects such as strain rate sensitivity and temperature effects. A quarter symmetry model using eight nodes brick (C3D8R) and six nodes prism (C3D6) reduced integration and hourglass control continuum elements is used. The blast load is modelled by means of a rectangular pressure pulse.

The predicted plate responses: mid point displacement, permanent deformed shape and rupture are compared to the experimental data. High temperatures and severe element elongations due to very high strain in localised area indicates where tearing is most likely to take place. The prediction compares very well with measured experimental results.

Conclusions drawn are that the results obtained essentially exhibited both Mode I and phases of Mode II failures. Deflection and tearing appear to be dependent on both stiffener sizes and configurations. Results obtained from the new approach of using material properties that include temperature dependence to model the plate response to uniform blast loads are very encouraging. Predictions for permanent central deflection, final deformation shape and tearing compare well with the experimental work presented.

It is recommended, therefore, that further experiments should be extended to include other load configurations (localised load & load on the side of the stiffener) and other stiffener configurations (running along the plastic hinges).

With such encouraging results from the new approach using temperature dependent material properties, it is also recommended to improve the model by incorporating new technique that implements an equation of state to determine the material behaviour of the explosive to model structures such as plates subjected to blast loading conditions.

Table of Contents

List of Tables

List of Figures

Page

Page

Page

Page

Page

Page

Notation

Upper Case

A	Material parameters measured at or below $\theta_{transition}$
A_s	Cross sectional area of stiffener
B	Plate breadth
D	Material constant ($40.4s^{-1}$)
E	Young's modulus
H	Height of stiffener
I	Impulse applied to the plates
L	Plate length
L_B	Beam length
M	Total mass of pendulum
M_o	Fully plastic bending moment
S	Material parameters measured at or below $\theta_{transition}$
T	Time period of pendulum
T_s	Modified plate thickness
V_b	Burn speed of the explosive
V_o	Initial impulsive velocity
W_f	Maximum permanent transverse displacement
W_p	Width of plate
W_s	Width of stiffener
Z	Length of pen

Lower Case

a	Distance between paper and pendulum
c	Specific heat
n, m	Material parameters measured at or below $\theta_{transition}$
q	Material constant (5)
t	Plate thickness

Greek Characters

β	Damping constant
δ	Mid-point deflection
$\dot{\varepsilon}$	Strain rate
$\dot{\varepsilon}_o$	Material constant (40.4 s^{-1})
ε_{nom}	Nominal strain
$\bar{\varepsilon}^{pl}$	Equivalent plastic strain
$\Delta\bar{\varepsilon}^{pl}$	Increment of the equivalent plastic strain
$\bar{\varepsilon}_f^{pl}$	Strain at failure
θ	Current temperature
$\hat{\theta}$	Non-dimensional temperature
θ_{melt}	Melting temperature
$\theta_{transition}$	Transition temperature
ϕ_q	Dimensionless Impulse (Damage number)
λ	Dimensionless impulsive velocity
η	Material constant (5)
μ	Mass per unit length
ν	Poisson's ratio
ρ	Material density
σ_O	Material static yield stress
σ_{yo}	Static yield stress at the reference temperature of the tensile test
σ_{true}	True stress
$\sigma^I{}_O$	Dynamic yield stress
σ_{nom}	Nominal stress
τ	Duration of pressure pulse

Acknowledgement

The author is indebted to the faculty staff and students who generously provided their valued advice and guidance throughout the course of his study and thesis. In particular, the author acknowledges the contributions of Mr. L. Watkins for making the test plates and the tensile test specimens; the assistance received from Mr. V Balden, Mr S. Courtney and Mr H. Bowles for their computational help. Also the author wishes to thank Mr A. Warburton for taking photographs of the cut specimens, Mr M. Briers of the department of Quantity Surveying for his help with the photogrammetry, the Centre for Research in Computational and Applied Mechanics (CERECAM) and the Department of Mechanical Engineering for their financial support. And finally but not least special thanks go to Prof. G. N. Nurick, the author's supervisor for his precious help and advice.

1.0 Introduction

Events involving impulsive loading occur in a wide variety of circumstances. All too frequently, the results of explosions and collisions; typical events involving impact; are reported in the news. These events often result in loss of life or injuries. An understanding of such events is crucial. By conducting research into the behaviour of beams and plates subjected to impulsive loading, a better understanding can be gained and this, in turn, can be used to guide the development of rational design procedures for a safer world.

The investigation into the failure of plates subjected to blast loading conditions has been on-going for some years as reported by Nurick and Martin [1,2]. The failure of thin plates under impulsive loading is important as a model of engineering structures undergoing large plastic deformations under dynamic loads.

Previous experimental work on quadrangular and circular plates subjected to explosive and impact loading was performed in order to measure large inelastic deformations - Mode I failure and to investigate the tensile tearing at support - Mode II failure and the transverse shear at support - Mode III failure[3], the effect of the boundary conditions [4]and effect of plate thickness[5].

Other works[6,7,8] include the response of one-way and two-way stiffened plates subjected to air blast load. The response of the latter is of the order of 200ms[6,7] compared to the 150μs time response of plates subjected to explosive blast load as reported by Nurick[9]. However, only a few experimental studies have been attempted to determine the response and damage of plates having more than two stiffeners subjected to uniform blast load. The primary concern of this investigation has been to investigate the link between the stiffener configuration and material failure.

Numerous attempts with varying degrees of success have been made to model impulsively loaded plate structures using finite element models[10,11]. The Mode I failure has been predicted with relatively good accuracy. However, aspects such as material failure due to tearing or fracture are less accurately modelled despite the numerous criteria, such as rupture strain, equivalent plastic work and damage models, applied. Nevertheless, not many of these models have included temperature dependent material properties. A successful numerical model would therefore offer substantial savings in cost and time in the long run and also helps to gain a better understanding of the blast load. The latter could hence be used to predict the response of objects with more complex geometry.

This thesis reports on the results of an experimental and numerical investigation into the dynamic response of stiffened quadrangular plates subjected to uniform blast loads. The effect of the stiffener configuration is also presented. The numerical analysis is an investigation using a general-purpose finite element package; ABAQUS/Explicit to simulate both the large inelastic deformation and tearing mode of the plate using temperature dependent material properties. The numerical predictions are compared with the experimental results.

A stiffened quadrangular plate consists of two components: a quadrangular plate and a rectangular beam that acts as reinforcement. In addition, there are two types of end fixing of plates: clamped plates where the plate and stiffener are clamped together by means of support plates and bolts; and built-in plates where the plate and the stiffener are machined out of same metal plate including the boundary.

The objectives of this report are to:

- determine the dynamic response of stiffened quadrangular plates subjected to uniform blast loads.
- investigate the effect of the stiffener on quadrangular plates subjected to uniform blast loads.
- investigate the effect of the stiffener configuration on quadrangular plates subjected to uniform blast loads
- perform a numerical analysis to model the dynamic response of the stiffened quadrangular plates subjected to uniform blast loads (Mode I).
- use the numerical model with temperature dependent material properties to attempt to predict Mode II failure of the quadrangular plates subjected to uniform blast loads.
- compare the numerical model with the experimental results
- draw conclusions and recommendations based on the findings.

The scope of the investigation was limited to quadrangular plates of fixed exposed area. The machining process, although very carefully monitored, did not produce plates of consistently similar thicknesses and stiffeners of consistently similar sizes. This was due to cutter wear and cumulative machining inaccuracies.

The entire report is based on information from a series of experiments undertaken in the blast laboratory of the University of Cape Town.

An extensive amount of research from previous experimental work in the form of theses or journals was carried out to provide additional information.

The report begins by discussing the results of the literature review that covers past theoretical work, experimental results and observations as well as numerical models. Past experimental work was introduced for comparison with the results of this investigation.

The experimental procedure and the physical indicators such as plate deformation, thinning, tearing and failure modes are briefly described in chapter 3 with the experimental results given in chapter 4. An analysis of the experimental results which includes graphs and comparisons with other work is given in chapter 5. Chapter 6 sets out the methods of finite element solutions. This included the steps taken to achieve a final working model and the justification for the modelling decisions. The results obtained from the numerical model are presented and compared with experimental results in chapter 7 for purpose of validation. Conclusions are drawn and recommendations are made based on the findings.

2.0 Literature Review

The response of thin plates clamped at the outer edges and built-in plates subjected to both uniform and localised blast loading conditions has been studied for a number of years. Extensive experimental studies have been carried out to understand the large permanent ductile deformations and rupture of beams, plates and shells. Nurick and Martin [1,2] present an overview of the theoretical and experimental results from which it is evident that most of the investigations deal with a plate that is loaded uniformly over the entire plate area. Further studies referred to such as Teeling-Smith[12], Lumpp[13], Olson et al[14] and Nurick et al [15,16] show that the focus of such studies has been on circular plates, circular plates with singular stiffener, square plates, square plates with singular stiffener and rectangular plates with two stiffeners. The recorded responses of these structural elements have been compared with the responses predicted analytically and numerically. Reviews of the work conducted in this field have been published by many researchers[6,7,10, 17,18].

2.1 Blast Loads

A blast wave generated by detonating an explosive interacts with any object in its path by imposing impulsive or dynamic blast loads causing the object to deform or tear. The actual explosion pressure-time loading is a complex decaying pressure oscillation that requires, for practical reasons, simplification before applying in any structural analysis. Figure 2.1 shows the smoothed pressure-time history for a typical blast wave. The peak over-pressure is much larger than the peak under-pressure so that the negative phase of the blast wave can be ignored.

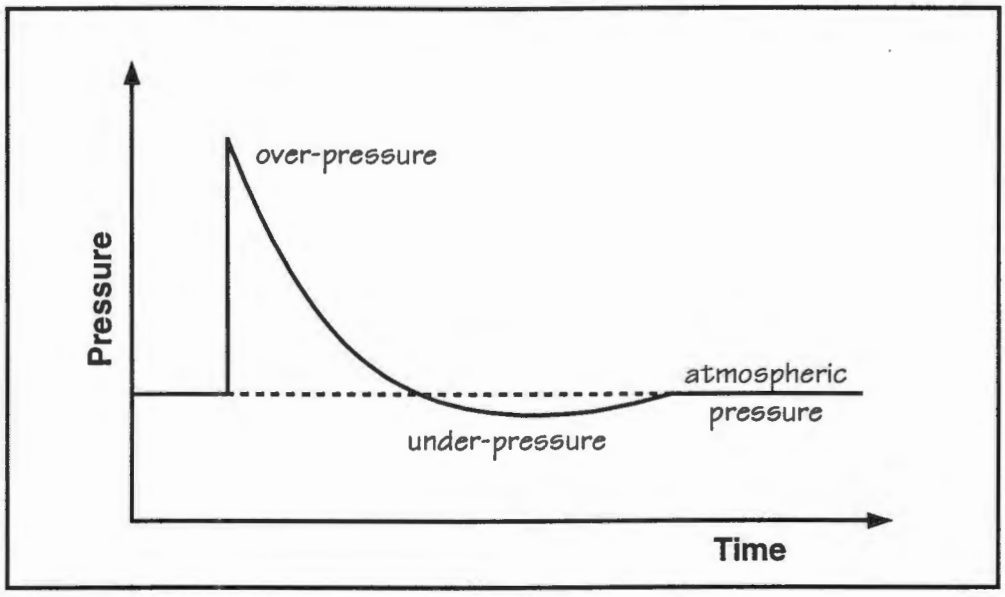

Figure 2.1 Pressure as a function of time for blast loads.

Shen and Jones [19] characterised impulsive loading as a pressure pulse having a finite impulse with an infinitely large magnitude and an infinitesimally short duration. The Steel Construction Institute [20] classified blast loads as 'impulsive' if the duration of the load is significantly less than the natural period of the structure and the structure has insufficient time to fully respond to the load; and as 'quasi-static' if the duration of the loading is much longer than the natural period. Loading in the transition region between these two regimes is termed 'dynamic'.

Although blast load is a topic needing further research, the Steel Construction Institute [20] observed that for impulsive loading, that is, external pressure loading of peak intensities of several Megapascals in magnitude over durations typically of microseconds, preserving the exact peak load value and the exact load duration is not critical. It is, however, important to represent the impulse accurately. Figure 2.2 shows some "ideal" pressure-time impulsive loading histories found in the literature.

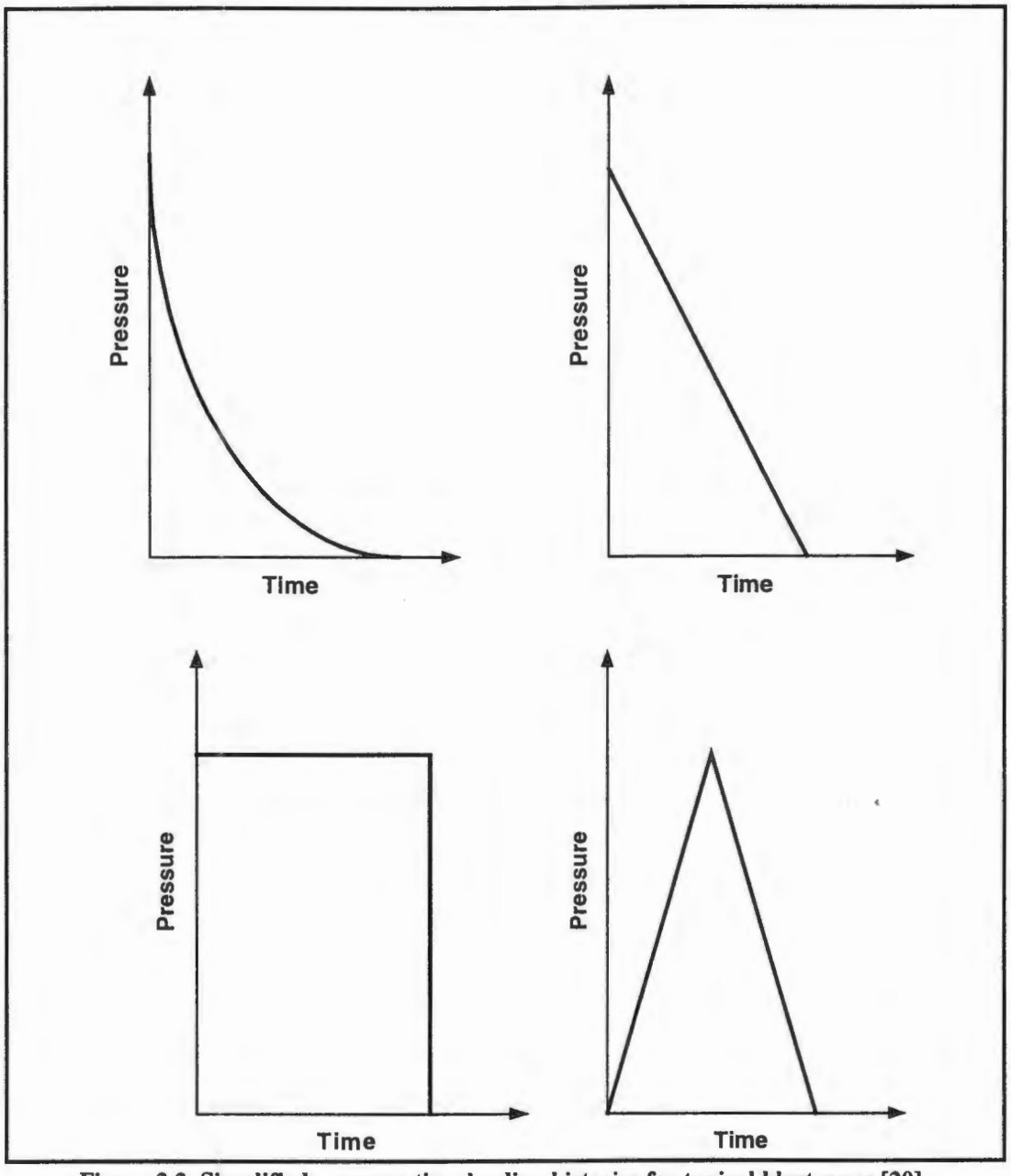

Figure 2.2 Simplified pressure-time loading histories for typical blast wave [20].

In the case where the pressure pulse is not well approximated by a blast-type pulse, the Youngdahl[21] method of representing the true pulse with a rectangular pulse of equivalent impulse has given good results. Farrow, Nurick and Mitchell[17] used both a rectangular and a triangular pressure pulse to predict the plate deflections, deformation shapes, residual strains and dynamic yield stress of a circular plate subjected to uniformly distributed explosive loading using the Abaqus finite element code. The rectangular pulse gave results which corresponded more favourably with the experiment compared to the triangular approximation because of either the difference in pressure peaks or the duration of applied load.

2.2 Experimental Studies

2.2.1 Modes of Failure

Menkes and Opat [3] reported different failure modes for fully clamped metal beams loaded impulsively. They reported that as the impulse increased, three distinctly different damage modes were noted. The failure modes were classified as:

Mode I : Large inelastic deformation of the entire beam
Mode II : Tearing (tensile failure) of the beam material at or over the support
Mode III : Transverse shear failure of the beam material at the supports.

These three failure modes are shown schematically in Figure 2.3.

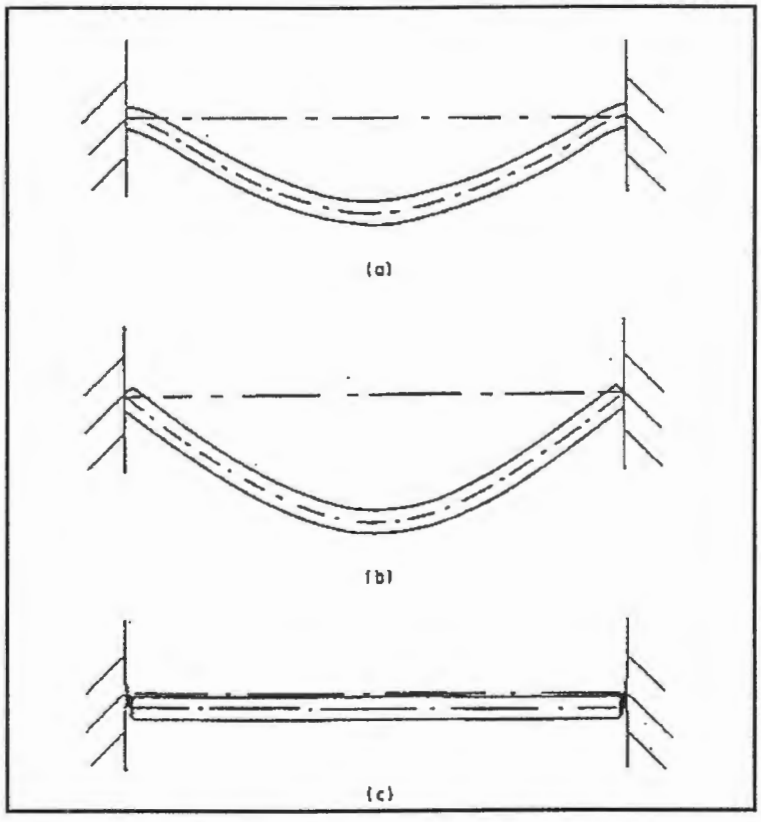

Figure 2.3 Failure associated with clamped metal beams loaded impulsively. (a) Mode I, Large permanent ductile deformation. (b) Mode II, Tensile tearing at supports, (c) Mode III, Transverse shear failure at supports.

Similar failure modes have also been observed for square plates by Olson, Fagnan and Nurick[14] and for circular plates by Teeling-Smith and Nurick[12]. Some additions to Mode II failure, which appear to be related to the shape of the plates, were reported by Nurick and Shave[22].These were classified as:-

Mode II* : Partial tearing at the boundary
Mode IIa : Complete tearing with increasing mid point deformation.
Mode IIb : Complete tearing with decreasing mid point deformation.

It must, however, be noted that while most experiments have been done on plates considered fully clamped at the boundary, with fewer experiments done on plates with fully built-in conditions at the boundary (see for example Thomas [4]) the predictions have either assumed fully built-in conditions at the boundary or considered simply supported plates.

2.2.2 STRUCTURAL RESPONSE

Several investigations have been reported on beams and on plates subjected to uniform impulsive load.

Nurick et al [23] reported on the large inelastic deformations of T-section aluminium alloy beams with fully clamped ends, which are subjected to a uniform impulsive load distributed over the entire span. The resulting response of the beams was categorised into two groups: global deformation and local deformation. The global deformation referred to the transverse deflections of the beam mid-plane while the local deformation referred to the bending and shear distortion of the flanges. The local deformation was small and occurred only at the mid-point. It was also observed that compressive stress was developed in the web at the clamped boundary. At large impulses, there were signs of onset of tearing of the flanges at the supports.

Olson, Nurick and Fagnan[14] observed that tearing of the clamped blast loaded non-stiffened square plate occurred first at the middle of the sides and then progresses towards the corners with increasing impulse. Also in cases where some corners were torn out, the specimen rotated about the other corners. Their experiments also revealed a "pulling-in" of the mid-sides of the plates during Mode II failure (including initiation). The springback effect decreased with increasing impulse. For Mode II failure, as the impulse increased from low to high values, the mid-point deflection reached a maximum and then decreased again.

In another set of experiments on clamped square plates subjected to impulsive loads, Nurick and Shave[22] observed that a shear lift occurred on the unloaded side of the plate when the plate deformed inelastically. The shear lift, although not symmetrical, was evenly distributed on each side of the plate. The total shear lift never exceeded about 50% of the total boundary length before tearing begun on the one side. Similar observations on tearing to those of Olson, Nurick and Fagnan[14] were also made.

Nurick and Lumpp[13] and Nurick and Conolly[16], investigated the response of clamped single stiffened circular plates and clamped single and double stiffened rectangular plates subjected to blast loads respectively. In both sets of experiments it was observed that the permanent mid-point deflection of the beam was greater than the mid-point displacement of the plate with a gap created between the plate and the stiffener. That was attributed to the springback effect referred to in Ref [14].

Nurick and Lumpp[13] also observed that the tearing of the circular plate or the stiffener at the boundary occurred in a small range of impulses. For stiffener of sizes 8x3mm and 8x4mm, the beam tore at the boundary at impulses lower than that required for plate tearing, while the inverse happened for stiffener sizes 8x5mm and 8x6mm.

On the other hand, Nurick and Connolly[16] observed tearing along the long side (that is the side closest to mid point of the plate) for isotropic plates. However, for the stiffened plates – both single and double stiffeners, tearing was observed along the short side of the plate.

Previous experimental work on stiffened square plates was carried out by Nurick, Olson, Fagnan and Levin[15]. They reported on the deformation and tearing of stiffened square plates where the stiffener and the plate were manufactured as a single unit referred to as a built-in plate. Their observations showed that for Mode I failure, all the experimental results showed a generally satisfactory trend of increasing permanent deflection with increasing impulse.

The onset of tearing in the plate occurred at the fixed boundary for the small stiffeners (3 x 2mm and 3 x 4mm) and at the stiffener for the larger stiffeners (3 x 5mm and 3 x 9mm). The mid-point displacement decreased with increasing stiffener size.

In similar studies, Schubak, Olson and Anderson[6,7] observed that for a very high intensity pulse (several times the static collapse pressure) the displacements of the stiffeners and nearby plating were approximately the same. It was suggested that, away from the lateral edges, the one-way stiffened plates behave much like a singly symmetric beam with the plate acting as a large flange. Similarly, a two-way stiffened plate might behave like a grillage of singly symmetric beams.

Schubak, Olson and Anderson[24] investigated the response of a five bay, T-beam stiffened steel plate (DRES panel) to blast loads. The panel was flush-mounted on a foundation and bare high-explosive charges were detonated above it. Heavy concrete walls were constructed above the ground along two edges of the panel so that the shock front would be reflected from the walls. As a result of the blast, the longitudinal edges of the panel slipped inward while the maximum permanent displacement occurred at the middle of the panel.

Recent experimental work on blast loading of stiffened plates on a larger scale was carried out by Schleyer, Hsu and White[18]. Their tests were conducted on 1m square, stiffened plates with and without in-plane restraint. The in-plane restraint condition was achieved by using 60 studs to clamp the frame up against the test plate. On the other hand, by virtue of a 1-3mm gap between the frame and the plate and the absence of studs no direct in-plane restraint was achieved. No use of explosives or hydrocarbons to generate the pressure pulse was made.

Instead, the pulse was generated by a transient differential pressure, triangular in form with a peak nominal pressure of approximately 0.1Mpa, created by the timed blow-down of two pressure loading chambers on either side of the test plate. The test programme consisted of static and dynamic tests on clamped plates including multiple and reverse loading tests.

The test results showed that in-plane restraint was responsible for reducing the maximum transient deflections in the stiffened plates by almost 50% and permanent deformations by more than a factor of 4. There was also no sign of lateral buckling in the stiffeners. On the other hand, the stiffeners appeared to have had little or no effect on the deflections of the plates without in-plane restraint.

2.2.3 The Effect of Boundary Conditions on Failure

An experimental investigation into the effect of boundary conditions on the failure of thin plates subjected to impulsive loading was carried out by Thomas[4]. The results showed that Mode I failure is not affected by the boundary conditions whereas for the onset of Mode II failure they are significant. These boundary fixation conditions are critical in assessing the tearing mechanisms which occur when the blast load is large enough to cause partial or complete tearing on the boundaries of the plate. With the observations of thinning at the boundary for plate diameters with sharp edge conditions and larger deformations occurring before thinning and tearing occur for relaxed boundary edge condition, Nurick, Gelman and Marshall[25] identified other modes of failure. These modes were identified as different phases within Mode I (large inelastic deformations) and were classified as follows:-

Mode I : Large inelastic deformation with no necking at the boundary.
Mode Ia : Large inelastic deformation with necking around part of the boundary.
Mode Ib : Large inelastic deformation with necking around the entire boundary.

2.3 Theoretical Predictions

Theoretical models of dynamic response of thin plates far outnumber experimental studies. Simple closed form solutions can often provide a rapid and sufficiently accurate design estimate to, for example, plate deflection, deformed profiles and residual strains. However, little insight into areas such as transient behaviour and tearing failure has been provided.

The predictions for cases where thin clamped quadrangular plates are subjected to impulsive and blast loads include the final mid-point deflection and in some cases; the shape of the plate and the response time. The correlation between the predictions and the experiments has been shown to be favourable for all these parameters.

Nurick and Martin[1,2] list numerous approximate methods for predicting the dynamic global response of thin plates. A dimensionless impulse; ϕ_q (or damage number) proposed by Nurick and Martin[1,2] provides a method to relate the plate geometry, impulse and material properties of plates of different thicknesses. This relationship is given by:-

$$\phi_q = \frac{I}{2t^2 \left(BL\rho\sigma_0\right)^{0.5}} \tag{2.1}$$

where I : applied impulse; B : plate breadth; L : plate length;
t :plate thickness; ρ : material density; σ_0 : material static yield stress.

This relationship, however, holds for plates that have been deformed and showed no tearing and for quadrangular plates with no stiffener.

From the above relationship (equation 2.1) , Nurick and Martin [1,2] obtained an empirical relationship of:-

$$\frac{\delta}{t} = 0.471\phi_q + 0.001 \tag{2.2}$$

where δ : Mid-point deflection; t : Plate thickness; ϕ_q : Dimensionless Impulse

for quadrangular plates, with a correlation coefficient of 0.984, where the number of data points were 156.

Jones[26] proposed rigid-plastic theoretical models that consider the influence of finite displacements for the dynamic plastic response of impulsively loaded fully clamped beams and quadrangular plates both with rectangular shaped cross-sections. The models account for the influence of membrane and bending forces for large permanent ductile deformation and tensile tearing at supports using a square yield criterion. The influence of material hardening is not taken into account. However, the strain rate sensitivity was included in the models. The approximate theoretical procedure uses the conservation of energy to obtain solutions for the maximum permanent transverse displacements.

The maximum permanent transverse displacement, W_f, of a beam which is fully clamped at both ends and impulsively loaded, with a uniform velocity, V_o, across the entire span, $2L_B$, is given by:-

$$\frac{W_f}{H} = \frac{1}{2}\left\{\left(1+\frac{3\rho V_o^2 L_B^{\,2}}{n\sigma_o H^2}\right)^{1/2} - 1\right\} \tag{2.3}$$

where strain rate enhancement; $n = \frac{\sigma_o'}{\sigma_o} = 1+\left(\frac{V_o W_f}{3\sqrt{2}DL_B^{\,2}}\right)^{1/q}$ (2.4)

For a quadrangular plate of length 2L and width 2B which is fully clamped around the entire boundary and subjected to a uniformly distributed impulsive velocity, V_o, the maximum permanent transverse displacement, W_f, is given by:-

$$\frac{W_f}{H} = \frac{(3-\xi_o)\left\{\left(1+\Gamma/n\right)^{1/2} - 1\right\}}{2\left\{1+(\xi_o-1)(\xi_o-2)\right\}} \tag{2.5}$$

where

loading parameter ; $\Gamma = \frac{2\rho V_o^2 L^2 \beta^2}{3\sigma_o H^2}(3-2\xi_o)\left(1-\xi_o+\frac{1}{2-\xi_o}\right)$, (2.6)

geometry parameter ; $\xi_o = \beta\left\{(3+\beta)^{1/2} - \beta\right\}$, (2.7)

aspect ratio; $\beta = \frac{B}{L}$ (2.8)

and strain rate enhancement; $n = 1+\left(\frac{V_o W_f}{3\sqrt{2}DB^2}\right)^{1/q}$ (2.9)

Jones[26] also presented a dimensionless initial kinetic energy. This relationship is given by:-

$$\lambda = \frac{\mu V_o^2 L^2}{M_o H} \tag{2.10}$$

These approximate theoretical procedures give reasonable agreement with the experimental results in predicting Mode I response.

So far, theoretical solutions that deal with either flat quadrangular plates or simple beams have been discussed.

Schubak, Olson and Anderson[6,7] developed a simplified analytical procedure to predict the dynamic response of stiffened plates to high intensity load pulses by modelling them as rigid-plastic beams or grillages. Partial end fixity of a stiffened plate was modelled by connecting the beams to rigid supports with rigid-plastic links of zero length and reduced plastic capacities. The true beam yield curve was approximated by four linear segments. As a consequence, the response of the beam was divided into two distinct linear phases; firstly an initial plastic hinge mechanism phase (small-displacement) where the beam resisted the load primarily through bending and a later plastic string phase (large-displacement) when the beam's bending resistance disappeared. The response was solved by two methods. In the first method, the two phases were governed by linear differential equations that were solved in closed form. In the second method, the response was approximated as a sequence of "instantaneous" mode responses, in which the velocity field was a separable function of the spatial and temporal variables. This response was solved by an instantaneous mode solution algorithm wherein the "instantaneous" modes were taken to be valid over time steps of small but finite duration Δt.

The solution methods were applied to several examples such as five bay T-beam stiffened steel plates (DRES panel) and square plates stiffened by three identical and evenly spaced T-beam crossing each other subjected to high explosive charges. Good comparison was obtained from the analytical solution and from the non-linear beam and stiffened plates finite element program. Some success was achieved in comparison with experimental results.

Schleyer, Hsu and White[18] adopted a pseudo elastic-plastic approach to predict the maximum dynamic deflection and permanent deformation of both stiffened and unstiffened plates under pulse pressure loading. The analysis is based on simple structural models that are assumed to deform as a whole within a prescribed form and the stiffening ribs deforming with the transverse deflections of the plate. However, the stiffening ribs were not assumed to develop membrane action.

The contribution of the plate to flexural rigidity of the rib was taken into consideration in the analysis. The critical moment in these members was based on either lateral buckling of the cross-section when the free edge of the rib was in compression or the fully plastic moment capacity of the cross-section or the lower of the two values.

The generalised displacement is achieved by applying the fourth order Runge-Kutta numerical time-stepping scheme up to a point of maximum displacement. The rebound of the plate was not considered in the analysis. The predictions showed encouraging correlation with the experimental results. However, the pseudo elastic-plastic procedure needs further development, particularly when plastic flow and yield line mechanisms become significant in the deformation process.

In general, theoretical techniques are based upon assumptions and simplifications and are therefore well suited to the preliminary design of blast-loaded structures.

2.4 Computational Predictions

Predictions using computational and numerical techniques of the large deformation of structural components, as a result of a blast load, have been reported widely in the literature. Radford and Nurick[10], Olson et al[14] and Farrow et al. [17], modelled circular and square plates with symmetrical cross-sections. The predictions of deformation of asymmetrical cross-sections such as stiffened plates (a combination of beams and plates) and T-beams have also been reported in the literature [Ref 6,7,11,15,27,28].

Houslton and DesRochers[8] performed a finite element analysis to determine the time-displacement history of stiffened panels subjected to air-blasts. Schubak et al[6,7] developed a simplified method to predict the dynamic response of the stiffened panels subjected to air-blasts. The finite element analysis mentioned is specifically concerned with air-blast loading, where the duration of the applied load is very much longer than that investigated in this study. Houslton and DesRochers[8] used a response time of pressure pulse of approximately 200ms, whereas the response time of blast load is about 140μs[6].

Nurick, Olson, Fagnan and Levin[14,15] used a computer program called NAPSSE (Non-linear Analysis of Plate Structures using Super Elements) to successfully predict both maximum deflection and deformation shape of uniformly blast loaded non-stiffened and stiffened square plates. The displacement fields incorporated into these super elements were represented both analytically and by polynomial functions to reduce the number of elements used for design level accuracy.

Nurick et al[14,15] also observed that the influence of strain rate via its effect on the yield stress and the plate response was significant. A plot of the predicted strain rate, the dynamic yield stress and the time of occurrence for first yield versus impulse is shown in Figure 2.4. The strain rates are very high, ranging from 850 to 3000 per second as the impulse increases from 5 to 30Ns, with the corresponding dynamic yield stress varying from 750 to 890MPa. The time to first yield decreases from 7 to 2.8μs, with increasing impulse, all less than the load duration of 15μs.

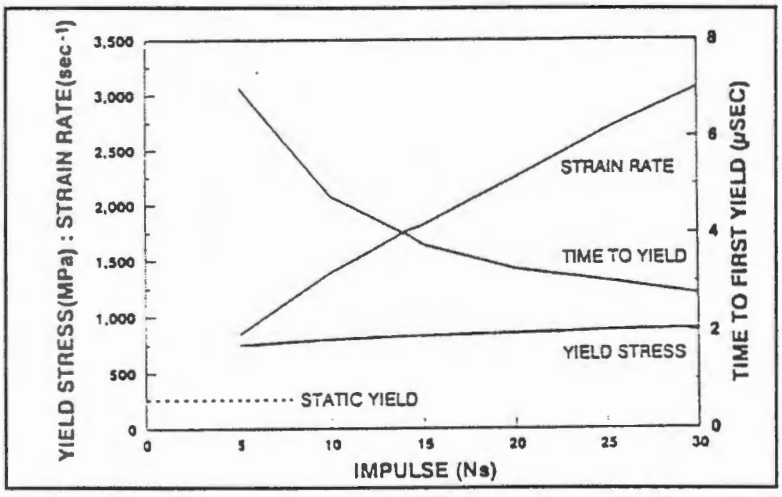

Figure 2.4 : First yield results vs impulse for a 3x4mm single stiffened square plate[15]

Figure 2.5 shows a comparison of the deflection-history of the mid-point displacement of a square plate subjected to an impulsive load of 15Ns of a model with rate dependence included and excluded. The strain rate effect not only decreases the maximum displacement but also the associated time to reach the maximum displacement.

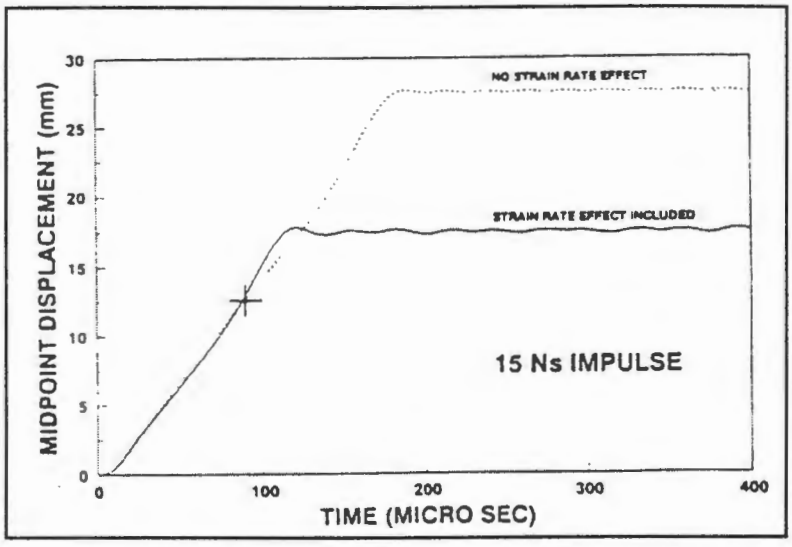

Figure 2.5 : Plate mid-point displacement response [14]

Consequently, the plate profile was affected as shown by the centreline profile plots in Figure 2.6. The non-strain rate profile has a larger slope near the boundary and a longer developed length.

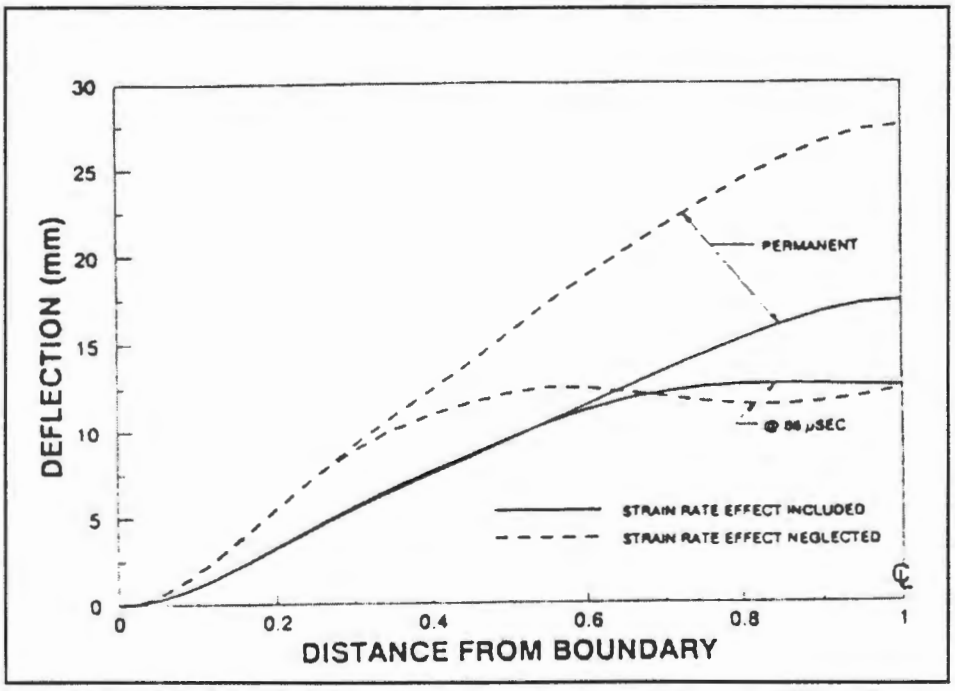

Figure 2.6 : Centre line profiles of a square plates at impulse 15Ns [14]

The analysis of the rigidly clamped square plate[14] was carried out using two finite element grids to represent one quarter of the plate. The results from the two grids exhibited the same trends. As the impulses were increased from zero, the predicted permanent deflection increased for the case of Mode I failure retaining a characteristic shape. However, it was observed for impulses 20Ns and above, Mode II failure was predicted. The predicted profile at the times of first failure exhibited a relatively flat portion in the central area of the plate while the deformations became more concentrated near the boundary. The predicted failure profiles are shown in Figure 2.7.

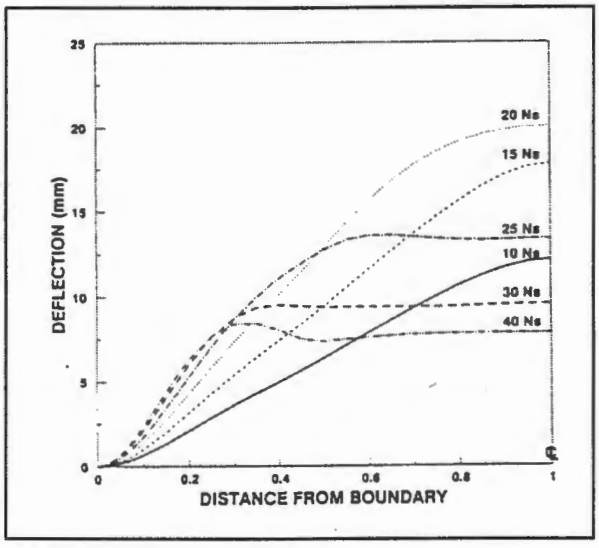

Figure 2.7 : Predicted centreline failure profiles [14]

The maximum strain distribution is shown in Figure 2.8 for impulses of 20, 25, 30 and 40Ns. Based on a strain criterion, it was observed that for an impulse of 20Ns, Mode II failure would occur first at the centre of each side. For higher impulses the failure would occur simultaneously along the central region of each side.

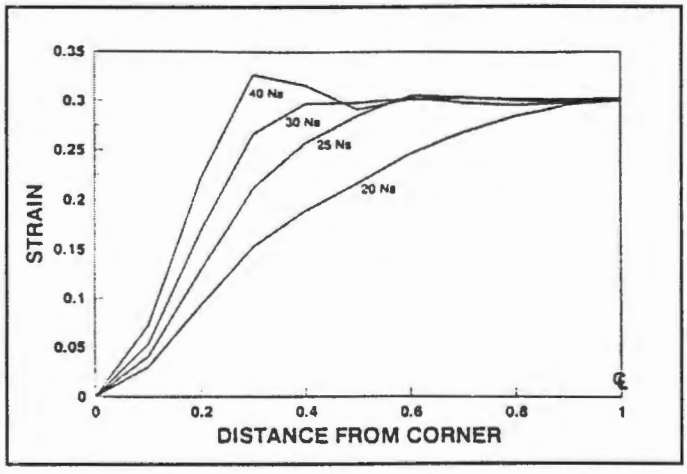

Figure 2.8 : Strain distribution at Mode II failure [14]

The stiffened plates were modelled in a rigorous continuum manner with the analogous geometric and material non-linearities included in both the plates and the stiffeners[15]. The analysis was carried out for each stiffener case. It was observed that the plate initially responded faster than the stiffener. For small stiffeners, the maximum displacement occurred at the stiffener centre whereas for larger stiffener it occurred in the plate between the boundary and the stiffener.

The initiation of Mode II failure was predicted to occur at the boundary by a maximum strain criterion, but no confirmation was obtained due to the lack of experimental data. Figure 2.9 shows the predicted Mode II failure profiles for the 3x4mm stiffened plate for a sequence of impulses. The Mode II failure was indicated by a very high plate bending slope at the boundary. Also the predicted critical impulse for Mode II failure at the boundary was found to be independent of stiffener size.

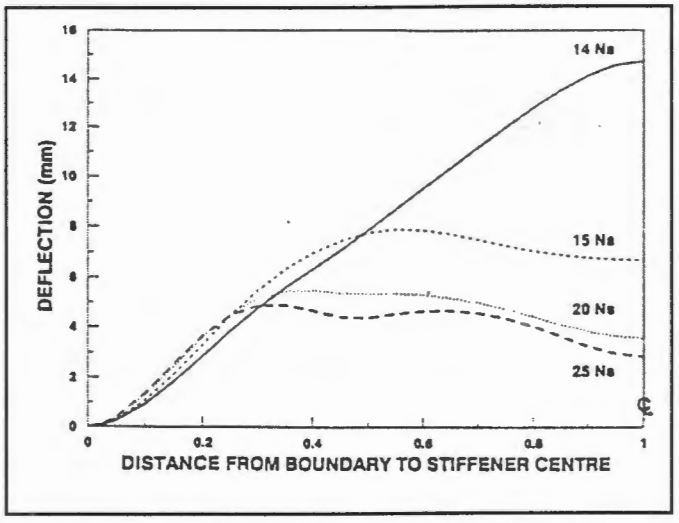

Figure 2.9 : Predicted failure profiles for 3x4mm stiffened plate[15]

Bimha, Nurick & Mitchell [11] modelled the deformation of blast loaded fully built-in single stiffened plates successfully for large ductile deformation. Their numerical analysis was carried out with the general finite element package; ABAQUS; using non-linear geometry and material effects as well as strain rate sensitivity. The S4R shell elements and B3I beam elements were used to model the plate and the stiffener respectively. Although the prediction of tearing was not carried out, it was suggested that Mode II (tensile tearing) failures were likely to occur first at the boundaries from the plastic strain distribution (Figure 2.10). The predicted strains at the stiffener were significantly less than at the boundary for

small stiffeners. For large stiffeners, the strains at the stiffener approached those at the boundary.

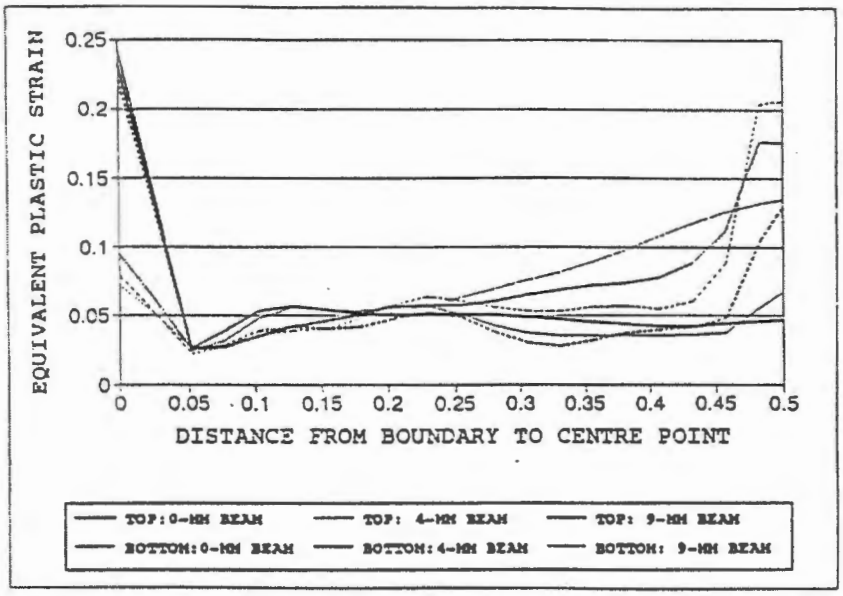

Figure 2.10 : Equivalent plastic strain distribution for the top and bottom sections of the plate for 10Ns impulse [11]

Until recently, the effects of temperature dependent material properties have been excluded in numerical predictions of structural response of thin plates subjected to blast loads. Wiehahn et al[29] used the temperature dependent material properties to indicate failure occurring as a result of a thermo-mechanical instability and localised shear banding. These localised shear bands provided new insights into the subsequent failure and tearing mechanism through the thickness of the plate undergoing deformation at strain rates in the range of 10^2 s^{-1} to 10^4 s^{-1}. Comparisons between experimental and numerical results showed good correlations with a temperature independent simulation being a slightly better correlation than a temperature dependent simulation for cases where tearing did not occur. Deflections obtained from a model using a temperature dependent material is slightly higher than those using a temperature independent material. However, simulations using temperature dependent properties showed severe necking as a result of unrealistically large strains in the localised region clearly indicating the point of failure for cases where tearing occurred when a coarse mesh was used (Figure 2.11). On the other hand, fine meshes predicted formations of shear bands at an angle of either 45° or 135° to the mid-plane of the plate for the same cases (Figure 2.12). The exact method of failure is thus highly dependent on mesh density.

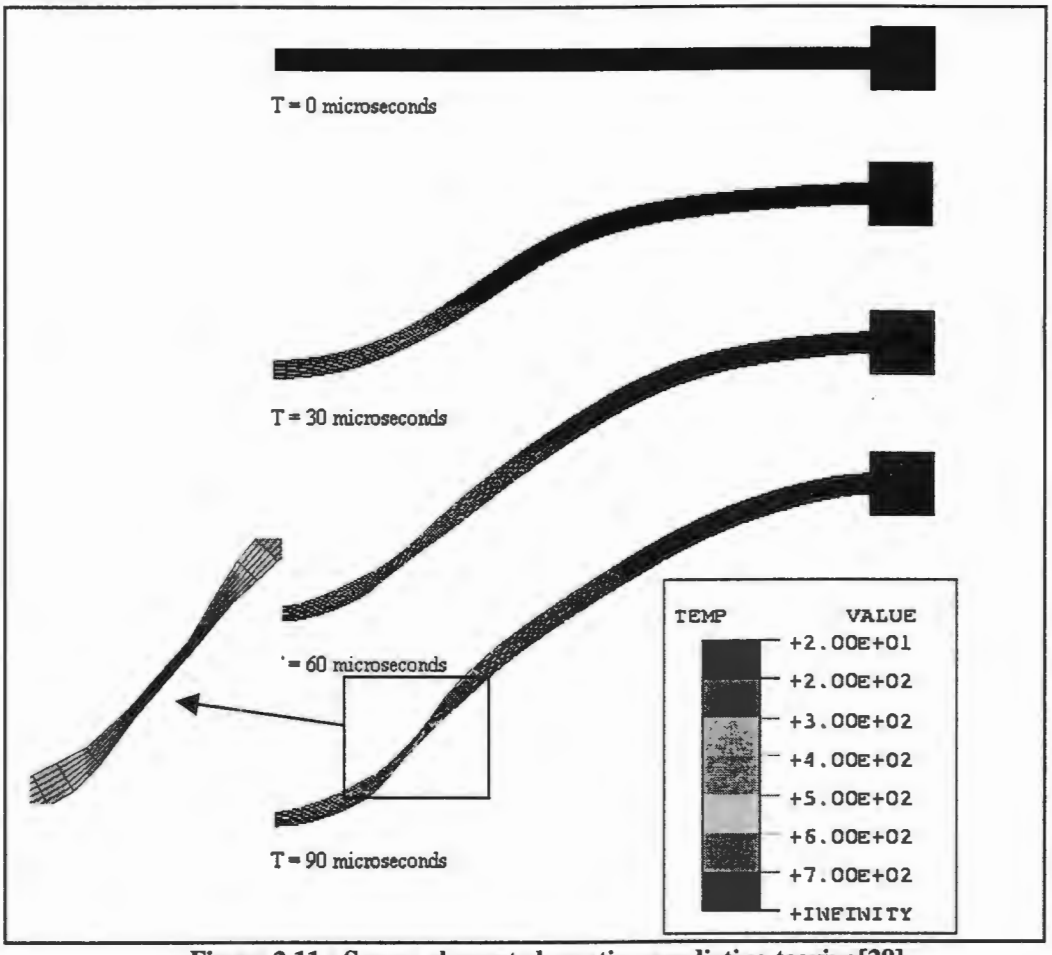

Figure 2.11 : Severe element elongation predicting tearing[29]

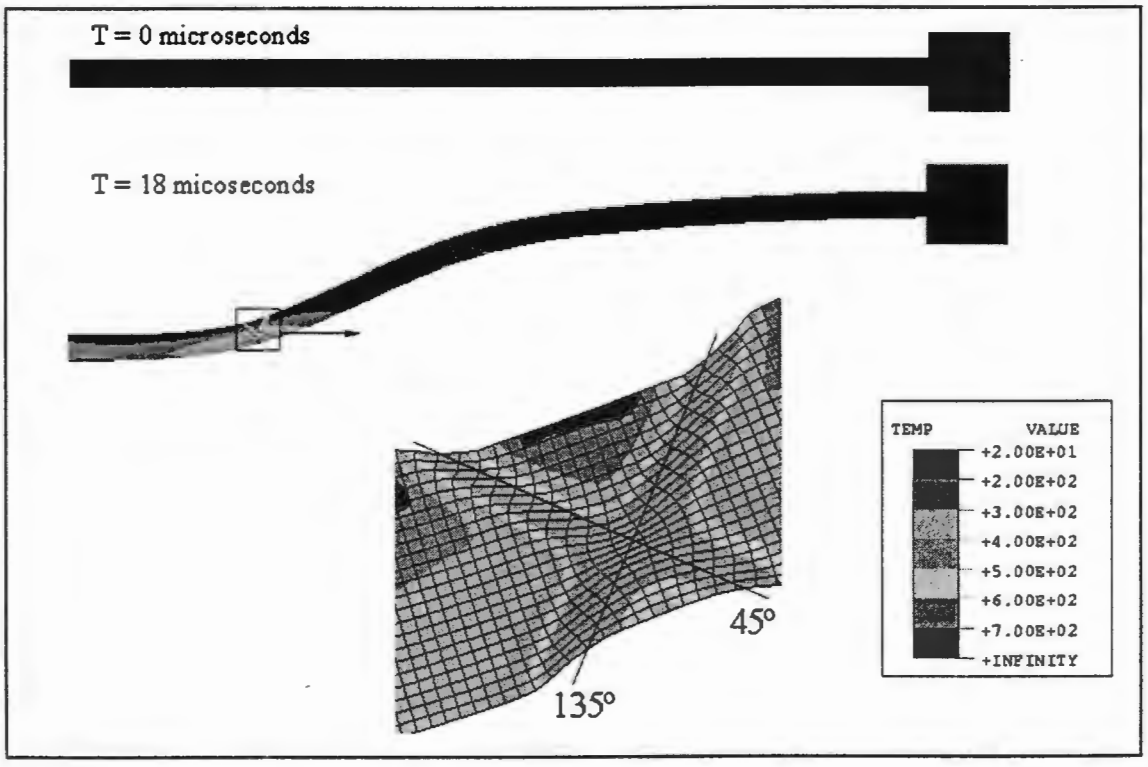

Figure 2.12 : Formation of shear band at 45° and 135° predicting tearing[29]

The emphasis of the numerical analyses, so far, has been on the prediction of the response of the structures. Recently Grobbelaar[30] made use of computational techniques to model the behaviour of the explosive to acquire a better understanding of the blast process and the material behaviour. Until now, the loading conditions have been modelled based on assumptions of blast time and constant pressure[11,14,17,27]. Grobbelaar[30] recently made use of the Jones-Wilkins-Lee equation of state to define the material behaviour of the explosive to model the detonation and subsequent expansion of the plastic explosive. In this way the explosive material and its interaction with the structure is investigated. This provides an insight into the spatial distribution of the explosive process and eliminates the need to assume a pressure-space-time distribution for the loading. The explosive model was assessed by considering its interaction with experimental data for localised blast loaded circular plates. Four loading conditions were investigated (load/plate diameter ratio of 0.18, 0.25, 0.33 and 0.40) and the trends predicted exhibited satisfactory correlation with the experimental results.

Three phases of the explosive process and its plate interaction were defined:

Phase I : The expansion of the explosive from time of detonation to interaction with the plate (0-5μs)

Phase II : Explosive plate interaction (6-30μs)

Phase III : Expansion of explosion from time of separation from plate to time of plate equilibrium (40-450μs)

The expansion of the explosive and its interaction with the plate is shown in Figures 2.13. The result shows the explosive expansion at different time increments during its expansion. The model shown depicts the 0.25 load/plate diameter ratio and 7.7 Ns impulse.

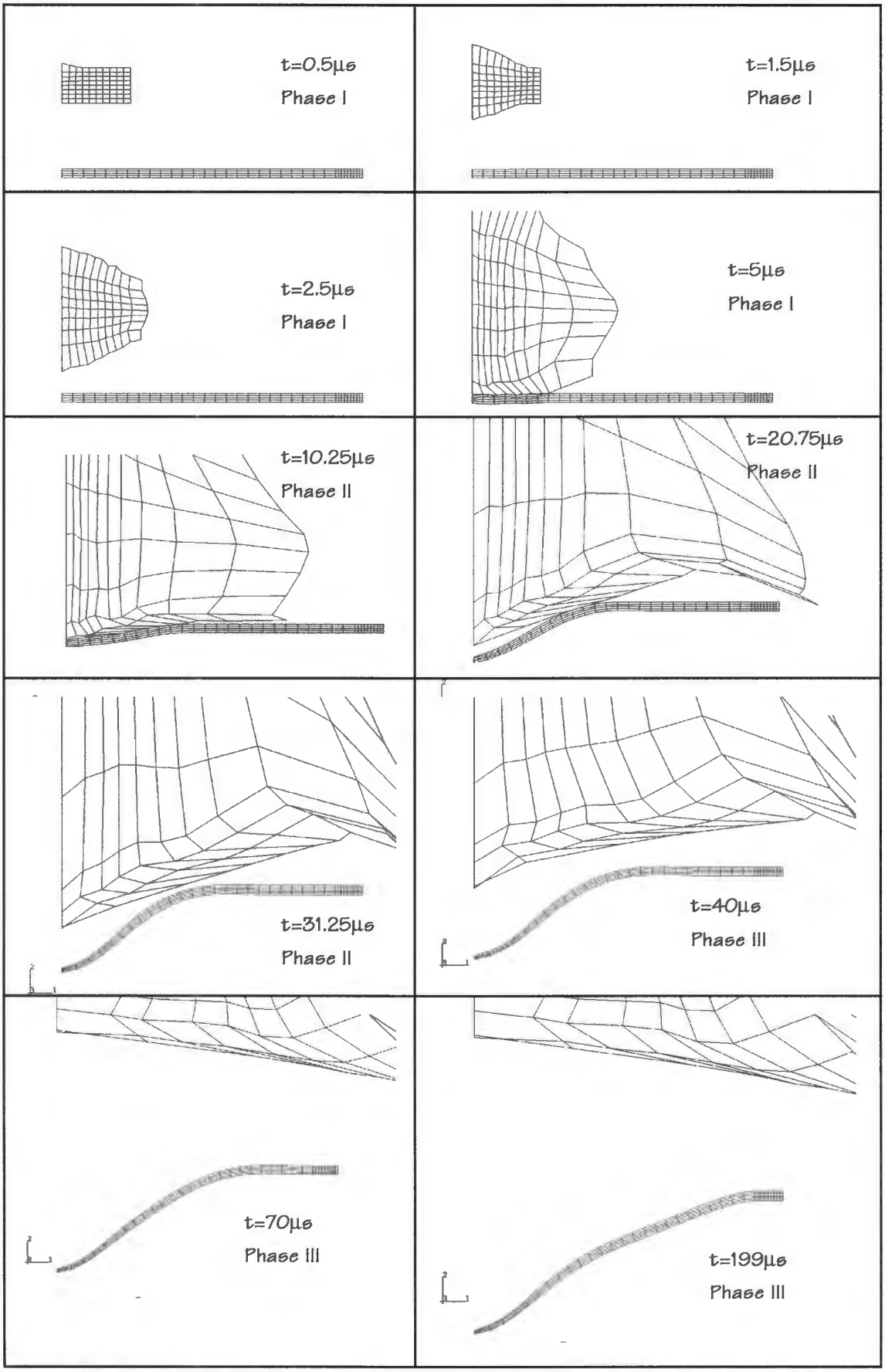

Figure 2.13 : Expansion of explosive and its interaction with the plate for a load diameter 25mm and impulse 7.7Ns [30]

3.0 Experimental Details

The experimentation reported on in this document was done by the author in the Blast Laboratory at the University of Cape Town. The following sections give the experimental procedures, material tested, explosive material used and the observations that were made. Results obtained from the experimentation are discussed in the next chapter.

3.1 Experimental Procedure

The experimental procedure; the method of creating an impulsive load using plastic explosive and the measurement of the impulse using a ballistic pendulum; used in this investigation and presented in this report is similar to that used in many previous experimental investigations. The ballistic pendulum is the same as that used by Nurick et al.[2,4,5,6] involving explosive impact on plates. This experimental technique has been proven to give consistent and reproducible results.

The experiments described herein differ from previous experiments in that the size of the plates and the configurations and size of the stiffeners are different.

The apparatus used in these experiments can be classified as follows:-

- Ballistic pendulum used to measure the impulse.
- Plastic explosive used to impart the impulse.
- Test specimens, Built-in Plates.

3.1.1 BALLISTIC PENDULUM

A ballistic pendulum was used to measure the uniform impulse applied to the plates. It consists of a steel I-beam suspended from a solid concrete roof by four spring steel wires, as shown in Figure 3.1. The spring steel wires have adjustable screws attached to them, enabling the pendulum to be levelled. At one end of the pendulum the built-in test plate (experimental rig) is positioned and at the other end balancing masses are attached. These balancing masses are to ensure that each spring steel wire carries approximately the same mass thus ensuring that the impulse acts through the centroid of the pendulum. Also attached to the ballistic pendulum is a recorder pen. This pen is used to record the oscillation amplitude of the pendulum on to a sheet of tracing paper. The oscillation amplitude relates directly to the impulse imparted on to the test specimen.

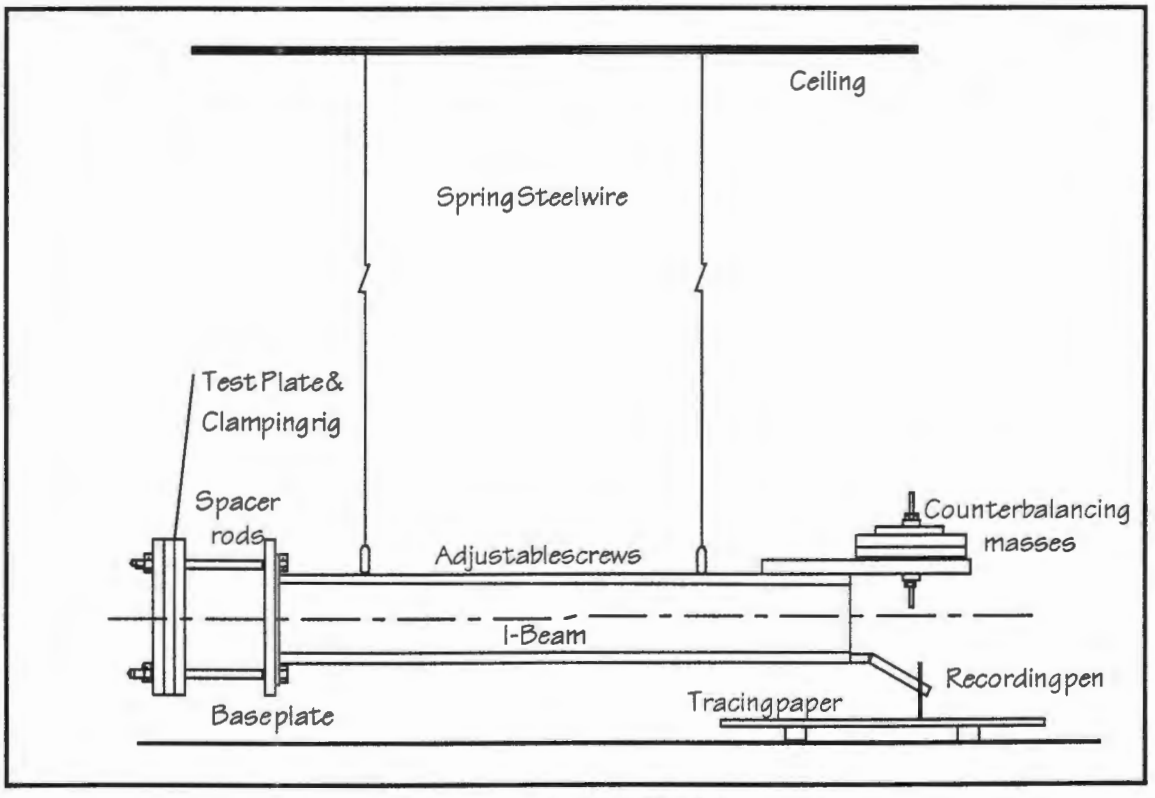

Figure 3.1 Ballistic Pendulum

In order to calculate the impulse from the trace several measurements need to be taken of the apparatus. These are presented in Table 3.1. The equations relating the motion of the pendulum to the impulse applied to the test plates are given in the appendix C.

Table 3.1 gives the ballistic pendulum constants used in the experiments.

Mass of I-Beam	28155g
Mass of Clamping Rig	15385g
Mass of Counter Balance	23690g
Total Pendulum Mass (M)	67230g
R (see appendix C)	2584mm
Z (see appendix C)	119.62mm
A (see appendix C)	62.7mm
T (see appendix C)	3.19s

Table 3.1 Ballistic pendulum details.

3.1.2 Explosive Load Geometry and Material Properties

The plates were uniformly loaded using plastic explosive (PE 4), with an approximate burn speed of 7500m/s. This explosive was laid out on a 12mm thick polystyrene foam pad which has the dimensions of the exposed plate in two concentric quadrangular annuli made by rolling the sheet explosive into cylinders and arranged in such a way that there was on average a uniform distribution of explosive mass over the specimen. Two perpendicular strips of explosive at the centre called cross-leaders interconnected the annuli. A short tail of 1g of explosive holding the detonator was then attached to the centre of the cross-leaders. The foam pad disintegrates on detonation but attenuates the shock transmitted to the plate, provides a uniform impulse and prevents spallation of the specimen without interfering with the outcome of the test. The mass of the explosive tail and the cross-leaders was kept constant for all the tests. Differing masses of the annuli explosive were used, giving different impulses, resulting in plate responses ranging from Mode I deformations to complete tearing. The plate and load configuration is illustrated in Figure 3.2.

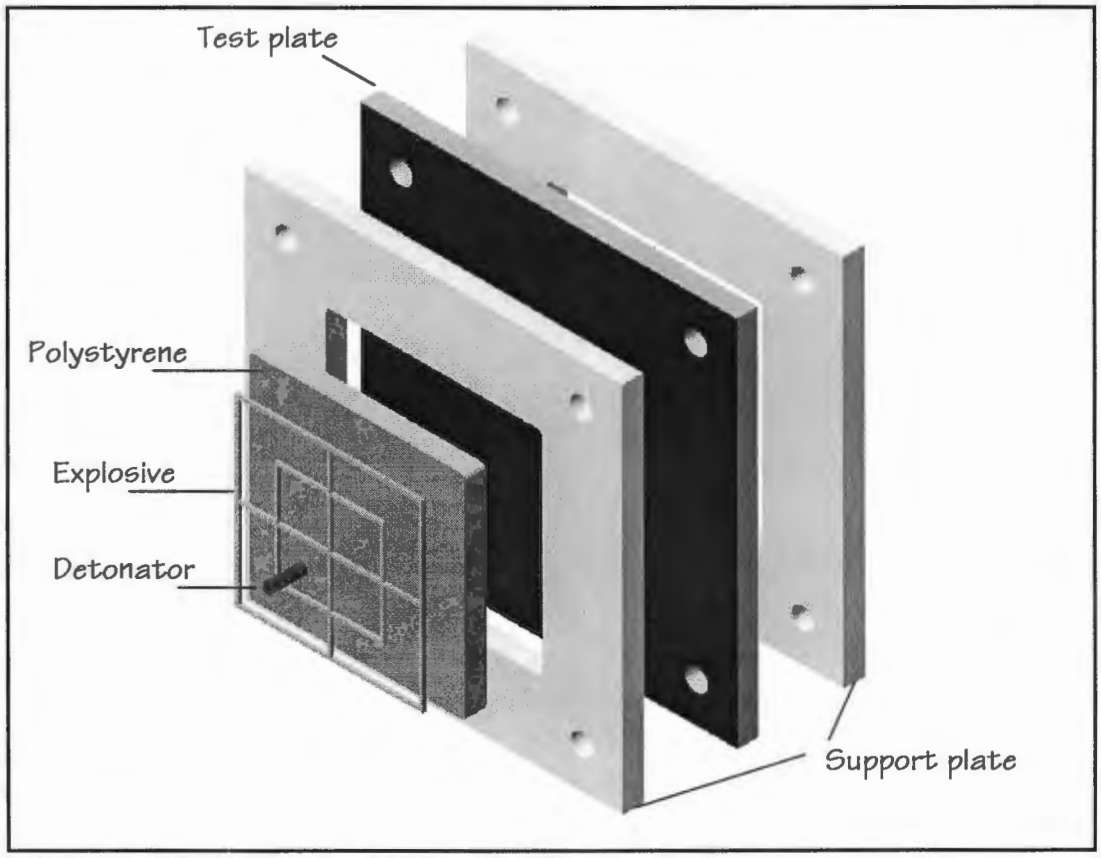

Figure 3.2 Plate and Load configuration

3.1.3 BUILT-IN TEST PLATE

The built-in test plate consists of a 12mm thick and approximately 220mm square hot rolled steel. One surface of each plate was ground to provide a flat surface for the machining process. A numerically controlled milling machine was used to cut a quadrangular section of dimensions 126 x 126mm (square plates) and 159 x 100mm (rectangular plates) leaving a 1.6mm thick plate with a rectangular stiffener 3mm or 4mm wide. Different stiffener heights of 3 and 7mm were cut as well as plates without a stiffener. The dimensions were chosen so that the exposed area of the two geometries were similar. Table 3.2 shows the different configurations of stiffener. Diagrams of typical plates are shown in Appendix E.

Name	Description	Sketch	Stiffener Size
Square (S)	No stiffener within exposed square area	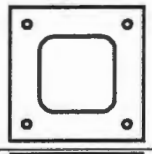	none
Single Stiffener (S-S)	A single stiffener machined within exposed square area	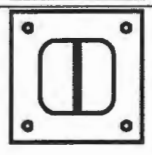	3x3mm 3x7mm 4x3mm 4x7mm
Double Stiffener (S-DS)	Two stiffeners machined parallel to each other within the exposed square area dividing the plate into three equal areas	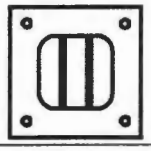	3x3mm 3x7mm
Double-cross Stiffener (S-DCS)	Three stiffeners machined within the exposed square area dividing the plate into six equal areas		3x3mm 3x7mm
Cross Stiffener (S-CS)	Two single stiffeners machined perpendicular to each other dividing the exposed square area into four equal areas	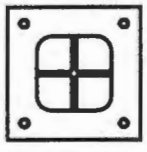	3x3mm 3x7mm
Rectangular (R)	No Stiffener within the exposed rectangular area	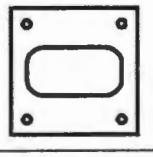	3x3mm 3x7mm
Rectangular Double stiffener (R-DS)	Two stiffeners machined parallel to each other within the exposed square area dividing the plate into three equal areas	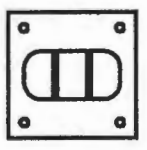	3x3mm 3x7mm

Table 3.2 : Stiffener configurations

In order to take into account the variable dimensions of each plate, the plate thickness as well as the width and height of the stiffeners were measured at several places and the average reading was taken. Variations in the measurements were mainly due to tool wear of the mill cutter. The dimensions of the plates are shown in Appendix F.

The test plate is heat treated to remove all residual stress caused by the machining and drilling processes. It is attached to the ballistic pendulum by means of four high tensile steel bolts. This is illustrated in Figure 3.3. The clamping force applied to the test plates was assumed to be sufficient to prevent slippage of the specimen.

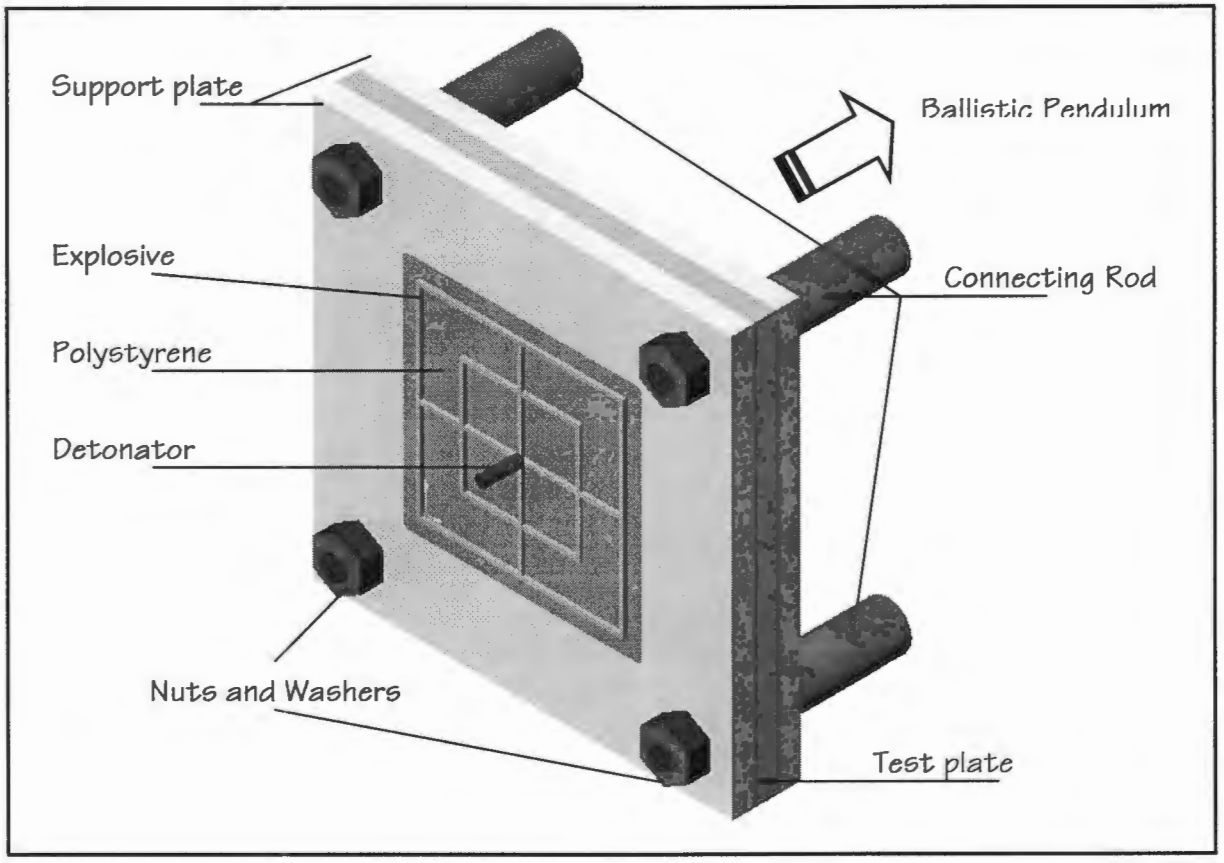

Figure 3.3 Built-In test plate set-up

Standard uni-axial tensile test specimens cut from the thick parts of the test plates after being blasted were tested at different strain rates. Assuming the mild steel plates to be rigid-viscoplastic, static yield stresses were computed by substituting the test results into the Cowper-Symonds relation:-

$$\frac{\sigma_0^1}{\sigma_0} = 1 + \left(\frac{\dot{\varepsilon}}{\dot{\varepsilon}_0} \right)^{1/\eta} \tag{3.1}$$

where σ^1_0 : Dynamic yield stress; σ_0 : Static yield stress; $\dot{\varepsilon}$: Strain rate; $\dot{\varepsilon}_0$ and η are material constants. $\dot{\varepsilon}_0 = 40\ s^{-1}$ and $\eta = 5$ are commonly used and acceptable values for mild steel [26].

The results of the tensile tests are shown in Appendix B.

A summary of the material properties and geometry of the test plate is given in the Table 3.3.

Exposed Area (A) square plates	15876mm²
Exposed Area (A) rectangular plates	15900mm²
Nominal plate thickness (t)	1.6mm
Density (ρ)	7769Kg/m³
$\dot{\varepsilon}_o$	40.4
η	5
Poisson's Ratio (ν)	0.33
Uniaxial Tensile Stress	242MPa
Young's Modulus (E)	210Gpa
% Uniaxial Tensile Strain at failure	34.73

Table 3.3 Plate material properties and geometry

3.2 Experimental Measurements

For each experiment, two measurements are needed:

- the measurement of the impulse.
- after deformation where no tearing has taken place, the final mid-point deflection of the plate.

Plate profile and contour plots are also taken for a number of plates to compare the experimental results with the numerical models.

3.2.1 Impulse

The impulse is determined by the displacement of the ballistic pendulum. The equations relating the displacement of the ballistic pendulum to the impulse are given in Appendix C.

3.2.2 Mid-point Deflection

The final mid-point deflection is measured mechanically using a height gauge.

3.2.3 Plate profile

The vertical cross-section of the deformed plate that is plate profile is measured by means of a coordinate measuring machine (CMM). The accuracy of the machine is of the order of 10μm. The plate profile is taken along the lines of symmetry of the plates and 20mm from the centre of the plates parallel to the stiffener.

3.2.4 Contour plot

An outline of the different levels of displacement of the deformed plates that is contour plot is obtained from digital photogrammetry. Digital images of the deformed test plates are processed into a computer using pixels and image processing technique to obtain the geometric information of the deformed plates. The order of accuracy of the plot is less than 0.2mm.

4.0 Experimental Results

A total of 40 tests were conducted in this project. These tests were performed over a period of two months. This chapter presents the observations made on examining the plates after testing.

Tables A.1 to A.7 in appendix A list the test readings with all the measured data. The analysis of the experimental results is discussed in detail in chapter 5.

4.1 General Plate Deformation

In all the tests of Mode I category of large inelastic deformation, the plate profiles were characterised by a uniform global dome with hinges formed from the corner to the central part of the plate. The hinges were formed at 45° from the corners of the plate. The global deformation was dictated by symmetry in all cases. During the first few tests which involved single stiffened plates, the boundary was deformed (see Figure 4.1) due to insufficient support at the boundary. This was corrected by attaching an additional support plate at the boundary of the plates.

Figure 4.1 : Deformed boundary of a single stiffened square plate with stiffener size 3x7mm at impulse 34Ns

4.1.1 NO STIFFENER (S AND R)

Similar to past experiments on beams, circular plates and square plates, the mid-point displacement of both the square and rectangular plates increased as the impulse increased with the highest displacement occurring in the central area of the plate. Typical responses of the square and rectangular plates are shown in Figures 4.2 - 4.5. Unlike the square plates where the maximum displacement occurred in the central area of the plate, the rectangular plates exhibited two peaks along the centre profile of the longest side of the plates at either side of the centre line of the longest side of the plate (see Figure 4.4).

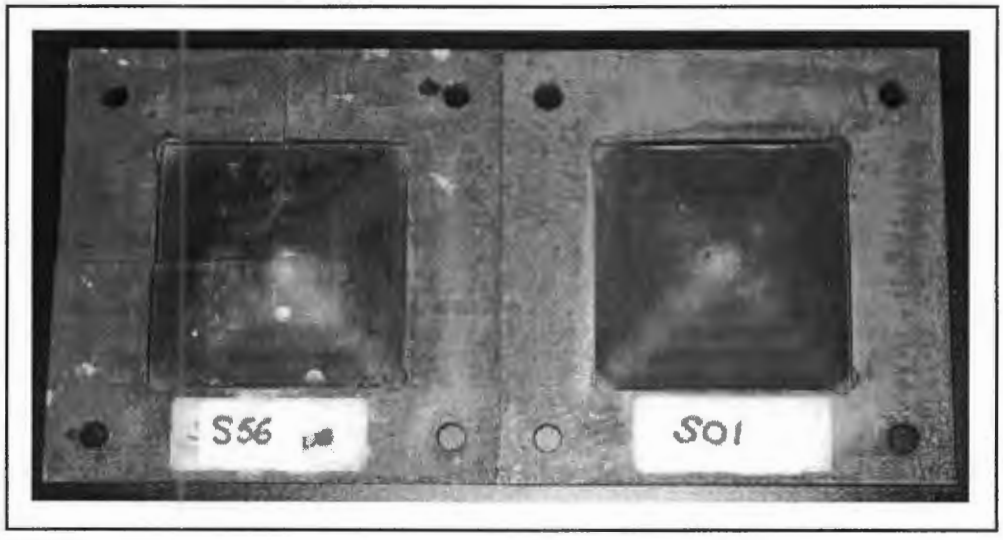

Figure 4.2 : Deformed square plates
From left to right : Impulse 31Ns and 43Ns;
mid point displacements : 25.5mm and 32.8mm

Figure 4.3 : Side view of cut square plate at impulse 31Ns

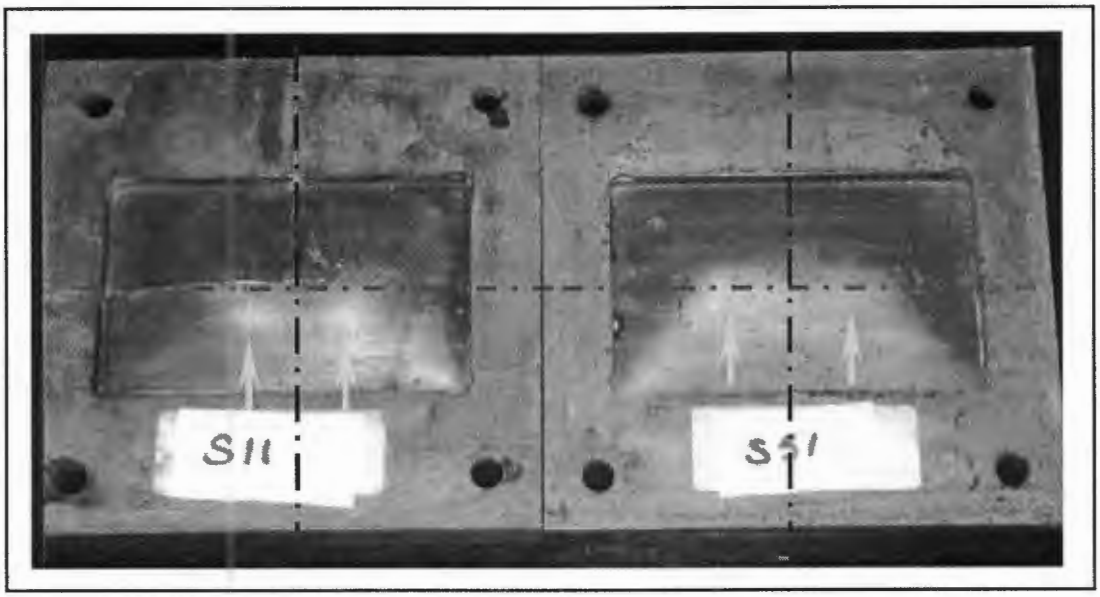

Figure 4.4 : Deformed rectangular plates
From left to right : impulses 24Ns and 34.8Ns (arrows showing peak)
Mid point displacement : 15.8mm and 23.2mm
(red line denotes centre line of shortest sides; blue line denotes centre line of longest sides)

Figure 4.5 : Side view of cut rectangular plate at impulse 24Ns
(Arrow showing peak height)

4.1.2 SINGLE STIFFENER (S-SS)

This configuration response is shown in Figures 4.6 and 4.7. The response is generally similar to that already described in section 4.1.1. However, the mid-point deflection of the stiffened plate (S-SS) was less than the mid-point of the square plate (S) for the same load intensity. The latter is discussed in chapter 5. Moreover, the mid-point displacement decreased with increasing stiffener size.

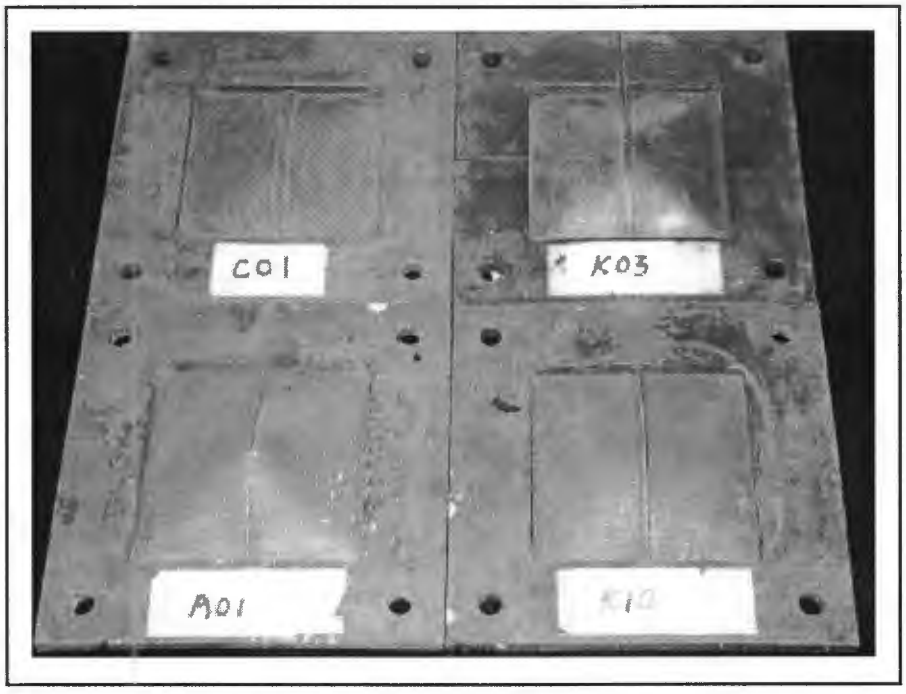

Figure 4.6 : Deformed single stiffened square plates
Clockwise from top : (C01);stiffener size 4x3mm at impulses 18Ns; mid point displacement 11.8mm, (K03); stiffener size 4x7mm at impulses 40.5Ns, mid point displacement 26.6mm, (K10); stiffener size 3x7mm at impulses 34Ns, mid point displacement 24.7mm, (A01); stiffener size 3x3mm at impulses 35.8Ns, mid point displacement 30.1mm

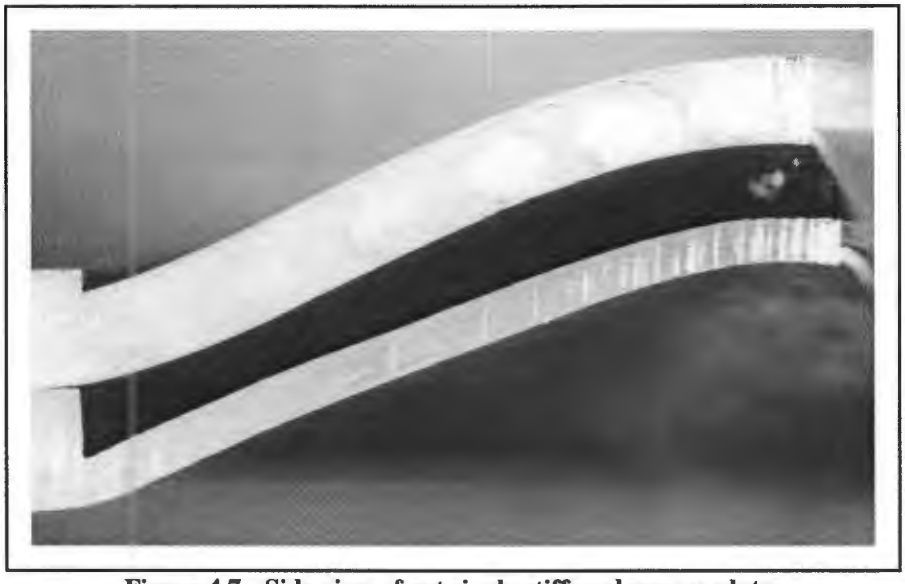

Figure 4.7 : Side view of cut single stiffened square plates
From top to bottom : stiffener size 4x7mm at impulse 40.5Ns, stiffener size 3x3mm at impulse 35.8Ns

4.1.3 Cross Stiffener (S-CS)

The cross stiffened plates deformed symmetrically about the x-y and z-y planes like the square plates with the highest mid-point deflection occurring in the central area of the plate as shown in Figures 4.8 and 4.9. For all the stiffened plates, the mid-point displacement increased as the impulse increased.

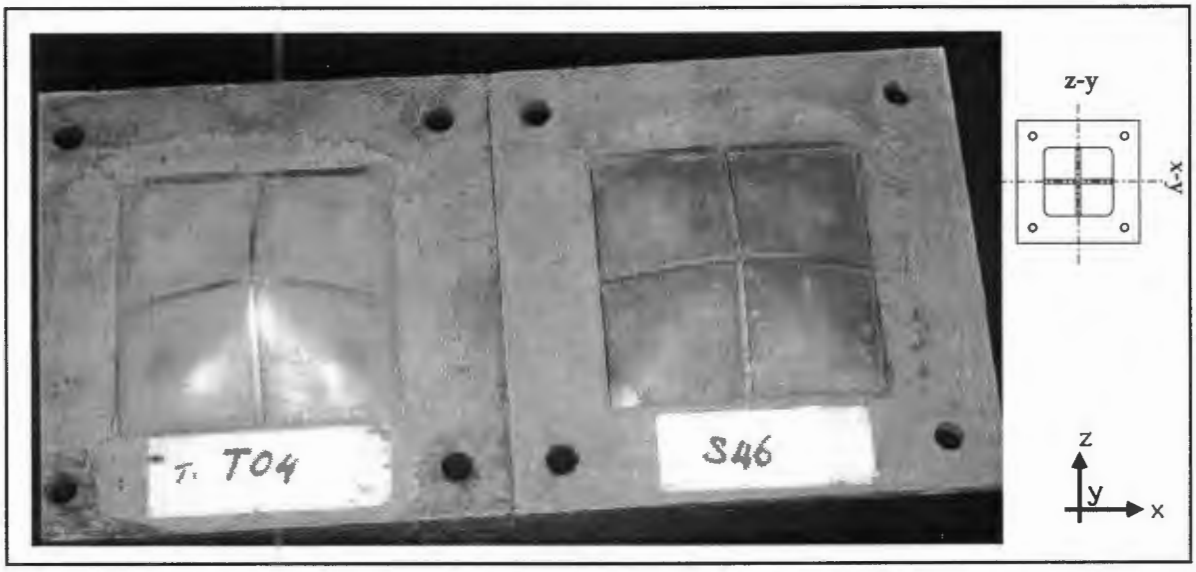

Figure 4.8 : Deformed cross stiffened square plates
From left to right : stiffener size 3x3mm impulses 36Ns, mid point displacement 25.9mm; stiffener size 3x7mm impulse 32Ns, mid point displacement 17mm

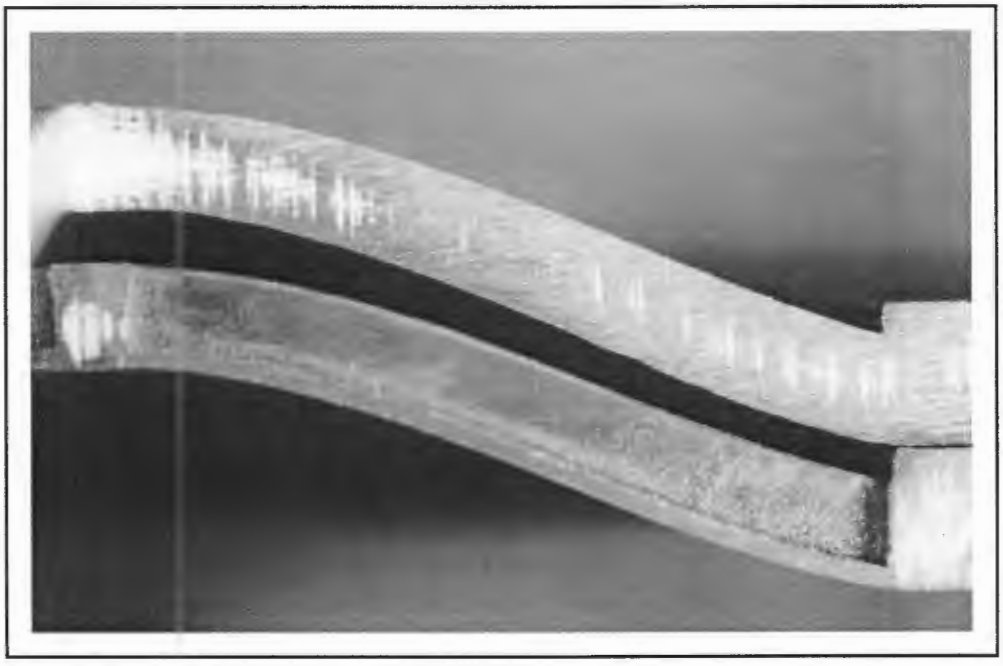

Figure 4.9 : Side view of cut cross stiffened square plates
From top to bottom : stiffener size 3x7mm at impulse 35.6Ns and impulse 36Ns

4.1.4 DOUBLE STIFFENER (S-DS) AND (R-DS)

The response of this configuration was generally similar to that described for the single stiffened plates (S-SS). Typical plate response is shown in Figures 4.10 to 4.13. The mid-point displacement of the plate (S-DS) is smaller than the single stiffener configuration. For the square plate, the maximum displacement occurred over a small central area between the parallel stiffeners whereas for the rectangular plates it occurred over a central area that included both parallel stiffeners. It was also observed that the distance between the parallel stiffeners; referred to as the gap (shown by arrows in Figure 4.10); increased as the impulse increased for stiffeners of the same size and same failure mode of the plate. As the stiffener size increased the gap size decreased for the same impulsive load. Tabulated in Table 4.1 is the percentage increase in the gap size.

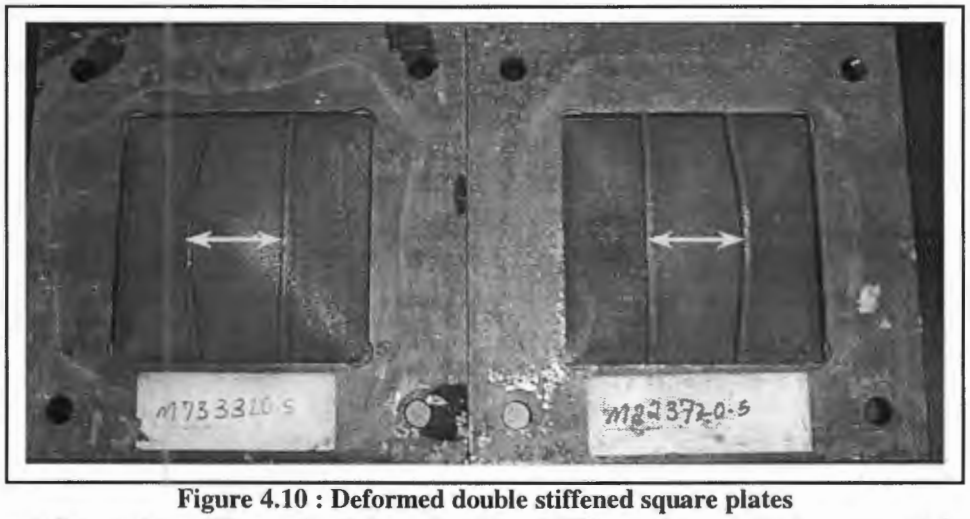

Figure 4.10 : Deformed double stiffened square plates
From left to right : stiffener size 3x3mm impulses 36.9Ns, mid point displacement 25.2mm; stiffener size 3x7mm impulse 45.9Ns, mid point displacement 23.0mm
(arrows show distance between the parallel stiffeners referred to as gap)

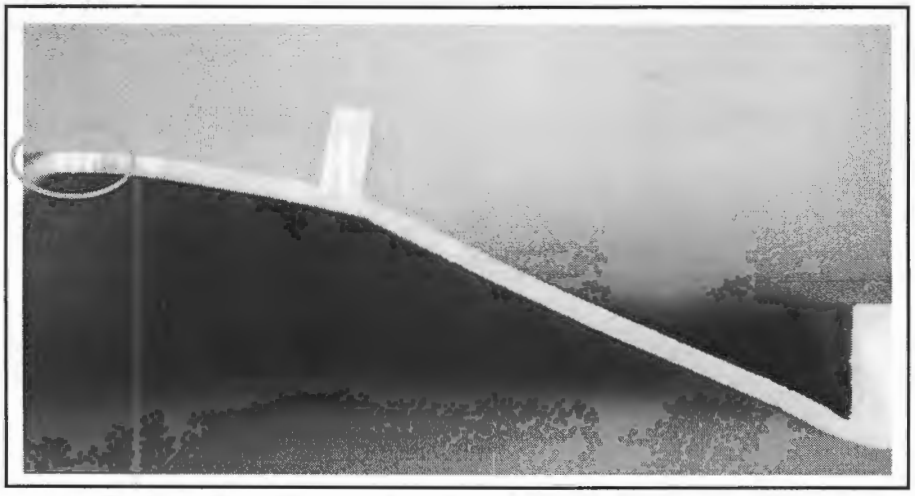

Figure 4.11 : Side view of cut double stiffened square plate with stiffener size 3x7mm at impulse 45.9Ns

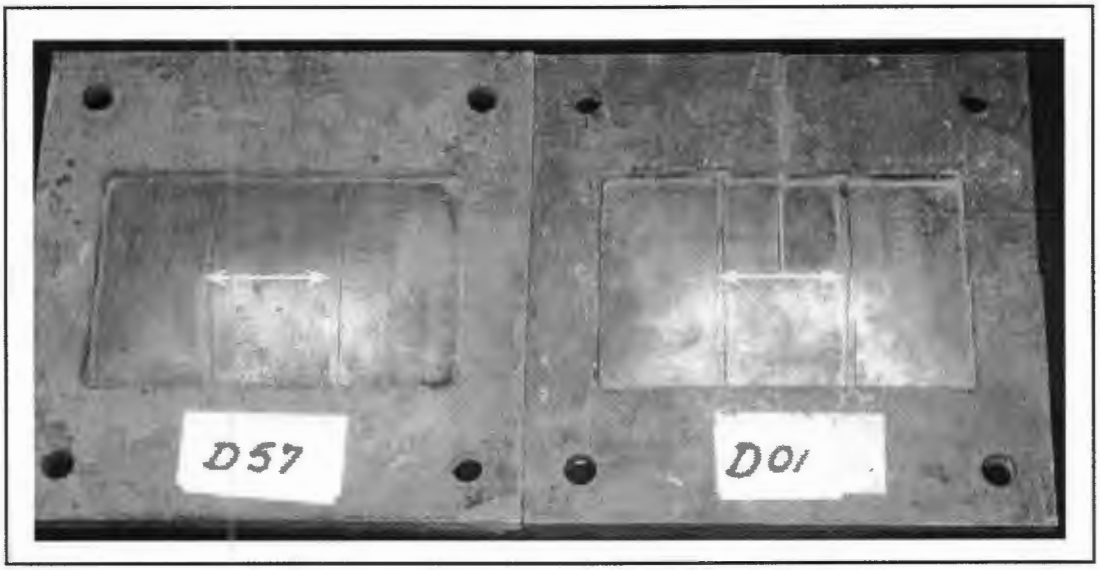

Figure 4.12 : Deformed double stiffened rectangular plates
From left to right : stiffener size 3x3mm impulses 29.2Ns mid point displacement 15.9mm; stiffener size 3x7mm impulse 35.5Ns mid point displacement 18.5mm
(arrows show distance between the parallel stiffeners referred to as gap)

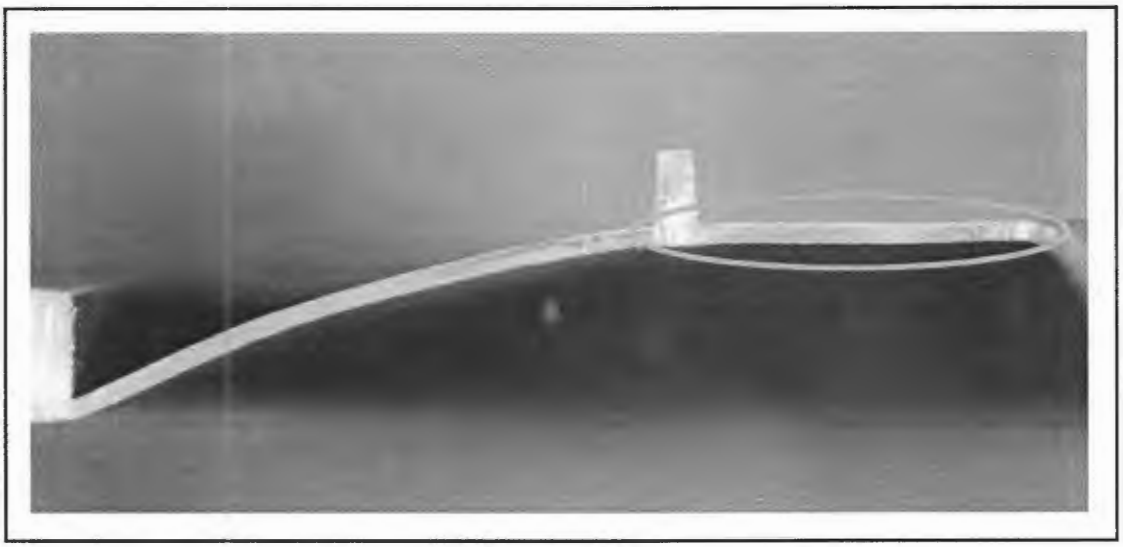

Figure 4.13 : Side view of cut double stiffened rectangular plate with stiffener size 3x7mm at impulse 35.5Ns

4.1.5 DOUBLE CROSS STIFFENER (S-DCS)

The plate response for the double cross stiffener (S-DCS) configuration as shown in Figures 4.14 and 4.15 was similar to that of the double stiffened plates (S-DS). The double cross stiffened square plates, however, showed more resistance to the impulsive load than the double stiffened plate. A decrease in mid point displacement was observed for the same load intensity.

Figure 4.14 : Deformed double cross stiffened square plates
From left to right : stiffener size 3x3mm impulses 35.8Ns, mid point displacement 24.4mm; stiffener size 3x7mm impulse 36.7Ns, mid point displacement 19.8mm

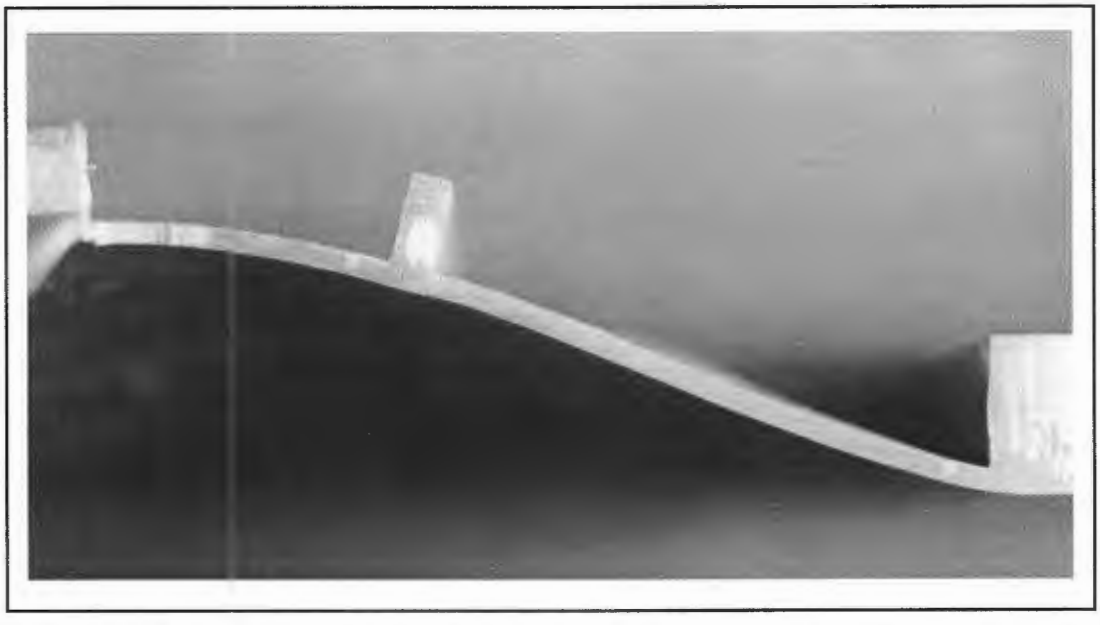

Figure 4.15 : Side view of cut double cross stiffened square plate with stiffener size 3x7mm at impulse 36.7Ns

Table 4.1 shows the distance between the two parallel stiffeners (gap size) for double stiffened and double cross stiffened plates. Originally the gap size is 40mm for the double stiffened and double cross stiffened square plates and 50mm for the double stiffened rectangular plates. For the same stiffener size and impulsive load the distance between the parallel stiffeners of double stiffened square plate (S-DS) is larger than the distance between the parallel stiffeners of the double cross stiffened square plate (S-DCS). The percentage increase in gap size is generally higher for the square plates than the rectangular plates.

Specimen	Stiffener Configuration	Stiffener size (mm)	Impulse Ns	Gap size (mm)	% increase	Comments
D57	R-DS	3 x 3	29.2	52.58	3.10	Mode I
D36	R-DS	3 x 3	33.4	52.56	3.06	Mode I
D11	R-DS	3 x 7	31.8	52.74	3.41	Mode II*
D01	R-DS	3 x 7	35.5	52.12	2.20	Mode I
M73	S-DS	3 x 3	36.9	43.32	8.30	Mode I
T01	S-DCS	3 x 3	35.8	42.78	6.95	Mode I
M22	S-DS	3 x 7	37.5	42.18	5.45	Mode I
M17	S-DS	3 x 7	42.3	41.28	3.20	Mode II*
M27	S-DS	3 x 7	45.9	41.84	4.60	Mode II*
T02	S-DCS	3 x 7	36.7	41.74	4.35	Mode I
T10	S-DCS	3 x 7	36	42.00	5.00	Mode II*

Table 4.1 : Gap size for different stiffener sizes and impulses

4.2 Thinning of the quadrangular plates

4.2.1 Plate thinning at the boundary

At higher impulses, the plates deformed with thinning occurring at different parts of the plate. Thinning in the form of necking, as seen in typical tensile tests of mild steel (see Figure 4.16), was not visible in any cases. A similar observation about the thinning mechanism of built-in square plates subjected to blast load was made by Thomas[20], hence showing good repeatability of results.

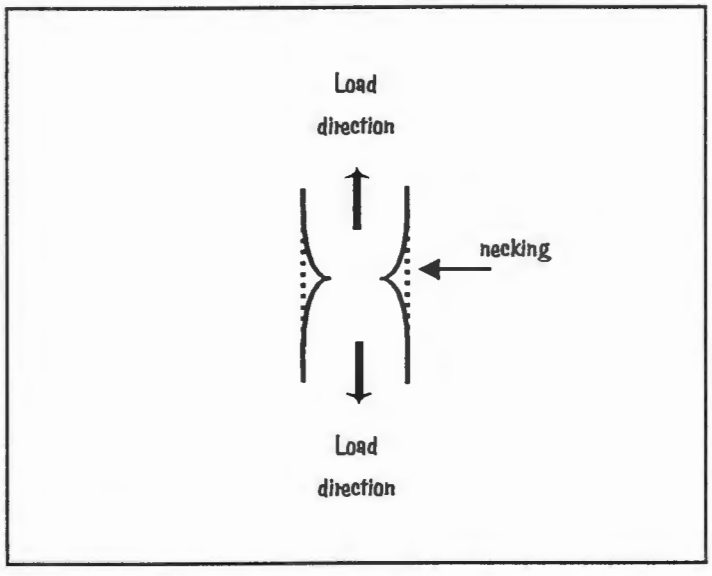

Figure 4.16 : Necking as seen in typical tensile tests of mild steel

Thinning mechanisms at the boundary were observed for all plates irrespective of stiffener sizes and configurations as shown in Figure 4.17. Thinning occurred due to the larger displacement of the loaded side of the plate towards the centre of the plate. Figure 4.18 shows a schematic sketch of boundary thinning. However, thinning was not consistent all around the boundary.

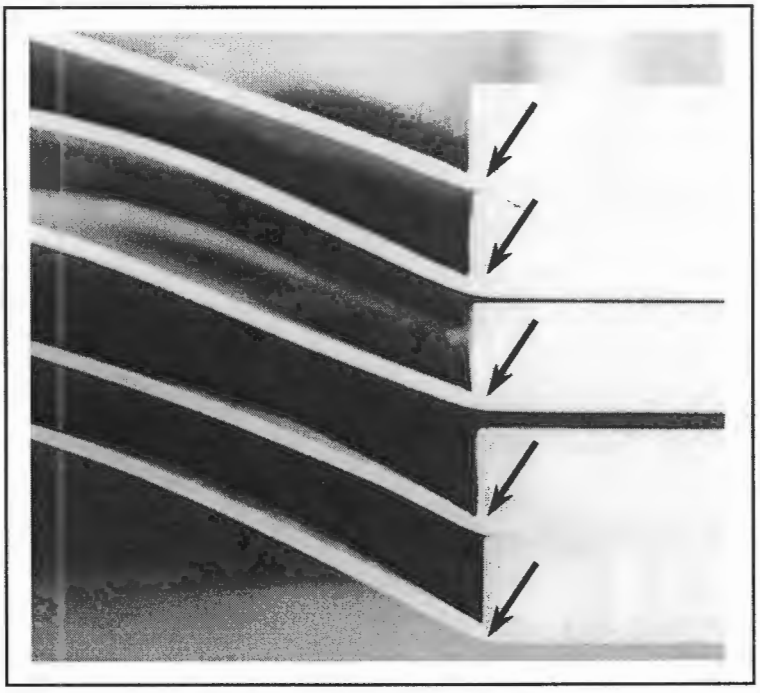

Figure 4.17 : Boundary thinning for square plates of all stiffener configurations (denoted by blue arrows)
From top to bottom: double cross stiffeners size 3x7mm at impulse 36.7Ns, cross stiffeners size 3x7mm at impulse 36Ns, double stiffeners size 3x7mm at impulse 37.5Ns, single stiffener size 4x7mm at impulse 40.5Ns, no stiffener at impulse 31Ns

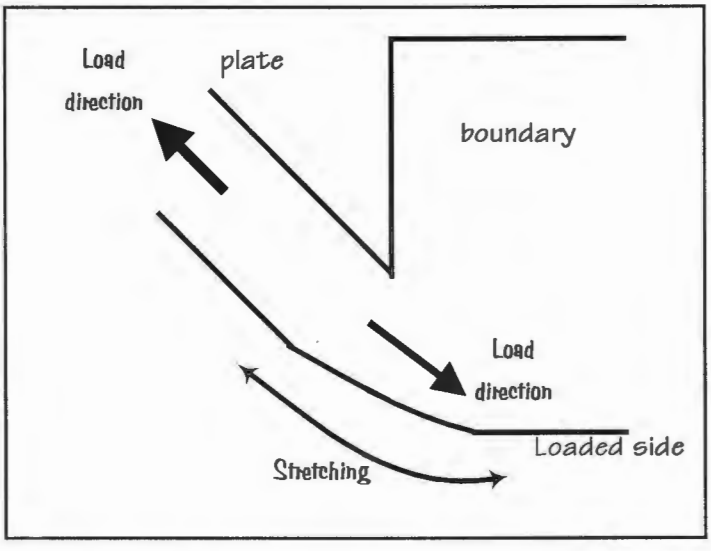

Figure 4.18 : Schematic sketch of boundary thinning

4.2.2 Plate thinning at the stiffener

For double and double cross stiffened plates (S-DS, R-DS and S-DCS), it was observed that the plate thins at only one side of the stiffener. In all such cases, thinning occurred at the side of the stiffener that is closest to the boundary as shown in Figures 4.19 and 4.20 No sign of thinning is observed at the other side of the stiffener. The plate thinning was more visible in the double stiffened square plates (S-DS) than in the double cross stiffened square plates (S-DCS) and the double stiffened rectangular plates (R-DS).

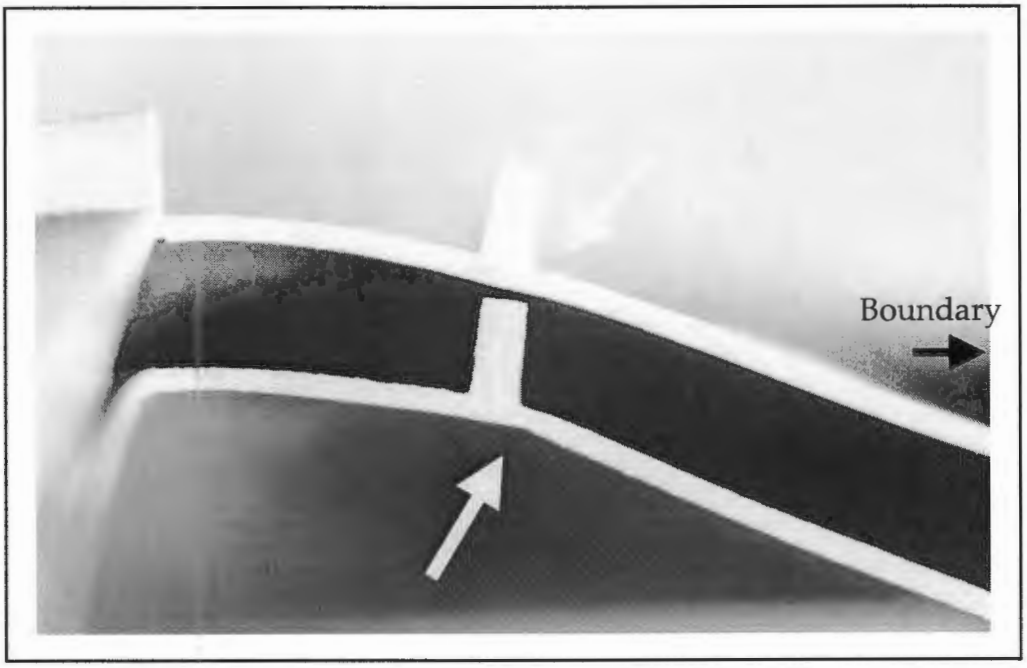

Figure 4.19 : Plate thinning in the vicinity of the stiffener of square plates (denoted by arrow) From top to bottom : double cross stiffened square plate with stiffener size 3x7mm at impulse 36.7Ns double stiffened square plate with stiffener size 3x7mm at impulse37.5Ns

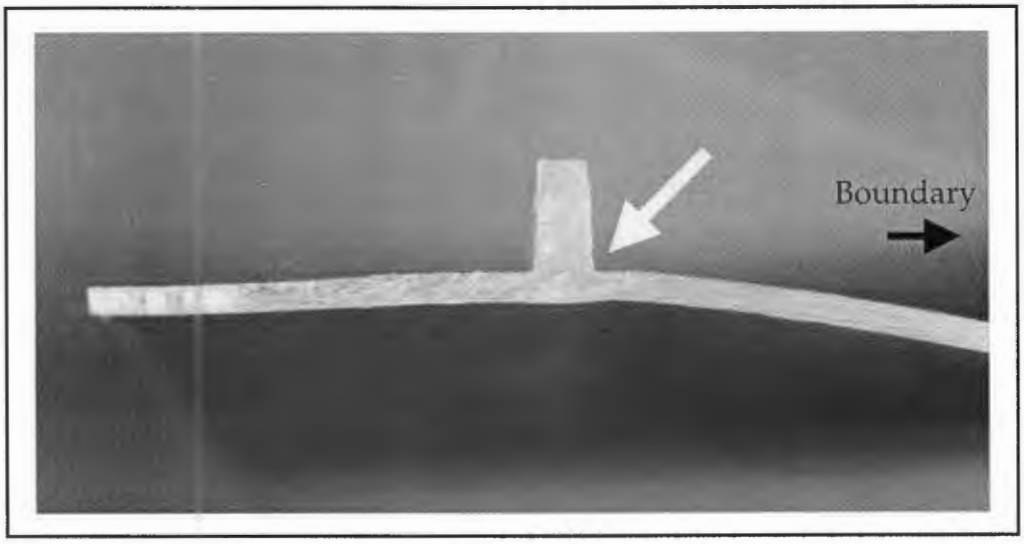

Figure 4.20 : Plate thinning in the vicinity of the stiffener of a double stiffened rectangular plate with stiffener size 3x7mm at impulse 36.7Ns (denoted by arrow)

4.2.3 Thinning of the stiffener

Thinning was also observed in the stiffener. A reduction in the stiffener width; illustrated in Figures 4.21 and 4.22; was observed. These occurred only in cases where the two stiffeners crossed each other perpendicularly; cross-stiffened and double-crossed stiffened square plates. The thinning only took place at the top of the stiffener. The latter is shown in Figure 4.22. This could be the result of the stretching of the stiffeners as the plate deformed.

Figure 4.21 : Stiffener thinning of a double cross stiffened square plate with stiffener size 3x3mm at impulse 36Ns (denoted by arrow)

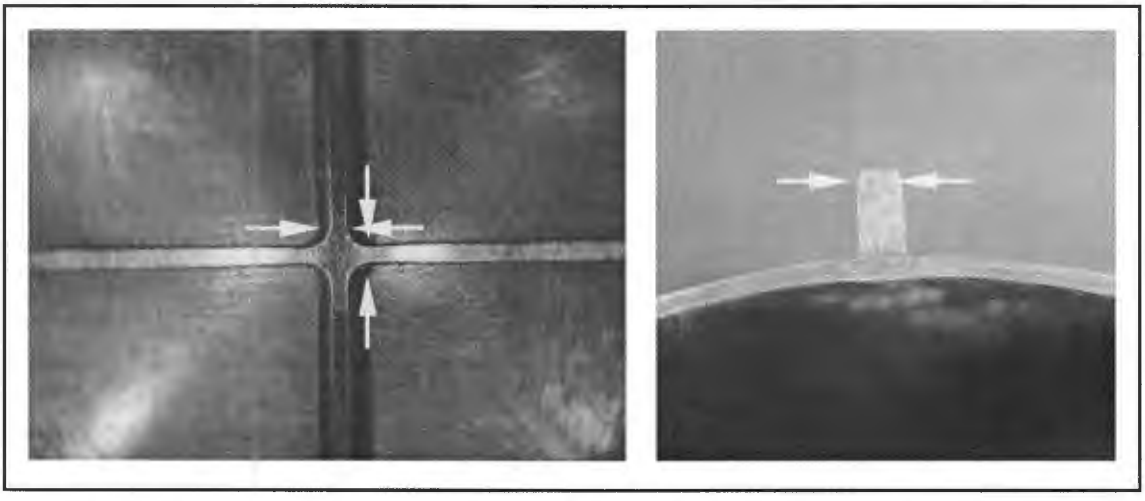

Figure 4.22 : Stiffener thinning of cross stiffened square plates (denoted by arrow)
From left to right : stiffener size 3x3mm at impulse 36Ns; stiffener size 3x7mm at impulse 36Ns yellow arrows highlights thinning in stiffener width

4.3 Tearing of the quadrangular plates

The plate deformation increased as the impulse increased causing the plate to thin. After the occurrence of thinning, the subsequent rupture of the plate was observed. Tearing first occurred at the middle of one side of the square plates and then progressed towards the corners as the load intensity increased; also reported by Olson et al [14, 15]. For the rectangular plates, tearing first occurred at the centre of one of the longest sides; that is the sides closest to the mid-point of the plate; and then progressed towards the corners as the impulse increased. Figure 4.23 shows tearing initiation in both the square and rectangular plates.

Figure 4.23 : Tearing of non-stiffened plates(shown by arrows)
From left to right : square plate at impulse 43.4Ns; Rectangular plate at impulse 34.8Ns

For stiffened plates, Mode II failure (tearing at the supports) always occurred first at the middle of one of the supported boundaries parallel to the stiffener. As the impulse increased, the number of torn sides increased, progressing from one side of tearing to two sides of tearing to three sides of tearing. These cases are designated as Mode II-1, Mode II-2 and Mode II-3 respectively. Figures 4.24 and 4.25 show the different Modes II failures at which tearing took place for single stiffened square plates (S-SS) and double stiffened square plates (S-DS) respectively.

Figure 4.24 : Tearing of single stiffened square plates –
From left to right : stiffener size 4x3 at impulse 39.8Ns; stiffener size 4x7 at impulse 41Ns; stiffener size 3x3 at impulse 40.6Ns

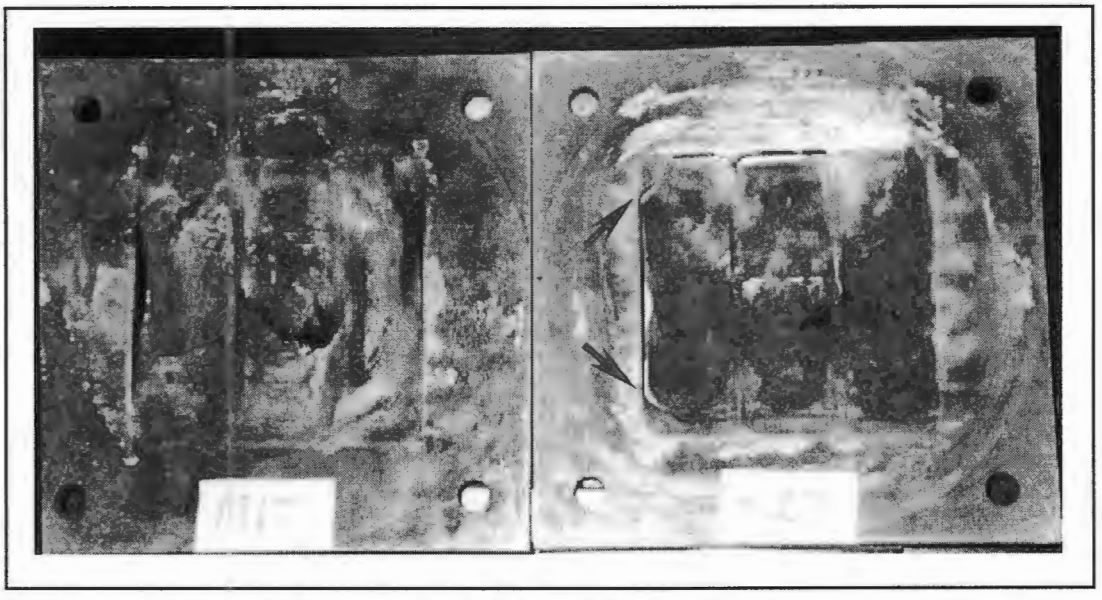

Figure 4.25 : Tearing of double stiffened square plates
From left to right : stiffener size 3x7 at impulse 42.3Ns; stiffener size 3x7 at impulse 45.9Ns
red arrows shows tearing across corner

Moreover, it was observed that in most cases where two sides perpendicular to each other tore, the plate sides tore across the corner of the plate as seen in Figure 4.25 (red arrow).

During the Mode II* failure phase, some "pulling-in" along the mid-sides of the plate was observed as the plate tore away at the boundary. This "pulling-in" seemed to result from the deformation of the plate which continued after one side of the plate had torn. The latter can be seen in all cases where at least one side of the plate has torn.

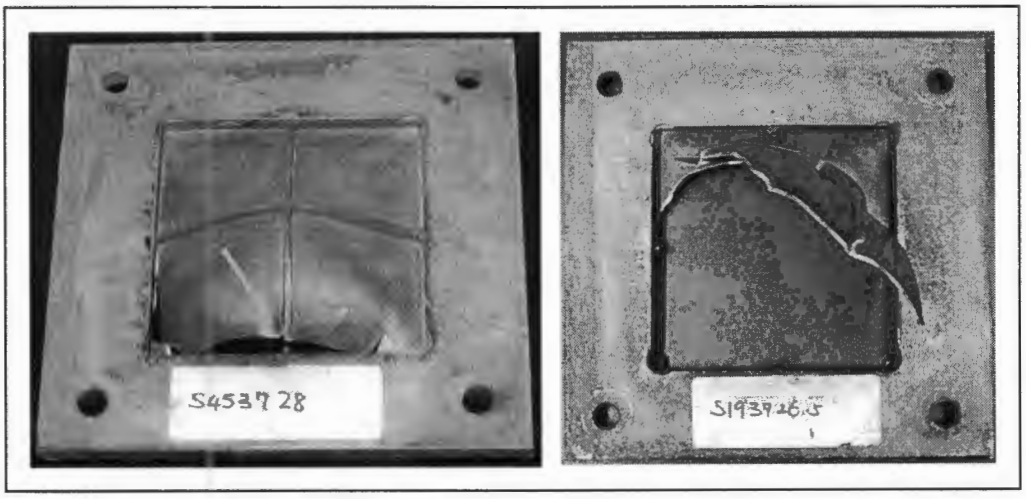

Figure 4.26 : Tearing of cross stiffened square plates (green arrow points out "pulling-in") From left to right : stiffener size 3x7 at impulse 37.6Ns; stiffener size 3x7 at impulse 45.8Ns

Furthermore, no sign of tearing was observed along the stiffener even if thinning was observed in the vicinity of the stiffener. In all cases of tearing the plates tore across the stiffener at the boundary as seen in Figures 4.24-4.26. Also none of the plates had all four sides torn in a specific test. When three sides had torn, the plates tended to bend backwards as seen in Figures 4.24 and 4.26.

Illustrated in Figure 4.27 and 4.28 are the first sign of tearing of a double cross stiffened square plate (S–DCS) and a double stiffened rectangular plate (R–DS) respectively.

Figure 4.27 : Tearing of double cross stiffened square plates with stiffener size 3x7mm at impulse 36Ns

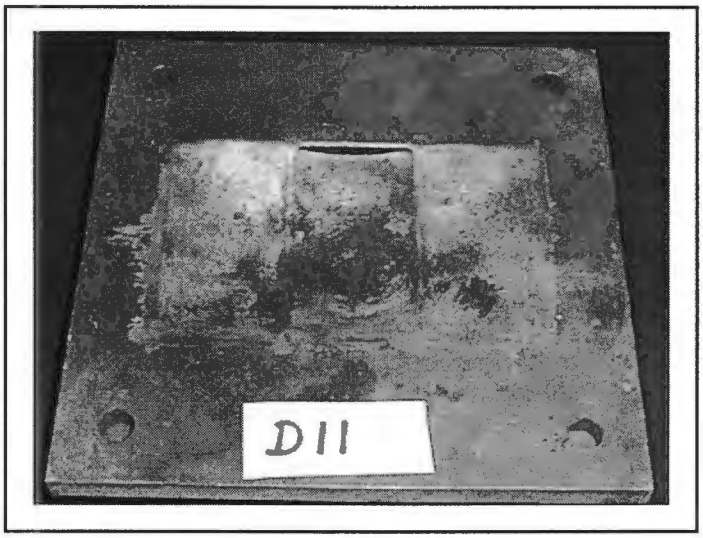

Figure 4.27 : Tearing of double stiffened rectangular plates with stiffener size 3x7mm at impulse 31.8Ns

Moreover, when the tearing occurred little sign of thinning was observed at the point of failure at the boundary to suggest tensile tearing. Figure 4.29 below shows a close-up of boundary tearing of a single stiffened square plate.

Figure 4.29 : Boundary tearing of single stiffened square plate with stiffener size 3x3mm at impulse 37.8Ns

5.0 Analysis of Experimental Results

This chapter of the report examines the experimental results from a dimensional parameters perspective in terms of material properties and the plate geometry. In particular, the relationship between the mid-point deflection and impulse is investigated.

The section closes with a discussion of the overall effects of the configuration and size of the stiffeners on the material failure.

5.1 The Relationship between Plate Deflections and Impulse

The results of mid-point deflection versus impulse for the various stiffener configurations and stiffener sizes are shown in Figure 5.1. The graph only shows the failures that fall into the Mode I category. The results show a general trend of increasing permanent deflection with increasing impulse for the same stiffener configurations and sizes. Some data points do, however, differ slightly from the general trend because of the fact that the plate and stiffener dimensions deviate from the nominal values.

Nevertheless, when grouped in terms of the stiffener thickness, the results confirm the generally linear relationship between the mid-point deflection and the impulse. The results are categorised into three groups:

1. single stiffened square plates with stiffener height of less than 5mm and non-stiffened plates.
2. single stiffened square plates with stiffeners height of 7mm and other plates with different configurations of 3mm thick stiffeners.
3. stiffened plates with different configuration of 7mm thick stiffeners.

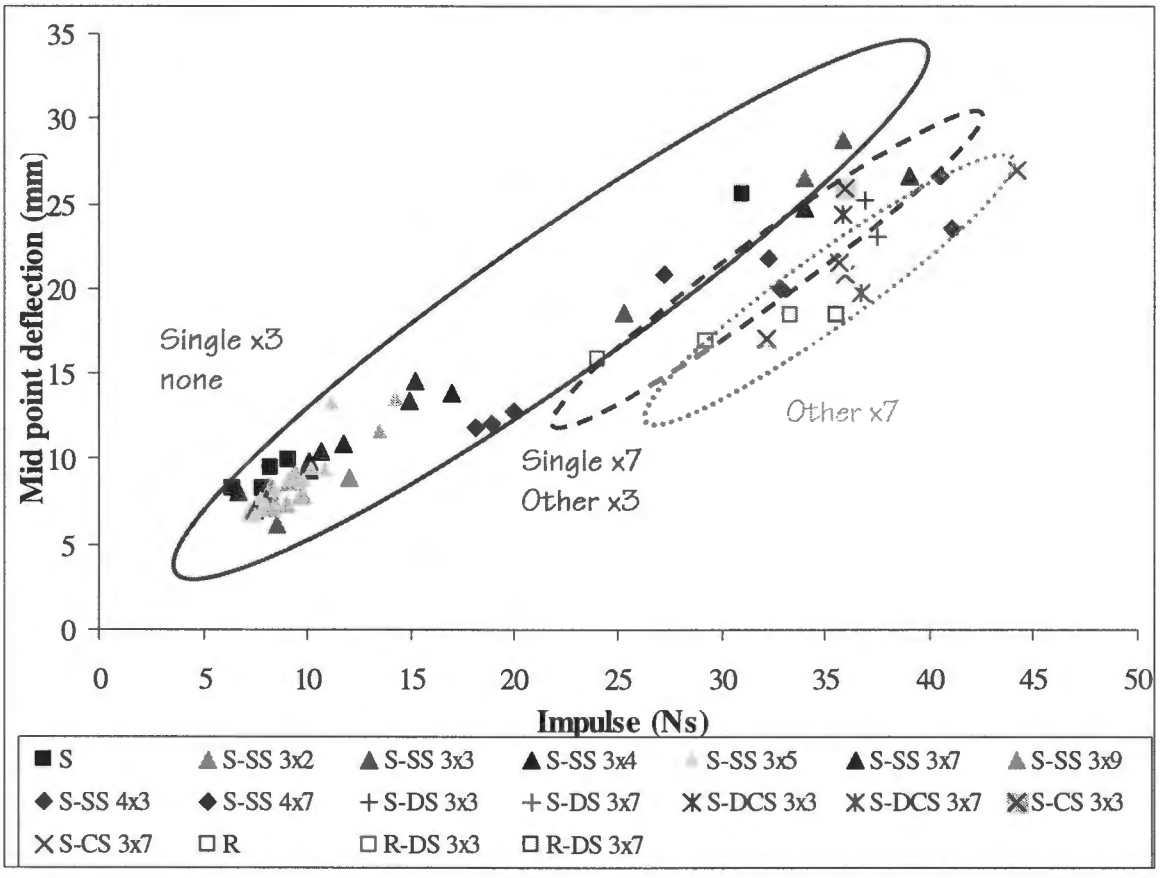

Figure 5.1 Mid-point deflection versus Impulse showing the various stiffener configurations and sizes. (axb refers to the size of the stiffener); S-SS 3x2, S-SS 3x4, S-SS 3x5 and S-SS 3x9 are results obtained by Olson [6]

The graph includes results obtained by Olson[6](see Appendix A). The data obtained by Olson[6] correlates well with those of the present experiment showing repeatability of such experiments; except for the case where the square plates have a single 9mm thick stiffener (S–SS 3x9). The latter could be because of a difference in static yield stress of the material.

A procedure to resolve the problem of differences in thicknesses is to use dimensionless numbers. However, because of the stiffeners, the thickness of the plate is modified by adding the ratio of total cross-sectional area of the stiffeners to the width of the plate and the thickness of the plate as illustrated in equation 5.3. Figure 5.2 shows a schematic sketch of how the plate thickness is modified.

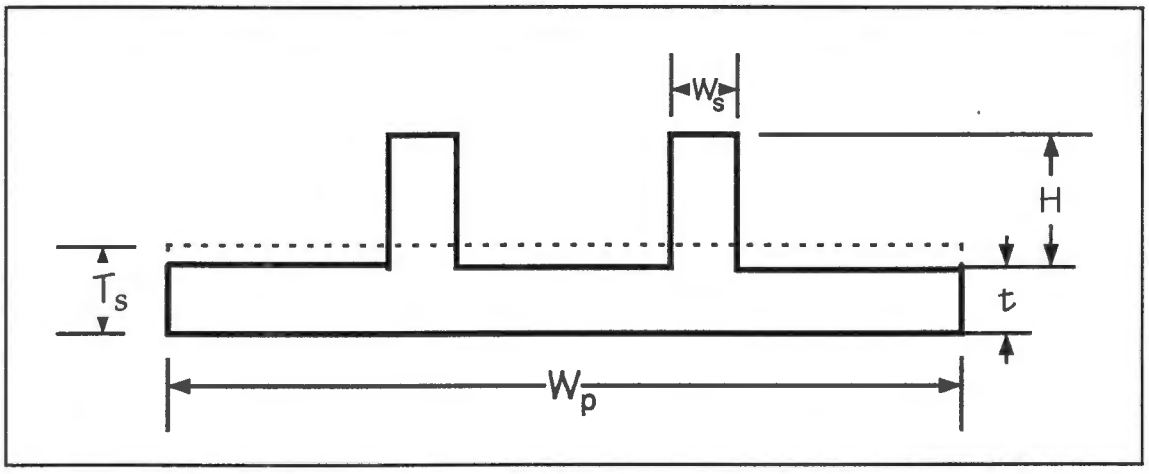

Figure 5.2 : Schematic sketch of modified plate thickness

$$w_p T_s = w_p t + A_s \tag{5.1}$$

where Total cross sectional area of stiffeners; $A_s = \sum w_s H$ (5.2)

thus Modified plate thickness; $T_s = \frac{A_s}{w_p} + t$ (5.3)

where T_s: modified plate thickness; w_p : width of plate;
w_s : width of stiffener; H : Height of stiffener
A_s : Total cross sectional area of stiffeners; t : plate thickness

When this data is plotted in the dimensionless form; that is mid-point deflection modified thickness ratio versus dimensionless impulse; the influence of plate thickness, stiffener size and configuration is no longer as evident.

The deflection modified thickness ratio (δ/t) plotted against ϕ_q, in which a least square analysis performed on the results of 30 untorn plate is shown in Figure 5.3 with a ±1 mid-point deflection thickness ratio repeatability bound.

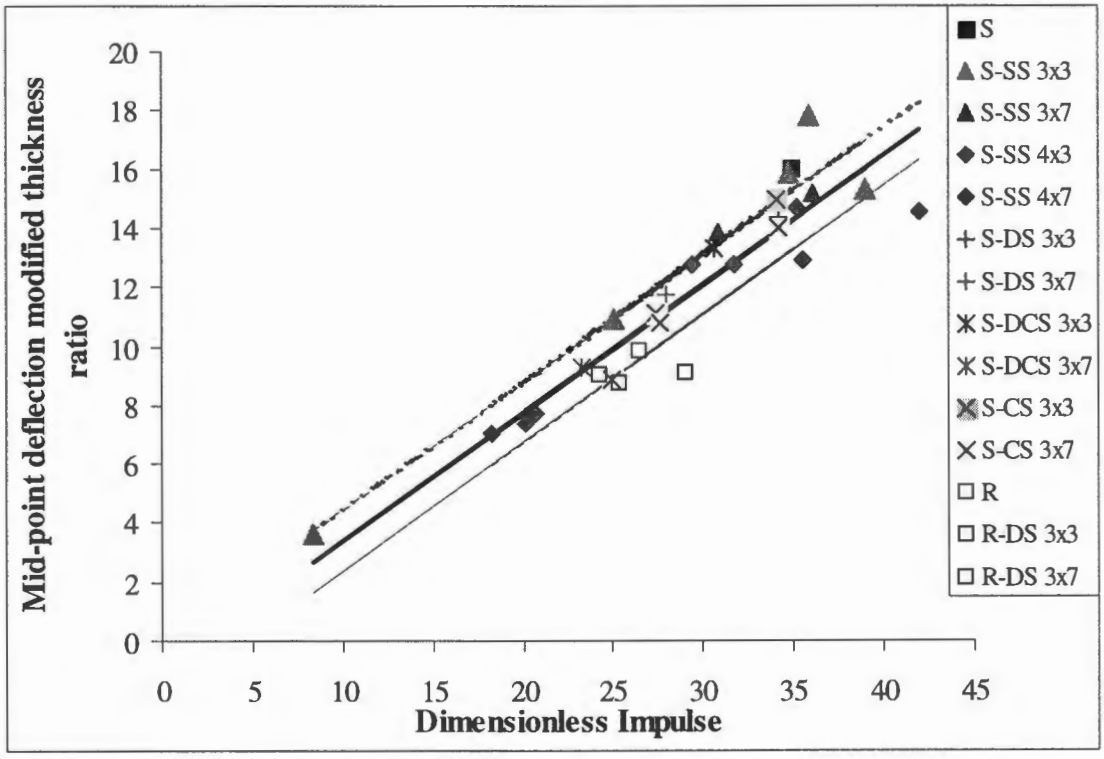

Figure 5.3 : Graph showing Mid-point deflection modified thickness ratio vs dimensionless impulse

The analysis resulted to a relationship of:-

$$\frac{\delta}{t} = 0.435\phi_q - 0.97$$

with a correlation coefficient of 0.857, where the number of data points was 30.

The gradient obtained from analysis is smaller compared to the relationship of $\frac{\delta}{t} = 0.471\phi_q + 0.001$ for non-stiffened square plates obtained by Nurick and Martin[1,2].

5.2 The effect of the size of the stiffener

The permanent displacement profiles along the lines of symmetry of single stiffened square plates (S-SS) exposed to approximately the same impulse (nominal 34Ns) are shown in Figures 5.4 and 5.5. It can be seen that the central maximum displacement decreases as the stiffener height increases from 3 to 7mm, and the overall plate profile changes along the centre line that lies across the stiffener. For the small stiffener (3x3), the maximum displacement clearly occurs over a small area at the stiffener centre thus resulting in a small peak unlike for the larger stiffeners (3x7 and 4x7) where it occurs over a larger area resulting in a relatively flat peak. A similar pattern was observed for other stiffener configurations; see Table 5.1. Further investigations on the effect of the size of the stiffener are carried out in the Finite Element section (chapter 7) using data from the numerical analysis.

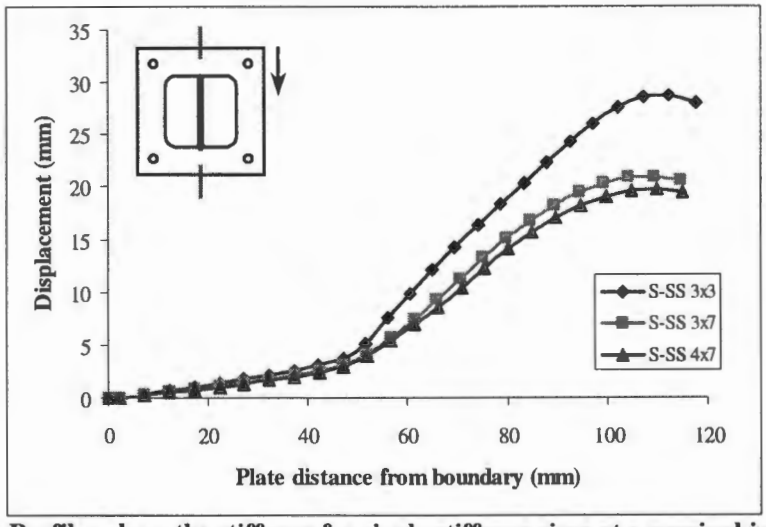

Figure 5.4 : Profiles along the stiffener for single stiffener sizes at a nominal impulse 34Ns

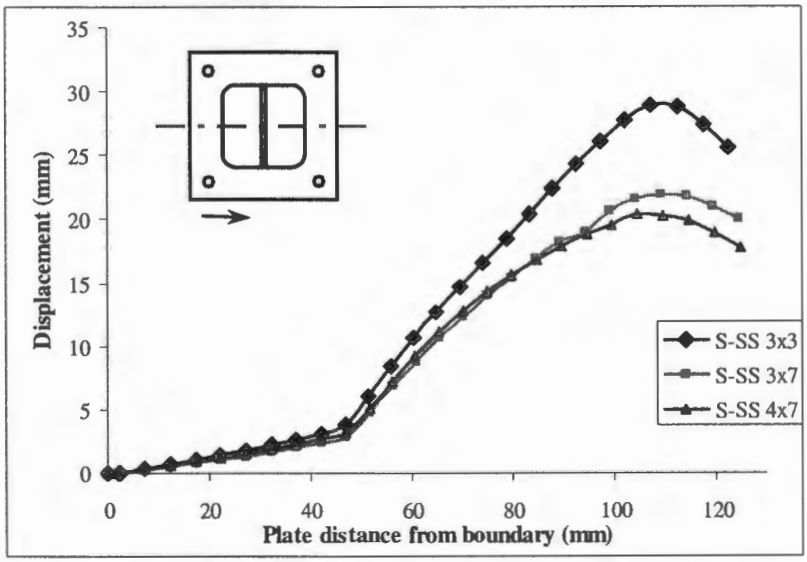

Figure 5.5 : Profiles centreline across the stiffener for single stiffener sizes at a nominal impulse 34Ns

A method to assess the effect of the size of the stiffener is to compare the highest mid-point displacement for the corresponding impulse for the different stiffener configurations and sizes for both square and rectangular plates. Due to experimental scatter a nominal impulse value of 35Ns is considered for all plates. Using a non-stiffened plate as a reference, (square plate and rectangular plate) a percentage difference in impulse and maximum deflection is calculated. The results are tabulated in Table 5.1 and plotted on a bar chart; Figure 5.6. It is observed that despite the fact that there is an increase in impulse (refer to Table 5.1), the maximum deflection of the plate decreases as the stiffener height increases. From Figure 5.6, it is observed that the percentage decrease in deflection increases as the cross sectional area of the stiffener increases.

Plate configuration	X- section area of stiffener (mm^2)	Impulse (Ns)	% impulse difference from square plate	Maximum deflection (mm)	% deflection difference from square plate
S	-	31	-	25.54	-
S-SS 3x3	9	35.8	+9.7	30.1	+17.8
S-SS 3x7	21	34	+19.4	24.7	-3.3
S-SS 4x3	12	32.3	+14.8	21.74	-14.8
S-SS 4x7	28	32.9	+18.4	20	-21.7
S	-	31	-	25.54	
S-DS 3x3	18	36.9	+19	25.2	-1.3
S-DS 3x7	42	37.5	+21	23.01	-9.9
S	-	31	-	25.54	
S–DCS 3x3	27	35.8	+15.5	24.4	-4.5
S-DCS 3x7	63	36.7	+18.4	19.8	-22.7
S	-	31	-	25.54	
S-CS 3x3	18	35.9	+15.8	25.9	+1.4
S-CS3x7	42	35.6	+14.8	21.5	-15.8
R	-	34	-	Torn at boundary	
R-DS 3x3	18	33.4	-1.8	16.45	-
R-DS 3x7	42	35.5	+4.4	18.45	-

Table 5.1 : Comparison of mid-point displacement for different stiffener sizes at a nominal impulse 35 Ns

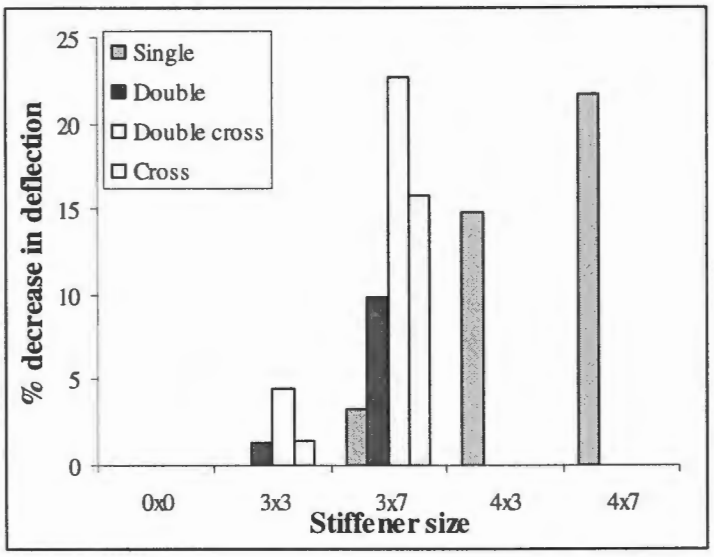

Figure 5.6 : Bar chart of percentage decrease in maximum displacement for different stiffener configurations of different sizes for square plates

5.3 The effect of the configurations of the stiffener

The highest mid-point displacement for the different stiffener configurations of stiffener size 3x7mm is tabulated in Table 5.2 for a nominal impulse of 34.8Ns. Using a non-stiffened square plate as a reference a percentage difference in impulse and maximum deflection is calculated. It is observed that as the plates become stiffer (with the addition of more stiffeners) the maximum displacement decreases. Furthermore, the cross-stiffened square plates offer more resistance to the blast load than the double stiffened square plates even though both stiffener configurations use two stiffeners. From Figure 5.7 it can be noted that percentage decrease in maximum displacement shows a seemingly linear relationship with stiffness of the plate.

Plate configuration	X- section area of stiffener (mm^2)	Impulse (Ns)	% difference from square plate	Maximum displacement (mm)	% difference from square plate
S	-	31	-	25.54	-
S-SS 3x7	21	34	+9.7	24.7	-3.3
S- DS 3x7	42	37.5	+21	23	-7.8
S-CS 3x7	42	35.6	+14.8	20.84	-18.4
S-DCS 3x7	63	36.7	+18.4	19.76	-22.6
R	-	34	+9.7	Torn at boundary	
R-DS 3x7	42	35.5	+14.5	18.45	-27.8

Table 5.2 : Comparison of mid-point displacement for different stiffener configurations at a mean impulse 34.8 Ns

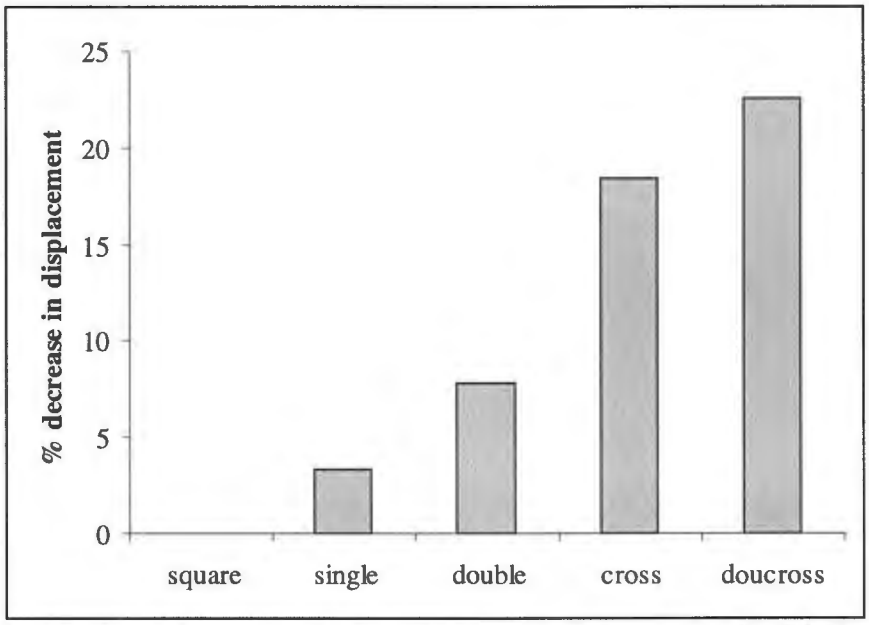

Figure 5.7 : Bar chart of percentage decrease in maximum displacement for different stiffener configurations

Figures 5.8 – 5.11 show the profile of the stiffened plates compared with a non-stiffened plate. Although no quantitative comparison of the stiffened plate and the non-stiffened plate can be made due to the difference in impulse, an assessment of how the stiffened plates deform relative to the non-stiffened plate can be made.

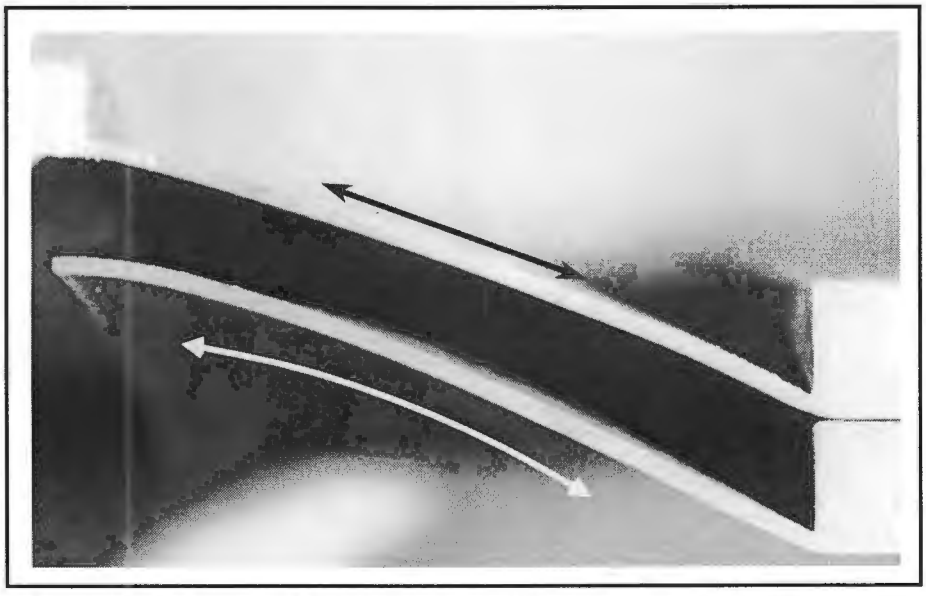

Figure 5.8 : Comparison of profile of a square plate at impulse 31Ns (bottom) and a single stiffened square plate with stiffener size 4x7mm at impulse 40Ns (top) (arrows denote curvature).

The shape profile of the square plate (S) shows a greater curvature compared to the single stiffened square plate (S-SS) between the boundary of the plate and the point of maximum displacement.

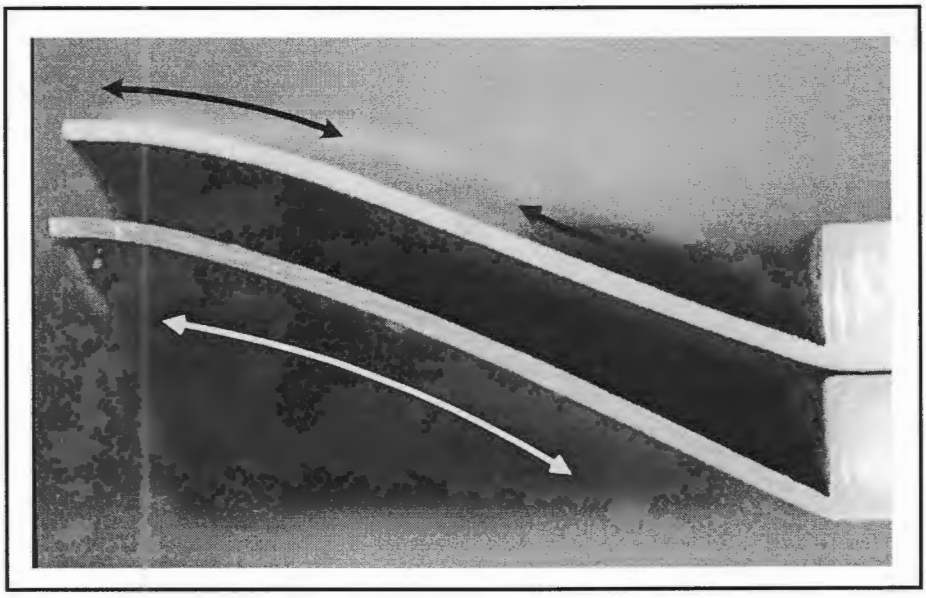

Figure 5.9 : Comparison of profile of a square plate at impulse 31Ns (bottom) and a double stiffened square plate with stiffener size 3x7mm at impulse 37Ns (top) (arrows denote curvature).

The double stiffened square plate (S-DS) shows a change in curvature along its profile; concaving up near the boundary and concaving down near the central area of the plate. However, in the case of the non-stiffened square plate (S) the concavity of the profile does not change.

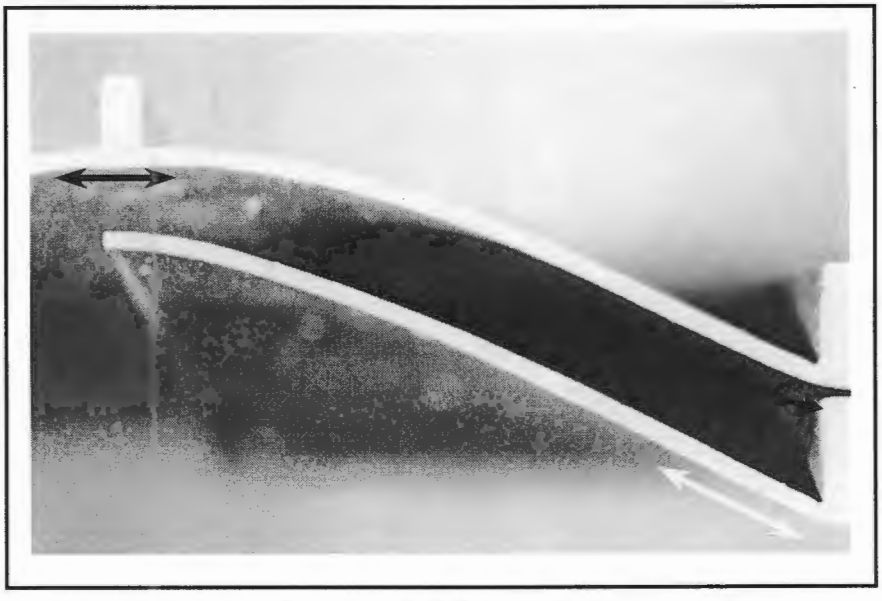

Figure 5.10 : Comparison of profile of a square plate at impulse 31Ns (bottom) and a cross stiffened square plate with stiffener size 3x7mm at impulse 36Ns (top) (arrows denote curvature).

The profile of the square plate (S) appears to rise in a linear manner from the boundary, whereas the cross stiffened (S-CS) plate shows a sharp curvature at the boundary. The cross stiffened plate also exhibits a flat region in the middle of the plate.

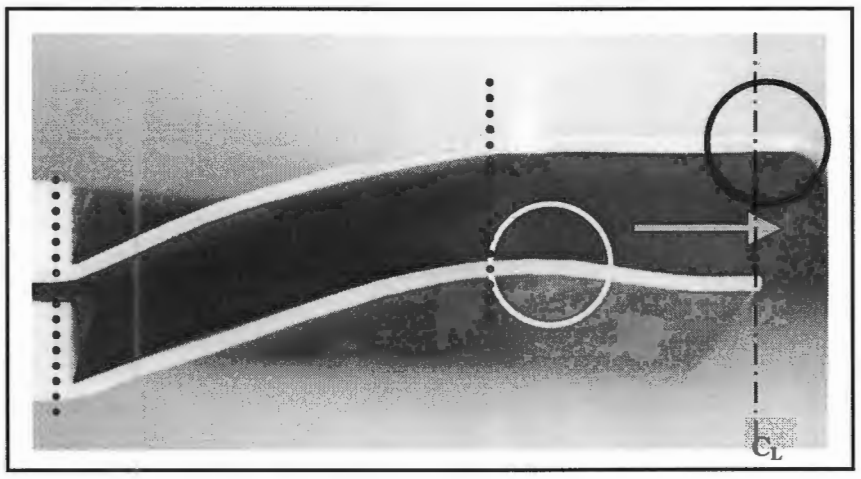

Figure 5.11 : Comparison of profile of a rectangular plate at impulse 24Ns (bottom) and a double stiffened rectangular plate with stiffener size 3x7mm at impulse 35.5Ns (top) (circle denotes area of maximum displacement)

A comparison of the profile of a rectangular plate (R) and double stiffened rectangular plate (R-DS) with stiffener size 3x7 is illustrated in Figure 5.11. The profile of both plates between the boundary and up to the maximum displacement (between the two vertical dotted lines) of the rectangular plate is similar. However, the maximum displacement of the double stiffened rectangular plate (R-DS) occurs at the centre of the plate while the maximum displacement of the rectangular plate (R) occurs on either side of the centreline of the plate.

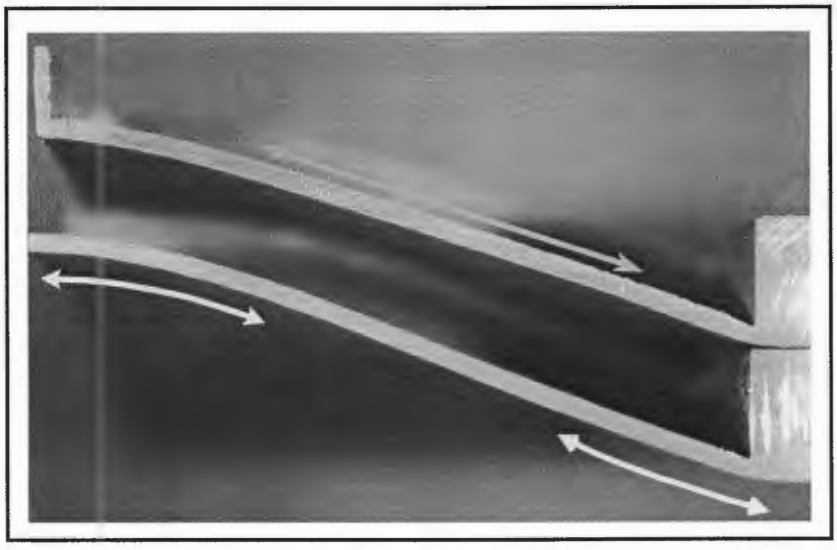

Figure 5.12 : Comparison of profile of a double stiffened square plate with stiffener size 3x7mm at impulse 37.5Ns (bottom) and a double cross stiffened square plate with stiffener size 3x7mm at impulse 36.7Ns (top) (arrows denote curvature).

The profile of the double cross square plate (S-DCS) appears to rise in a linear manner from the boundary concaving down near the maximum displacement. The double stiffened plate (S-DS) shows a change in curvature of its profile, concaving up near the boundary and concaving down near the central area of the plate

5.4 Tearing of the plate

Table 5.3 below shows results of an investigation of the relationship between maximum displacement, impulse and tearing of the stiffened quadrangular plates. It is observed that the maximum mid-point displacement at which tearing occurs for the double cross stiffened square plate is less than that for the square plate. Tearing is found to be a function of maximum displacement of the plate irrespective of the stiffener size and stiffener configuration as reported by Olson[5] and Shave[13]. The maximum central displacement associated with these Mode II failures decreases as the stiffener size increases. For plates that have more stiffeners the maximum central displacement deflection at which tearing occurs decreases.

Furthermore, the average length of tear does not show any relationship with either the maximum displacement or the impulse or the stiffener configurations or the stiffener sizes.

Specimen	Plate configuration	Impulse (Ns)	Maximum mid-point displacement (mm)	Average length of tear (mm)
S01	S	43.4	35.46	72.7
A03	S-SS 3x3	37.8	31.9	88.7
C17	S-SS 3x3	39.8	31.64	81.5
K04	S-SS 4x7	41.1	25.62	76.69
M17	S-DS 3x7	42.3	25.52	79.4
S45	S-CS 3x7	37.6	24.88	
T10	S-DCS 3x7	36	21.34	
S51	R	34.8	22.76	64.9
D11	R-DS 3x7	31.8	20.12	

Table 5.3 : Relationship between tearing and maximum mid-point displacement

6.0 Finite Element Formulation

The following chapter outlines the finite element method and data used for the numerical simulation of the mild steel plates.

6.1 Finite Element Analysis Method

The numerical analysis was carried out using ABAQUS; a general-purpose finite element program. In this case, ABAQUS/*Explicit* was used. ABAQUS/Explicit analysis incorporates non-linear geometry, material effects as well as strain rate sensitivity and temperature effects into its models requiring no iterations and tolerances or global tangent stiffness matrix. It is computationally efficient for the analysis of large models with relatively short dynamic response times as with the case with blast loading conditions. It solves the governing equations by using an explicit integration scheme together with the use of diagonal ("lumped") element mass matrices. The explicit integration is carried out with a central difference scheme using the accelerations calculated at time, t; to advance the velocity solution to time, $t+\Delta t/2$ (as opposed to direct-integration available in ABAQUS/Standard); and the displacement solution to time, $t+\Delta t$. Such a numerical integration is however, conditionally stable, with the stability being governed by the time step taken in the integration scheme. In the application of blast loaded plates, high frequency waves are propagated through the specimen. To resolve the high frequency components, the time step in the solution scheme must be smaller than the time it takes for a dilation wave to cover the length of an element. The critical time increment to ensure stability can be represent by the equation 6.1.

$$\Delta t \leq \min\left(L^{el} \sqrt{\frac{\rho}{\lambda + 2\mu}} \right) \tag{6.1}$$

where L^{el} : characteristic element length; ρ : the material density; λ and μ : Lame's material constants

ABAQUS/Explicit is unlike Standard in that convergence is not sought after each time increment, thus the time stepping in the explicit scheme is extremely small to maintain accuracy. For this reason the explicit scheme is ideally suited to short duration and high-speed dynamic events, as is the case with blast loading.

6.2 Geometrical modelling of the Built-in plate

In the finite element model, the object being modelled is discretised into a number of elements. The choice of these elements depends on the type of analysis and the geometry of the body.

6.2.1 Types of Elements used in the Finite Element Model

The ABAQUS element library provides a complete geometric modelling capability. For this reason any combination of elements can be used to make up the model. It is also possible to formulate and implement a user-defined element. However, the elements available in the library were sufficient for this study. From the library the following elements were chosen since they were applicable to the material and geometry being modelled. A number of different models were created, and the various elements used were:-

C3D6 Element

The C3D6 is a 6-noded linear prism, 3-d continuum element. It has reduced integration, hourglass control and three active degrees of freedom; U_x, U_y and U_z; at each of its nodes, namely translation in the X, Y and Z directions.

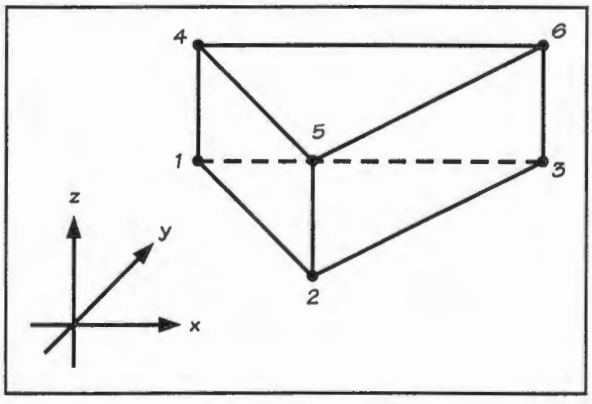

Figure 6.1 : A schematic of a C3D6 element, showing node numbering and co-ordinate system

C3D8R ELEMENT

The C3D8R is a 8-noded linear brick, 3-d continuum element, reduced integration and hourglass control. This element is similar to the C3D6 element with the exception of having 8 nodes and constituting a brick shape.

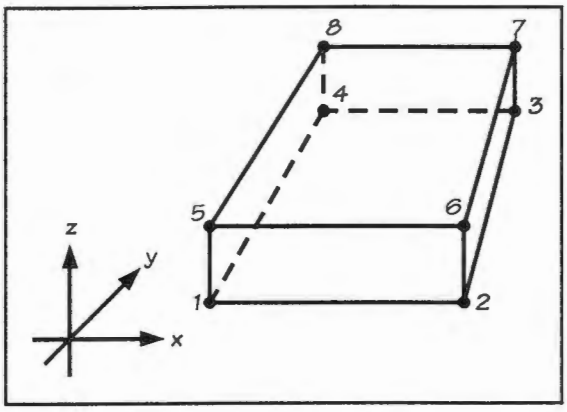

Figure 6.2 : A schematic of a C3D8R element, showing node numbering and co-ordinate system

6.2.2 MESHING THE FINITE ELEMENT MODEL

The number of elements used in a model has a significant effect on the finite element analysis. The solution approaches the exact solution of the governing equations as the number of elements approaches infinity in the finite element formulation. It is therefore essential that a sufficient number of elements be used to ensure that a satisfactory representation of the exact solution is found. However, as the number of elements increases so does the computational expense. The increase in computational time with the increasing number of elements can be attributed to two factors:-

- The number of degrees of freedom needing to be analysed increases.
- The stable time increment for the numerical integration decreases.

An ideal model must, thus, have sufficient elements to accurately describe the model history while minimising that number to reduce computational time. Another restriction on the model is the aspect ratio; the ratio between the longer and shorter dimensions of an element. If the aspect ratio is exceeded by a factor of more than 4 the element is considered excessively distorted and the analysis will be terminated. In the case of expansion in a single direction a small element can afford less expansion than a larger element due to it having a smaller adjacent side.

Applying symmetry conditions to the model reduces both computational time and file sizes of the analysis. This reduced model due to symmetry decreased the computational time by a factor of four while the results are still unaffected. In an attempt to reduce further computational time, the plate was modelled in such a way that the entire thick part of the plate (the boundary) was excluded. The simulation failed to give the appropriate deformed shape and was thus rejected. The failed attempt is shown in Figure 6.3. The failure at the boundary represented by extensively elongated elements was due to the high constraints at the boundary. The plates do not have enough "room" to thin at the edge.

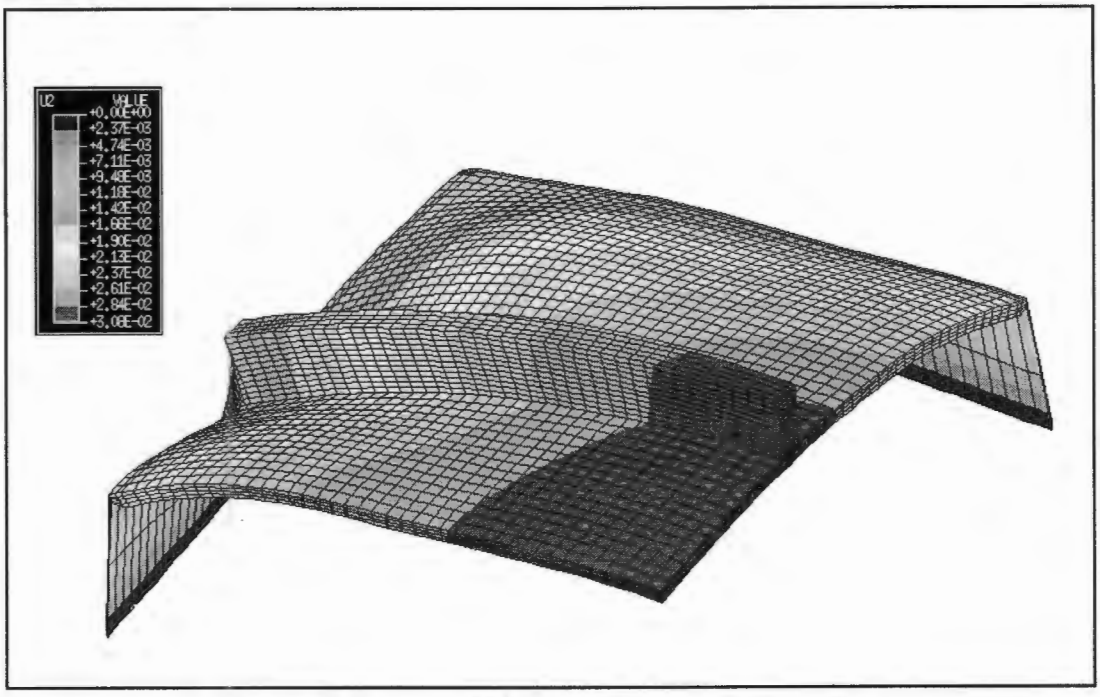

Figure 6.3 : Rejected model due to failure at the boundary

The finite element model was thus extended to include the actual plate geometry with its boundary. Only a quadrant of the built-in plate was modelled with symmetrical boundaries imposed about the y-z and x-y planes as shown in Figure 6.4. Figure 6.4 shows a typical double-crossed stiffened plate with the planes of symmetry.

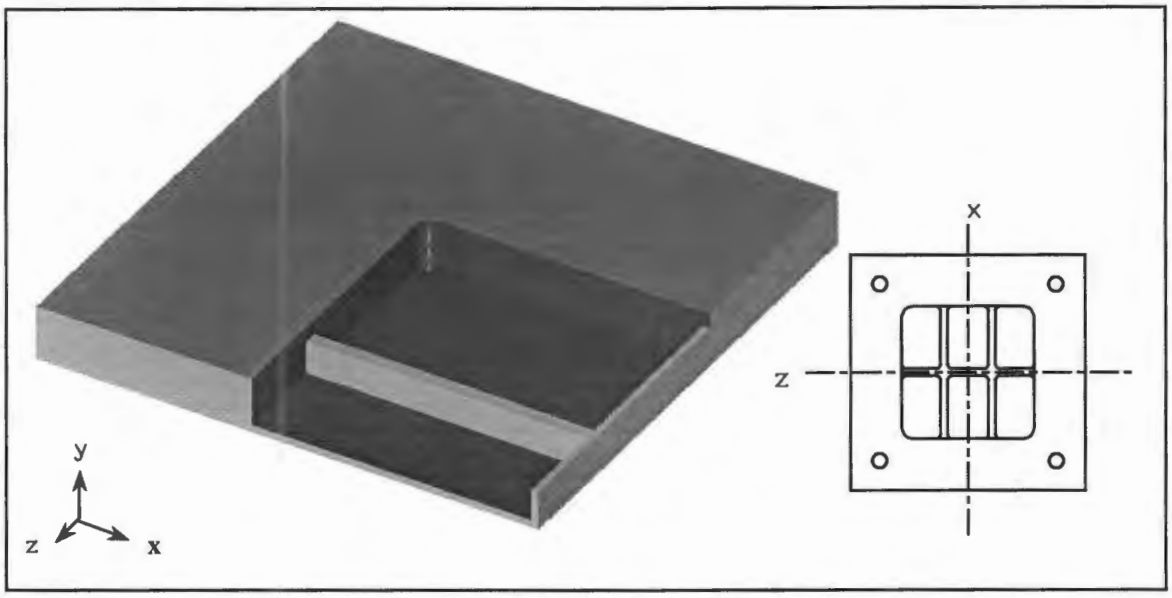

Figure 6.4 : Model of a double cross stiffened built-in square plate with symmetry conditions applied.

6.3 Material Properties of the built-in plate

Mild Steel plates undergoing blast-loading conditions plastically deform at high strain rates causing localised high temperatures due to the strain rate. Material properties at such strain rates and temperatures are still being investigated. ABAQUS/Explicit offers several material failure models. Two models can be used to model high strain rate deformation. They are :

- the Johnson-Cook plasticity model
- the Classical metal plasticity model

6.3.1 JOHNSON-COOK PLASTICITY MODEL

The Johnson-Cook plasticity model is a particular type of Mises plasticity model with analytical forms of the hardening law and rate dependence. It is typically used in adiabatic transient dynamic simulations. Johnson-Cook hardening is a particular type of isotropic hardening where the static yield stress; σ_o, is assumed to be in the form of :-

$$\sigma_o = \left[A + S\left(\bar{\varepsilon}^{pl}\right)^n\right]\left(1-(\hat{\theta})^m\right), \tag{6.2}$$

where $\bar{\varepsilon}^{pl}$: equivalent plastic strain; $\hat{\theta}$: non-dimensional temperature
A, S, n and m : material parameters measured at or below the transition temperature, $\theta_{transition}$.

The non-dimensional temperature is defined as:-

$$\hat{\theta} \equiv \begin{cases} 0 & \text{for} \quad \theta < \theta_{transition} \\ \left(\theta - \theta_{transition}\right)/\left(\theta_{melt} - \theta_{transition}\right) & \text{for} \quad \theta_{transition} \le \theta \le \theta_{melt} \\ 1 & \text{for} \quad \theta > \theta_{melt} \end{cases} \tag{6.3}$$

where θ : current temperature; θ_{melt} : melting temperature
$\theta_{transition}$: transition temperature defined as the one at or below which there is no temperature dependence on the expression of the yield stress.

The Johnson-Cook model is only valid up to the melting temperature. However, the Johnson-Cook model requires extensive information describing the material constants that depend on the transitional temperature that is difficult to find because of the high strain rates and temperatures. For this reason, it was not included in the scope of this study.

6.3.2 CLASSICAL METAL PLASTICITY MODEL

The classical metal plasticity model was adopted for this study. The classical metal plasticity models use standard Mises or Hill yield surfaces associated with plastic flow, which allow for isotropic and anisotropic yield respectively. It involves using stress-strain data from uni-axial tensile tests that are modified for yield hardening, strain rate and temperature dependencies. A strain based shear failure/predictor was also used.

6.3.3 YIELD HARDENING

Most materials that exhibit ductile behaviour yield at stress levels that are orders of magnitude less than the elastic modulus of the material, which implies that Young's modulus describes their elastic region. However, for the plastic region, true stress and logarithmic plastic strain data are required. For an isotropic material; mild steel in the case of this study; the nominal stress-strain data obtained from uni-axial tests is converted to true stress and logarithmic plastic strain as follows

$$\sigma_{true} = \sigma_{nom}\left(1+\varepsilon_{nom}\right) \tag{6.4}$$

$$\varepsilon_{\ln}^{pl} = \ln\left(1+\varepsilon_{nom}\right) - \frac{\sigma_{true}}{E} \tag{6.5}$$

where σ_{true} : true stress; σ_{nom} : nominal stress; ε_{nom} : nominal strain

$\varepsilon_{\ln}^{pl}$: logarithmic plastic strain; E : Young's Modulus

A graph of the true stress and logarithmic plastic strain for mild steel is shown in Figure 6.5

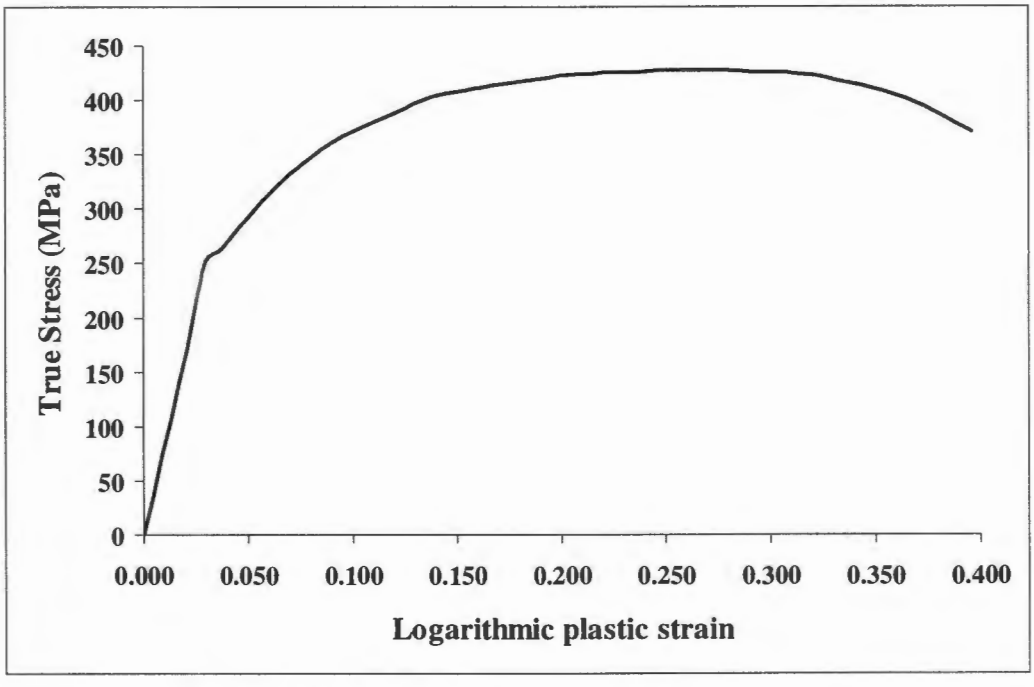

Figure 6.5 : Graph of true stress vs logarithmic strain

6.3.4 Strain Rate Dependence

Mild steel typically exhibits linear elastic and isotropic strain hardening plastic behaviour with a significant dependence on strain rate. The Von Mises yield criterion with isotropic hardening is an appropriate model to describe the elasto-plastic properties of the built-in steel plate. Hardening as a result of the strain rate effect was modelled using the Cowper-Symonds relation shown in equation 6.6.

$$\frac{\sigma_0^1}{\sigma_0} = 1 + \left(\frac{\dot{\varepsilon}}{\dot{\varepsilon}_0} \right)^{1/\eta} \tag{6.6}$$

where σ^1_0 : Dynamic yield stress; σ_0 : Static yield stress; $\dot{\varepsilon}$: Strain rate; $\dot{\varepsilon}_0$ and η are material constants. $\dot{\varepsilon}_0 = 40.1\ s^{-1}$ and $\eta = 5$ are the commonly used and acceptable values for mild steel [26].

6.3.5 Temperature Dependence

Plastic work results in heat generation causing the degradation of material properties. Since ABAQUS/Explicit allows adiabatic stress analysis to be performed where heat is generated by the plastic strain, temperature dependent material properties were incorporated in the numerical analysis. Masui et al.[31] reported the temperature dependence of Young's modulus and yield stress for mild steel, as shown in equations 6.7 and 6.8:

$$\begin{aligned} &E = 207\times10^9 - 58.34\times10^6 \cdot \tau && \text{for} \quad \tau \le 600\ ^0C \\ &E = 3.1\times10^5 \cdot (\tau - 1100)^2 + 97\times10^9 && \text{for} \quad 600^0C < \tau \ge 1100\ ^0C \end{aligned} \tag{6.7}$$

$$\begin{aligned} &\sigma_o = \sigma_{yo} && \text{for} \quad \tau \le 200\ ^0C \\ &\sigma_o = \sigma_{yo} \cdot [1 - 0.00178 \cdot (\tau - 200)] && \text{for} \quad 200^0C < \tau < 700\ ^0C \\ &\sigma_o = \sigma_{yo} \cdot [0.133 - (\tau - 700) \cdot 3.884X10^{-4}] && \text{for} \quad 700^0C \le \tau \le 1000\ ^0C \end{aligned} \tag{6.8}$$

where E : Young's Modulus; τ : material temperature; σ_o : static yield stress; σ_{yo} : static yield stress at the reference temperature of the tensile test.

The temperature rise due to the plastic strain is computed using the specific heat of the metal while the Young's Modulus and true stress-logarithmic plastic strain data are put in tabular form for different temperatures. ABAQUS/Explicit determines the exact Young's Modulus and strain by linearly interpolation of the tabulated values.

Figure 6.6 shows Young's Modulus as a function of temperature. The Young's modulus gradually decreases linearly from a value of 207GPa at room temperature to 175GPa at 600 ^{0}C. Thereafter for higher temperatures, it decays quadratically to 100.1GPa at 1000 ^{0}C.

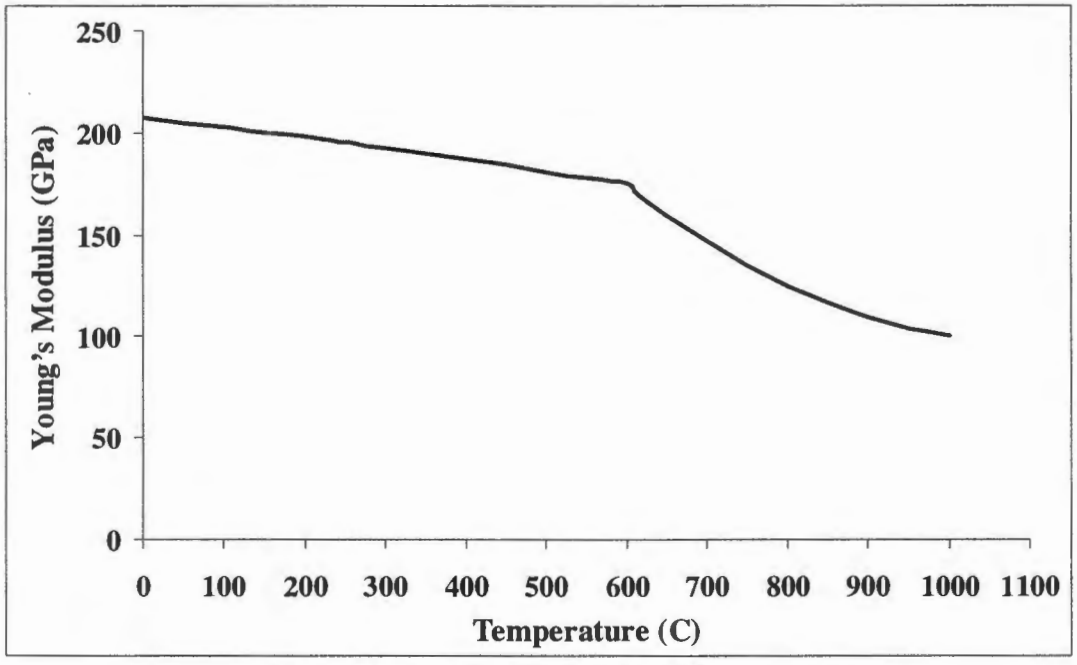

Figure 6.6 : Graph of Young's Modulus vs temperature

The static yield stress as a function of temperature is shown in Figure 6.7. In this case, the yield stress remains constant until the temperature reaches 200^{o}C, at which point it decays at a rate of 449kPa/^{o}C; (gradient of curve) until the temperature reaches 700^{o}C. From 700^{o}C to 1000^{o}C, the yield stress further decreases but at a slower rate of 100449kPa/^{o}C; (gradient of curve).

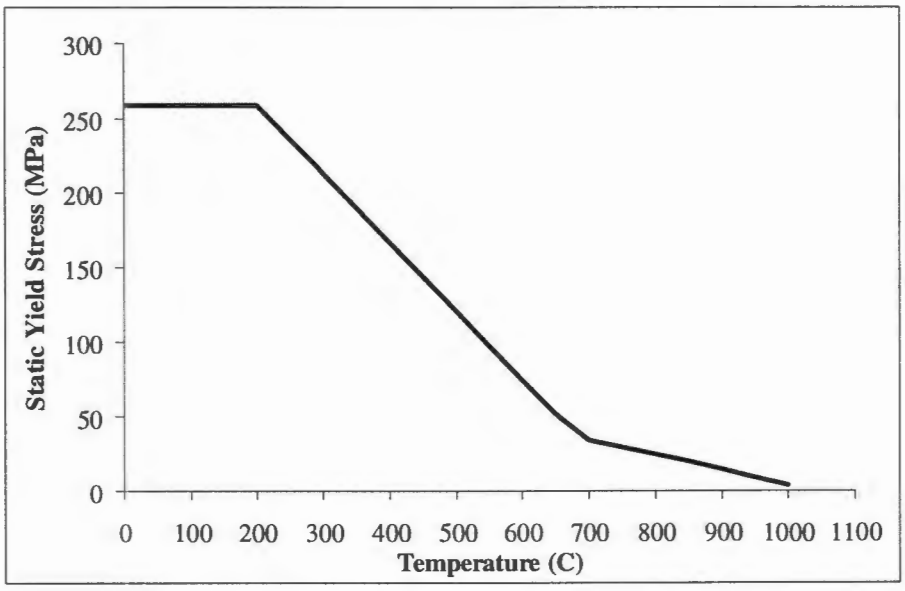

Figure 6.7 : Graph of yield stress vs temperature

A comparison of the temperature effect on the yield stress and Young's modulus is shown in Figure 6.8 The yield stress and Young's Modulus were normalised by dividing the yield stress and Young's Modulus at any temperature by the yield stress and Young's Modulus at 0^0C respectively. The yield stress is more affected than the Young's Modulus.

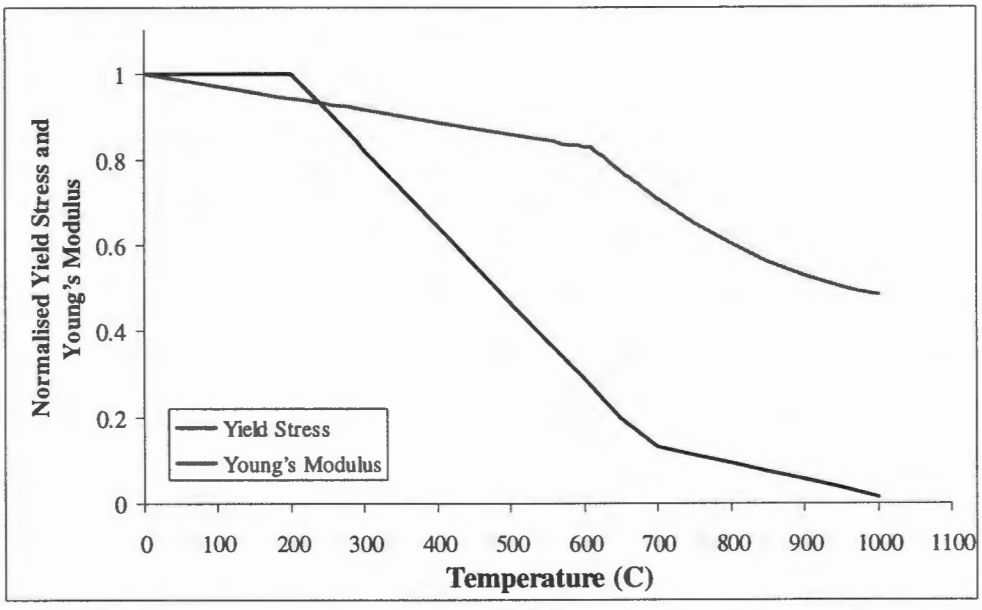

Figure 6.8 : A comparison of the normalised static stress and Young's Modulus as a function of temperature

It was assumed that 90% of the plastic work is converted into heat. Because of the short duration of the blast; (14.5μs) and the subsequent deformation of the plate; (150μs) allowing very little heat to be dissipated from the deformation area it was further assumed that the model is adiabatic. Furthermore it was assumed that the density and the specific heat of the material do not change with temperature.

6.3.6 STRAIN BASED SHEAR FAILURE CRITERIA

A shear failure criterion was also used for the numerical simulations. The failure criterion is based on the value of the equivalent plastic strain at element integration points. Failure is assumed to occur when the damage parameters exceeds 1. The damage parameter, ω, is defined as:-

$$\omega = \sum \left(\frac{\Delta \bar{\varepsilon}^{pl}}{\bar{\varepsilon}_f^{pl}} \right), \tag{6.9}$$

where $\Delta \bar{\varepsilon}^{pl}$: increment of the equivalent plastic strain

$\bar{\varepsilon}_f^{pl}$: strain at failure.

The summation is performed over all increments in the analysis. The shear failure criterion offers two failure choices, including the removal of elements from the mesh as a result of tearing or ripping of the structure.

A summary of the material properties of the test plate is given below.

Young's Modulus	E	200 GPa (at room temperature)
Poisson's Ratio	ν	0.3
Static Yield Stress	σ_o	259MPa
Density	ρ	7860 kg/m^3
Specific heat	c	452 J/kg/K

Table 6.1 Material properties of test plate

6.4 Blast Load modelling

The uniform blast load, generated by the use of plastic explosive in the experiments, was modelled as a pressure applied to the exposed area of the built-in test plates over a given time in the finite element model. The time is fixed by the explosive properties and geometry, but the pressure distribution and area over which it acts are complex for the actual explosion. The modelling of the blast load was, however, simplified by certain assumptions.

The duration of the pressure distribution; τ, was calculated from the burn time of the explosive and the length of the explosive annuli from the centre to the edge and from the edge to the corner (see Figure 6.9).

$$\tau = \frac{a}{V_b} \tag{6.10}$$

where a : length of explosive annuli; V_b : burn speed of the explosive.

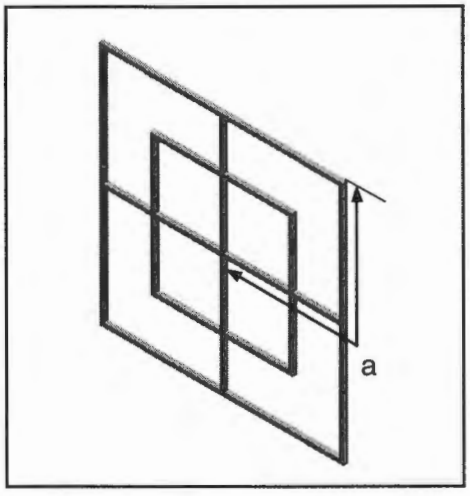

Figure 6.9 : Explosive annuli

In reality, the pressure distribution with time is complex, and consists of both an over-pressure and under-pressure (see section 2). However, the over-pressure is relatively large compared to the under-pressure. The under-pressure and its contribution to the deformation can thus be neglected.

A further assumption is made: the over-pressure is constant for the duration of the burn time.

These assumptions result in a rectangular pressure distribution with time which is shown in Figure 6.10. The magnitude of the pressure applied; P is then calculated from equation 6.11.

$$P = \frac{I_m}{A\tau} \tag{6.11}$$

where I_m : measured impulse; A : plate area exposed to the blast load;
τ : duration of pressure distribution

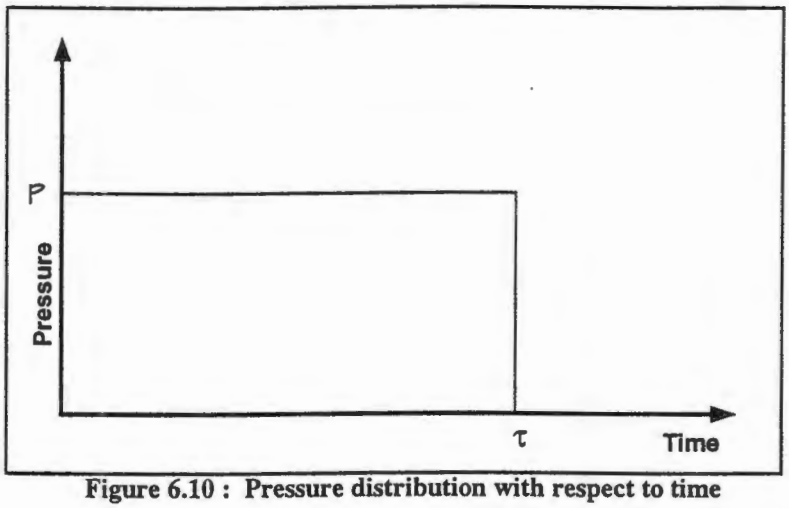

Figure 6.10 : Pressure distribution with respect to time

Typical pressure values for both square and rectangular plates are listed in Table 6.2.

Impulse (Ns)	Pressure (Pa)	
	Square plate	Rectangular plate
27	1.173E+08	1.171E+08
30	1.303E+08	1.301E+08
33	1.434E+08	1.431E+08
35	1.520E+08	1.518E+08
37	1.607E+08	1.605E+08
40	1.738E+08	1.735E+08
42	1.824E+08	1.822E+08
45	1.955E+08	1.952E+08

Table 6.2 : Typical pressure values for both square and rectangular plates

ABAQUS/Explicit employs a multiple step concept in the history data section to accurately define the different conditions to which the model is exposed. Although the maximum deflection of the specimens occurs at 150-200μs, a second unloaded step of 500μs is included in the input file to record the inertial response of the model to the impulsive load.

6.5 Boundary Conditions

In order to simulate the fully built-in boundary, boundary constraints limiting all degrees of freedom were assigned to the thin unloaded sides of the plates; thus allowing no rotational and translational movements.

As outlined in section 6.2.2 the built-in quadrangular plates and the application of the uniform blast load can be considered as symmetrical about the y-z and x-y planes. To reflect the latter, the model needed to have symmetry boundary conditions imposed on it. Thus, if one considers the edge created in the y-z plane, this edge can only move in the z and y directions and always has a constant x co-ordinate during the deformation. Similarly the edge created in the x-y plane can only move in the x and y directions and is fixed in the z direction.

By applying these boundary conditions the model shown in Figure 6.11 is obtained. This is effectively a quadrant of the quadrangular plate and was used for all the analyses. Figure 6.11 shows a double cross stiffened square plate with stiffener size of 3x7mm with the applied symmetrical boundary conditions. Models of other stiffener configurations can be found in Appendix I.

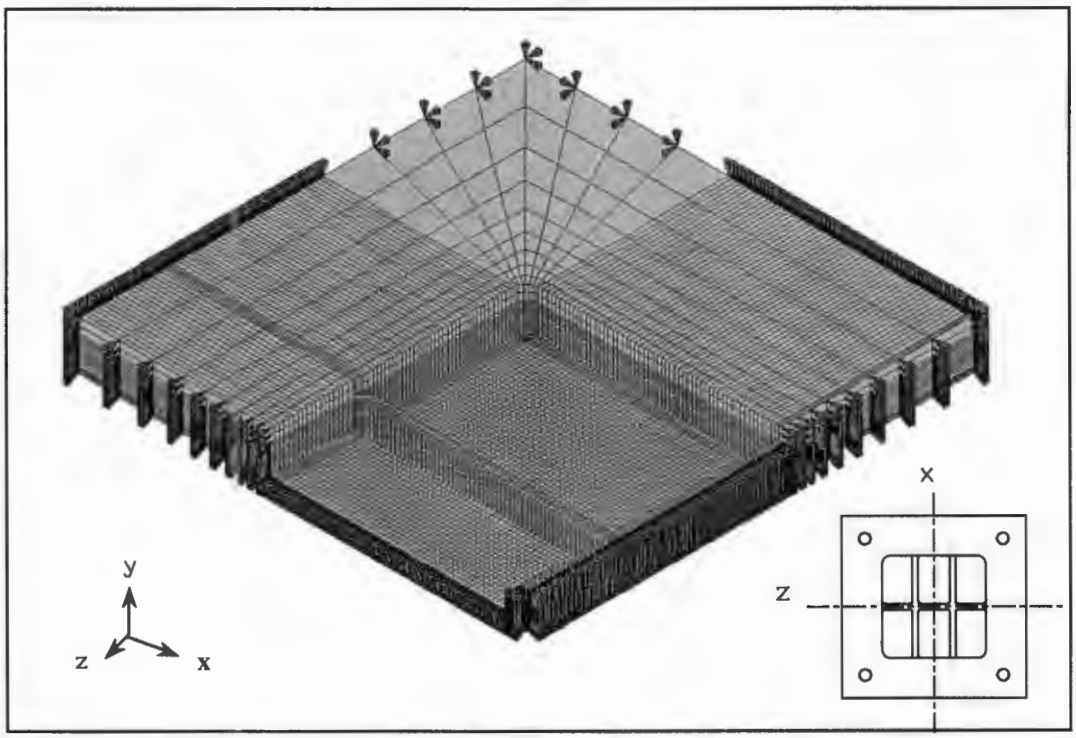

Figure 6.11 : Model of a double cross stiffened plate with boundary conditions

7.0 Simulation Results

The results obtained from the numerical simulations of the mild steel stiffened quadrangular plates undergoing a uniform blast load are presented in this chapter. The results include final mid-point displacement, vertical cross-sections and outline plots of the deformed plates with a comparison of solutions obtained from models that include or exclude temperature dependent material properties. Models for a wide range of impulses are discussed; including both Mode I and tearing failure modes. The ABAQUS input deck for the various models are included in Appendices G and H.

7.1 Mode I Response

Before modelling more complex behaviour of the stiffened quadrangular plates undergoing uniform blast loading conditions; such as failure through rupture; it was imperative to establish the level of correlation between the current model and the experiments for the range of impulses causing only permanent inelastic deformations. The level of correlation was established by comparing the final mid-point displacement, the plate profile and the contour plot obtained from both the numerical analysis and the experimentation. The analysis was carried out for each stiffener configuration and size for a range of impulses from 27Ns to 35Ns for the Mode I response. The models were investigated on only one criterion; material properties that include or exclude temperature dependency.

7.2 Time response of the plate

In this series of experiment, the exact time taken for the plate to reach its final deformed shape was not measured due to the high speed and nature of an explosion. However, numerically it is primordial to ensure that the analysis had continued long enough for the plate to reach equilibrium. Figure 7.1 shows the displacement history for nine points; taken at different intervals along the plate profile from the centre to the boundary. The displacement history plot represents a non-stiffened square plate that underwent an impulsive load of 31Ns.

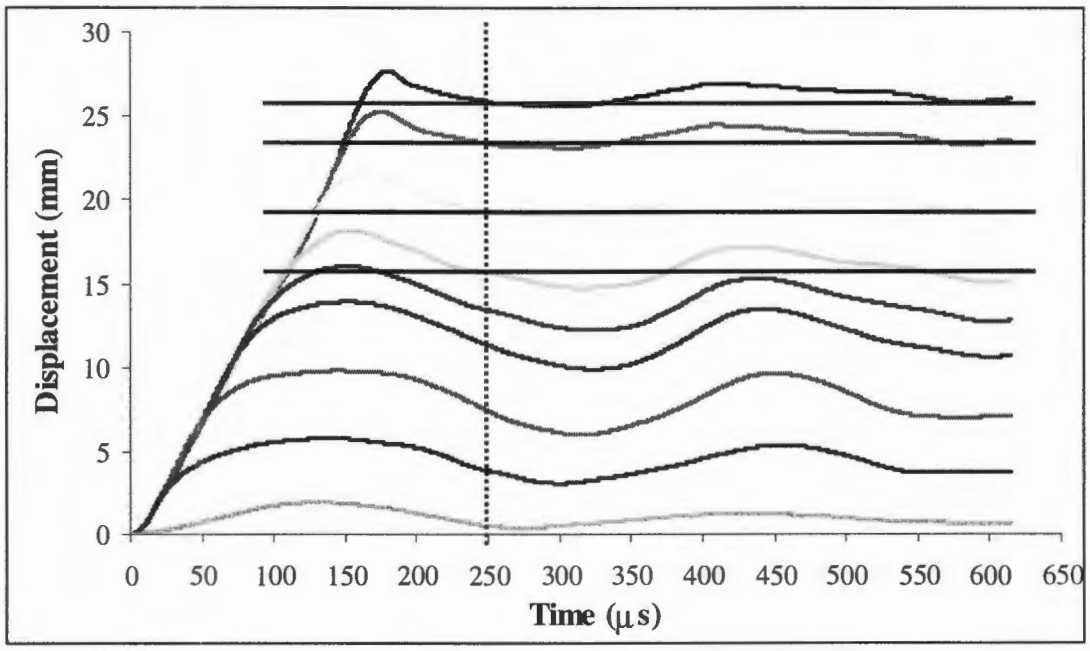

Figure 7.1 : Displacement history at various points along the profile of a non-stiffened square plate From top to bottom represents from centre of the plate to 5mm to the boundary

Figure 7.1 illustrates that all points monitored along the plate profile reach equilibrium at approximately the same time; 250μs (vertical dotted line in Figure 7.1). From the displacement history plot it can be seen that the stiffened plate responded to a large deformation almost linearly with time, reached a maximum and then exhibited a small amount of residual elastic vibration about a mean displacement (denoted by the horizontal lines in Figure 7.1) after approximately 250μs, with the magnitude of the vibration slowly decaying. The equilibrium point for other plates with different configurations and sizes of stiffener would be different to the equilibrium point of the non-stiffened square plate but was assumed to be in the same region as the latter. Thus it would be sufficient to stop the analysis after 515μs.

Table 7.1 tabulates the results of a comparison of mid-point displacement obtained by the model that include temperature dependent material properties and the experimental data. It can be seen that the results show a good correlation with a margin of error of less than 8%.

Type of plate	Stiffener width w (mm)	Stiffener height h (mm)	Impulse (Ns)	Measured Mid Point Displacement (mm)	Predicted Mid Point Displacement (mm)	% Error
S	0	0	31.0	25.54	26	+1.8
S-SS	3	3	34.0	26.53	27.21	+2.6
S-SS	3	3	35.8	30.10	27.99	-7.0
S-SS	4	3	27.2	20.86	19.73	-5.4
S-SS	3	7	34.1	24.71	23.28	-5.8
S-SS	4	7	32.9	19.99	21.03	-5.2
S-DS	3	3	36.9	25.20	27.78	+1.8
S-DS	3	7	37.5	23.01	22.6	-1.8
S-DCS	3	3	35.8	24.35	24.61	+1.1
S-DCS	3	7	36.7	19.76	20.17	+2.1
S-CS	3	3	35.9	25.92	24.79	-4.4
S-CS	3	7	35.6	21.50	19.83	-7.8
R	0	0	24.0	15.83	14.84	-6.3
R-DS	3	7	35.5	18.46	17.13	-7.2

Table 7.1 : Comparison of predicted mid-point displacement with experiments

The plates' responses to a uniform explosive blast are shown in Figures 7.2 to 7.8. The models show the plate response from just after the detonation of the explosive to the final deformed shape.

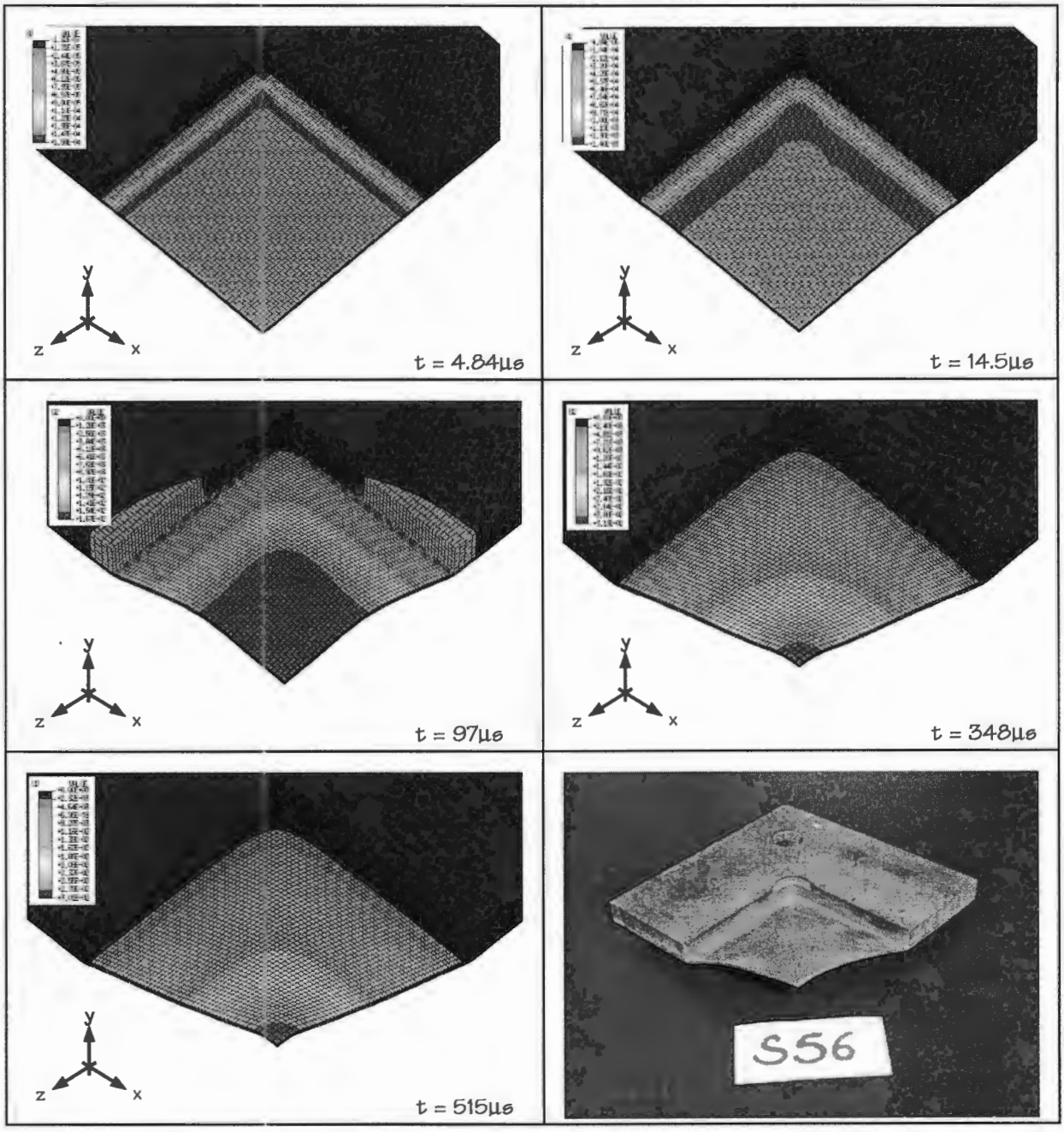

Figure 7.2 Response of a square plate at impulse 35Ns showing displacement in the y-direction

In Figure 7.2 it can be seen that the non-stiffened square plate started deforming at the boundary moving towards the centre of the plate as time increased. After detonation, the plastic hinge was displaced with the highest deflection occurring over a large flat central area of the plate. Thereafter, the plate continued to deform to its final shape with the maximum deflection occurring over a small area in the central part of the plate. Olson et al [14] observed the same transient response. The colour red in the contour plot denotes the highest point of deflection at any time.

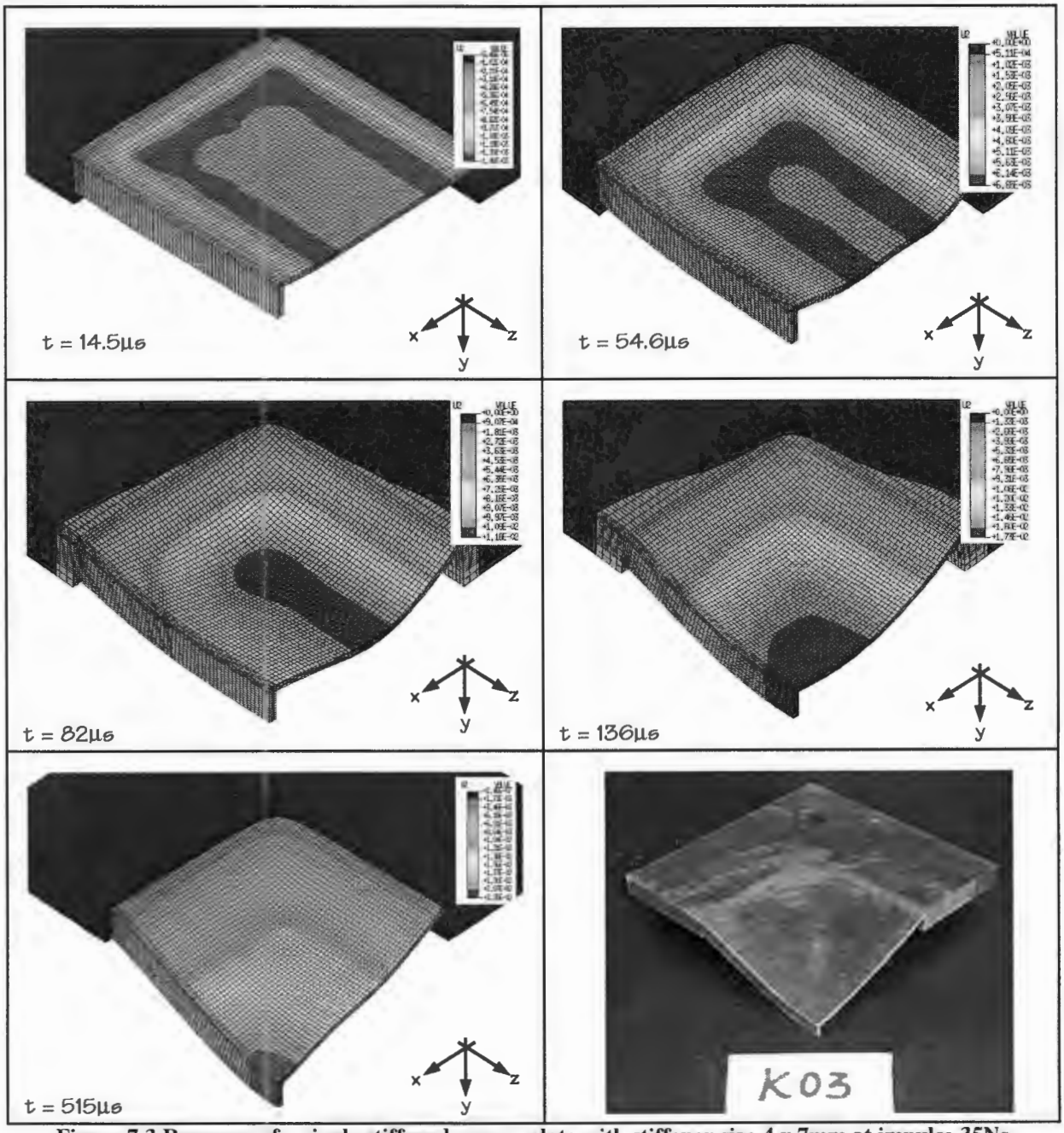

Figure 7.3 Response of a single stiffened square plate with stiffener size 4 x 7mm at impulse 35Ns showing displacement in the y-direction

Figure 7.3 shows the response of a single stiffened square plate with deformation initially occurring between the boundary and the stiffener. The highest point of deflection close after detonation occurred between the stiffener and the boundary. However, as time increased the plate deformed to its final shape with the highest point of deflection moving from the area between the stiffener and the boundary to the central area of the plate. Olson et al[15] observed a similar transient response.

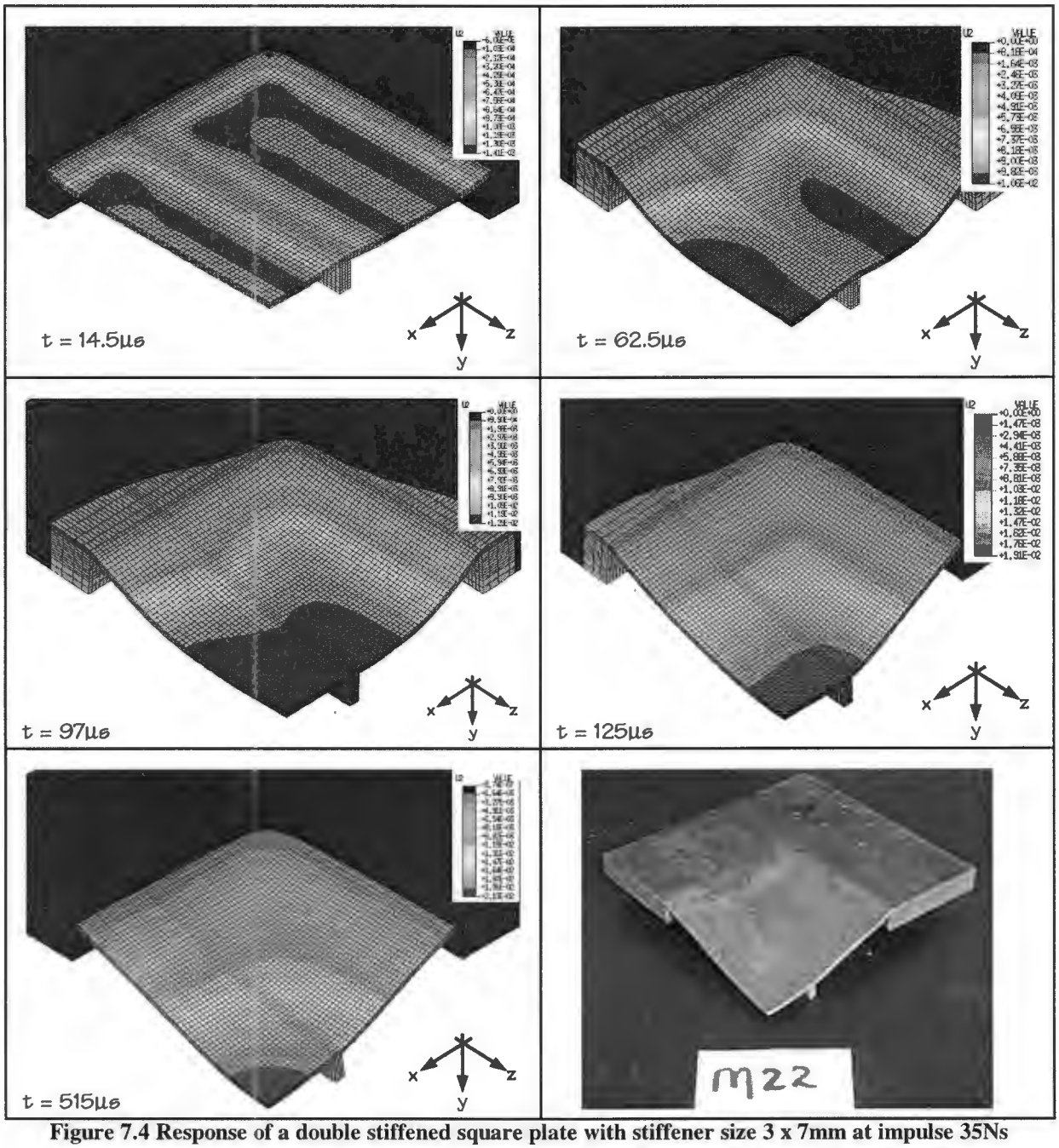

Figure 7.4 Response of a double stiffened square plate with stiffener size 3 x 7mm at impulse 35Ns showing displacement in the y-direction

From Figure 7.4 it can be noted that the double stiffened square plate response was similar to the single stiffened square plate with deformation initially occurring between the boundary and the stiffener. As time increased the plate continued to deform with the plastic hinge gradually moving towards the centre of the plate. After the maximum displacement has reached the central area of the plate the plate response was similar with small variations in displacement due to the residual elastic vibration.

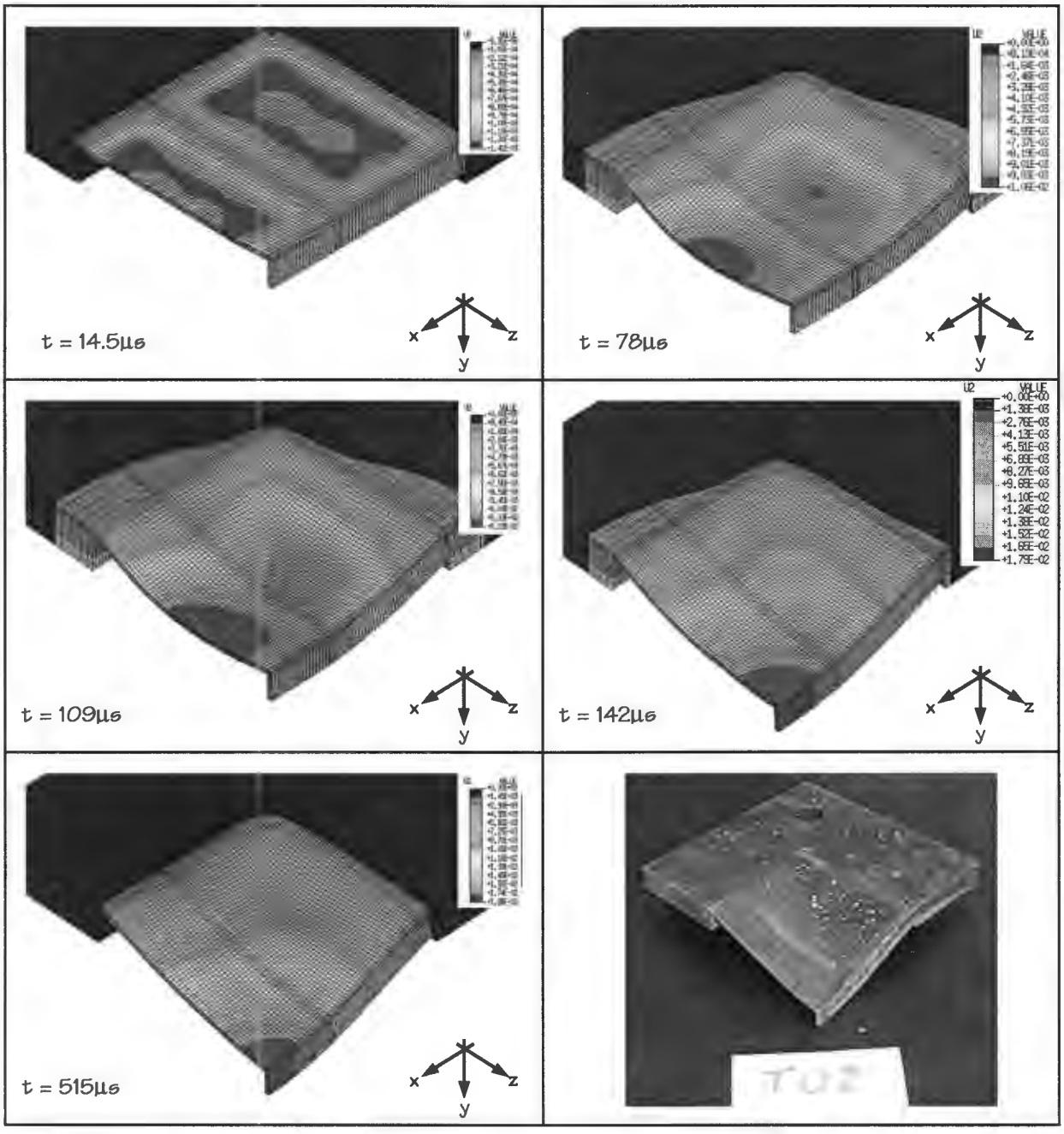

Figure 7.5 Response of a double cross stiffened square plate with stiffener size 3 x 7mm at impulse 35Ns showing displacement in the y-direction

Figure 7.5 shows the response of a double cross stiffened square plate. A similar response pattern to that of a double stiffened square plate was observed. However, the plastic hinges moved from between the two parallel stiffeners and adjacent to the cross stiffener towards the centre of the plate as time increased. The final highest point of deflection occurred over a small area at the centre of the plate.

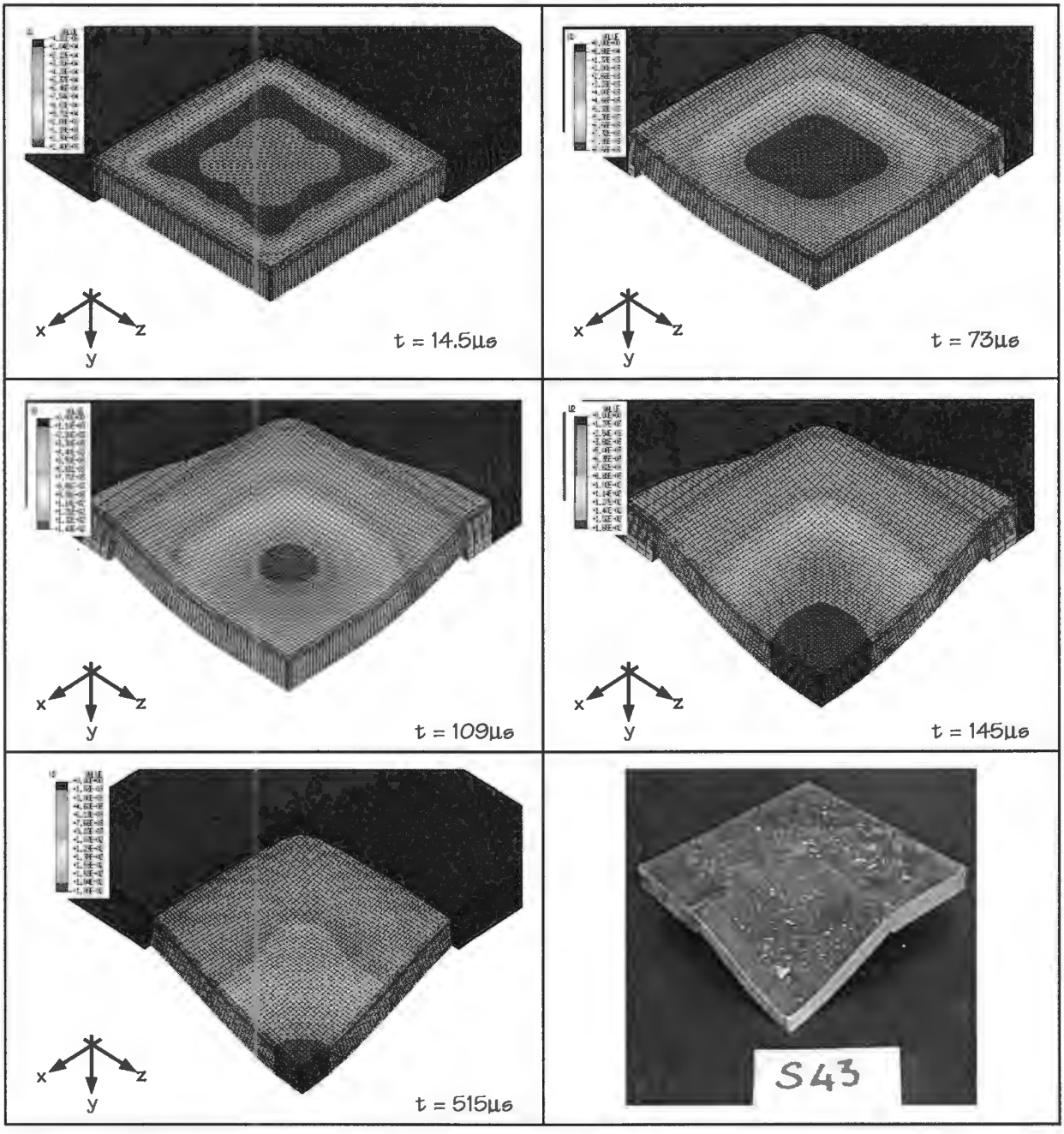

Figure 7.6 Response of a cross stiffened square plate with stiffener size 3 x 7mm at impulse 37Ns showing displacement in the y-direction

The response of a cross stiffened square plate is illustrated in Figure 7.6. The plate started deforming within the area bordered by the boundary and cross stiffeners. The plastic hinges then progressed to the centre of the plate until its equilibrium position.

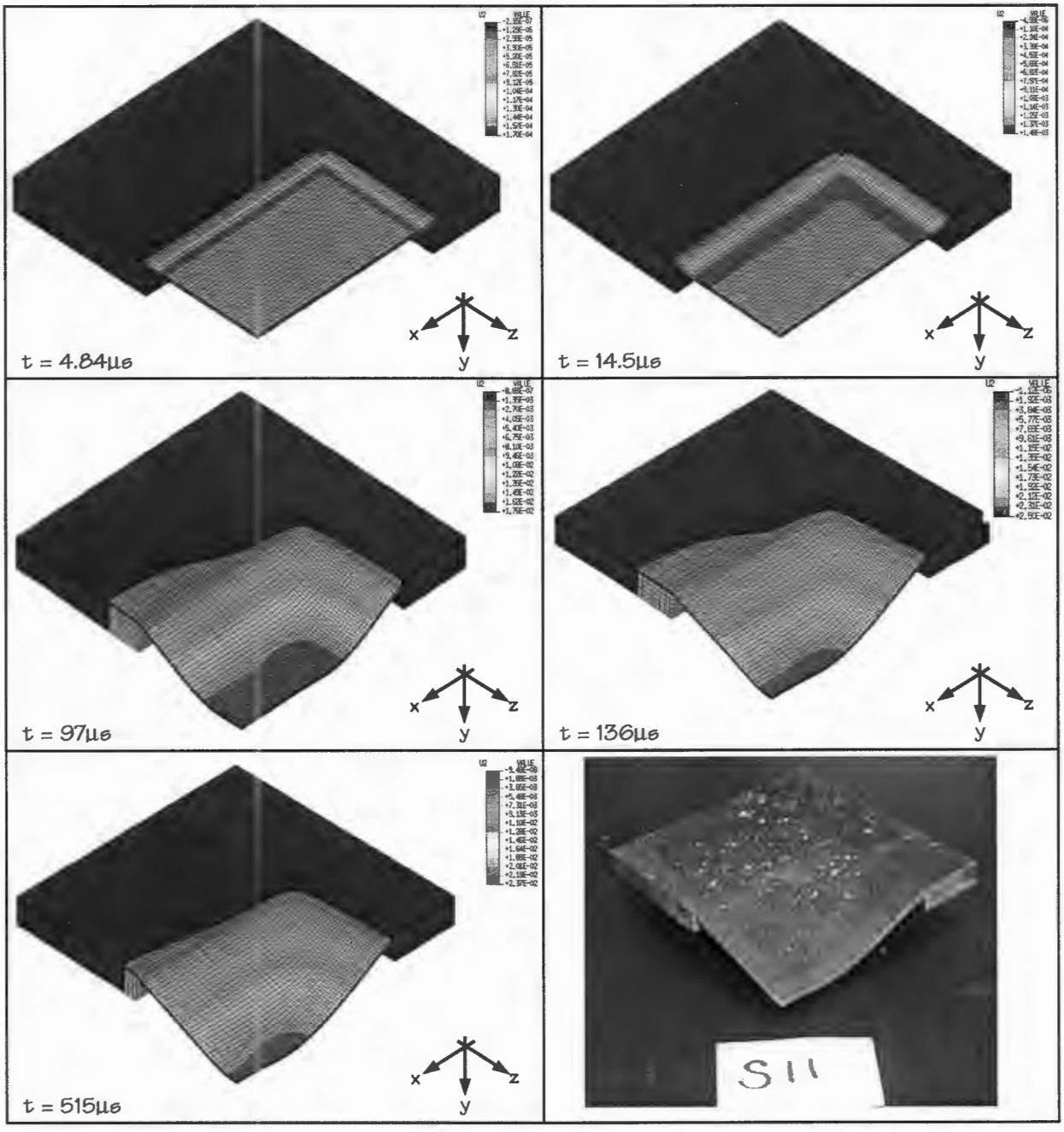

Figure 7.7 Response of a rectangular plate undergoing at impulse 37Ns showing displacement in the y-direction

The response of the non-stiffened rectangular plate (R) as shown in Figure 7.7 is similar to that of a non-stiffened square plate (S) with the only difference being the highest point of displacement. The highest point of displacement of the rectangular plate occurred over a larger area compared to the square plate. Also, the boundary of the longest side of the plate was slightly displaced.

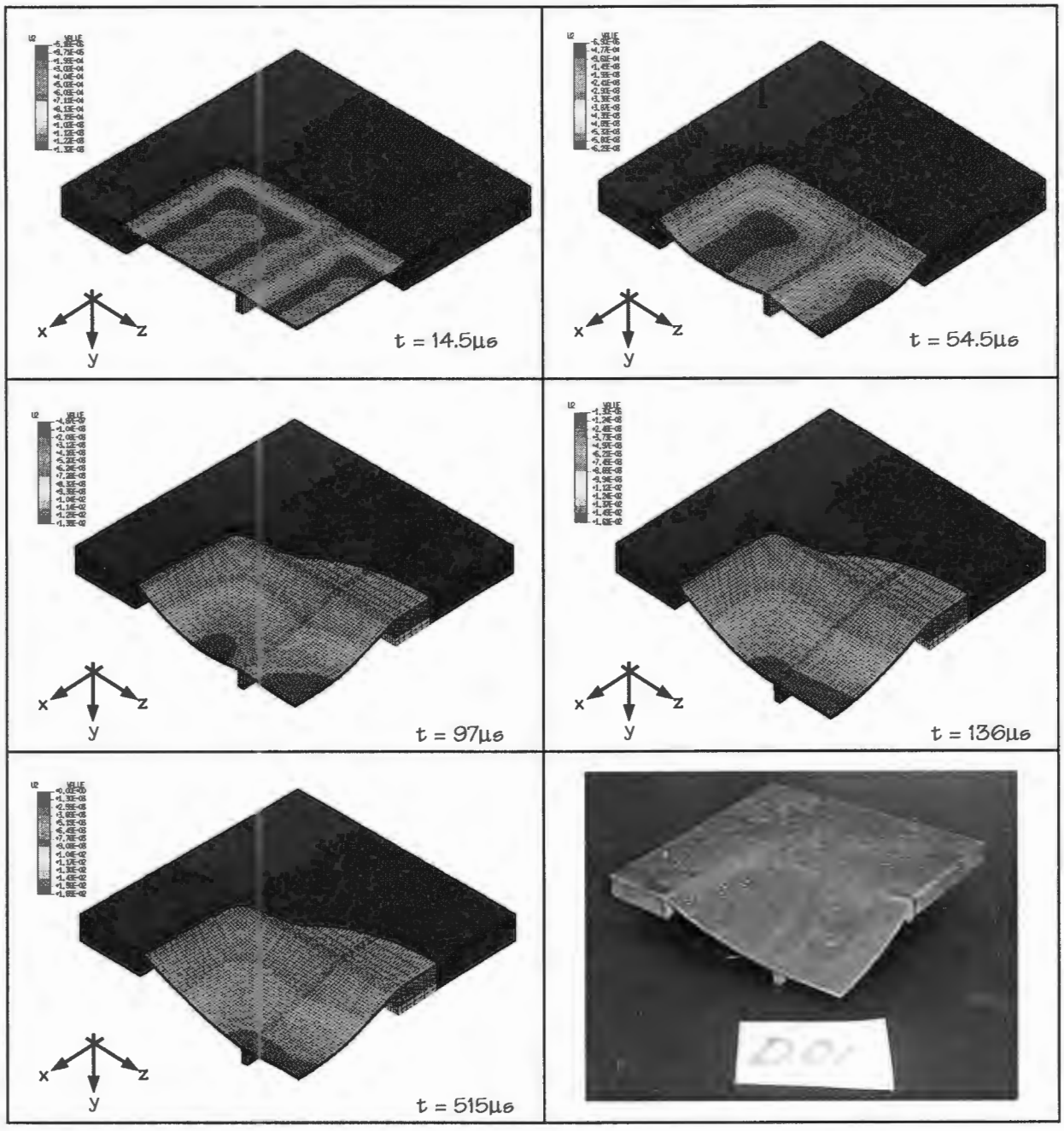

Figure 7.8 Response of a double stiffened rectangular plate with stiffener size 3 x 7mm at impulse 33Ns showing displacement in the y-direction

Figure 7.8 shows the response of a double stiffened rectangular plate (R-DS). The response is analogous to that of the double stiffened square plate (S-DS). However, the longest side of the plate was slightly displaced. After the plastic hinges have reached the central area of the plate (136µs) the plate response remained almost constant until its equilibrium was reached.

The Mode I response of the different stiffened plates shows that the stiffener affects the behaviour of the deformation process close to detonation. The simulation shows that after detonation, all the plates; irrespective of the stiffener configuration and size; behave in a similar way with the maximum displacement occurring between the stiffener and the boundary. As time increases the maximum displacement moves towards the central area of the plate. This indicates that the plate initially responds faster than the stiffener. However, the maximum point of displacement of the plates is highly dependent on the stiffener configuration and size. The numerical analysis shows that the highest displacement of the plate with same stiffener size and impulsive load is less for plates that have a more stiffened structure. This were also observed by Olson et al[15].

7.3 Effect of Temperature dependent material properties

Both torn and un-torn plates were modelled using material properties that include or exclude temperature dependence. Profile and contour plots of the un-torn plates were examined. The effect of the temperature dependence material properties on the torn plates is discussed in section 7.6. While the contour plot gave an overview of the plate deformation the plate profile gave a more accurate plate response to the uniform blast load. The plate profile was measured along the lines of symmetry of the quadrangular plates.

The contour plots predicted by the models; both including and excluding temperature dependent material properties; as shown in Figures 6.9 to 6.15, correspond well to the experimental plot. The contour plots obtained from the experiments show the entire plate area unlike the predictions which show only the quarter symmetry. Both models predict the deformed shapes and hinges correctly.

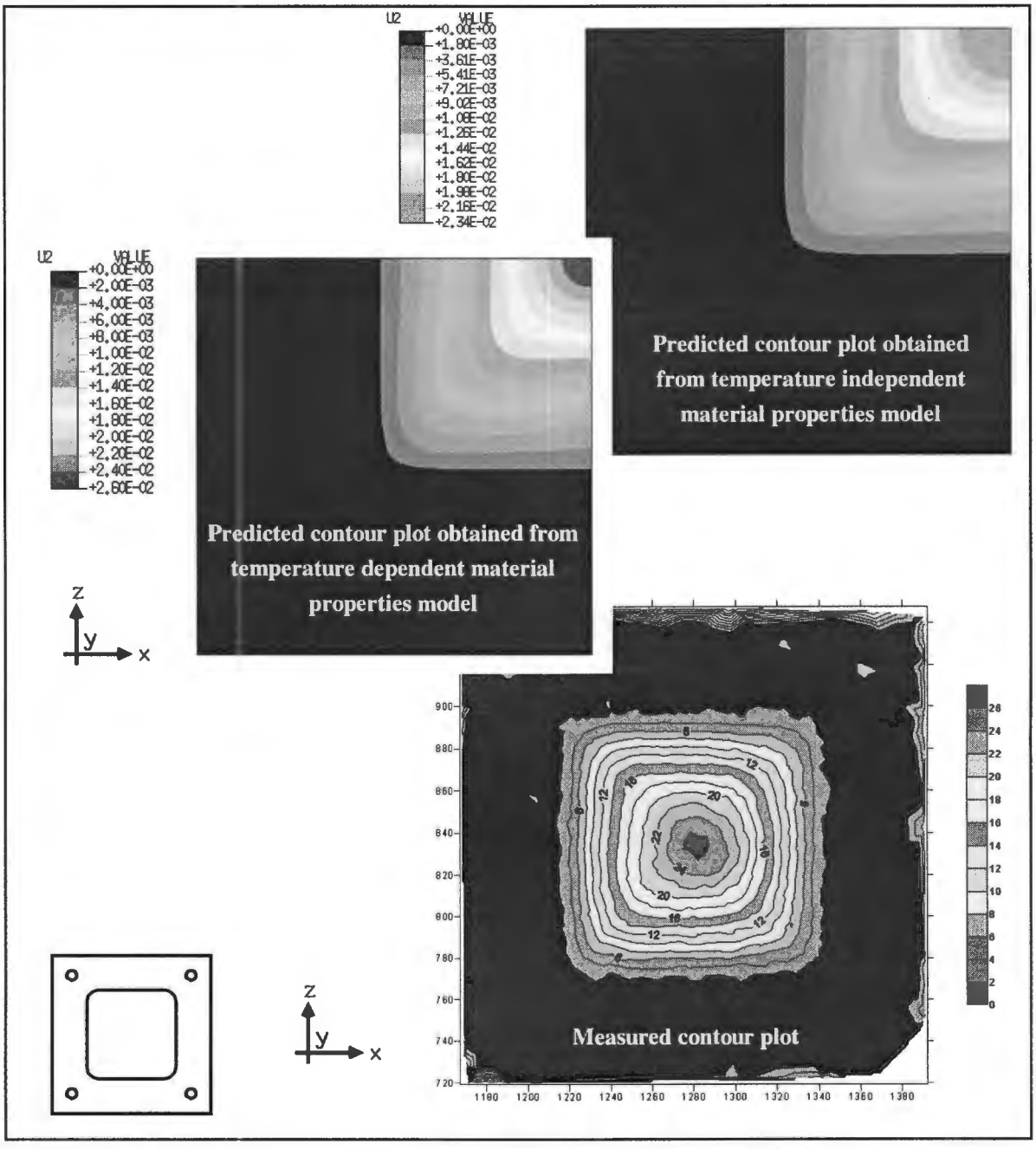

Figure 7.9 Comparison of predicted contour plot of a square plate at impulse 31Ns

From Figure 7.9, it can be seen that the predicted deformed shape corresponds well with the experiment. Both models using material properties that are temperature dependent and temperature independent show similar results. The model using material properties that include temperature effects shows a higher level of displacement. The data obtained from the model that uses material properties that include temperature dependency shows better correlation quantitatively with the experimental data than the model that neglects the temperature effect on material properties.

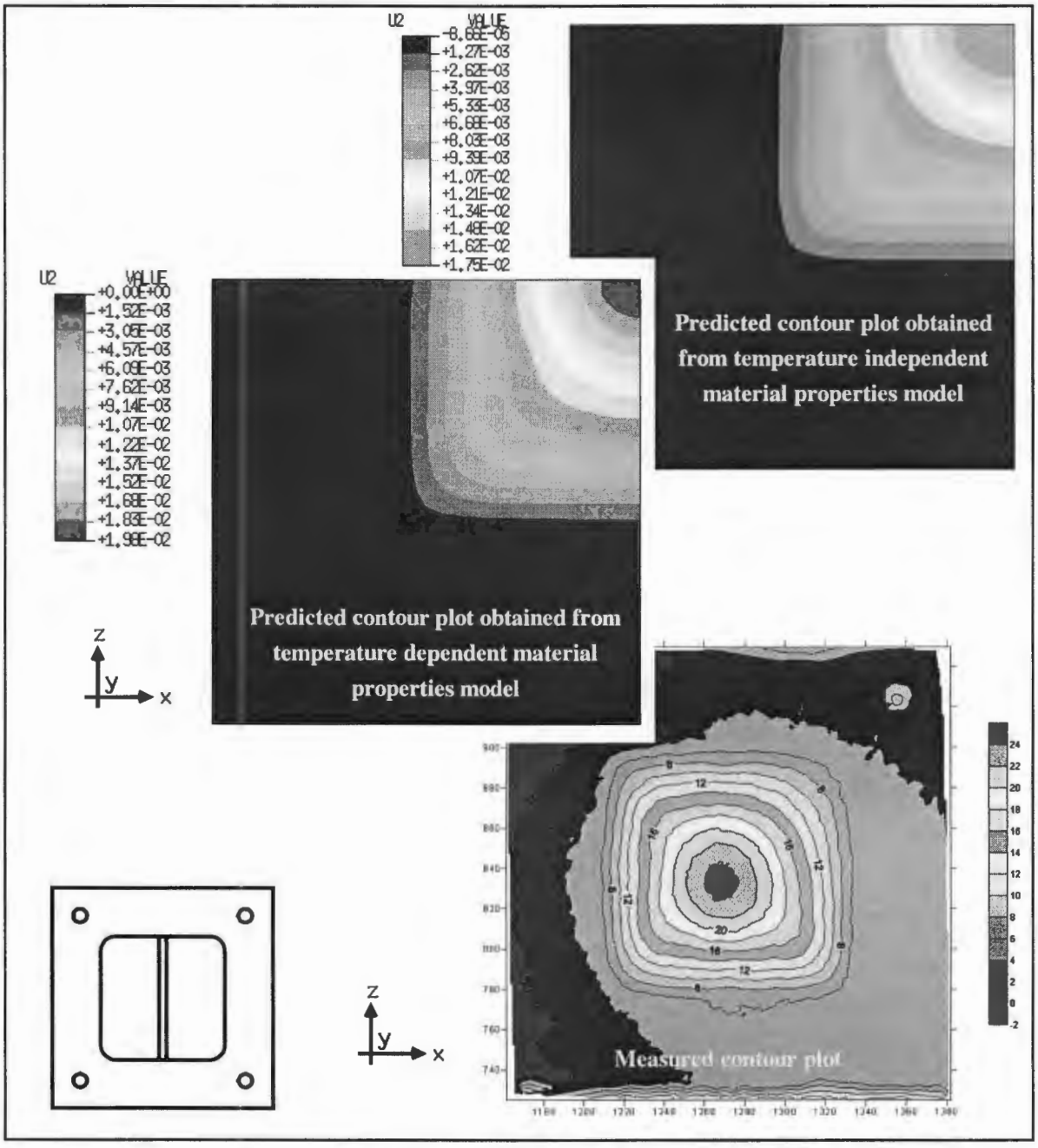

Figure 7.10 Comparison of predicted contour plot of a single stiffened square plate with stiffener size 4x3mm at impulse 27Ns

The predicted contour plots of the single stiffened square plate as shown in Figure 7.10 is compared to that of the deformed square plate. Qualitatively, the predictions correlate well with the experiment. The contour plot from the experiment reveals a relatively large displacement at the boundary due to the lack of adequate support at the boundary.

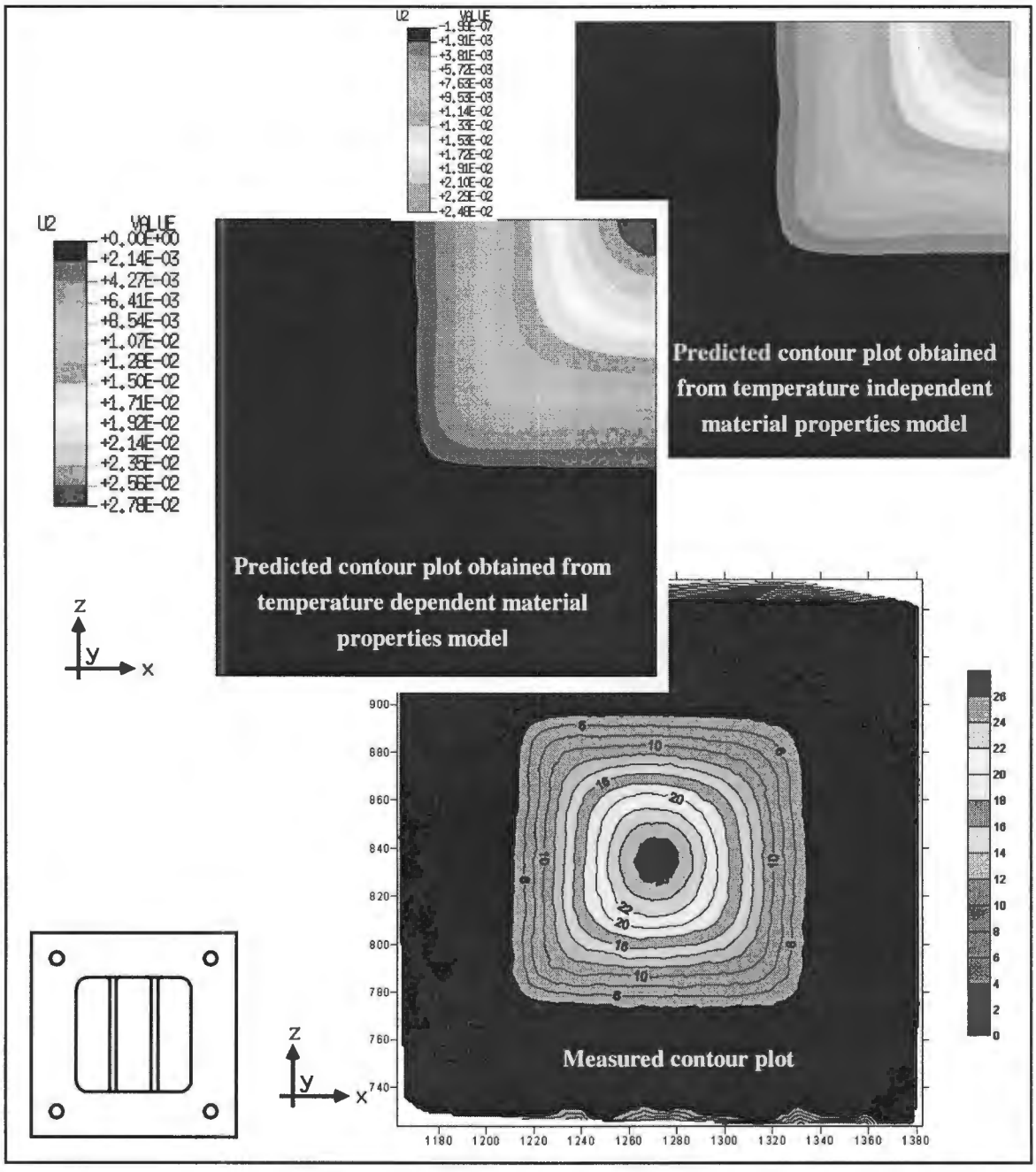

Figure 7.11 Comparison of predicted contour plot of a double stiffened square with stiffener size 3x3mm plate at impulse 37Ns

The contour plot of a deformed double stiffened square plate; shown in Figure 7.11; is compared to that obtained from the numerical analysis. The two models that use material properties that include and exclude temperature dependency predict the deformed shape correctly. The displacement obtained by the model using temperature dependent material properties is closer to the experimental data compared to the model that excludes temperature dependency.

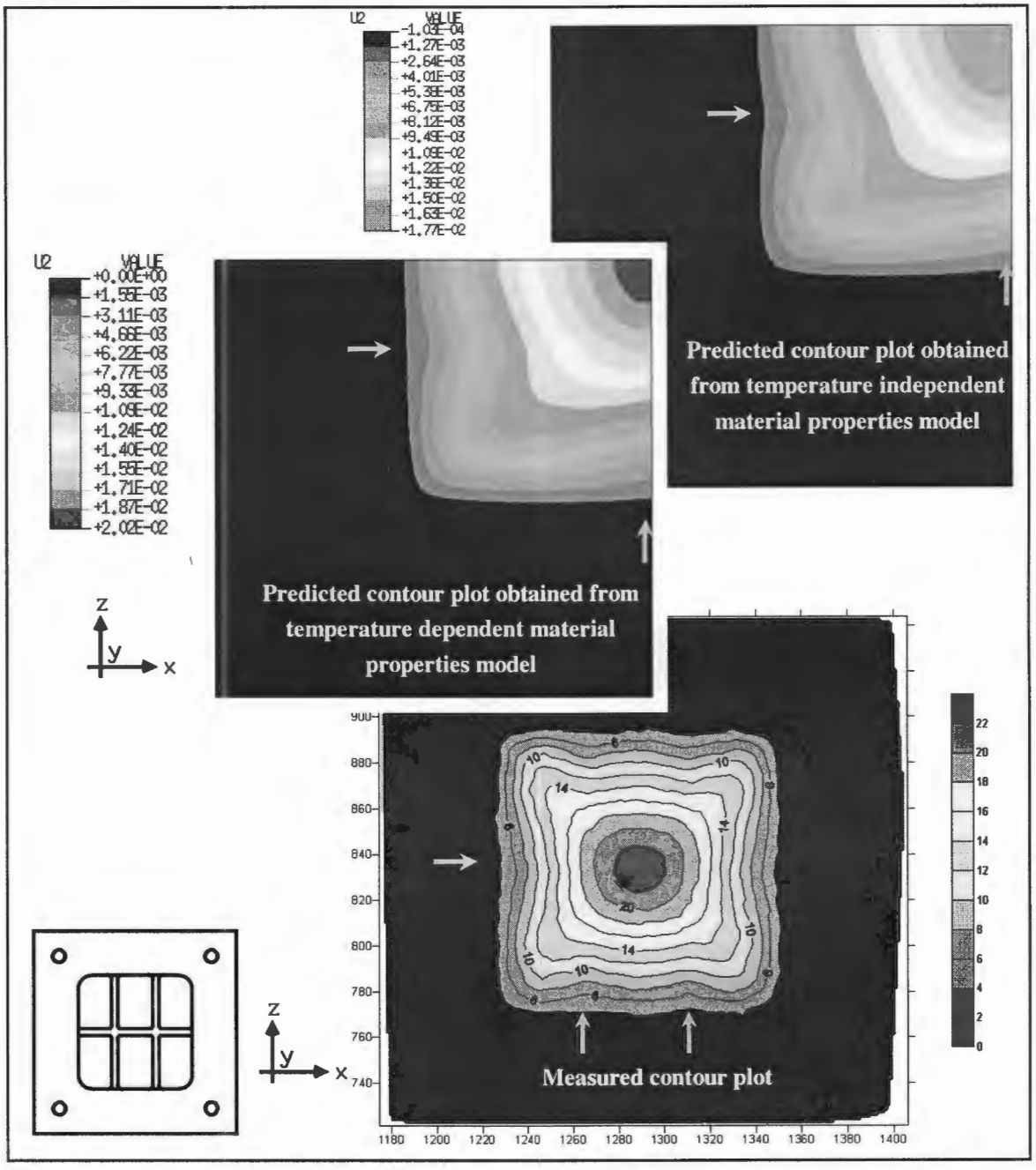

Figure 7.12 Comparison of predicted contour plot of a double cross stiffened square with stiffener size 3x7mm plate at impulse 37Ns (arrows show locations of stiffeners)

The predicted contour plots by two models that use material properties that include and exclude temperature dependency and the contour plot of a deformed double cross stiffened square plate are illustrated in Figure 7.12. The two models predict the deformed shape correctly. However, the model using temperature dependent material properties gives a better correlation than the model using material properties that exclude temperature dependency.

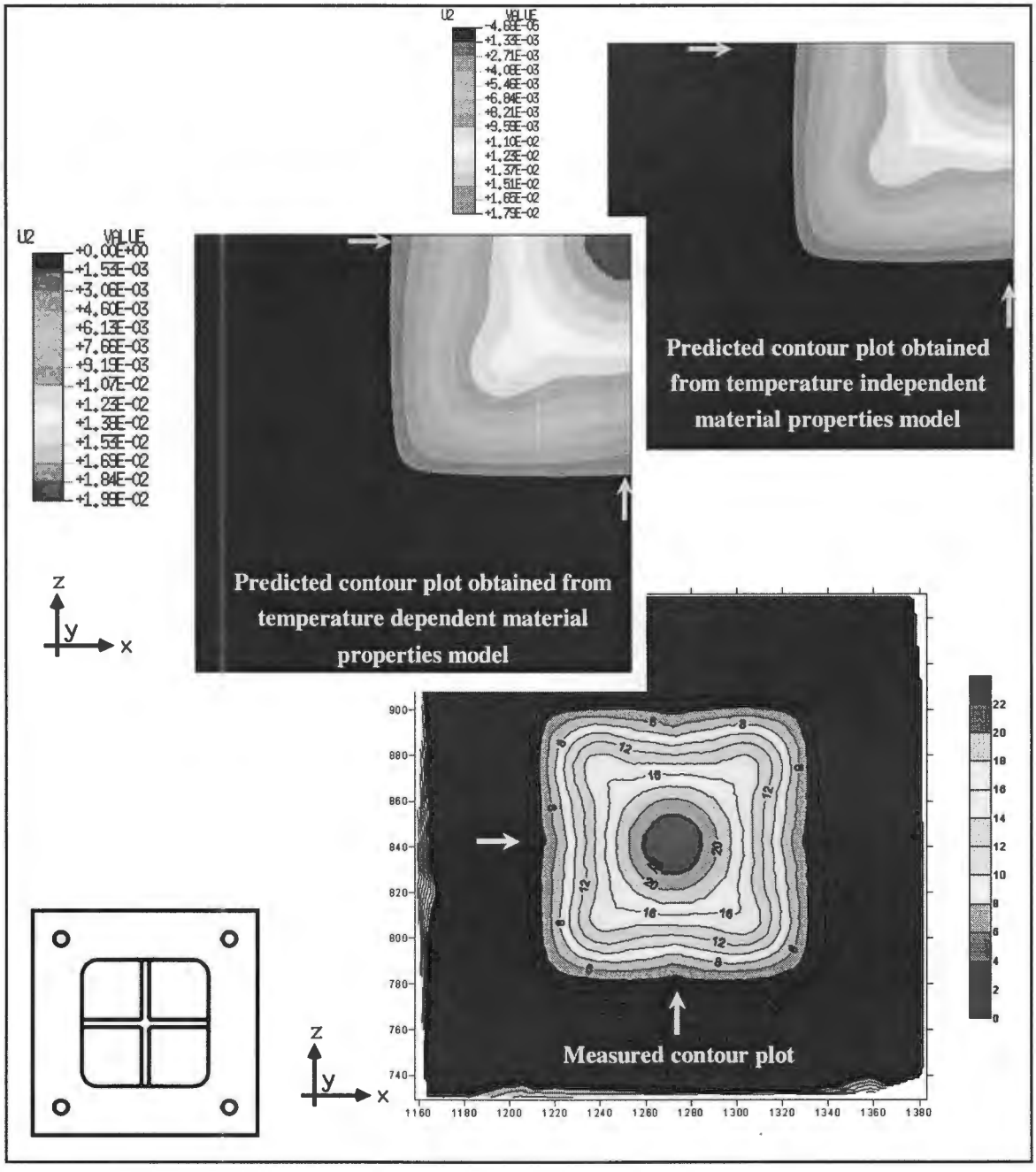

Figure 7.13 Comparison of predicted contour plot of a cross stiffened square with stiffener size 3x7mm plate at impulse 35Ns (arrows show locations of stiffeners)

The numerical analyses using material properties that include and exclude the effect of temperature on material failure show good agreement with the experiment as illustrated in Figure 7.13. Like the double cross stiffened square plate (S-DCS), the contour plot of the cross stiffened square plate (S-CS) reflects the effect of the stiffener. A change in the contour line of the contour plot of the deformed plate near its boundary indicates the locations of the stiffeners (shown by arrows).

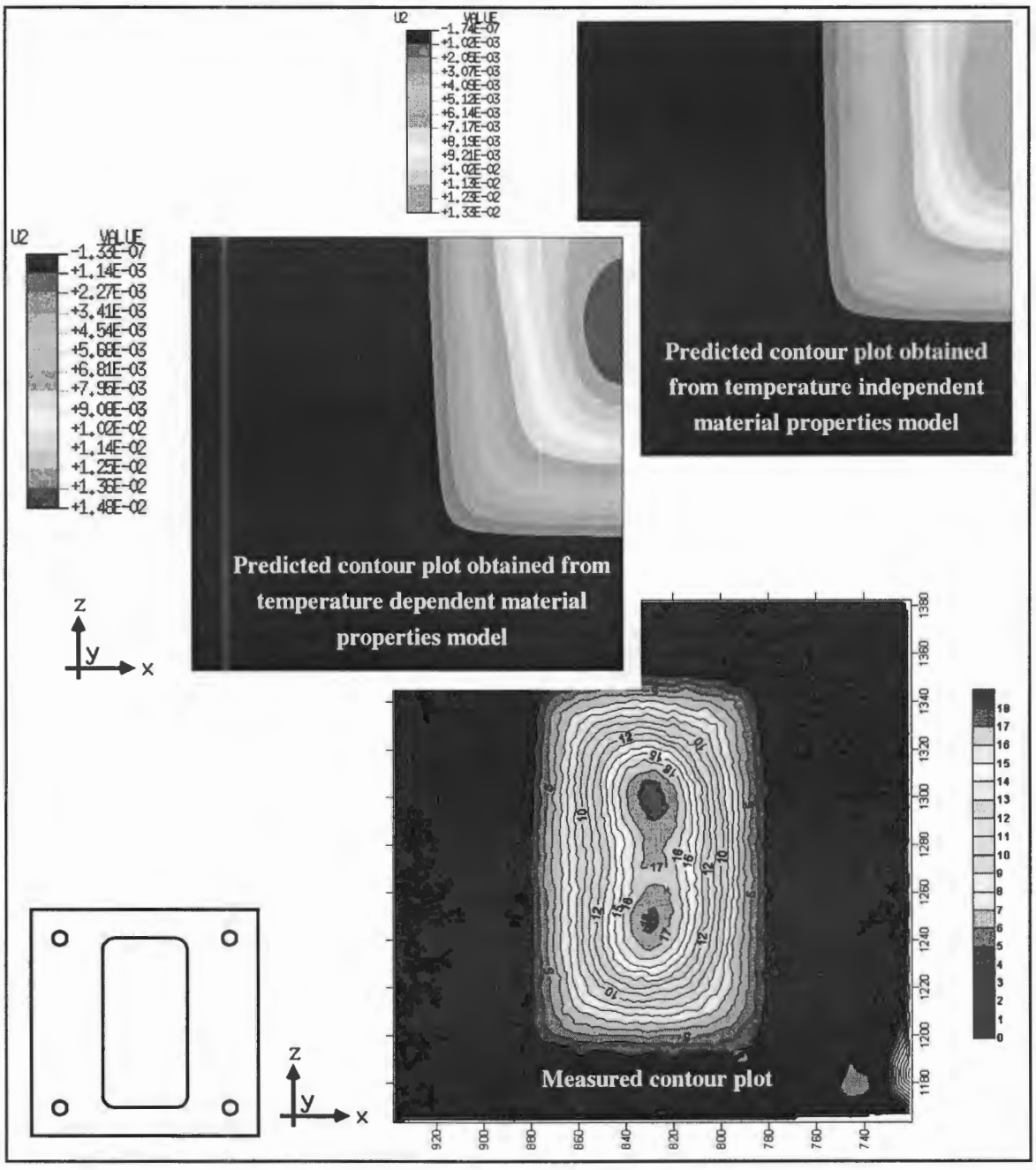

Figure 7.14 Comparison of predicted contour plot of a rectangular plate at impulse 24Ns

The predicted mode I permanent displacement contour plots of a rectangular plate using material properties that include and exclude temperature dependency are shown in Figure 7.14. The numerical models show favourable correlation with the experimental data; both showing the highest displacement occurring at two locations at either side of the centre line of the longest side of the plate (z-axis) giving a double bump effect along the plate profile.

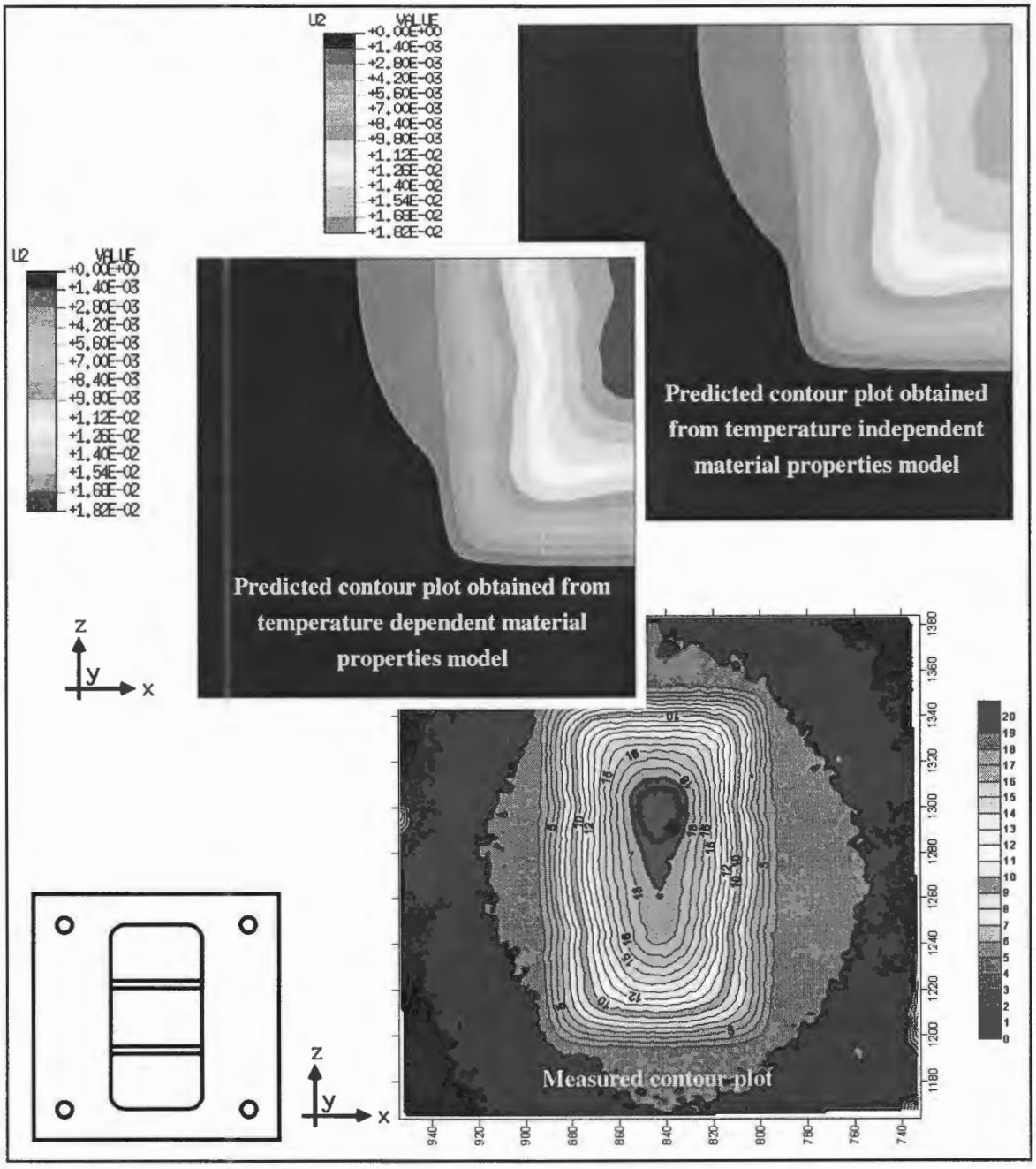

Figure 7.15 Comparison of predicted contour plot of a double stiffened rectangular plate with stiffener size 3x7 at impulse 35Ns

The contour plot of a double stiffened rectangular plate and the predicted models are shown in Figure 7.15. Good correlations are obtained from numerical models that use temperature dependent and non-temperature dependent material properties. The measured contour plot does not show any symmetry about the centre line of the longest side of the plate (z-axis). This may be due to the loading conditions and the difficult nature of the explosive.

More accurate comparisons of the results of the numerical analysis using material properties that include or exclude temperature dependence and experimental solutions as shown in Figures 7.16 to 7.27 are obtained by investigating the deformed quadrangular plate profile along its lines of symmetry. In all cases the models show good correlation with the experimental data. No sign of high strain localisation at the boundary or the central area of the plate is exhibited by the simulations.

The profiles shown represent an example of results for each stiffener configuration. The results obtained from the temperature dependent material properties models show higher mid-point displacement and plate profile than the non-dependent temperature material properties model. This is due to the weakening of material properties as temperature increases because of plastic work.

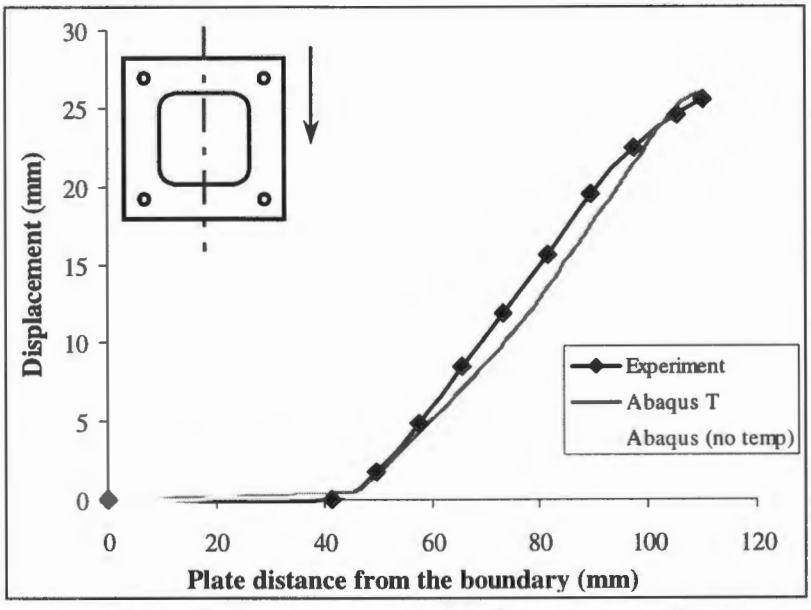

Figure 7.16 : Comparison of predicted and measured Mode I profile centreline along a square plate at impulse 31 Ns

Experiment denotes experimental values, Abaqus T denotes results obtained from the model that uses material properties that include temperature dependency, Abaqus (no temp) denotes results obtained from the model that uses material properties that exclude temperature dependency

The predicted mode I permanent displacement profile of a square plate is compared with the experimental data in Figure 7.16. Despite the slight difference in the plate profile the correlation is good. Both predicted profiles show a convex profile at plate distance of 60 to 85 mm, unlike the measured profile which a homogenous curvature.

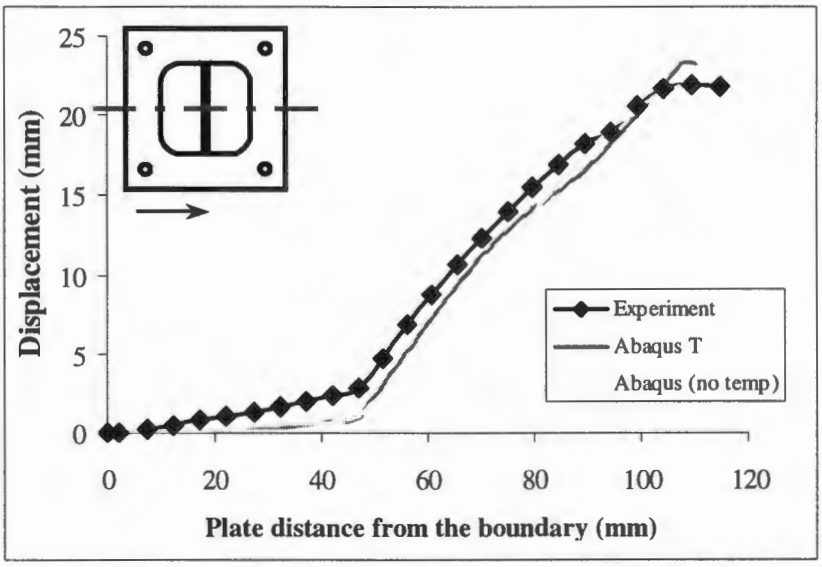

Figure 7.17 : Comparison of predicted and measured Mode I profile centreline across the stiffener of a single stiffened square plate with stiffener size 3x7mm at impulse 34 Ns

Experiment denotes experimental values, Abaqus T denotes results obtained from the model that uses material properties that include temperature dependency, Abaqus (no temp) denotes results obtained from the model that uses material properties that exclude temperature dependency

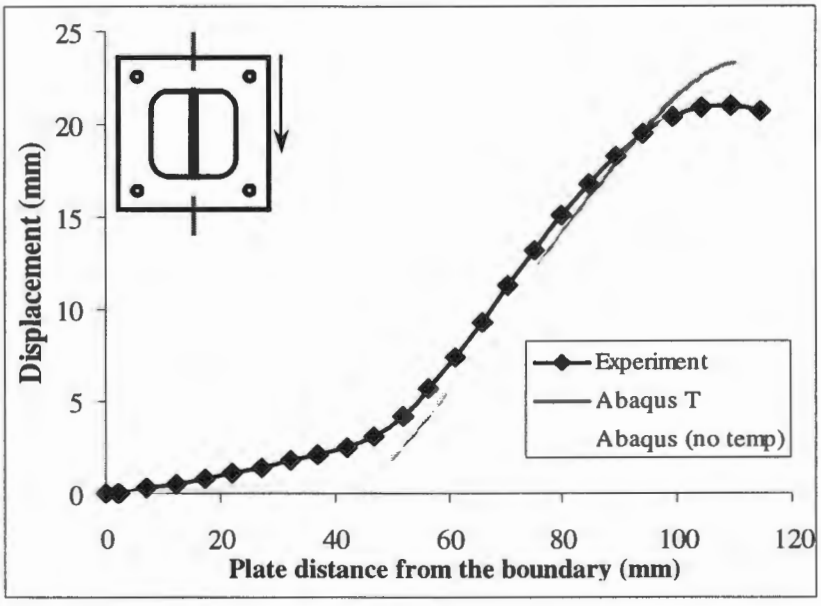

Figure 7.18 : Comparison of predicted and measured Mode I profile centreline along the stiffener of a single stiffened square plate with stiffener size 3x7mm at impulse 34 Ns

Experiment denotes experimental values, Abaqus T denotes results obtained from the model that uses material properties that include temperature dependency, Abaqus (no temp) denotes results obtained from the model that uses material properties that exclude temperature dependency

The predicted deformation profiles of a single stiffened square plate obtained from models that use material properties that include and exclude the effect of temperature compared well with the experimental data in Figures 7.17 and 7.18. The models slightly underestimate the deformed shaped but overestimate the highest displacement.

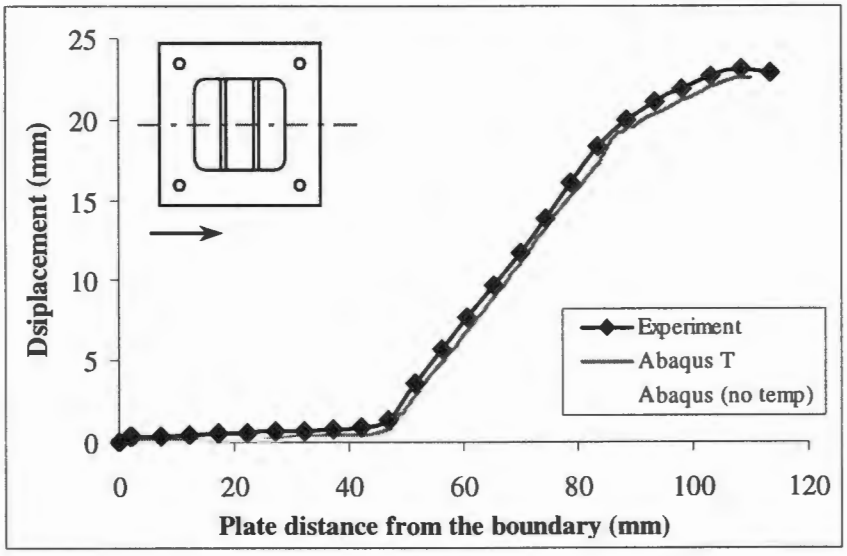

Figure 7.19 : Comparison of predicted and measured Mode I profile centreline across the stiffeners of a double stiffened square plate with stiffener size 3x7mm at impulse 37 Ns

Experiment denotes experimental values, Abaqus T denotes results obtained from the model that uses material properties that include temperature dependency, Abaqus (no temp) denotes results obtained from the model that uses material properties that exclude temperature dependency

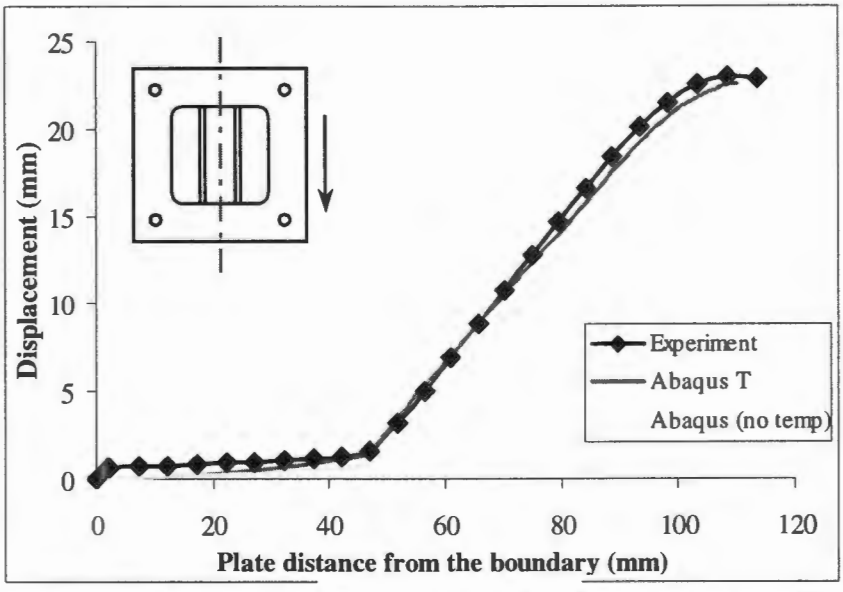

Figure 7.20 : Comparison of predicted and measured Mode I profile centreline parallel the stiffeners of a double stiffened square plate with stiffener size 3x7mm at impulse 37 Ns

Experiment denotes experimental values, Abaqus T denotes results obtained from the model that uses material properties that include temperature dependency, Abaqus (no temp) results obtained from the denotes model that uses material properties that exclude temperature dependency

Figures 7.19 and 7.20 represent the results of the numerical analyses that predicted the deformed profile of a double stiffened square plate using material properties that include and exclude the temperature effect on material failure. The solution obtained from the model using the temperature dependent material properties shows very good agreement with the experiment.

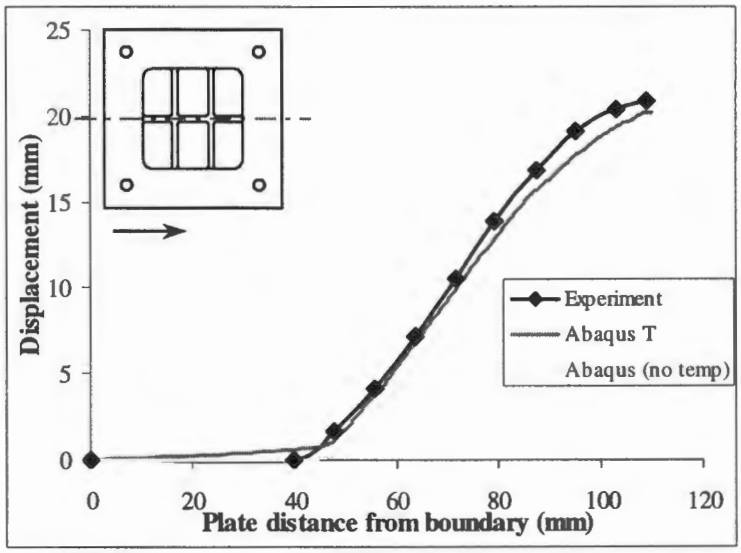

Figure 7.21 : Comparison of predicted and measured Mode I profile centreline across the stiffeners of a double cross stiffened square plate with stiffener size 3x7mm at impulse 37 Ns

Experiment denotes experimental values, Abaqus T denotes results obtained from the model that uses material properties that include temperature dependency, Abaqus (no temp) results obtained from the denotes model that uses material properties that exclude temperature dependency

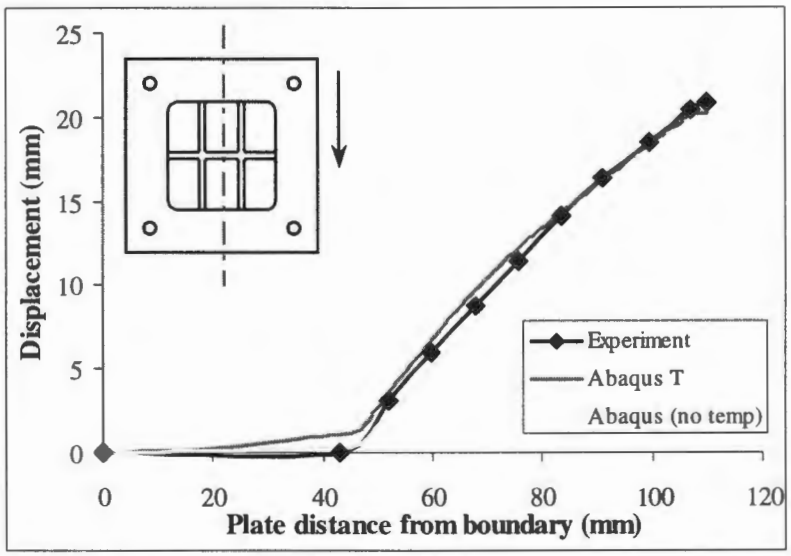

Figure 7.22 : Comparison of predicted and measured Mode I profile centreline parallel to the stiffeners of a double cross stiffened square plate with stiffener size 3x7mm at impulse 37 Ns

Experiment denotes experimental values, Abaqus T denotes results obtained from the model that uses material properties that include temperature dependency, Abaqus (no temp) results obtained from the denotes model that uses material properties that exclude temperature dependency

The predicted and measured profiles of a double cross stiffened plate are shown in Figures 7.21 and 7.22. The model that uses material properties that include temperature dependency shows better correlation with the experiment than the model that uses material properties that exclude temperature dependency. However, both models estimate the correct deformed shape.

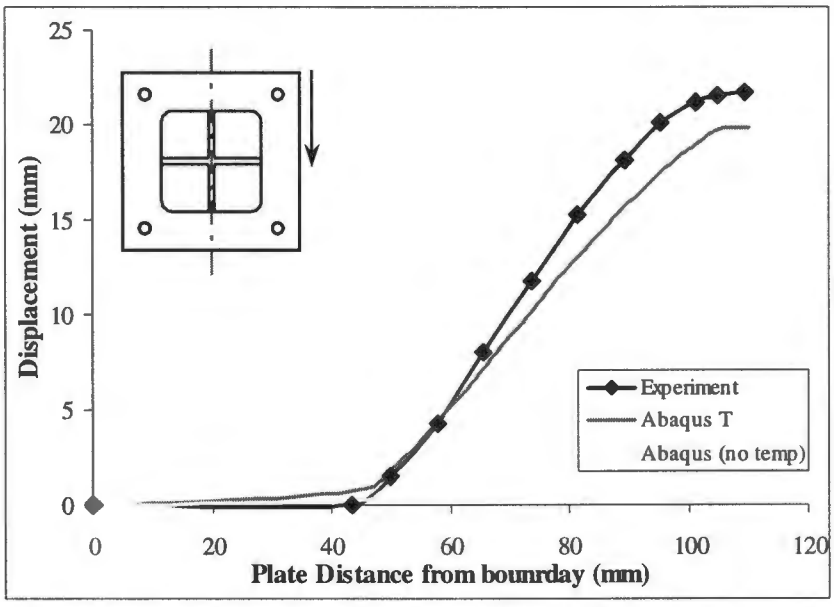

Figure 7.23 : Comparison of predicted and measured Mode I profile along centreline of a cross stiffened square plate (S-CS) with stiffener size 3x7mm at impulse 35 Ns
Experiment denotes experimental values, Abaqus T denotes results obtained from the model that uses material properties that include temperature dependency, Abaqus (no temp) results obtained from the denotes model that uses material properties that exclude temperature dependency

Because of symmetry only one profile along the centre line of the cross stiffened square plate illustrated in Figure 7.23 is examined. Both models underestimate the profile and the highest point of deflection. However, the predicted plate profile correlates well with the experimental data.

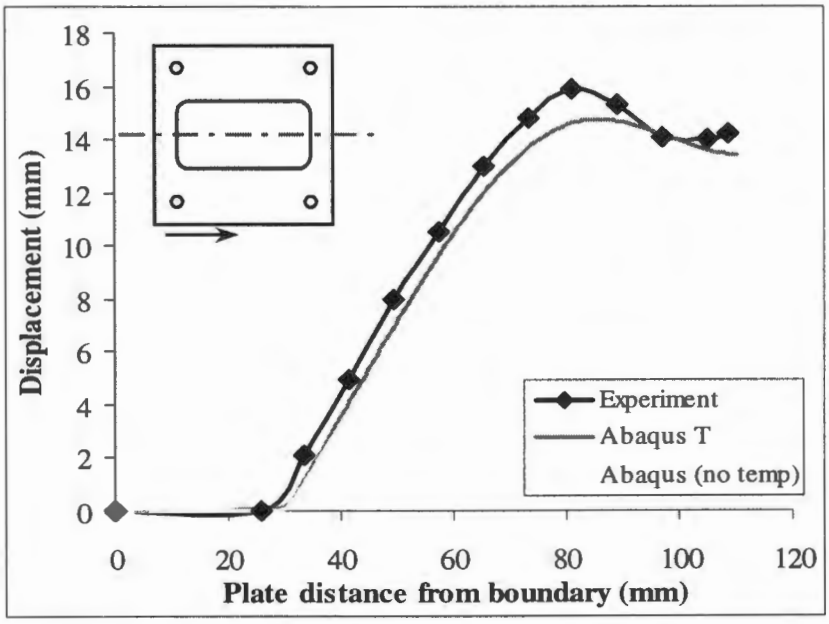

Figure 7.24 : Comparison of predicted and measured Mode I profile along centreline of shortest side of a rectangular plate (R) at impulse 24 Ns

Experiment denotes experimental values, Abaqus T denotes results obtained from the model that uses material properties that include temperature dependency, Abaqus (no temp) results obtained from the denotes model that uses material properties that exclude temperature dependency

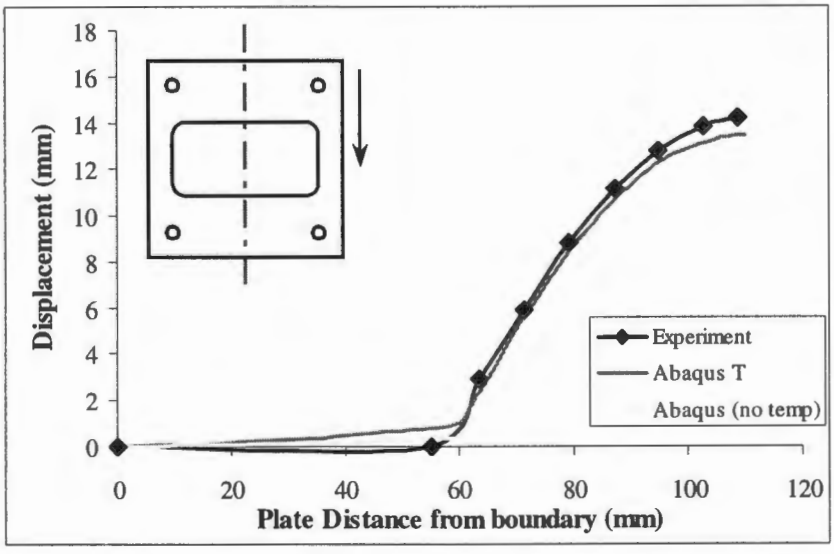

Figure 7.25 : Comparison of predicted and measured Mode I profile along centreline of longest side of a rectangular plate at impulse 24 Ns

Experiment denotes experimental values, Abaqus T denotes results obtained from the model that uses material properties that include temperature dependency, Abaqus (no temp) results obtained from the denotes model that uses material properties that exclude temperature dependency

The overall response of the rectangular plates is shown in Figures 6.24 and 6.25. It can be seen from both figures that the response of the temperature dependent model is very close to the experimental data. However, both models exhibit the same shape profile as the experimental data.

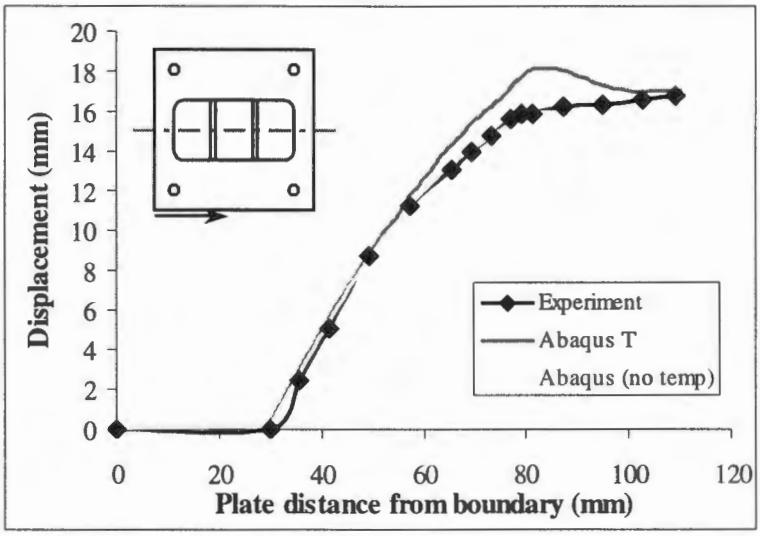

Figure 7.26 : Comparison of predicted and measured Mode I profile centreline across the stiffeners of a double stiffened rectangular plate with stiffener size 3x7mm at impulse 35 Ns
Experiment denotes experimental values, Abaqus T denotes results obtained from the model that uses material properties that include temperature dependency, Abaqus (no temp) results obtained from the denotes model that uses material properties that exclude temperature dependency

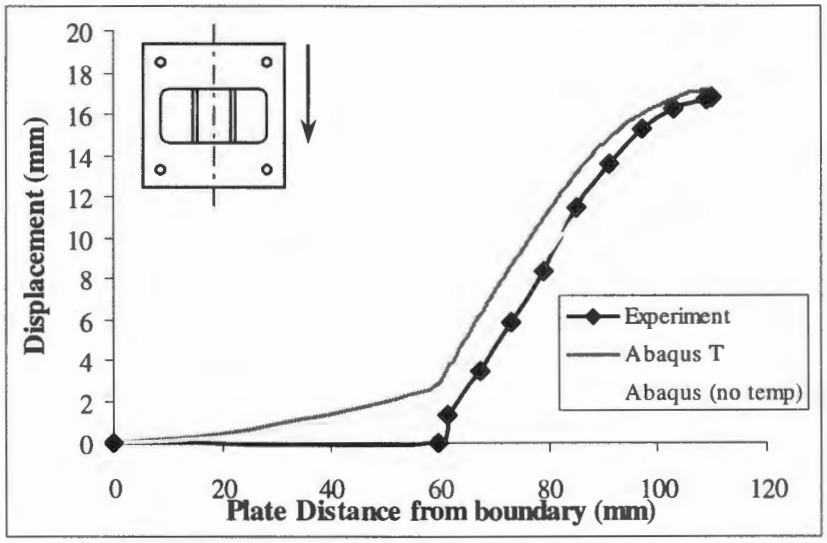

Figure 7.27 : Comparison of predicted and measured Mode I profile centreline parallel to the stiffeners of a double stiffened rectangular plate with stiffener size 3x7mm at impulse 35 Ns
Experiment denotes experimental values, Abaqus T denotes results obtained from the model that uses material properties that include temperature dependency, Abaqus (no temp) results obtained from the denotes model that uses material properties that exclude temperature dependency

The predicted mode I permanent displacement profiles of a double stiffened rectangular plate compares relatively well with the experimental data as shown in Figures 7.26 and 7.27. There is however, a slight difference in the profile along the centre line of the short side of the plate (Figure 7.26). The models exhibit the maximum displacement at 82mm from the boundary of the plate whereas according to the experimental data the maximum displacement lies at the plate centre.

7.4 The effect of the stiffener sizes on mode I response

The predicted mode I permanent displacement profiles at three locations; both lines of symmetry of the square plates and 20mm parallel to the centre line parallel to the stiffener (lies along the stiffener); are shown in Figures 7.28 – 7.30 for the different single stiffened square plates for the same impulse of 35Ns. It is seen that the central maximum displacement decreases by up to 26% as the cross sectional area of stiffener increases from 0 to 28 mm^2, and the overall shape changes. The percentage decrease in the maximum displacement as a function of stiffener sizes is tabulated in Table 7.1. For the small stiffeners, the profile curvature is approximately linear whereas for the larger stiffeners, there is a change in the curvature of the profile that forms the line of symmetry across the stiffener. The transition for this clearly occurs for a stiffener height of 7mm for the experiments described herein. Furthermore, from Figure 7.29, the predicted profiles across the stiffener suggest the existence of a relatively flat sector in the middle of the plate on both sides of the stiffener. The flat region increases as the stiffener height increases.

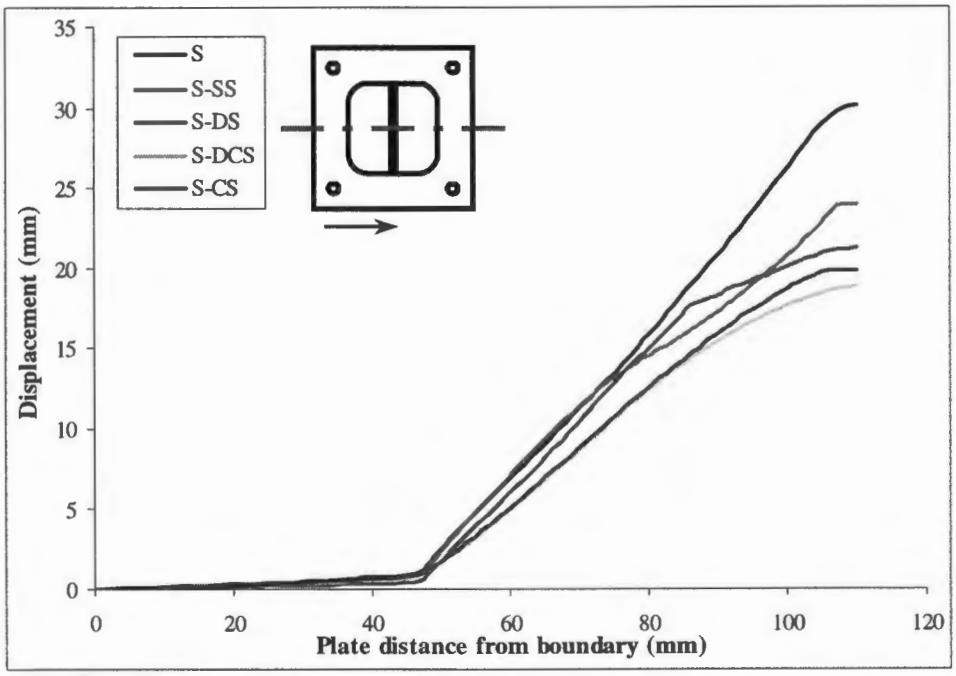

Figure 7.28 : Predicted Mode I profiles centreline across the stiffener of single stiffened square plates with various stiffener sizes at impulse 35Ns

Plate configuration	X- section area of stiffener (mm^2)	Mid-point displacement (mm)	Difference in mid-point displacement	% difference in mid-point displacement	Time to reach max displacement (μs)
S		30.14	-		184
S-SS 3x3	9	27.21	2.93	10	181
S-SS 4x3	12	26	4.14	13	180
S-SS 3x7	21	23.99	6.15	20	185
S-SS 4x7	28	22.4	7.74	26	188

Table 7.2 : Maximum displacement and time response of single stiffened square plates at impulse 35 Ns

Plate configuration	X- section area of stiffener (mm^2)	Mid-point displacement (mm)	Difference in mid-point displacement	% difference in mid-point displacement	Time to reach max displacement (μs)
S		30.14	-		184
S-DS 3x3	18	26.25	3.89	13	182
S-DS 3x7	42	21.27	8.87	29	185

Table 7.3 : Maximum displacement and time response of double stiffened square plates at impulse 35 Ns

Plate configuration	X- section area of stiffener (mm^2)	Mid-point displacement (mm)	Difference in mid-point displacement	% difference in mid-point displacement	Time to reach max displacement (μs)
S		30.14	-		184
S-CS 3x3	18	24.79	5.35	18	180
S-CS 3x7	42	19.83	10.31	34	185

Table 7.4 : Maximum displacement and time response of cross stiffened square plates at impulse 35 Ns

Plate configuration	Total cross section area of stiffener (mm^2)	Mid-point displacement (mm)	Difference in mid-point displacement	% difference in mid-point displacement	Time to reach max displacement (μs)
S		30.14	-		184
S-DCS 3x3	21	24.61	5.53	18	182
S-DCS 3x7	61	18.82	12.02	40	185

Table 7.5 : Maximum displacement and time response of double cross stiffened square plates at impulse 35 Ns

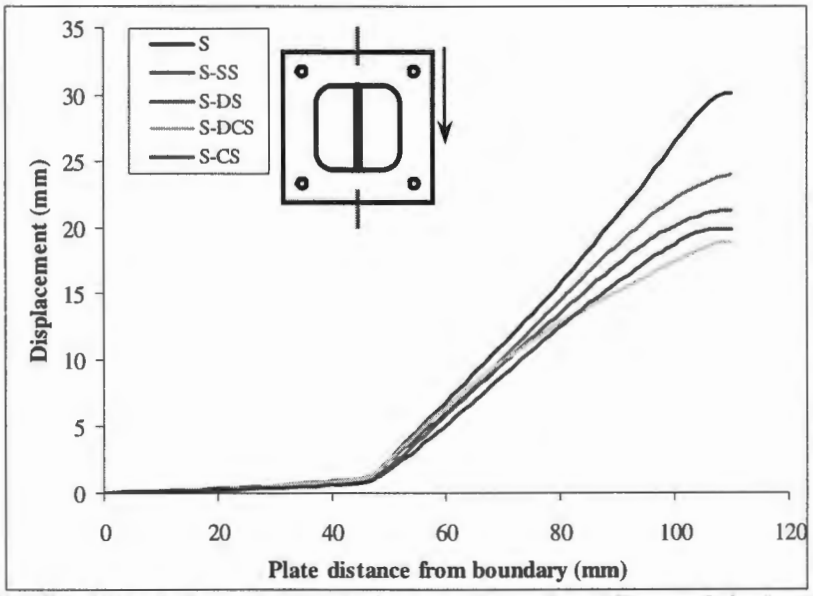

Figure 7.29 : Predicted Mode I profiles centreline parallel to the stiffener of single stiffened square plates with various stiffener sizes at impulse 35Ns

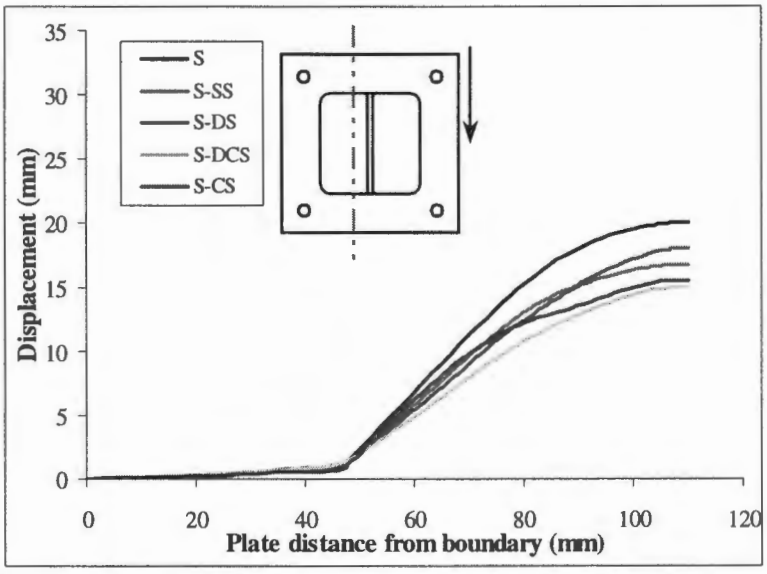

Figure 7.30 : Predicted Mode I profiles 20mm offset to the centre line parallel to the stiffener of single stiffened square plates with various stiffener sizes at impulse 35Ns

Using a non-stiffened square plate as a reference, the effect of the size of the stiffener is assessed by calculating the difference in mid-point displacement between the reference plate and the investigated plate. Tables 7.2 – 7.5 show the percentage decrease in mid-point displacement for each stiffener configuration as the stiffener height increases for an impulsive load of 35Ns. Depending on the stiffener configuration a decrease of up to 18% for stiffener size of 3x3mm and up to 40% for stiffener size 3x7mm in mid-point deflection can be achieved. Thus, by increasing the stiffener size from 3x3mm to 3x7mm the difference in mid-point displacement can be reduced by a factor of 2. This factor of 2 is also observed for all stiffener configurations.

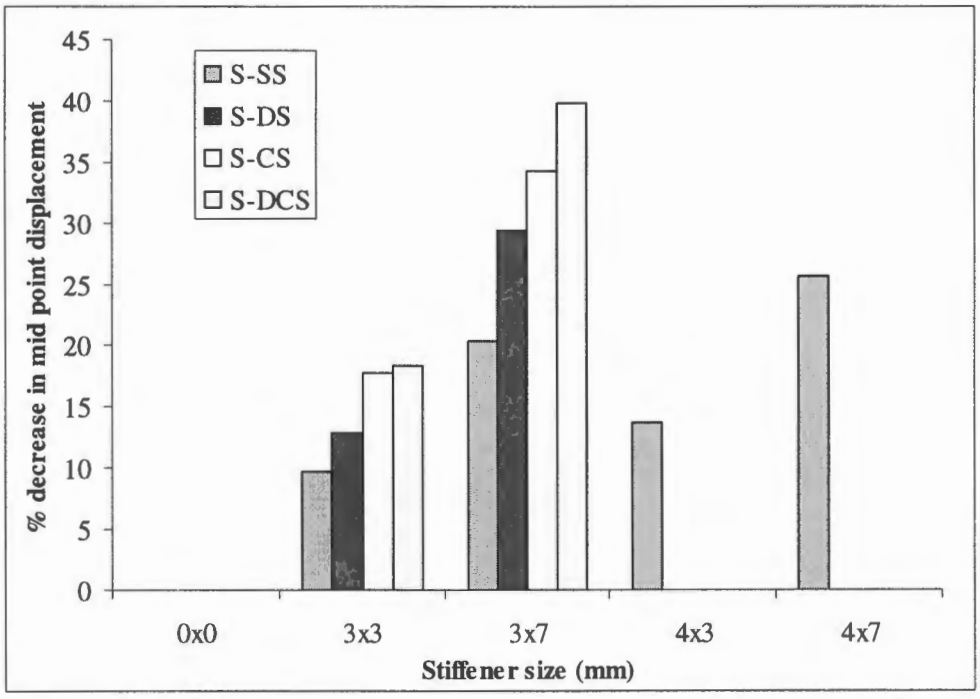

Figure 7.31 : Bar chart of predicted percentage decrease in mid-point deflection for each stiffener sizes and configurations.

Figure 7.31 shows the predicted percentage decrease in mid-point displacement (Tables 7.2 – 7.5) as a function of stiffener size for all stiffener configurations of square plates.

Figures 7.32 – 7.34 illustrate the predicted mode I permanent displacement profiles at three locations; both lines of symmetry of the rectangular plates and 25.5mm offset from the centre line parallel to the stiffeners (on the stiffener); for all double stiffened rectangular plates for the same impulse of 35Ns. Using the same procedure as for square plates, the difference in maximum displacement is calculated relative to the maximum displacement of an unstiffened rectangular plate. The central maximum displacement decreases up to 17% as the combined cross sectional area of stiffeners increases from 0 to 42mm^2, and the overall shape changes significantly. The results are tabulated in Table 7.6. Furthermore, as the stiffener height increases, the maximum displacement (seen as a peak in Figure 7.32) shifts to the left and the peak area also decreases. The profile centreline parallel to the stiffeners (Figure 7.33) shows that the displacement from the boundary to the mid point of the exposed area (up to vertical dotted line) is independent of the stiffener size. The profiles exhibited the same response.

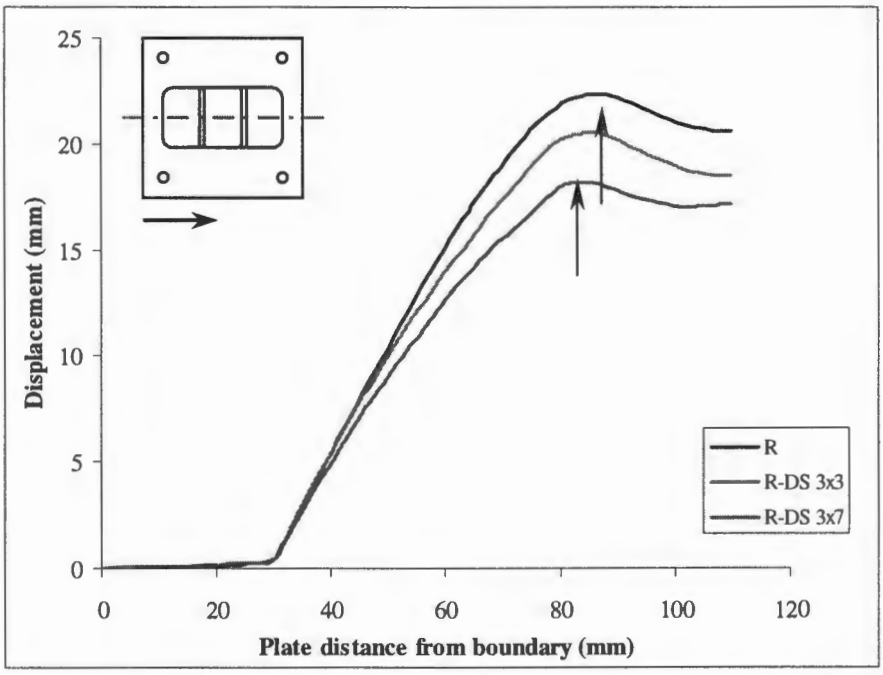

Figure 7.32 : Predicted Mode I profiles centre line across the stiffeners of double stiffened rectangular plates with various stiffener sizes at impulse 35Ns (arrows denote peak)

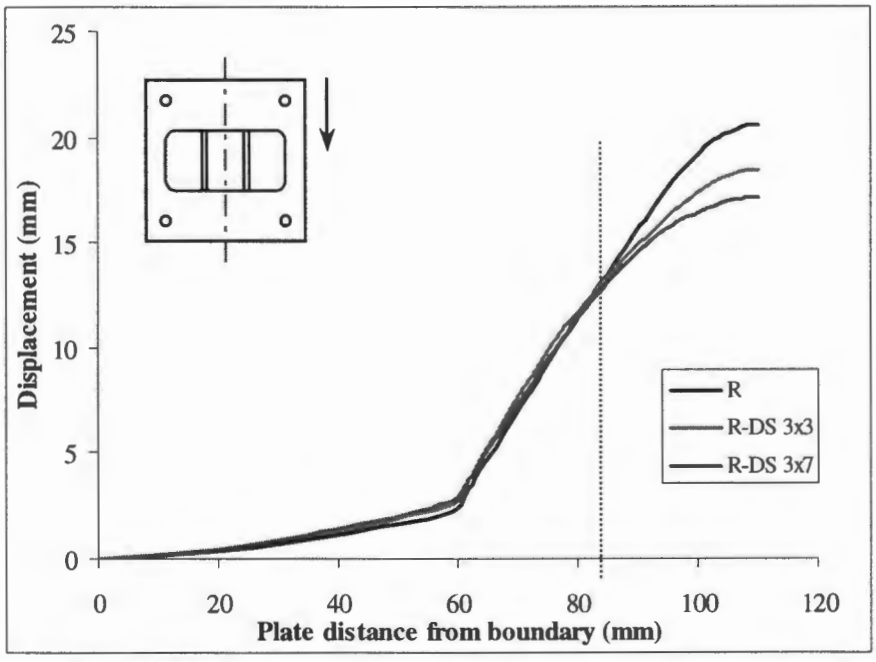

Figure 7.33 : Predicted Mode I profiles centreline parallel to the stiffeners of double stiffened rectangular plates with various stiffener sizes at impulse 35Ns

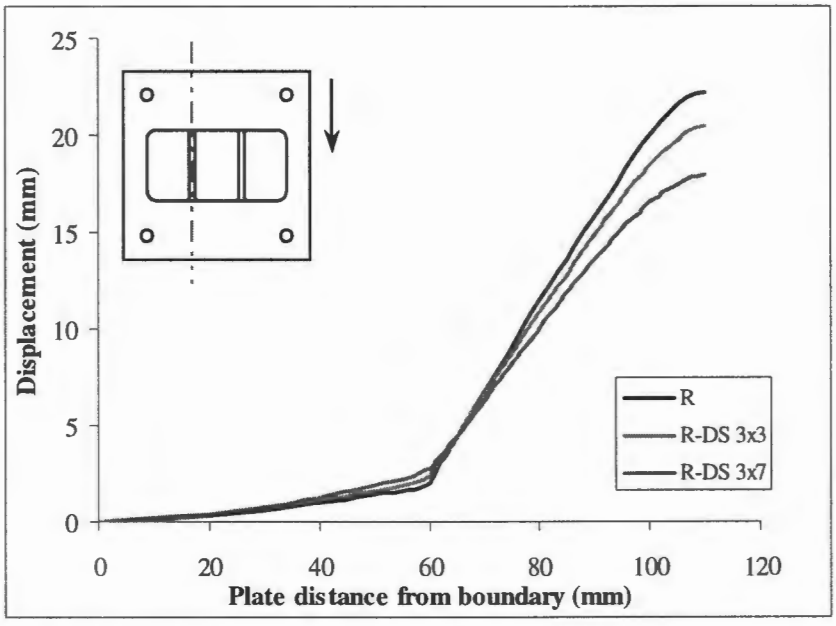

Figure 7.34 : Predicted Mode I profiles along centreline of one of the stiffeners of double stiffened rectangular plates with various stiffener sizes at impulse 35Ns

Plate configuration	Total cross section area of stiffeners (mm^2)	Mid-point displacement (mm)	Difference in mid point displacement	% difference in mid-point displacement	Time to reach maximum displacement (μs)
Rectangular		20.58	-		147
Recdou3x3	18	18.47	2.11	10	144
Recdou3x7	42	17.13	3.45	17	157

Table 7.6 : Mid-point displacement and time response of double stiffened rectangular plates at impulse 35 Ns

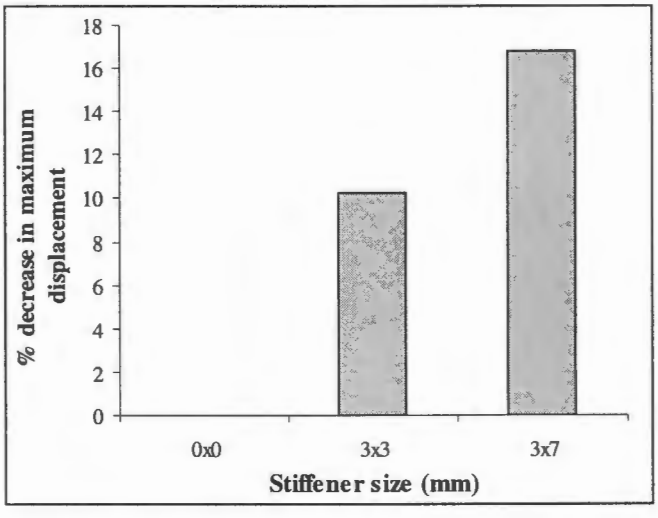

Figure 7.35 : Bar chart of predicted percentage decrease in maximum deflection for each stiffener size of double stiffened rectangular plates.

7.5 The effect of the stiffener configurations

The mode I permanent displacement profiles at three locations; both lines of symmetry of the square plates and 20mm parallel to the centre line parallel to the stiffener; predicted by the numerical analysis are shown in Figures 7.36 – 7.38 for all stiffened quadrangular plates for the same impulse of 35Ns. It is seen that by changing the configuration of the stiffeners the maximum displacement can be decreased by up to 40% and the overall shape changes significantly. As the plate structure stiffens the displacement decreases. The response of the double cross stiffened square plate shows the least mid-point displacement compared to the plates with other stiffener configurations. The profile curvature is homogeneous in all cases except for the double stiffened plate. A change in the profile that forms the centre line of the plate across the stiffeners is noted at the location of the stiffeners. Furthermore, it is observed that the cross stiffened plate offers more resistance to the blast load than the double stiffener despite the fact that the number of stiffeners is the same.

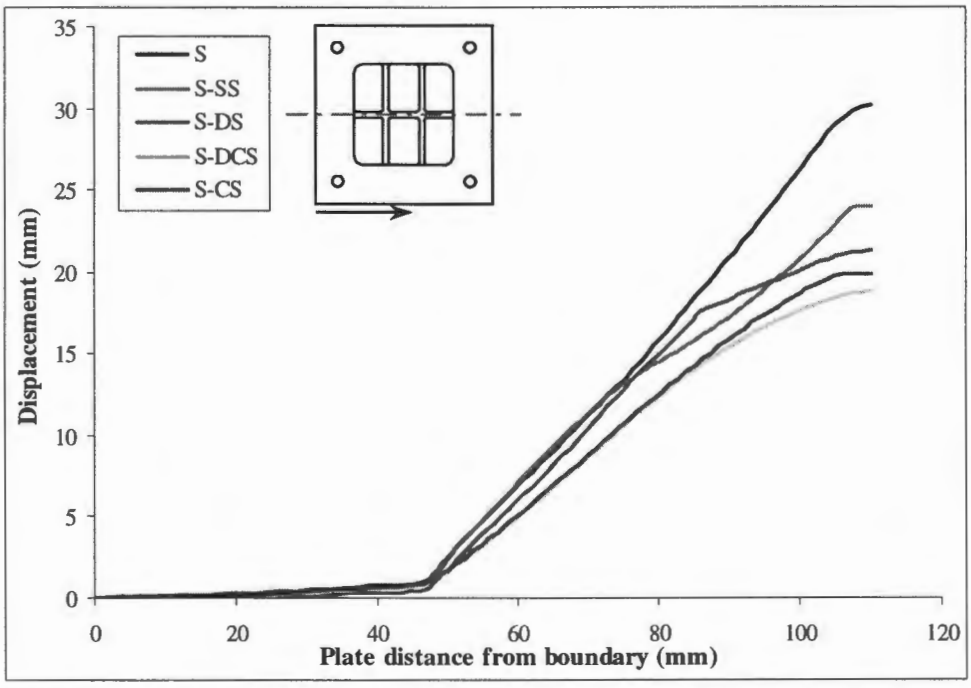

Figure 7.36 : Predicted profiles centre line across the stiffeners of square plates with stiffener size 3x7mm for various stiffener configurations at impulse 35Ns

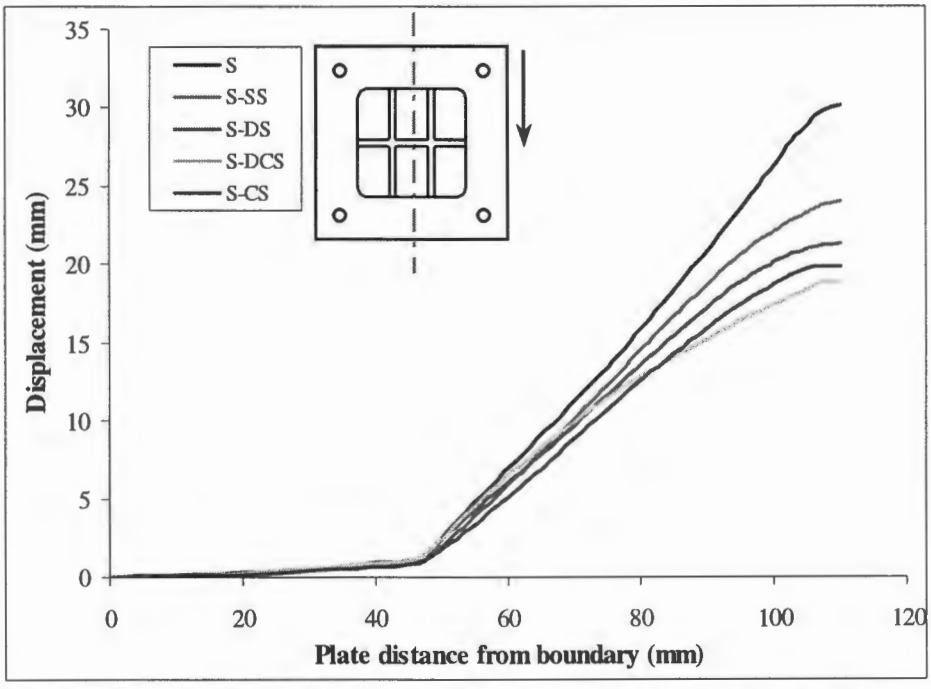

Figure 7.37 : Predicted profiles centre line parallel to the stiffeners of square plates with stiffener size 3x7mm for various stiffener configurations at impulse 35Ns

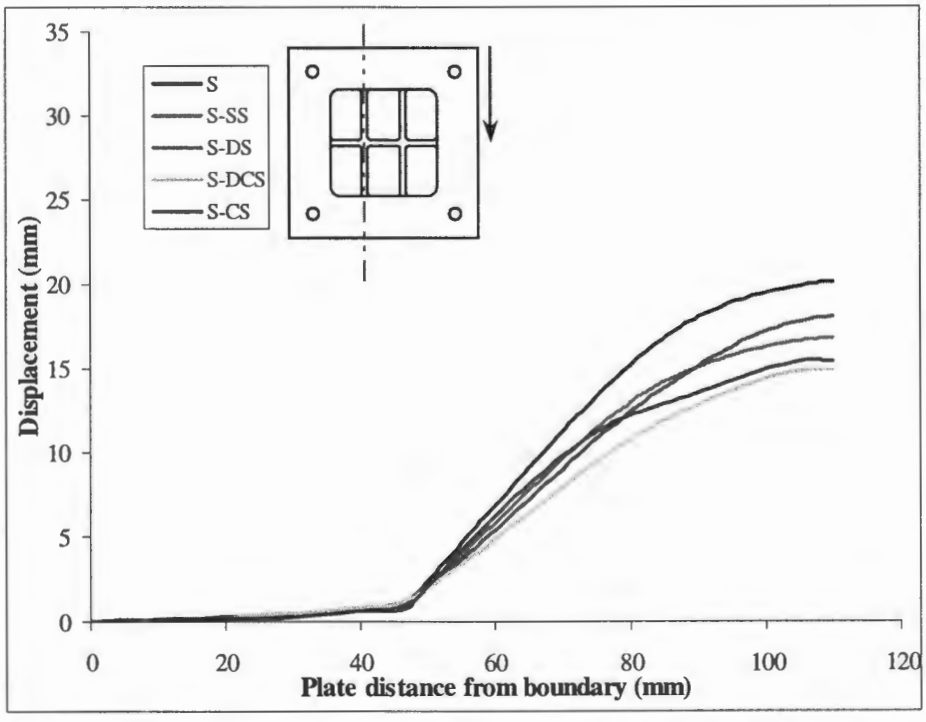

Figure 7.38 : Predicted profiles 20mm offset to centre line parallel to the stiffeners of square plates with stiffener size 3x7mm for various stiffener configurations at impulse 35Ns

Table 7.7 summarises the difference in maximum displacement from the unstiffened square or rectangular plate to the other plates with different stiffener configurations and size 3x7mm and the time taken for the plate to reach the maximum displacement. The time taken to reach the highest deflection is almost constant for plates of the same geometry. However, from Figure 7.39, it is noted that the rate at which the plate deforms decreases as the structure of the plate stiffens (more stiffeners). The average rate of deformation is defined by the ratio of the maximum displacement to the time taken to reach that displacement. For a square plate the average rate of deformation is 0.16mm/μs. On the other hand, the double cross stiffened square plate deforms at an average rate of 0.10mm/μs. The average rate at which the rectangular plate deforms; 0.15mm/μs, is found to be very close to that of the square plate. Both double stiffened quadrangular plates deform at the average rate of 0.12 mm/μs.

Plate configuration	X- section area of stiffener (mm^2)	Maximum displacement (mm)	Difference in maximum displacement (mm)	% difference in maximum displacement	Time to reach maximum displacement (μs)
S	-	30.14	-		184
S-SS 3x7	21	23.99	-6.15	-20.4	185
S-DS 3x7	42	21.27	-8.87	-29.4	185
S-CS 3x7	42	19.83	-10.31	-34.2	185
S-DCS 3x7	63	18.82	-11.32	-37.6	182
R	-	22.36	-	-	147
R-DS 3x7	42	18.2	-4.16	-18.6	157

Table 7.7 : Mid-point displacement and time response of stiffened quadrangular plates at impulse 35 Ns

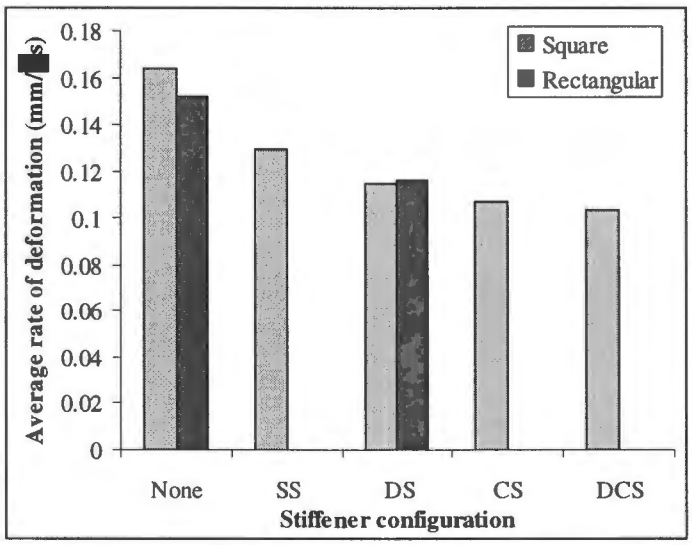

Figure 7.39 : Bar chart of average rate of deformation for plate of different stiffener configuration

Figure 7.40 shows that for the same plate size, the percentage decrease in maximum displacement increases as the plate stiffness increases. It can be seen that for the double stiffened plates, the percentage decrease for the square plate is higher than for the rectangular plate.

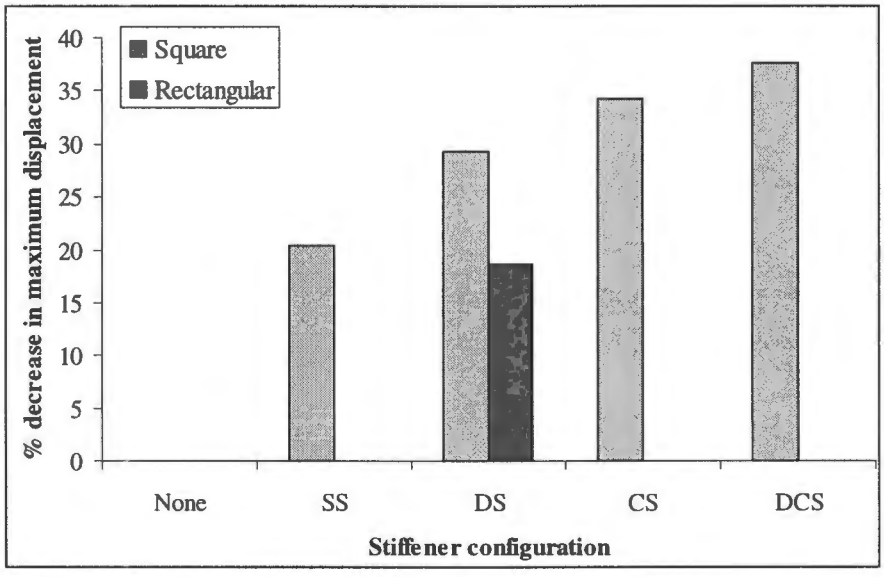

Figure 7.40 : Bar chart of predicted percentage decrease in maximum displacement for different stiffener configurations

7.6 Tearing Mode response

Experimental evidence has shown three distinct modes of failure of steel plates occurring in blast loading conditions. Mode I failure involves the large inelastic permanent deformation of the plate without any sign of tearing, and has been discussed in the previous section. The onset of Mode II failure is defined by the first sign of tearing occurring in the plate at the boundary. Thereafter all the tearing behaviour is described as Mode II until the Mode III failure where the energy of the blast is sufficient enough to cause shearing around the entire perimeter of the plate before any significant displacement has taken place in the remainder of the plate. The result of such failure mode is an almost flat disk of the size of the plate.

7.6.1 METHOD OF PLATE FAILURE

When tearing occurs the model is subjected to severe temperature rises in the region of fracture, forming a band of high temperatures due to a slightly larger amount of strain in the band compared to the surrounding areas. As a result of greater adiabatic heating due to the large amount of plastic work the material properties weaken. The weakening of material properties results in larger strains and higher temperatures until unrealistic element elongation occurs. As the temperature of the band becomes hotter, the elements in this band undergo extensive elongation in the direction of displacement (y-direction) exceeding realistic strain (70% - 300%). Hence, indicating that failure will occur within the high temperature band.

The reason for the severe element elongation can thus be ascribed to the effects of the temperature dependent material properties. Because of the thermal softening an unrealistic strain of 200% failure strain criterion was imposed on the model to ensure failure after extensive adiabatic heating in the localised region. If not, the elements in the localised area will keep on deforming as a result of the decaying material properties.

Failure by shear bands as reported by Wiehahn et al [27] is not investigated in this study. Because of the complex geometry, the mesh size of the model (1.2 x 1.2 x 0.4 mm^3) is considered to give satisfactory results and is kept constant. The effect of the mesh density is, therefore, not investigated.

7.6.2 PLATE RESPONSE

Figures 7.41 – 7.54 show the response of quadrangular plates which were partially or completely torn at the boundary (Mode II* and Mode II). In general, the finite element models show good correlation with the experimental results. However, because of the symmetry conditions the prediction fails to show how the Mode II failures progress from one side of the plate to two sides of the plate to three sides of the plates before the exposed area of the plate is blown out of the boundary as observed in the experiment. Tearing is not symmetrical in the experiment due to the complex nature of the loading conditions involving explosives.

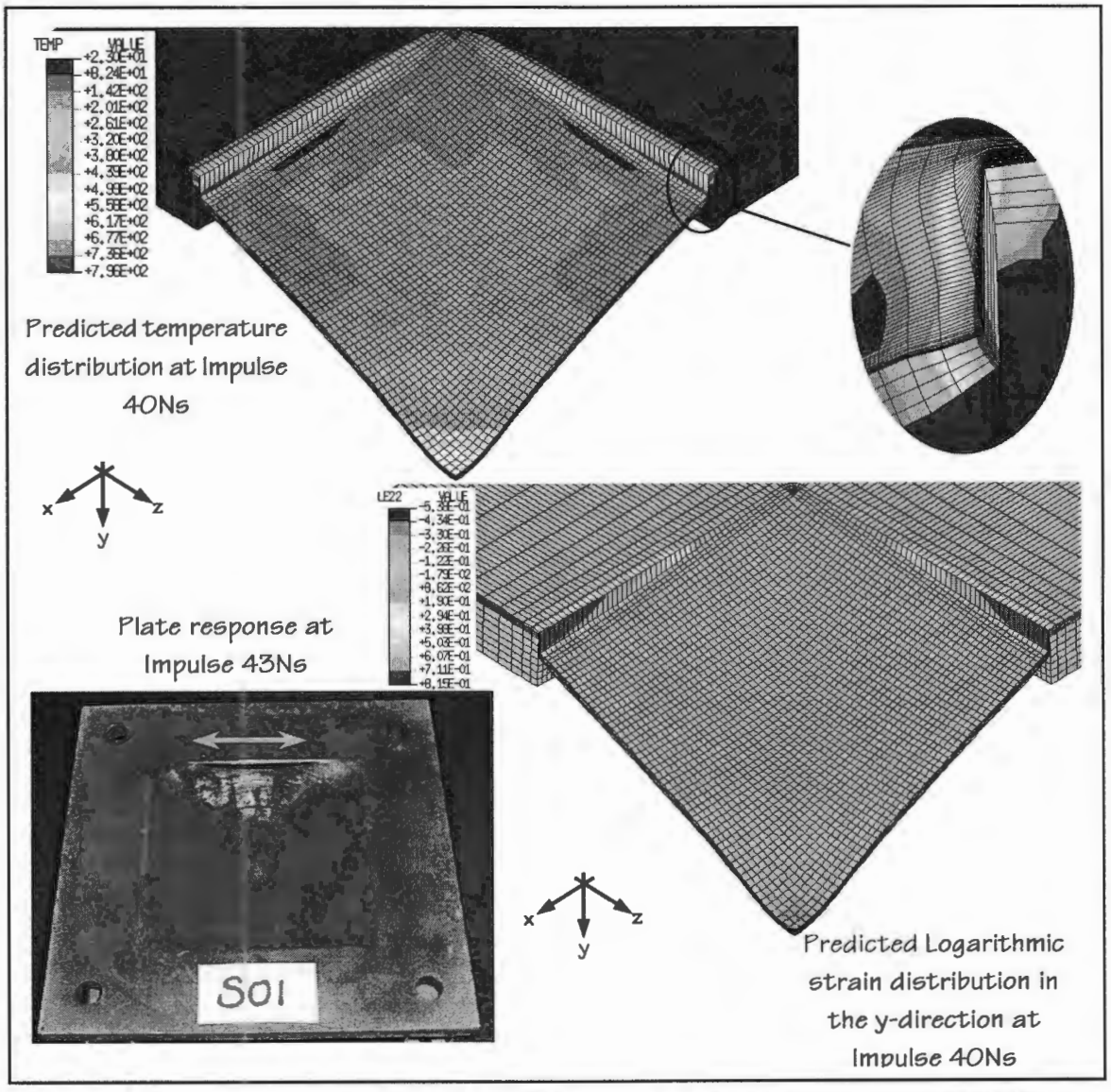

Figure 7.41 : Comparison of predicted Mode II* response of a square plate at impulse of 40Ns (arrow shows plate tearing)

Figure 7.41 shows the predicted response of a unstiffened square plate (S) which was partially torn at the boundary (Mode II*) under a uniform impulsive load of 40Ns. The numerical model predicted failure at a smaller impulsive load. Temperature and logarithmic strain values of 796 ^{0}C and 81.5% respectively at the elongated elements show that tearing occurs in the model.

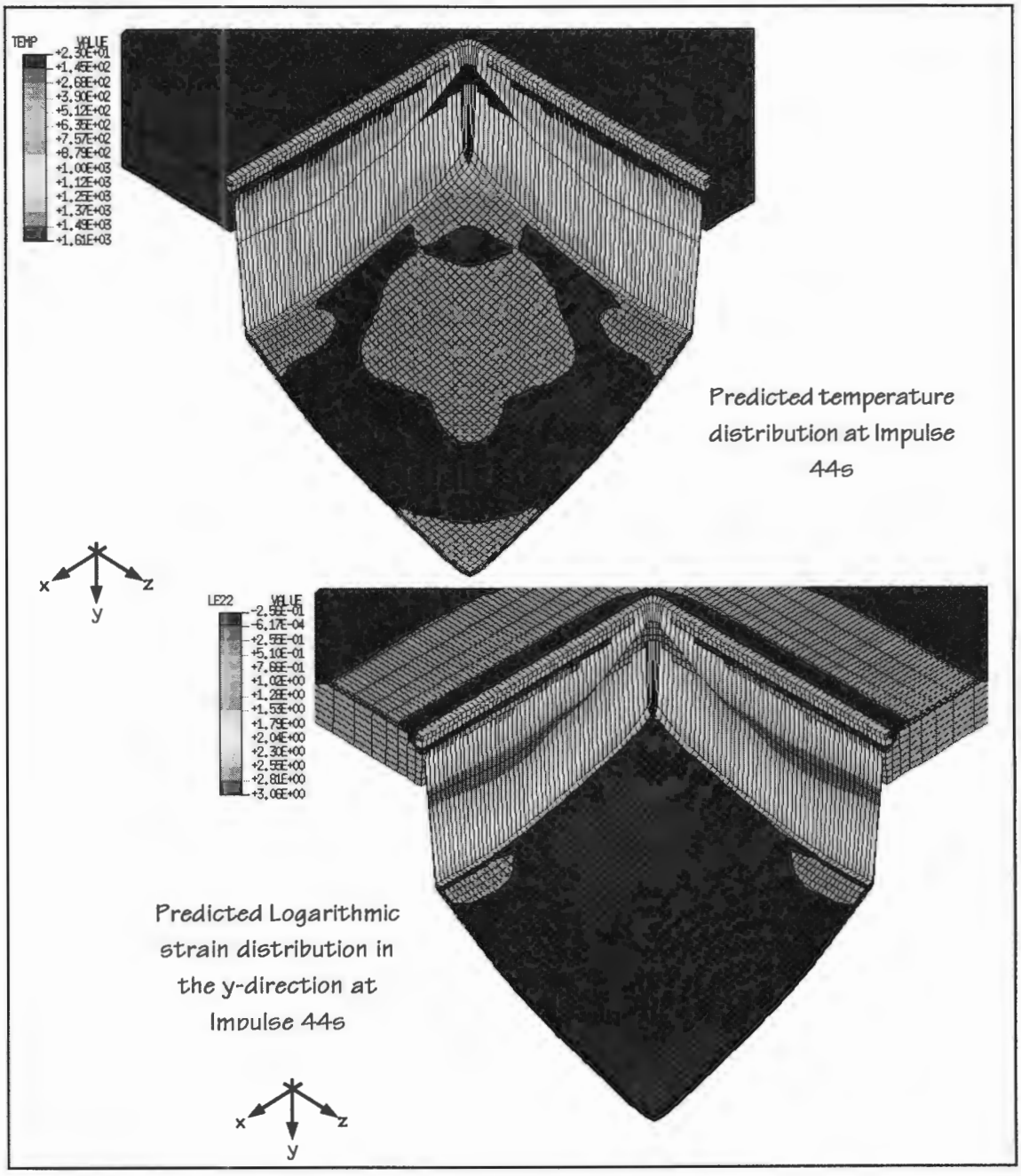

Figure 7.42 : Predicted Mode II response of a square plate at impulse 44Ns

Typical Mode II failure, illustrated in Figure 7.42, is predicted to occur at an impulse of 44Ns by the model. The severe element elongation at the boundary illustrates how the plate will shear. No experimental data is available to compare to the model data.

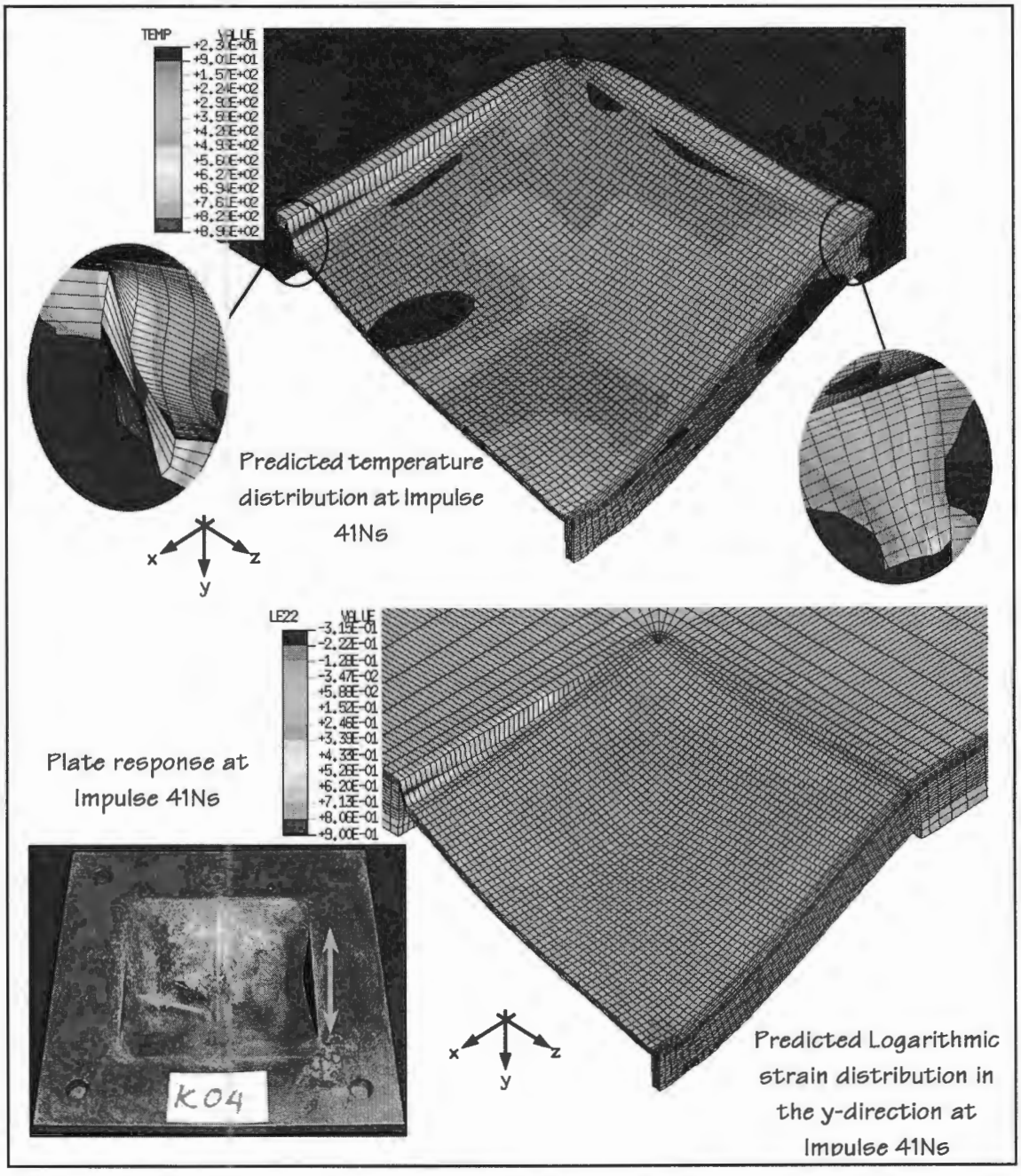

Figure 7.43 : Comparison of predicted Mode II* response of a single stiffened square plate with stiffener size 4x7mm at impulse 41Ns (arrows show plate tearing)

The Mode II* failure of a single stiffened square plate is well predicted by the numerical analysis as shown in Figure 7.43. A logarithmic strain of 90% and a temperature of 896 ^{0}C clearly indicate tearing at the support side parallel to the stiffener. High temperature spots are also formed at the maximum permanent displacement and at the boundary where the stiffener joins the plate; indicating where thinning occurs.

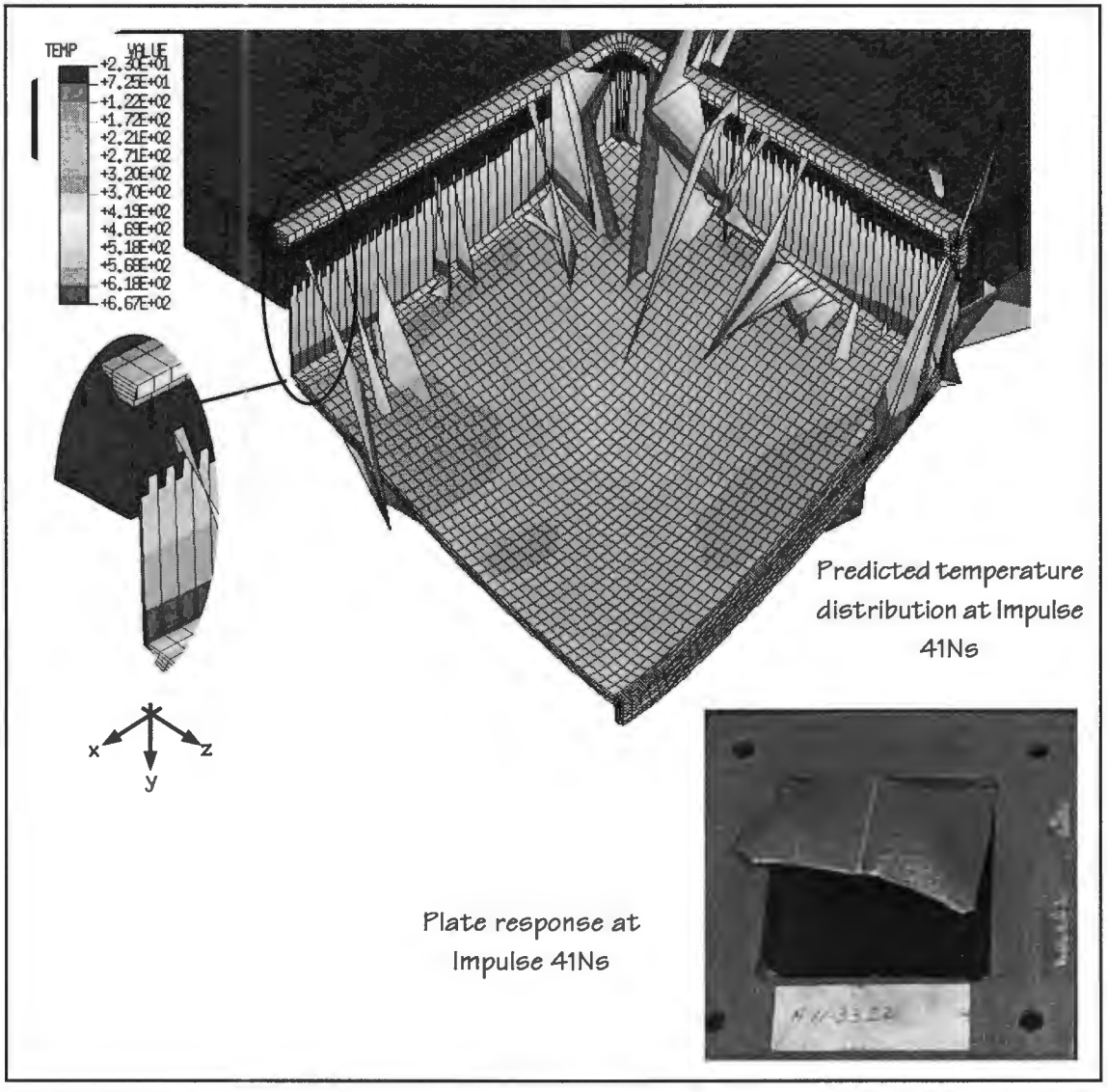

Figure 7.44 : Comparison of predicted Mode II response of a single stiffened square plate with stiffener size 4x3mm at impulse 41Ns

The severe element elongation and element distortion in Figure 7.44 show a Mode II failure of a single stiffened square plate. The distorted elements are failed elements that have undergone an equivalent plastic strain of 200% or more. The numerical analysis compares well with the experiment. Because of symmetry, the model does not exhibit a three torn sides plate as observed in the experiment.

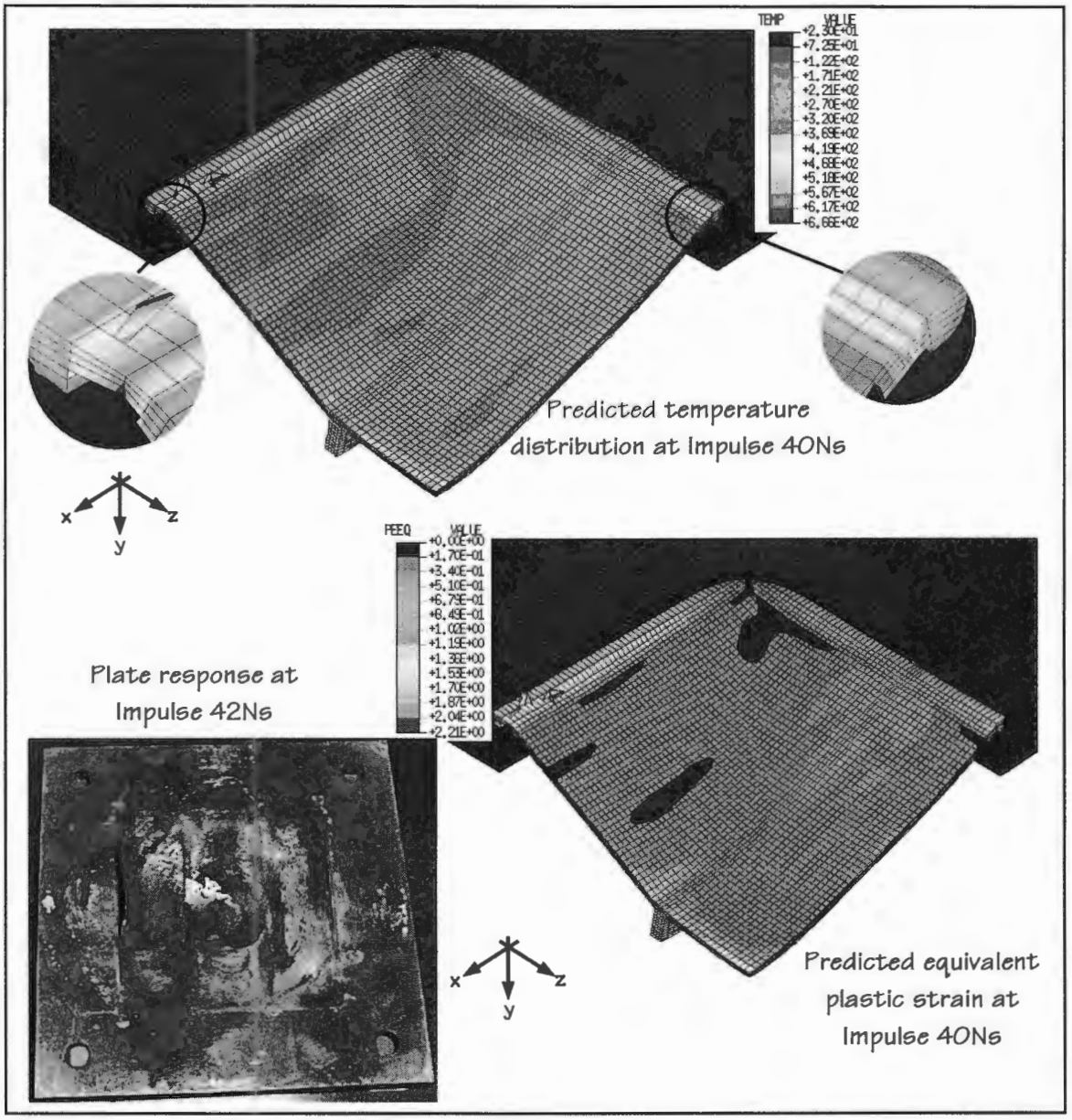

Figure 7.45 : Comparison of predicted Mode II* response of a double stiffened square plate with stiffener size 3x7mm at impulse 40Ns

A partially torn double stiffened square plate (Mode II*) under a uniform impulsive load of 40Ns is modelled and shown in Figure 7.45. The finite element model shows good correlation with the experimental results. Distorted elements due to very high equivalent plastic strain value (221%) and high temperature (666°C) clearly indicate tearing at the middle of the side that is parallel to the stiffeners of the plate. Other high temperature spots without element elongation in the numerical model suggest thinning occurring in the central part of the plate and on the stiffener side closer to the plate boundary.

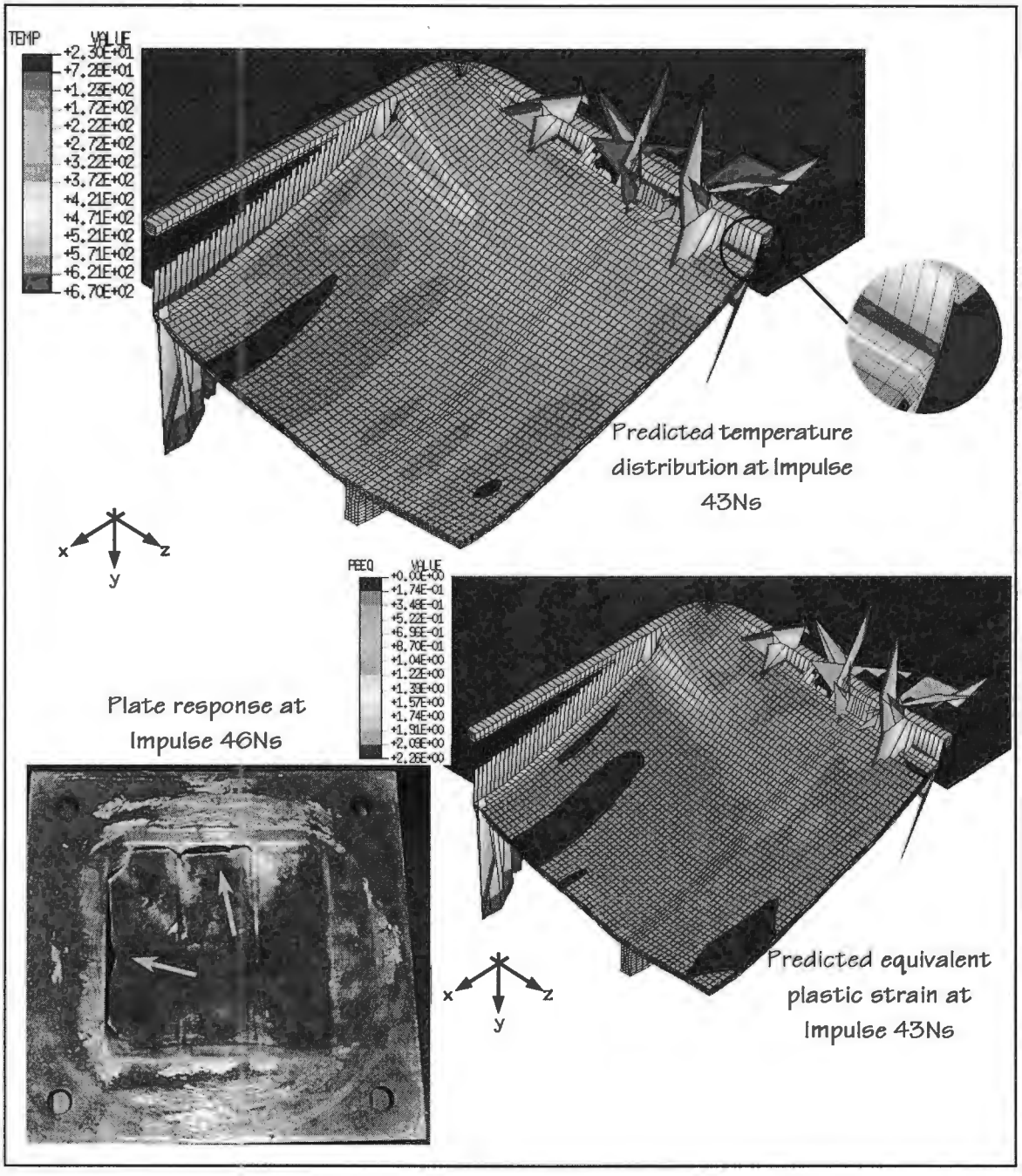

Figure 7.46 : Comparison of predicted Mode II response of a double stiffened square plate with stiffener size 3x7mm undergoing at impulse 43Ns

The double stiffened square plate model is analysed at higher load intensity. At an impulsive load of 43Ns, the temperature rises up to 670 ^{0}C in localised area at the boundaries. Elements in that localised area either undergo extensive elongation or distort indicating tearing as illustrated in Figure 7.46. The numerical analysis compares well with the experiment. The model indicates that failure occurs across the corner of the plate.

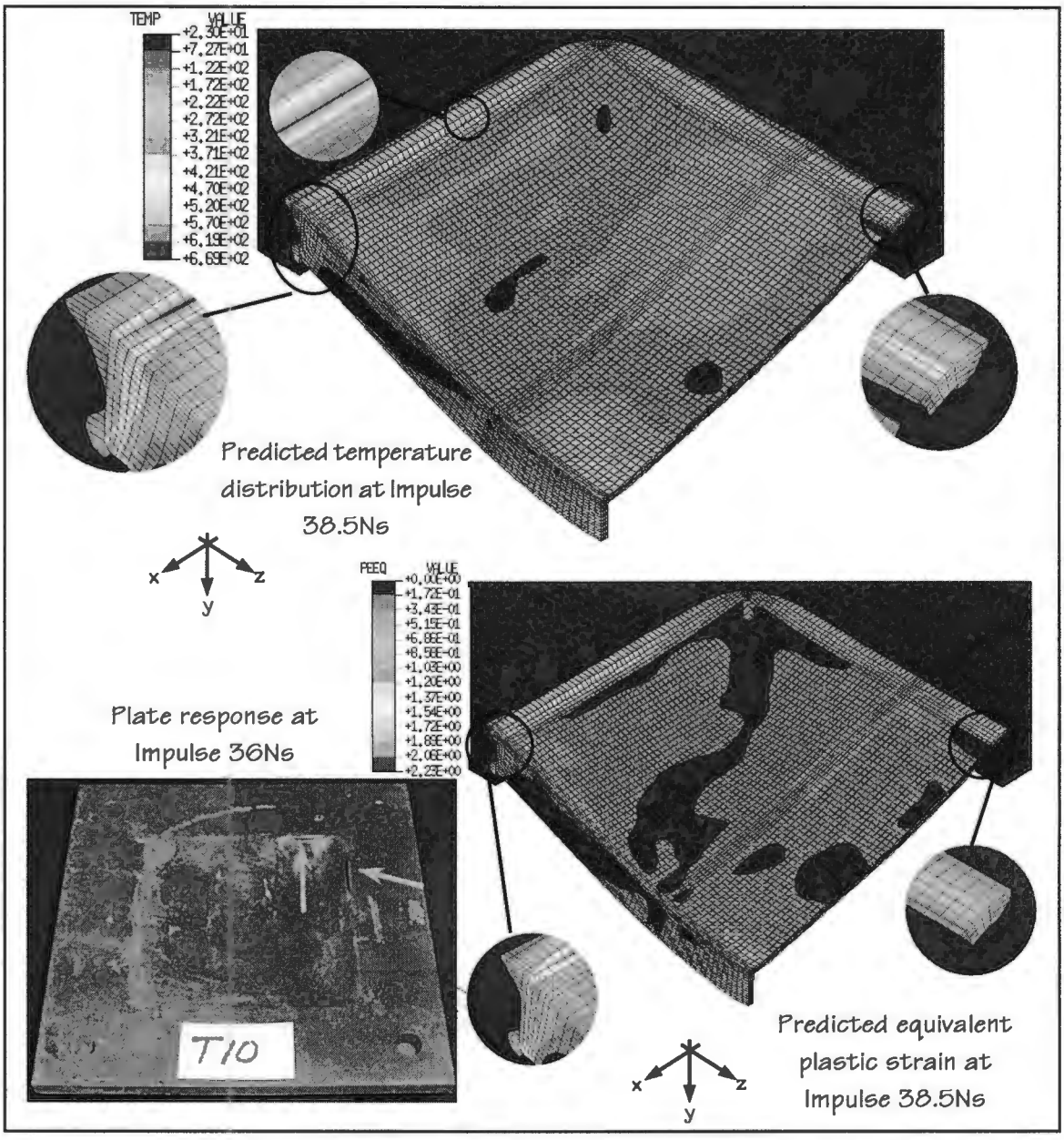

Figure 7.47 : Comparison of predicted Mode II* response of a double cross stiffened square plate with stiffener size 3x7mm at impulse 38.5Ns

Figure 7.47 illustrates a comparison of the numerical analysis and experimental test of a double cross stiffened square plate that undergoes a uniform load intensity of 38.5Ns. The numerical analysis predicts very high equivalent plastic strain values of 223% and temperature of 669°C at a localised area of the plate side parallel to the double stiffeners. The model predicts tearing at the sides parallel to the two stiffeners with good accuracy. A high temperature band at the boundary of the stiffener that runs across the two parallel stiffeners reveals that the cross stiffener is on the verge of tearing.

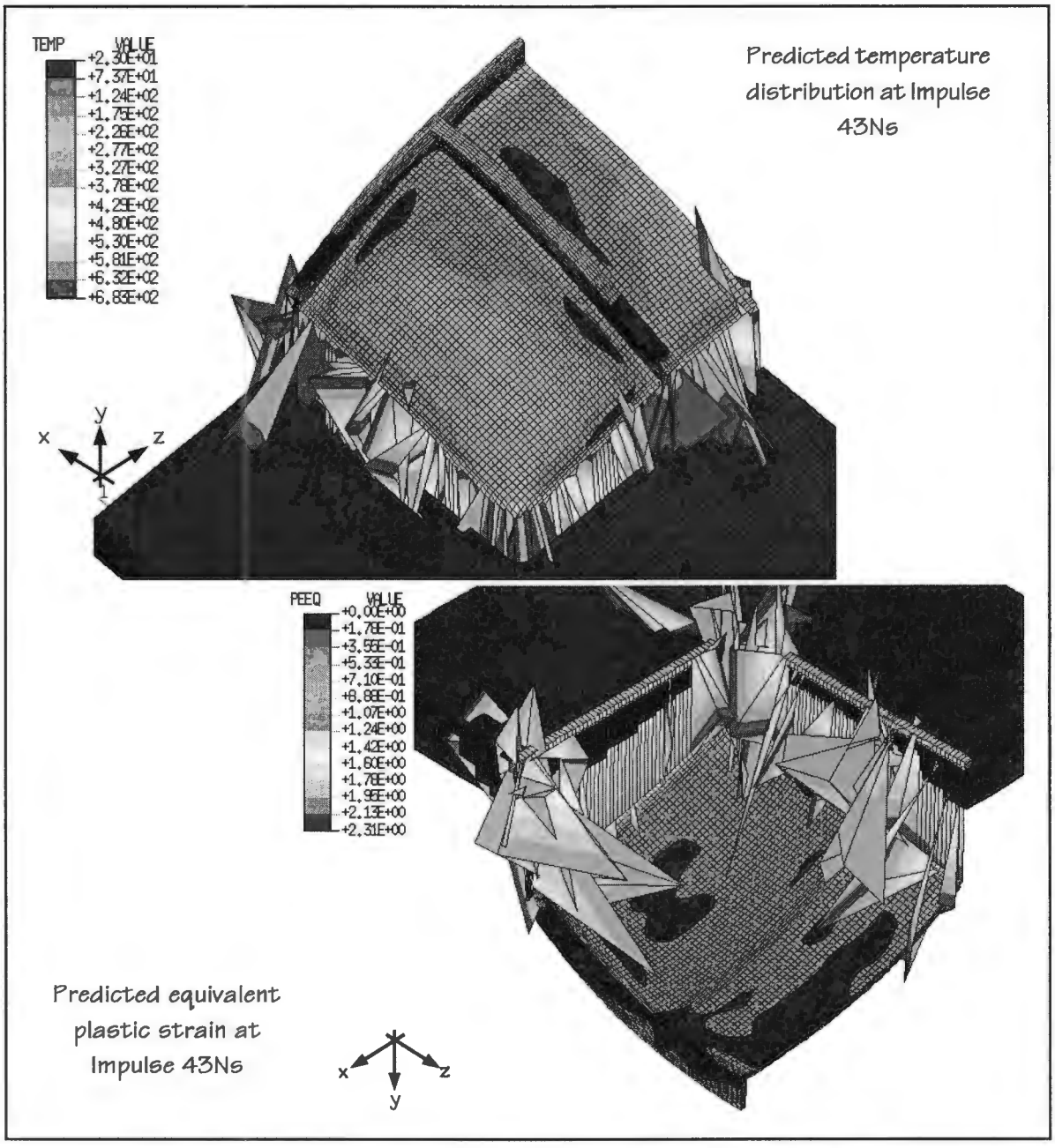

Figure 7.48 : Prediction Mode II response of a double cross stiffened square plate with stiffener size 3x7mm at impulse 43Ns

In Figure 7.48 the prediction shows how the double cross stiffened plate will fail in Mode II. The elements around the boundary are all distorted due to the fact that they have exceeded the shear failure criterion of 200%. The predicted equivalent plastic strain around the boundary is of the order of 213% and the temperature is as high as 632^{0}C. No experimental data is available to compare with the model.

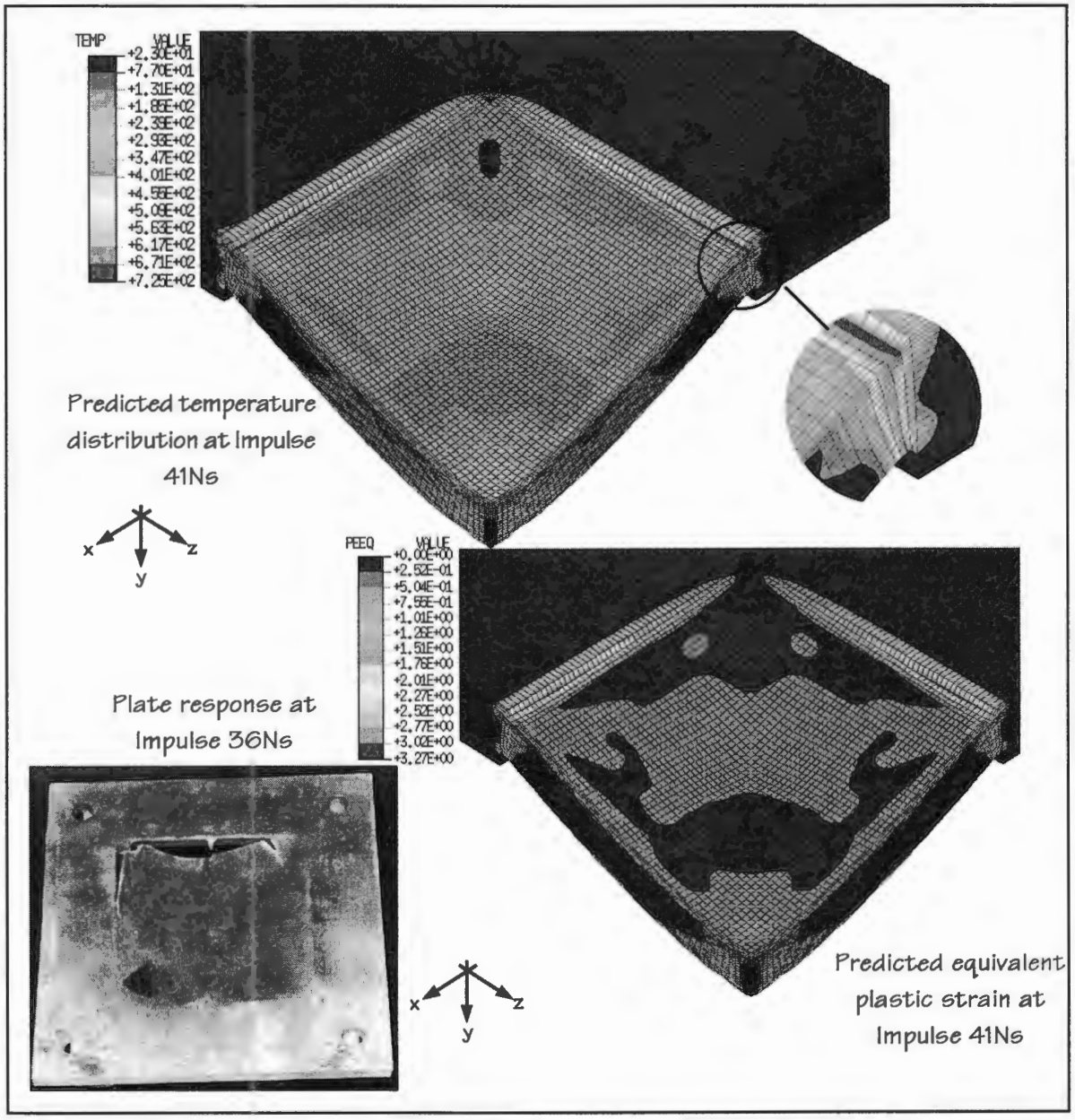

Figure 7.49 : Comparison of predicted Mode II* response of a cross stiffened square plate with stiffener size 3x7mm at impulse 41Ns

An analysis of the temperature and strain predicted by the model of a cross stiffened square plate at an impulse of 41Ns; as seen in Figure 7.49; confirms failure at the boundary of the plate. The numerical model compares well with the experiment. The model also shows thinning of both the plate and the stiffener at the central area of the plate.

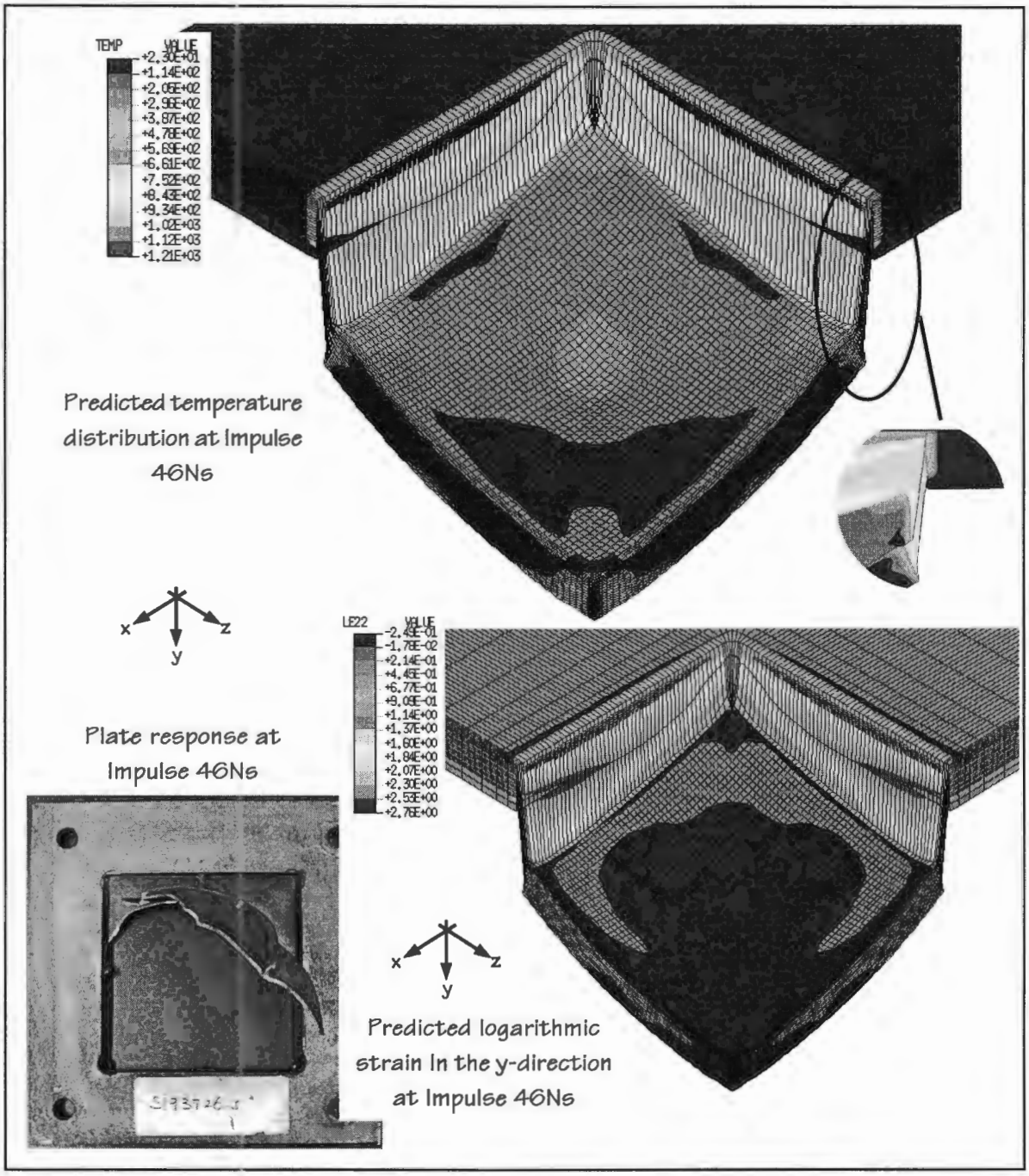

Figure 7.50 : Comparison of predicted Mode II response of a cross stiffened square plate with stiffener size 3x7mm at impulse 46Ns

At logarithmic strain of 276% in the y-direction and temperature of 1000°C, the model predicts Mode II failure at the boundary of the cross stiffened square plate where the elements are severely elongated as shown in Figure 7.50. The result compares well with the experimental result in which three sides of the cross stiffened plate tore. Experimentally, it is difficult to get all four sides of the plate to tear due to the difficult loading conditions.

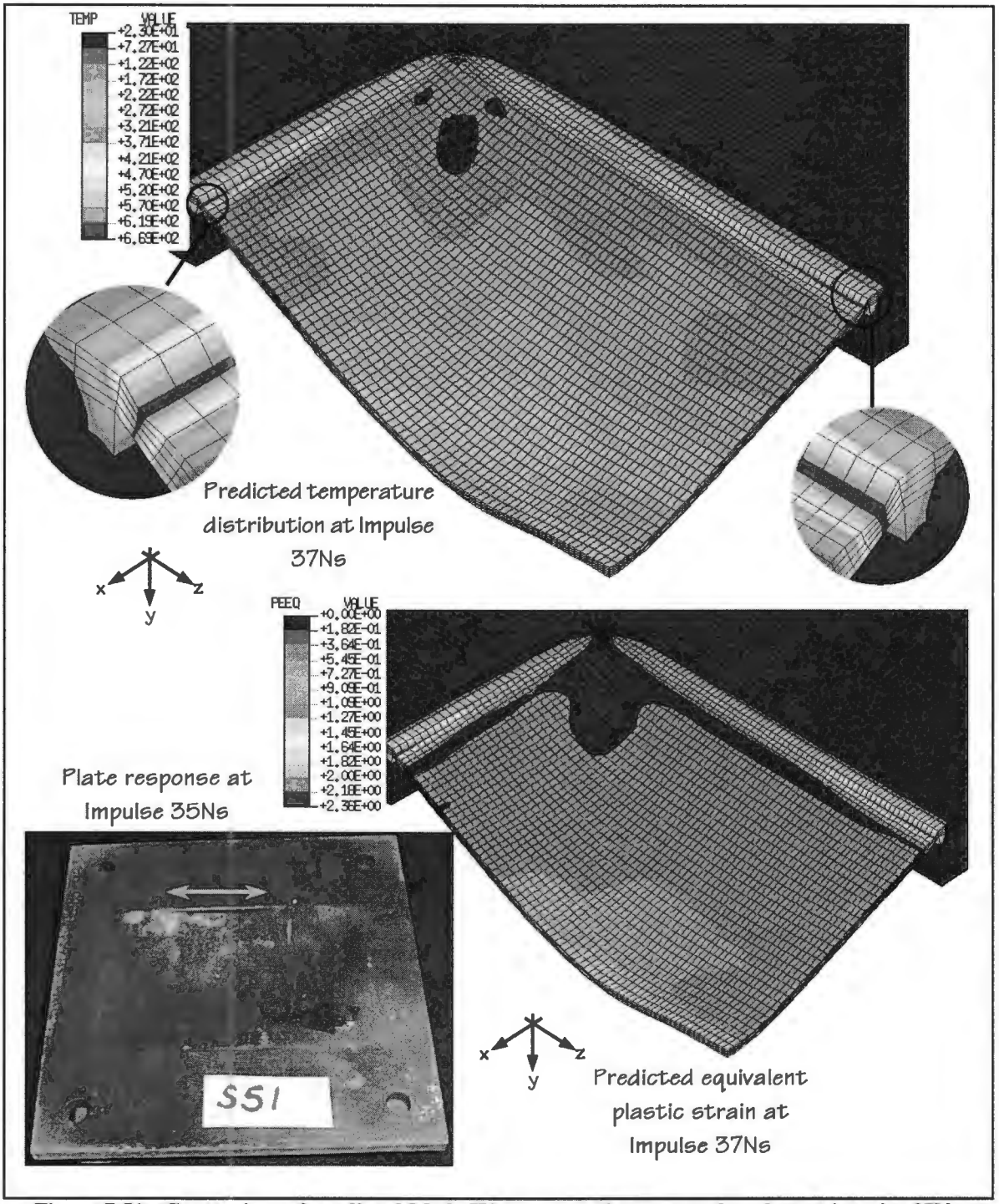

Figure 7.51 : Comparison of predicted Mode II* response of a rectangular plate at impulse 37Ns

At an impulse of 37Ns, high equivalent plastic strain (236%) and high temperatures (669^{0}C) through the plate thickness at the boundary indicates failure to occur at both sides of the rectangular plate as shown in Figure 7.51. A good correlation between the prediction and the experiment is achieved.

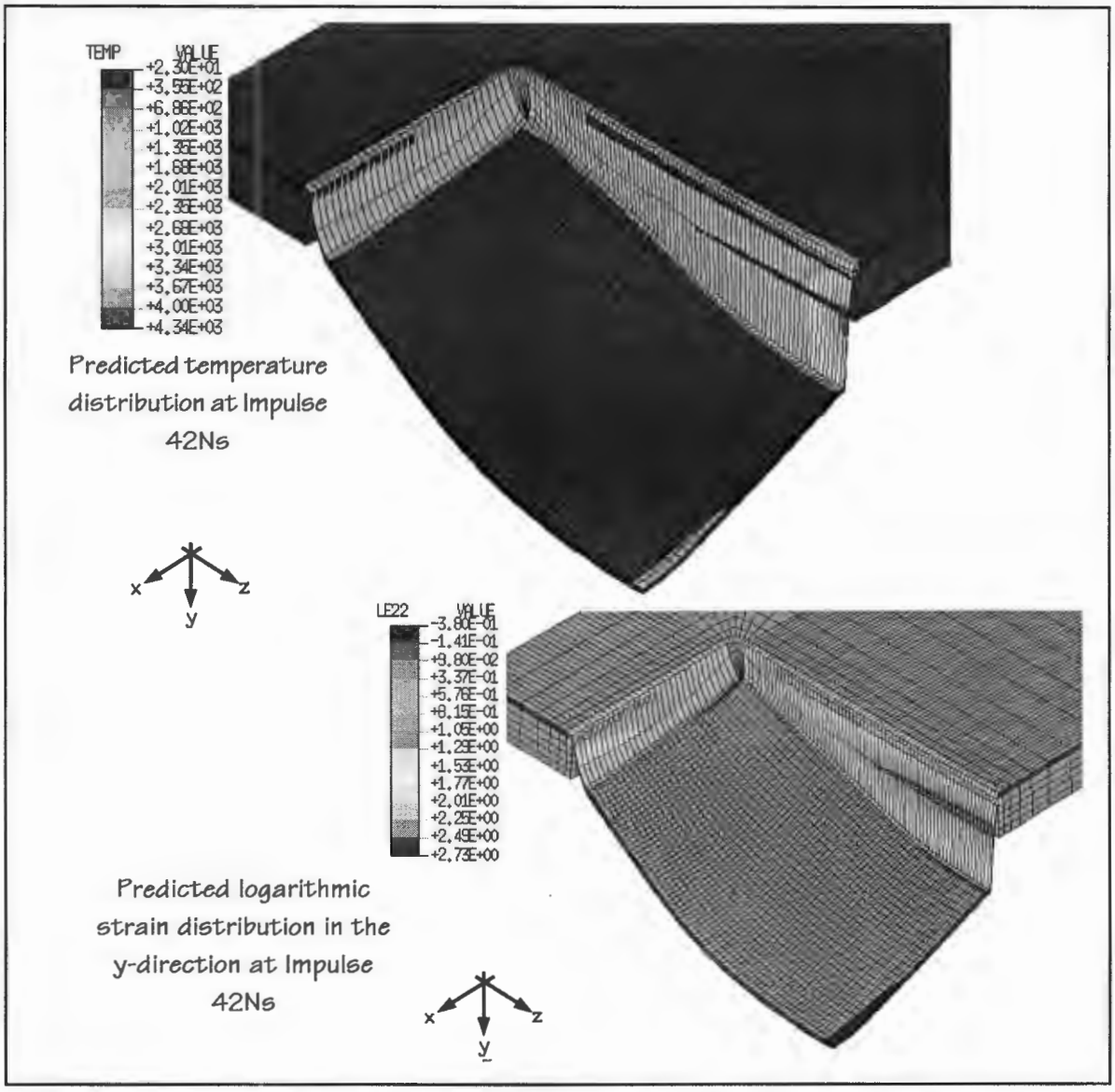

Figure 7.52 : Prediction Mode II response of a double stiffened rectangular plate with stiffener size 3x7mm at impulse 42Ns

Figure 7.52 illustrates the prediction of a typical Mode II failure of a rectangular plate at an impulsive load of 42Ns. The severe element elongation at temperatures of the order of 1350^0C around the boundary together with strain of over 129% illustrates that the plate will shear at both sides of the boundary. No experimental data is available to compare with the model data. In the impulse range from 37Ns to 42Ns, the length of tear at the boundary increases.

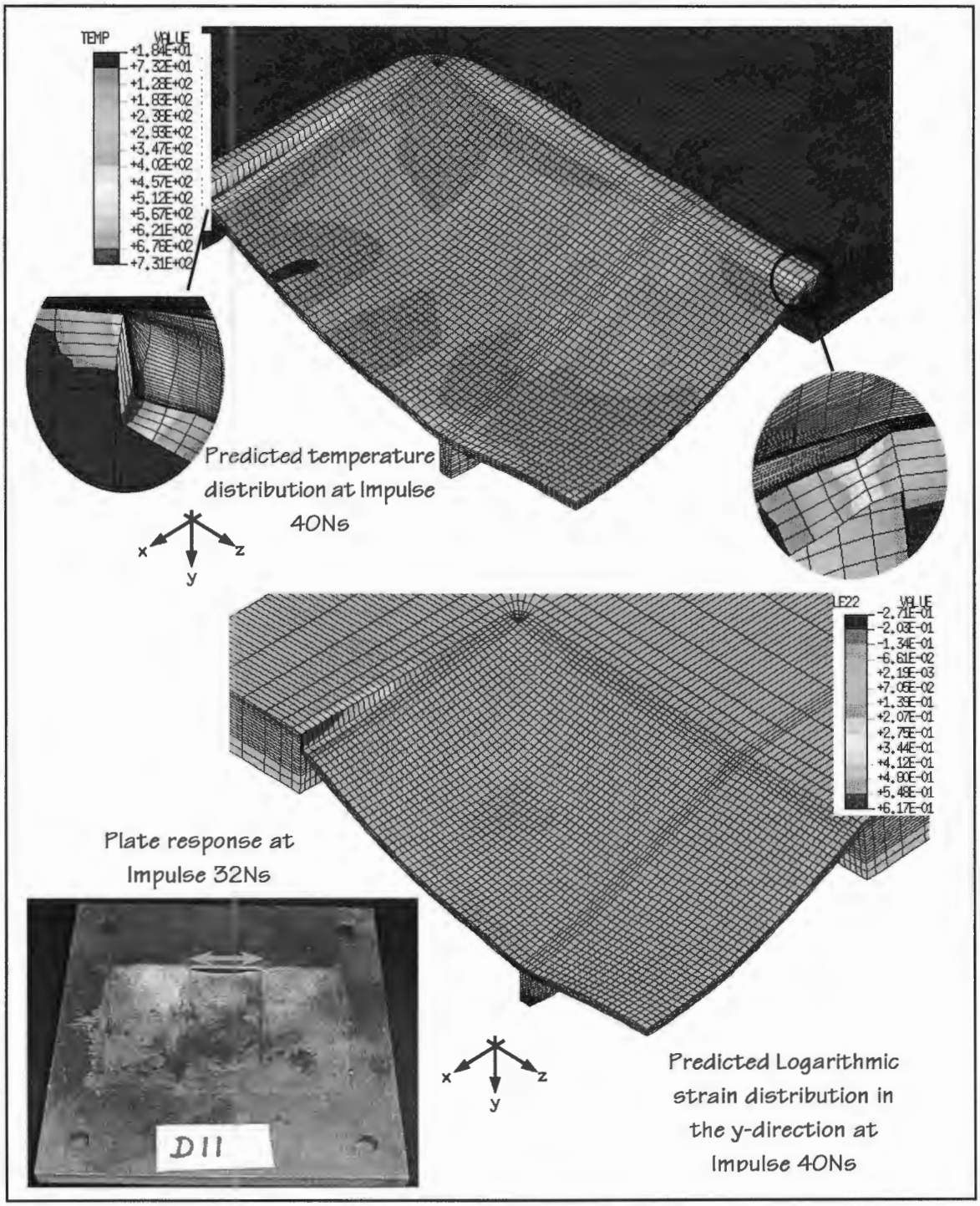

Figure 7.53 : Comparison of predicted Mode II* response of a double stiffened rectangular plate with stiffener size 3x7mm at impulse 40Ns

The prediction of tearing of the double stiffened rectangular shows a slightly different trend from the experimental result as shown in Figure 7.53. The model predicted tearing along the short side of the rectangular plate whereas tearing is observed along the longest side of the plate. This might be a phenomenon which needs more investigation or tearing may have happened as a result of machining of the plate.

Connolly[16], however, observed that tearing of the stiffened rectangular plates first occurred along the short side of the plate (tearing occurs along a boundary closest to the maximum deflection of the plate). Thus, the prediction correlates well with Connolly's results[16] . However, Connolly[16] used clamped plates in his investigation.

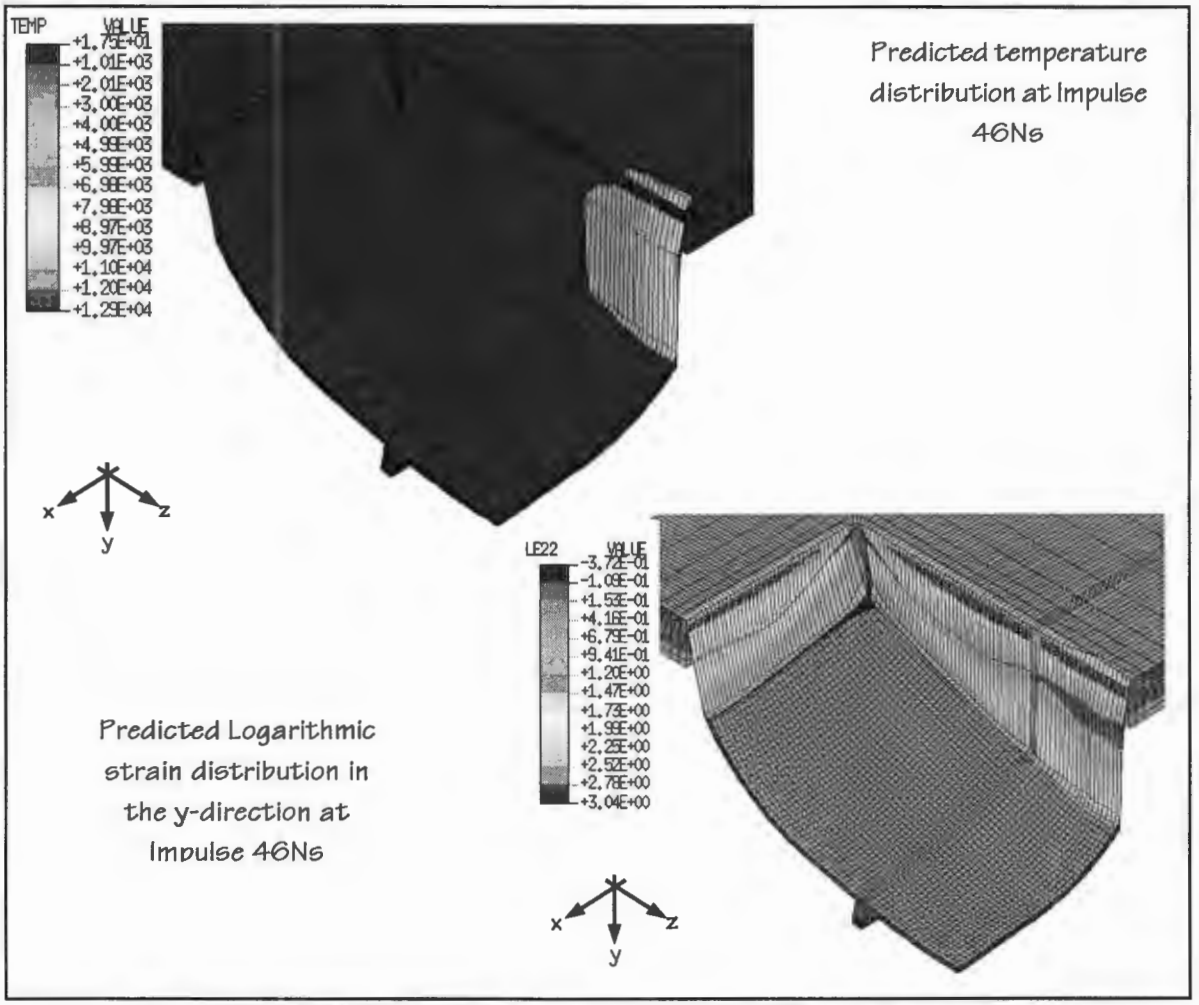

Figure 7.54 : Prediction Mode II response of a double stiffened rectangular plate with stiffener size 3x7mm at impulse 46Ns

Shown in Figure 7.54, is the response of a double stiffened rectangular plate to an impulse of 46Ns. The severe elements elongation at the boundary indicates Mode II failure. The logarithmic strain in the y-direction in the localised area is over a 100%. In the impulse range from 40Ns to 46Ns, the length of tear at the boundary gradually increases.

Table 7.8 shows the predicted maximum displacement and critical impulse at the onset of Mode II failures. It can be seen that the predicted impulse at which Mode II failures will occur is highly dependent on the maximum central displacement of the plates which in turn is dependent on the configuration and size of stiffener (see Figure 7.55). As the size of the stiffener increases or the plate structure becomes stiffer the maximum central displacement prior to the Mode II failure decreases. These results correlate well with experimental results obtained by Olson[14, 15] and Shave[22]. However, the impulses at which the onset of failure occurs are similar for all cases.

Plate configuration	Impulse (Ns)	Maximum central displacement (mm)
S	38.5	32.8
S-SS 3x3	36	28
S-DS 3x3	37	27.8
S-SS 3x7	38	25.7
S-DS 3x7	39	23.8
S-CS 3x7	39	22.2
S-DCS 3x7	37.5	20.2
S-SS 4x7	37	23.8

Table 7.8 : Predicted maximum displacement at the onset of tearing

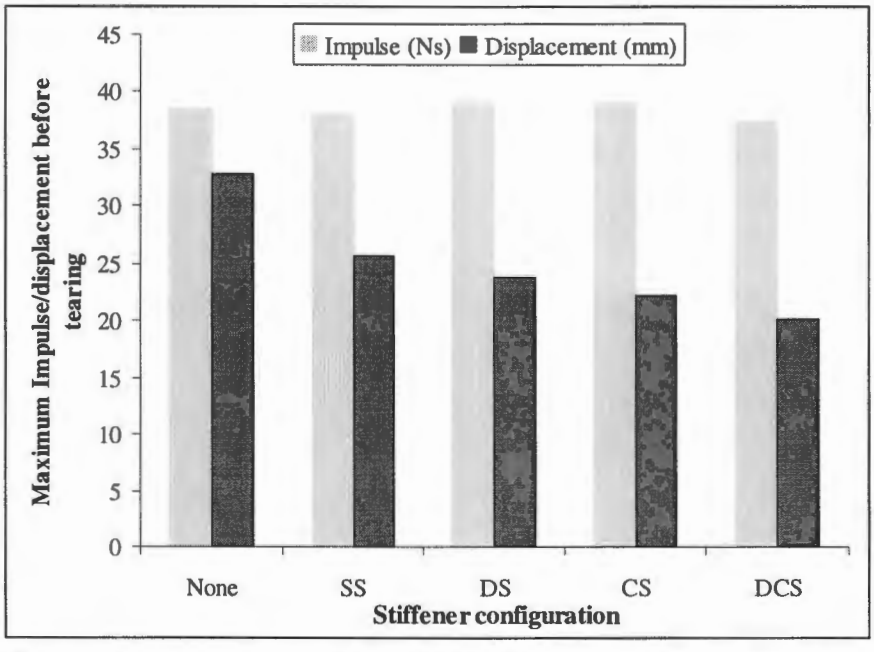

Figure 7.55 : Bar chart showing maximum impulse and displacement before tearing occurs for plates with different stiffener configurations and stiffener size 3x7mm

8.0 Conclusions

The deformation and tearing of uniformly blast-loaded quadrangular stiffened plates were investigated experimentally and numerically with emphasis laid on the effect of the stiffener sizes and configurations. Two finite element models were applied using material properties that included and excluded temperature dependency. Based on the findings of this investigation, the following conclusions may be drawn:

Mode of failure

The results obtained from this experimental investigation show that the plates exhibit essentially Mode I failure (permanent larger deformation) and only a few cases of Mode II failure (tensile tearing at supports) as previously observed for circular plates. Other phases in the Mode II failure region are also exhibited. These include Mode II-1, Mode II-2 and Mode II-3 which designate Mode II failure at the number of sides of the plate that tore and Mode II* which is defined where partial tearing of the boundary occurs. No Mode III failure (transverse shear at supports) is observed for any plate geometry.

Mode I failure

Deflection appears to be dependent on both stiffener sizes and configurations. As expected, for a specific size and configuration of stiffeners for the same plate geometry, permanent deflection increases with increasing impulse for Mode I failure. However, the central maximum displacement decreases as the stiffener height increases from 0 to 7mm, and the overall plate profile changes especially along the centre line that lies across the stiffener. As the stiffener size increases the central area over which the maximum displacement occurs increases resulting in a relatively flat peak at the highest point of deflection.

Furthermore, the shape and maximum central displacement of a deformed plate are highly dependent on the stiffener arrangement; the cross stiffened square plates deform less than the double stiffened square plates despite the fact both configurations have two stiffeners.

For a given plate geometry with stiffeners of the same size, the maximum mid-point displacement decreases as the number of stiffener increases. From single stiffened square plates to double cross stiffened square plates a reduction of about 20% in maximum mid-point displacement is achieved for the same load intensity.

For unstiffened rectangular plates, the highest point of deflection occurs at either side of the centreline of the longest sides. However, for the double stiffened rectangular plates, the highest point of deflection occurs in the central area of the plate.

THINNING MECHANISM

Thinning at the boundary is observed for all plates irrespective of stiffener sizes and configurations but is not consistent all around the boundary.

However, thinning at any other part of the plate seems to be dependent on the stiffener configuration. Plate thinning at the stiffener is observed only for double and double cross stiffened plates. In all such cases, the plate only thins at the side of the stiffener that is closest to the boundary. No sign of thinning is observed between the parallel stiffeners.

Thinning of the stiffener is only observed in the case where two stiffeners cross each other perpendicularly; cross stiffened and double cross stiffened plates. Thinning only takes place at the top of the stiffener. No thinning is observed for the one way stiffeners.

Mode II failure

Tearing always occurs first at the centre of one side of the non-stiffened square plates. However, for single or double stiffened square plates tearing first takes place at the centre of one of the sides parallel to the stiffeners whereas for rectangular plates, tearing first occurs at the centre of one of the longest sides.

These Mode II failures (tensile tearing) are found to be a function of maximum displacement of the plate irrespective of the stiffener sizes and stiffener configurations. The maximum central displacement associated with these failures decreases as the stiffness of the plate increases.

During the Mode II failures the torn sides of the plate exhibited a "pulling-in" near its centre. This "pulling-in" apparently results from the deformation of the plate and seems to be a function of the length of the tear.

Finite element results

The explicit solution scheme in ABAQUS has proved to be successful in the analysis of stiffened quadrangular plates exposed to uniform blast loads, which involves highly non-linear material and geometric behaviour provided the parameters such as mesh density, material properties and element types are incorporated properly.
Correlation between the predicted results and the experimental data is very close.

This numerical investigation has highlighted the benefits of using the new approach to include temperature effects in the modelling of structures, such as plates, undergoing blast loads. The results obtained are very encouraging. So far, no other model has shown such good correlation especially for cases where tearing is involved.

The numerical solutions that include temperature dependent material properties show that plate failure involves a thermo-mechanical cycle whereby at localised areas, increasing strain results in increasing temperatures causing the material to weaken. The degraded material properties result in strain and temperature values high enough to indicate the occurrence of thinning or tearing.

MODE I PREDICTION

The analysis for Mode I failure is investigated using material properties that include and exclude temperature dependence in conjunction with a strain rate effect. In both cases, Mode I failure is well predicted for the various stiffener configurations and sizes for the different quadrangular plates. No sign of very high strain localisation at the boundary or in the central region of the plate is exhibited by the simulations. Comparisons with experimental data for mid-point deflection, contour plot and structure profiles exhibit a close relationship for the full range of impulses tested. However, in all cases the model using material properties that include temperature dependency compares slightly better than the model that uses material properties that exclude temperature dependency. The latter is due to the weakening of the material properties as the temperature increases.

MODE II PREDICTION

In the analysis, the prediction for Mode II failure is based on a criterion of maximum equivalent plastic strain and works in conjunction with a strain rate effect and temperature dependent effect. This failure mode is predicted to occur first at the middle of the side boundaries at a critical impulse. For higher impulses, complete tearing of the boundaries is predicted to occur by means of high strain and temperature values or severely elongated elements or distorted elements caused by the imposition of an unrealistic strain of 200% failure strain criterion. The experimental evidence provided herein compares favourably with the predicted Mode II failures.

The predicted critical impulse for Mode II failure at the boundary was found to be independent of the stiffener size. However, the predicted central displacement associated with these failures did decrease with increasing stiffener size.

9.0 Recommendations

As a result of the findings and conclusions of this report, the following recommendations are made:

- Further tests at load intensities that would cause the plate to tear should be carried out to investigate the link between the "pulling-in" of the torn side of the plate and the stiffener sizes and configurations. Additional tests should be done to investigate Mode III failures of stiffened plates.

- The effect of the stiffener configurations on thinning mechanisms should also be investigated further.

- The effect of stiffener configuration on the material failure should be extended to include other plate geometries and stiffener geometries (T-beam for example), and further other stiffener arrangements with the stiffener running along the plate diagonals where plastic hinges occur.

- Other type of loading conditions such as localised blast loads or explosives loaded on the side of the plate where the stiffeners are should be investigated.

- The finite element model should be further investigated using technique that implements the Jones-Wilkins-Lee (JWL) equation of state to determine the material behaviour of the explosive. Thereafter, apply a contact to contact boundary interaction between the explosive and the plate to model the plate response as opposed to the pressure loading technique used herein.

- Despite the fact that the strain rate and temperature dependence have given good results further investigations should be done on the effect of the strain rate on the temperature dependence of material properties and vice versa.

10.0 References

1. Nurick, G. N. and Martin, J. B., Deformation of thin plates subjected to impulsive loading - a review. Part I: Theoretical considerations, *International Journal of Impact Engineering*, 1989, **8** (2), 159-169.

2. Nurick, G. N. and Martin, J. B., Deformation of thin plates subjected to impulsive loading - a review. Part II: Experimental Studies, *International Journal of Impact Engineering*, 1989, **8** (2), 171-186.

3. Menkes, S. B. and Opat, H. J., Tearing and shear failures in explosively loaded clamped beams, *Explosion Mechanics*, **13**, 480-486 (1973).

4. Thomas, B. M. and Nurick, G. N., The effect of boundary conditions on thin plates subjected to impulsive loads, *The 5th International Symposium on Plasticity and its Current Application*, Osaka, Japan, July 1995, pp 85-88.

5. Chung Kim Yuen, S. and Nurick, G. N., The significance of the thickness of a plate when subjected to localised blast load, *16th International Symposium on Military Aspects of Blast and Shock, (MABS16)*, Oxford, UK, 10-15 September 2000, pp 491-499.

6. Schubak, R. B., Olson, M. D. and Anderson, D. L., Rigid-plastic modelling of blast loaded stiffened plates – Part I: one way stiffened plates, *International Symposium on Structural Crashworthiness and Failure*, Liverpool, UK, 14-16 April 1993.

7. Schubak, R. B., Olson, M. D. and Anderson, D. L., Rigid-plastic modelling of blast loaded stiffened plates – Part II: partial end fixity, rate effects and two-way stiffened plates, *International Symposium on Structural crashworthiness and Failure*, Liverpool, UK, 14-16 April 1993.

8. Houlston, R. and DesRochers, C. G., Non-linear structural response of ship panels subjected to air-blast loading, *Computers and Structures*, 1987, Vol 26, pp 1-15.

9. Nurick, G. N., The prediction of the deformation response of a structure subjected to an explosive load using a light interference technique, *Proceedings of the SEM Spring Conference on Experimental Mechanics*, 1986, 105-114.

10. Radford, A. M. and Nurick, G. N., Circular plates subjected to localised central blast loads, *Transient loading and response of structures*, An International Symposium Honouring Mr Arnfinn Jenssen, Trondheim, Norway, 25-27 May 1998, pp 503-548.

11. Bimha, R. E., Nurick, G. N. and Mitchell, G. P., Modelling the deformation of blast-loaded stiffened square plates, *Proceedings of the 1st South African Conference on Applied Mechanics (SACAM) '96*, Midrand, South Africa, 1 - 5 July 1996.

12. Teeling-Smith, R.G. and Nurick, G. N., The deformation and tearing of thin circular plates subjected to impulsive loads, *International Journal of Impact Engineering*, 1991, **11** (1) 77-91.

13. Nurick, G. N. and Lumpp, D. M., Deflection and tearing of clamped stiffened circular plates subjected to uniform impulsive blast loads, *Structures Under Shock and Impact (SUSI) IV*, (Ed N Jones, CA Brebbia, AJ Watson), Published by Computational Mechanics Publications, pp 393-402, 1996.

14. Olson, M. D., Fagnan, J. R. and Nurick, G. N., Deformation and Rupture of Blast Loaded Square Plates - Predictions and Experiments, *International Journal of Impact Engineering*, 1993, **12** (2), 279-291.

15. Nurick, G. N., Olson, M. D., Fagnan, J. R. and Levin, A., Deformation and tearing of blast-loaded stiffened square plates, *International Journal of Impact Engineering*, 1995, **16** (2), 273-291.

16. Nurick, G, N. and Conolly, A. G., Response of clamped single and double stiffened rectangular plates subjected to blast loads, *Structures Under Shock and Impact (SUSI)*, (Ed P Bulson), Published by Computational Mechanics Publications, pp 207-220, 1994.

17. Farrow, G. H., Nurick, G. N., Mitchell, G. P., Modelling of impulsively loaded circular plates using the ABAQUS finite element code, *Proceeding 13th Symposium Finite element methods in South Africa*, Stellenbosch, South Africa, Jan 18-20, 1995.

18. Schleyer, G. K., Hsu, S. S. and White, M. D., Blast loading of stiffened plates: Experimental, analytical and numerical investigations, *Structures Under Extreme Loading Conditions*, (Ed by HS Levine), published by ASME, PVP-Vol 361 , 1998.

19. Shen, W. Q. and Jones, N., Dynamic response and failure of fully clamped circular plates under impulsive loading. *International Journal of Impact Engineering*, 1993, **13** (2), 259-278.

20. The Steel Construction Institute, The effects of simplification of the explosion pressure-time history, *British Gas Research and Technology*,1992.

21. Youngdahl, C. K., Correlation parameters for eliminating the effect of pulse shape on dynamic plastic deformation, *ASME J. Appl. Mech.*, Vol. 37, No. 3, pages 744-752, 1970.

22. Nurick, G. N. and Shave, G. C., Deformation and tearing of thin square plates subjected to impulsive loads, *International Journal of Impact Engineering*, 1996, **18** (1) 99-116.

23. Nurick, G. N., Jones, N. and von Alten-Reuss, G. V., Large inelastic deformations of T-beams subjected to impulsive loads, *Structures Under Shock and Impact (SUSI)*, (Ed P Bulson), Published by Computational Mechanics Publications, pp 191-206, 1994.

24. Schubak, R. B., Olson, M. D. and Anderson, D. L., Non-linear rigid-plastic analysis of stiffened plates under blast loads, *Structures Under Shock and Impact II (SUSII)*, (Ed P Bulson), Published by Computational Mechanics Publications, pp 521-532, 1992.

25. Nurick, G. N., Gelman, M. E. and Marshall, N. S., Tearing of blast loaded plates with clamped boundary conditions, *International Journal of Impact Engineering*, 1996, **18** (7-8), 803-827.

26. Jones, N., Structural Impact, *Cambridge University Press*, 1989.

27. Tollner, M. E. and Nurick, G. N., Predictions of stiffened circular plates subjected to impulsive loads, *Structures Under Extreme Loading Conditions, Fluid-Structure Interaction and Structural Mechanics, Problems in reactor safety*, (Ed by D. M. Jerome), PVP vol.394, 1999.

28. Nurick, G. N. and Jones, N., Prediction of large inelastic deformations of T-beams subjected to uniform impulsive loads, *High Strain Rate Effects on Polymer, Metal and Ceramic Matrix Composites and Other Advanced Materials*, AD-Vol. 48, pp 127- 153,ASME 1995,

29. Wiehahn, M. A., Nurick, G. N. and Bowles, H .C., Some insights into the mechanism of the deformation and tearing of thin plates at high strain rates incorporating temperature dependent material properties, *Structures Under Shock and Impact (SUSI)*, (Ed P Bulson), Published by Computational Mechanics Publications, pp 207-220, 2000.

30. Grobbelaar, W. P. and Nurick, G. N., An investigation of structures subjected to blast loads incorporating an equation of state to model the material behaviour of the explosive, *Proceedings of the 7th International Symposium on Structural Failure and Plasticity (IMPLAST 2000)*, Melbourne, Australia, 4-6 October 2000, pp185-194.

31. Masui, T., Nunokawa, T. and Hiramatsu, T., Shape correction of hot rolled steel using an on line leveller, *Journal of Japan Society for Technology of Plasticity*, (1), 1987.

11.0 Bibliography

1. Bimha, R.E., Response of thin circular plates to central loading, MSc thesis, University of Cape Town (1996).

2. Farrow, G. H., The response of impulsively loaded sandwich plates, MSc thesis, University of Cape Town (1995).

3. Grobbelaar, W., An investigation of structures subjected to blast loads incorporating an equation of state to model the material behaviour of the explosive, MSc thesis, University of Cape Town (1999).

4. Hibbit, Karlson and Sorenson, INC. ABAQUS/Explicit User's Manual Volume 1 v5.8, 1998.

5. Liu, D and Stronge, W.J., Shear and bending deformation of rigid-plastic circular plates by central pressure pulse, *International Journal of Impact Engineering*, 1996, **18** (4), 383-402.

6. Marshall, N.S., Investigate the boundary conditions of impulsively loaded plates, BSc thesis, University of Cape Town (1992).

7. Nurick, G.N., Large deformations of thin plates subjected to impulsive loading, PhD thesis, University of Cape Town (1987).

Results of blast tests

Test Data and results for square plates

Specimen	Mass of Explosive g	Stiffener width w mm	Stiffener height h mm	Thickness mm	Impulse Ns	Dimensionless Impulse ϕ_q	Measured Mid Point Deflection mm	.0471DImp +0.001	deflection/ thickness	Comment
S56	20.5			1.60	31.0	34.9	25.54	16.45	16.01	Mode I deformation
S01	23.5			1.63	43.4	46.7	35.46	0.22	21.73	Partial Tearing

Table A.1 Test Data and results for square plates

Test Data and results for double stiffened square plates

Specimen	Mass of Explosive g	Stiffener width w mm	Stiffener height h mm	Thickness mm	Impulse Ns	Dimensionless Impulse ϕ_q	Measured Mid Point Deflection mm	.0471DImp +0.001	deflection/ thickness	Comment
M73	20.5	3.10	3.00	1.61	36.9	40.8	25.2	19.22	15.65	Mode I deformation
M22	20.5	3.16	6.98	1.61	37.5	41.5	23.01	19.53	14.29	Mode I deformation
M27	23.5	3.14	7.00	1.48	45.9	60.1		28.29		Tearing
M17	25	3.18	6.99	1.61	42.3	46.7		22.02		Tearing // stiffener

Table A.2 Test Data and results for double stiffened square plates

Test Data and results for single stiffened square plates

Specimen	Mass of Explosive g	Stiffener width w mm	Stiffener height h mm	Thickness mm	Impulse Ns	Dimensionless Impulse ϕ_q	Measured Mid Point Deflection mm	.0471DImp +0.001	deflection/ thickness	Comment
A00	10	3.28	2.98	1.63	8.5	9.2	6.15	4.33	3.77	Mode I deformation
A13	16	3.35	3.08	1.62	25.3	27.7	18.56	13.03	11.45	Mode I deformation
A17	19	3.36	2.99	1.60	34.0	38.3	26.53	18.05	16.62	Mode I deformation
A01	20.5	2.96	3.06	1.62	35.8	39.2	30.1	18.45	18.58	Mode I deformation
A03	21.25	3.10	2.96	1.60	37.8	42.6	25.51	20.05	15.99	Partial Tearing
A11	22	3.33	3.02	1.60	40.6	45.9		21.60		Tearing
C01	13	4.16	2.97	1.51	18.1	22.7	11.84	10.68	7.86	Mode I deformation
C03	16	4.10	2.90	1.57	20.0	23.0	12.82	10.85	8.17	Mode I deformation
C13	16	4.16	2.95	1.63	18.9	20.3	12.1	9.54	7.44	Mode I deformation
C04	20.5	4.18	2.97	1.53	27.2	32.9	20.86	15.51	13.61	Mode I deformation
C07	21.25	4.16	2.97	1.61	32.3	35.3	21.74	16.65	13.51	Mode I deformation
C17	22	4.12	2.99	1.55	39.8	47.0	23.96	22.13	15.47	Partial Tearing
K10	19	3.22	6.97	1.60	34.1	38.1	24.709	17.95	15.43	Mode I deformation
K28	22.75	3.14	6.97	1.59	39.0	44.4	26.66	20.91	16.79	Mode I deformation
K24	19	4.14	6.98	1.61	32.9	36.2	19.99	17.05	12.39	Mode I deformation
K03	22	4.10	6.97	1.59	40.5	45.9	26.61	21.64	16.74	Mode I deformation
K04	23.5	4.12	6.99	1.59	41.1	46.5	23.48	21.92	14.76	Partial Tearing

Table A.3 Test Data and results for single stiffened square plates

Test Data and results for double cross stiffened square plates

Specimen	Mass of Explosive g	Stiffener width w mm	Stiffener height h mm	Thickness mm	Impulse Ns	Dimensionless Impulse ϕ_q	Measured Mid Point Deflection mm	.0471DImp +0.001	deflection/ thickness	Comment
T01	20.5	3.10	3.01	1.61	35.8	39.7	24.35	18.71	15.13	Mode I deformation
T02	20.5	3.14	7.01	1.60	36.7	40.9	19.76	19.29	12.32	Mode I deformation
T12	26.5	3.07	7.00	1.60	3.1	3.4	2.44	1.62	1.52	Mode I deformation
T10	26.5	3.12	7.00	1.61	36.0	40.0		18.86		Tearing

Table A.4 Test Data and results for double cross stiffened square plates

Test Data and results for cross stiffened square plates

Specimen	Mass of Explosive g	Stiffener width w mm	Stiffener height h mm	Thickness mm	Impulse Ns	Dimensionless Impulse ϕ_q	Measured Mid Point Deflection mm	.0471DImp +0.001	deflection/ thickness	Comment
T04	20.5	3.10	3.00	1.59	35.9	40.8	25.92	19.20	16.31	Mode I deformation
S43	20.5	3.10	6.98	1.59	35.6	40.4	21.5	19.05	13.53	Mode I deformation
S16	23.5	3.10	6.97	1.59	36.0	40.8	20.84	19.20	13.11	Mode I deformation
S46	25	3.10	6.98	1.58	32.1	36.9	17.01	17.38	10.77	Mode I deformation
S14	25	3.00	7.03	1.59	44.2	50.1	26.95	23.58	16.95	Mode I deformation
S19	26.5	3.10	7.01	1.60	45.8	51.1		24.05		Complete Tearing
S45	28	3.10	7.02	1.61	37.6	41.6		19.59		Tearing

Table A.5 Test Data and results for cross stiffened square plates

Test Data and results for rectangular plates

Specimen	Mass of Explosive g	Stiffener width w mm	Stiffener height h mm	Thickness mm	Impulse Ns	Dimensionless Impulse ϕ_q	Measured Mid Point Deflection mm	.0471DImp +0.001	deflection/ thickness	Comment
S11	21	0.00	0.00	1.61	24.0	26.5	15.83	12.48	9.84	Mode I deformation
S51	24	0.00	0.00	1.63	34.8	37.6	22.76	17.70	13.96	Tearing

Table A.6 Test Data and results for rectangular plates

Test Data and results for double stiffened rectangular plates

Specimen	Mass of Explosive g	Stiffener width w mm	Stiffener height h mm	Thickness mm	Impulse Ns	Dimensionless Impulse ϕ_q	Measured Mid Point Deflection mm	.0471DImp +0.001	deflection/ thickness	Comment
D57	21	3.10	2.99	1.63	29.2	31.5	15.91	14.83	9.75	Mode I deformation
D36	22.5	3.14	2.99	1.63	33.4	36.2	16.45	17.03	10.12	Mode I deformation
D01	21	3.14	6.99	1.61	35.5	39.4	18.46	18.54	11.47	Mode I deformation
D11	22.5	3.12	7.00	1.57	31.8	37.1	20.12	17.49	12.82	Tearing

Table A.7 Test Data and results for double stiffened rectangular plates

Test Data and results for single stiffened square plates (from Olson [15])

Test data and results for square plates

Test No	Stiffener width mm	Stiffener height mm	Plate Thickness mm	Impulse Ns	Dimensionless Impulse ϕ_q	Mid point Deflection mm	Deflection thickness ratio
31109241			1.64	6.36	9.24	8.3	5.06
31109242			1.57	8.20	13.00	9.51	6.06
31109243			1.53	7.89	13.17	8.27	5.41
31109244			1.54	9.13	15.04	9.92	6.44

Table A.8 : Test data and results for square plates from Olson[15]

Test data and results for single stiffened square plates with stiffener size 3x2mm

Test No	Stiffener width mm	Stiffener height mm	Plate Thickness mm	Impulse Ns	Dimensionless Impulse ϕ_q	Mid point Deflection mm	Deflection thickness ratio
30109233	2.96	2.02	1.6	8.20	12.52	8.36	5.23
30109234	3.01	2.03	1.6	7.58	11.57	7.25	4.53
30109235	3.03	2.08	1.57	8.20	13.00	7.91	5.04
30109236	2.98	1.99	1.62	9.44	14.06	9.12	5.63
30109237	3	1.96	1.6	9.13	13.94	8.68	5.43
30109238	3.04	1.95	1.61	7.28	10.98	6.83	4.24
30109240	3.12	1.9	1.62	8.20	12.21	7.8	4.81

Table A.9 : Test data and results for single stiffened square plates with stiffener size 3x2mm from Olson[15]

Test data and results for single stiffened square plates with stiffener size 3x4mm

Test No	Stiffener width mm	Stiffener height mm	Plate Thickness mm	Impulse Ns	Dimensionless Impulse ϕ_q	Mid point Deflection mm	Deflection thickness ratio
23109223	3.24	4.06	1.47	6.66	12.04	8.08	5.50
23109224	3.11	3.98	1.58	7.43	11.63	6.94	4.39
23109225	3.06	3.99	1.58	8.35	13.07	7.87	4.98
23109226	3.11	3.95	1.62	8.05	11.99	7.57	4.67
29109227	3.24	3.94	1.65	10.05	14.43	9.59	5.81
29109228	3.37	3.95	1.55	10.68	17.37	10.41	6.72
29109229	3.04	3.98	1.65	15.22	21.85	14.55	8.82
29109230	3.03	4.06	1.62	14.91	22.20	13.34	8.23
29109231	3.01	3.99	1.63	16.97	24.96	13.88	8.52
29109232	2.99	4.03	1.53	10.05	16.78	9.86	6.44

Table A.10 : Test data and results for single stiffened square plates with stiffener size 3x4mm from Olson[15]

Test data and results for single stiffened square plates with stiffener size 3x9mm

Test No	Stiffener width mm	Stiffener height mm	Plate Thickness mm	Impulse Ns	Dimensionless Impulse ϕ_q	Mid point Deflection mm	Deflection thickness ratio
30099201	2.93	9.04	1.56	9.74	15.64	7.8	5.00
30099202	2.74	9.1	1.5	8.35	14.50	7.06	4.71
30099203	3.03	9.02	1.53	8.97	14.97	7.37	4.82
30099204	2.97	9.01	1.51	9.67	16.57	7.78	5.15
30099205	2.99	9.01	1.51	12.00	20.57	8.84	5.85

Table A.11 : Test data and results for single stiffened square plates with stiffener size 3x9mm from Olson[15]

Test data and results for single stiffened square plates with stiffener size 3x5mm

Test No	Stiffener width mm	Stiffener height mm	Plate Thickness mm	Impulse Ns	Dimensionless Impulse ϕ_q	Mid point Deflection mm	Deflection thickness ratio
05109206	2.8	4.96	1.58	11.17	17.49	13.28	8.41
05109207	3.05	5.06	1.56	10.21	16.40	9.48	6.08
23109208	2.89	4.87	1.55	8.45	13.75	8.2	5.29
23109209	3.13	4.87	1.55	9.13	14.85	8.7	5.61
23109210	2.82	5.03	1.55	13.49	21.94	11.64	7.51
01109211	3.01	4.45	1.57	11.77	18.66	10.86	6.92
01109212	3.01	4.45	1.56	10.05	16.14	9.3	5.96
01109213	3.06	5	1.53	14.28	23.84	13.45	8.79
03109214	3.04	4.82	1.53	7.43	12.40	6.65	4.35
03109215	3.06	4.9	1.58	7.77	12.16	7.64	4.84
03109216	2.82	5.01	1.54	8.35	13.76	7.07	4.59
03109217	2.82	5.01	1.56	8.05	12.93	7.33	4.70
03109218	2.92	4.99	1.59	7.74	11.96	6.96	4.38
03109219	2.86	5	1.59	9.74	15.06	8.7	5.47
05109220	2.92	4.94	1.6	7.43	11.34	6.7	4.19
29109221	2.97	5.13	1.52	10.83	18.32	9.36	6.16
29109222	3.08	4.98	1.55	9.44	15.36	8.97	5.79

Table A.12: Test data and results for single stiffened square plates with stiffener size 3x5mm from Olson[15]

Results of uni-axial tensile tests

The values for forces and displacement were obtained from the "Zwick" machine and converted to stress and strain. The data were plotted on a stress vs strain curve (see Figure A.1) from which the dynamic stress was extrapolated. The static yield stress was then calculated from the dynamic yield stress using the Cowper-Symonds equation.

Specimen	Diameter	Crosshead speed	Yield Force	Strain Rate	Dynamic Stress	Static Stress	% Strain at Failure
	mm	mm/min	N	/s	MPa	MPa	
C2	5.06	100	6630	0.0859	329.7	225.2	35.5
C3	5.02	200	6570	0.1707	331.9	248.6	39.4
C4	5.00	200	6550	0.1673	333.6	250.1	35.5
C5	5.10	200	6840	0.1715	334.8	250.7	34.3
C6	5.04	300	6850	0.2538	343.4	251.9	33.4
C7	5.06	300	6940	0.2434	345.1	253.8	35.3
C8	5.02	100	6460	0.0797	326.4	253.5	34.4
C9	5.00	50	6200	0.0419	315.8	252.0	37.5
C10	5.02	5	5980	0.0046	302.1	260.0	38.4
				Average		**249.5**	**36.0**
A1	5.00	5	5860	0.0045	298.4	256.8	38.2
A2	5.00	50	6070	0.0424	309.1	246.6	34.4
A3	5.06	100	6400	0.0838	318.3	246.6	34.2
A4	5.08	100	6450	0.0900	318.2	245.7	35.7
A5	5.04	150	6380	0.1320	319.8	242.6	32.0
A6	5.00	200	6500	0.1733	331.0	247.8	35.6
A7	5.14	200	6780	0.1631	326.7	245.3	37.0
A8	5.06	300	6730	0.2352	334.7	246.6	34.3
				Average		**247.2**	**35.2**

Table A.1 Uniaxial Tensile test results

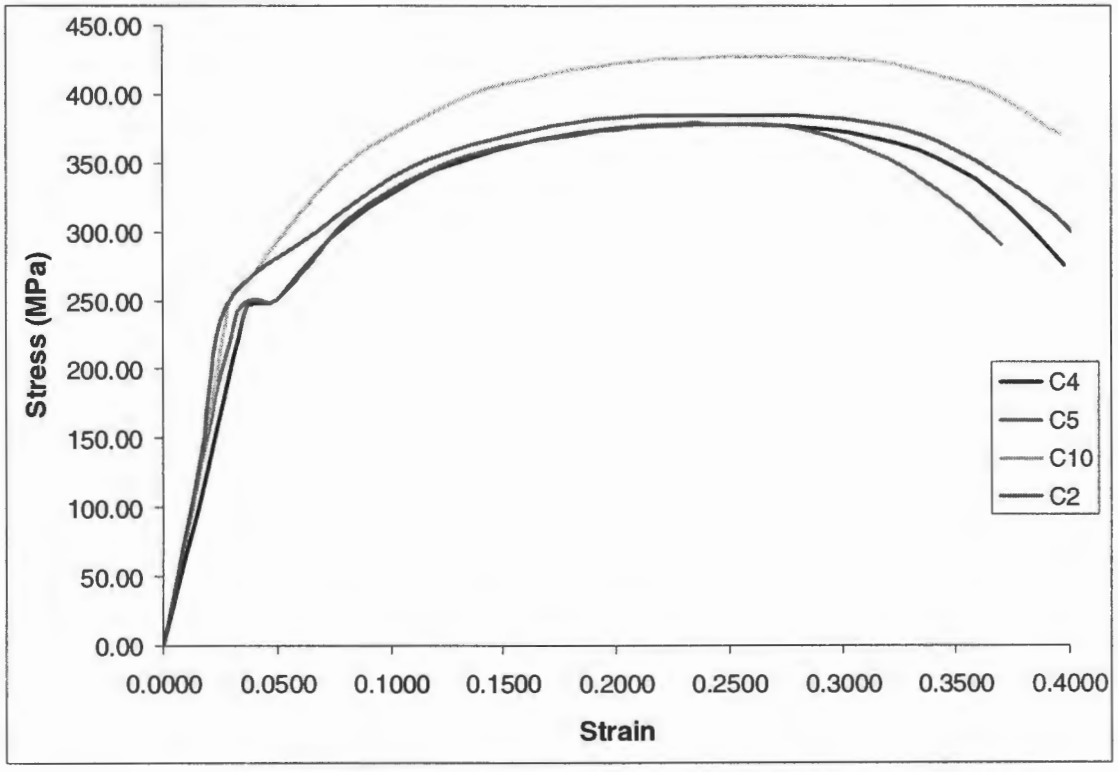

Figure A.1 : Typical stress vs strain curve from uni-axial tensile tests

Ballistic Pendulum

A general set up of the pendulum is shown in Figure C.1.

The linearised equation of motion of the ballistic pendulum, assuming viscous damping is

$$\ddot{X} + 2\beta.\dot{X} + \omega_n^2.X = 0 \qquad \text{(C.1)}$$

where

$$\beta = \frac{C}{2M}\ ,\ \omega_n = \frac{2\pi}{T} \text{ and } \omega_d = (\omega_n^2 - \beta^2)^{1/2}$$

and C is the damping coefficient, M is the total mass of the pendulum including the test rig, I-beam and balancing mass, and T is the natural period of the pendulum.

The solution of the equation C.1 is given by

$$X = \frac{e^{-\beta.t}.\dot{x}_o.\sin(\omega_d.t)}{\omega_d} \qquad \text{(C.2)}$$

where $\dot{x}_o$ is the initial velocity of the pendulum.

Let x_1 be the horizontal displacement at $t = \frac{T}{4}$

and $-x_2$ be the horizontal displacement at $t = \frac{3T}{4}$

Substituting into equation C.2 gives

$$x_1 = \frac{\dot{x}_o.T}{2.\pi}.e^{-0.25\beta.T} \qquad \text{(C.3)}$$

$$x_2 = \frac{\dot{x}_o.T}{2.\pi}.e^{-0.75\beta.T} \qquad \text{(C.4)}$$

Hence $$\frac{x_1}{x_2} = e^{0.5\beta.T} \quad \text{(C.5)}$$

giving $$\beta = \frac{2}{T}\ln\left(\frac{x_1}{x_2}\right) \quad \text{(C.6)}$$

and $$\dot{x}_o = \frac{2\pi}{T}.x_1.e^{0.25\beta.T} \quad \text{(C.7)}$$

The impulse can therefore be calculated from

$$I = M.\dot{x}_o \quad \text{(C.8)}$$

The natural period T is simply determined by averaging a number of measured pendulum oscillations. The damping constant; β; is calculated from equation C.6 where x_1 and x_2 are found from measurements taken from several pendulum oscillations in which the pendulum was drawn back and released.

From the pendulum geometry; (Figure C.1) below, it can be noted that the distance moved by the pendulum and that measured by the pen are not the same, and this must be accounted for.

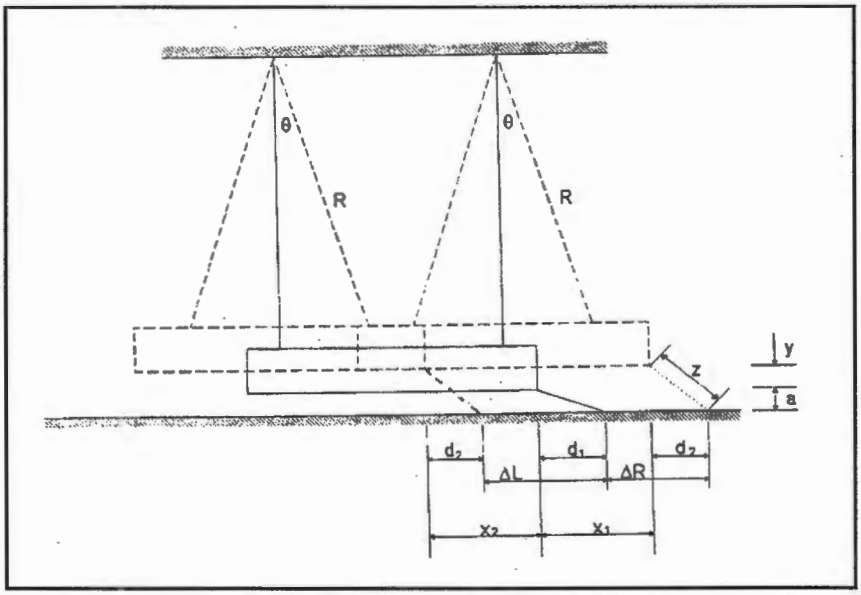

Figure C.1 Ballistic pendulum geometry

Considering Figure C.1, the horizontal distance between the end of the pendulum and the pen when then pendulum is stationary is given by

$$d_1 = (Z^2 - a^2)^{0.5} \quad \text{(C.9)}$$

while at its maximum amplitude, the distance decreases and is given by

$$d_2 = (Z^2 - (a + y)^2)^{0.5} \quad \text{(C.10)}$$

During testing, the pendulum oscillates at a very low amplitude thus giving a very small angle; θ and therefore it can be assumed that

$$x_1 = R.\theta \quad \text{and} \quad y = \frac{R.\theta^2}{2}$$

Hence

$$y = \frac{x_1^2}{2.R} \quad \text{(C.11)}$$

and

$$d_2 = \left(Z^2 - \left(a + \frac{x_1^2}{2.R} \right)^2 \right)^{0.5} \quad \text{(C.12)}$$

From Figure C.1

$$x_1 = \Delta R + d_1 - d_2$$

and

$$x_2 = \Delta L - d_1 + d_2$$

Substituting for d_1 and d_2, we have

$$x_1 = \Delta R + (Z^2 - a^2)^{0.5} - \left(Z^2 - \left(a + \frac{x_1^2}{2.R} \right)^2 \right)^{0.5} \quad \text{(C.13)}$$

and

$$x_2 = \Delta L - (Z^2 - a^2)^{0.5} + \left(Z^2 - \left(a + \frac{x_1^2}{2.R} \right)^2 \right)^{0.5} \quad \text{(C.14)}$$

where

ΔL, ΔR, Z, a, and R are measured and therefore x_1 and x_2 can be calculated.

Table C.1 shows the data of ballistic pendulum.

Mass of I-Beam	28155g
Mass of Clamping Rig	15385g
Mass of Counter Balance	23690g
Total Pendulum Mass (M)	67230g
R	2584mm
Z	119.62mm
a	62.7mm
T	3.19s

Table C.1 : Ballistic Pendulum Details

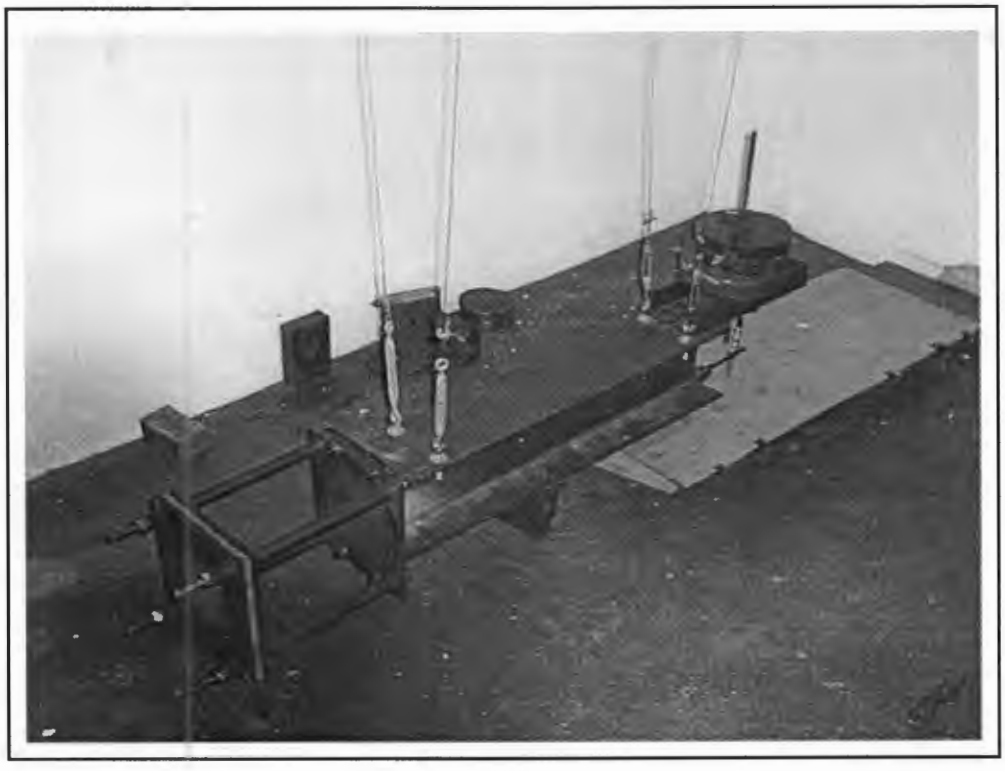

Figure C.2 : Ballistic pendulum

Explosive Layout

The physical layout of the plastic explosive was as used previously by Nurick[2]. For the set of experiments done, two quadrangular sections of areas 159mm x 100mm and 126mm x 126mm were loaded with PE4 of mass ranging from 13 to 26.5g. The dimensions of concentric rectangular annuli were obtained from the calculations shown below. The total exposed area of the test specimen was divided into two equal parts; A_1 and A_2. These two areas were subsequently divided into equal parts again and the appropriate width and breadth was calculated.

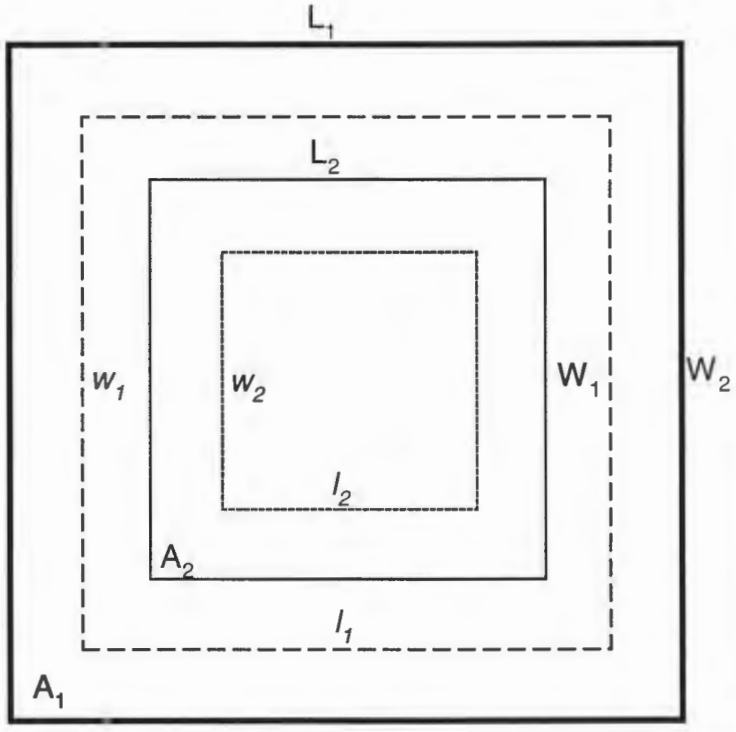

$L_1 W_1 = 2(L_2 W_2)$

$L_1 W_1 = 2(l_1 w_1)$ and $L_2 W_2 = 2(l_2 w_2)$

For the square plates	For the rectangular plates
$L_1 = W_1$	$L_1 = 1.59W_1$
$L_2 = W_2$	$L_2 = 1.59W_2$
$l_1 = w_1$	$l_1 = 1.59w_1$
$l_2 = w_2$	$l_2 = 1.59w_2$

Plate Geometry

E.1 Square Plate

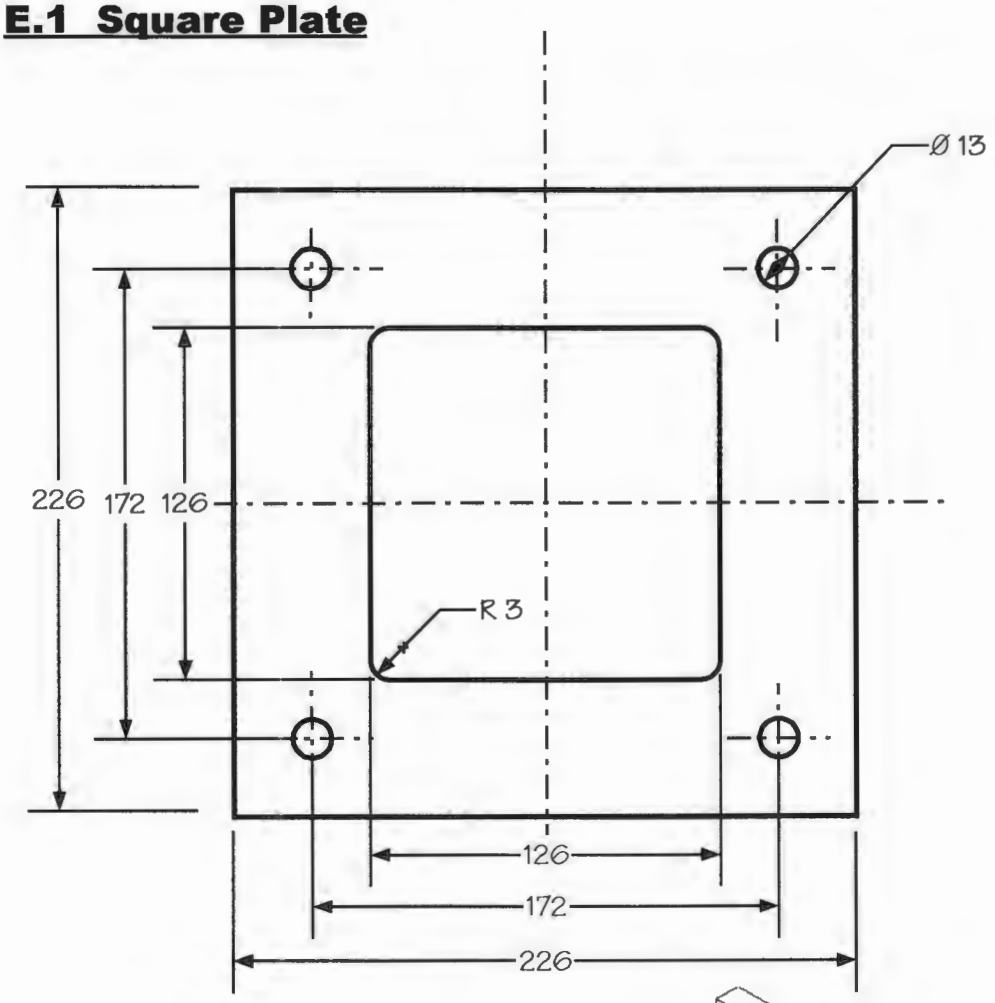

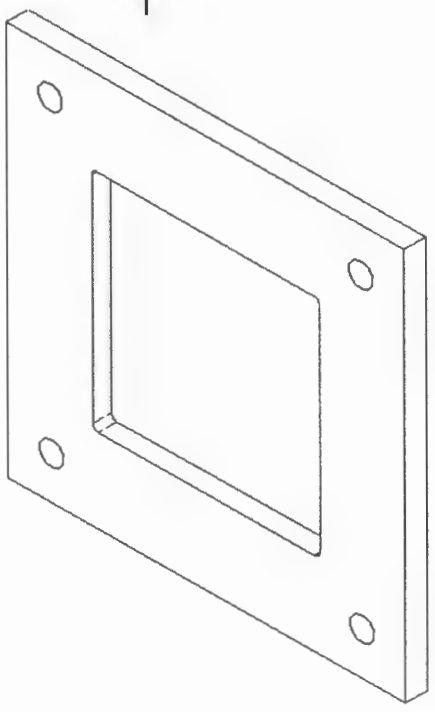

Plate thickness : 1.6mm

E.2 Single stiffened square Plate

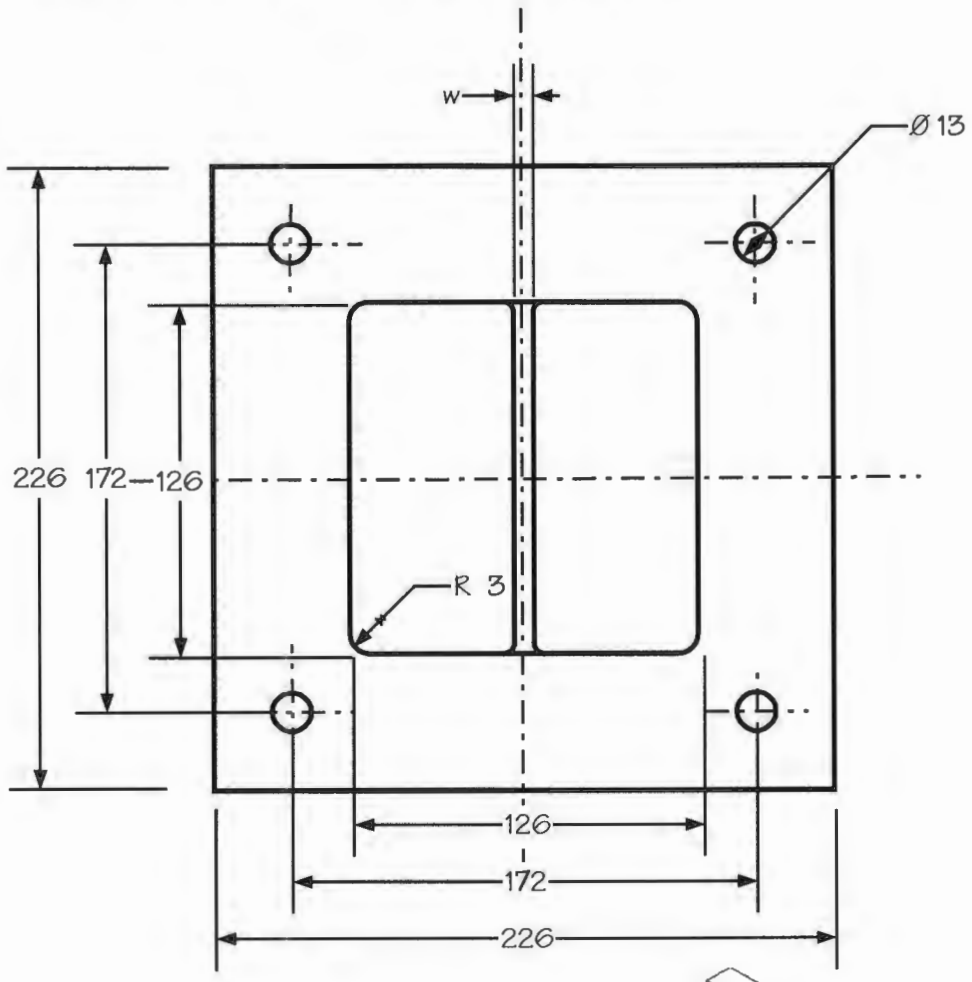

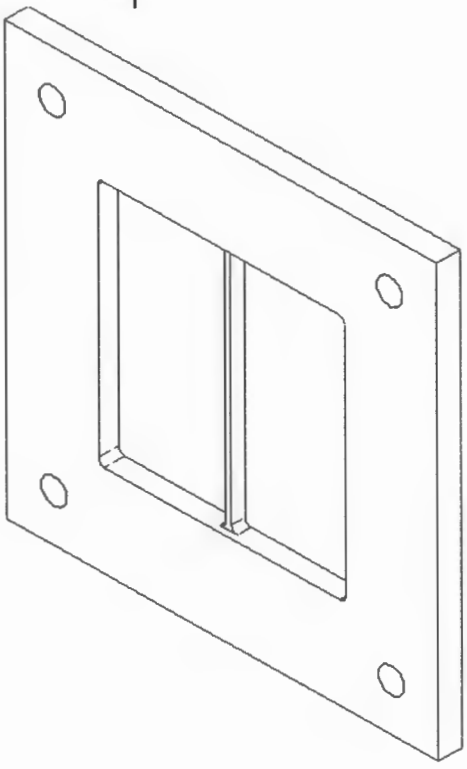

Plate thickness : 1.6mm

Stiffener width; w : 3, 4mm

Stiffener height : 3, 7mm

E.3 Double stiffened square Plate

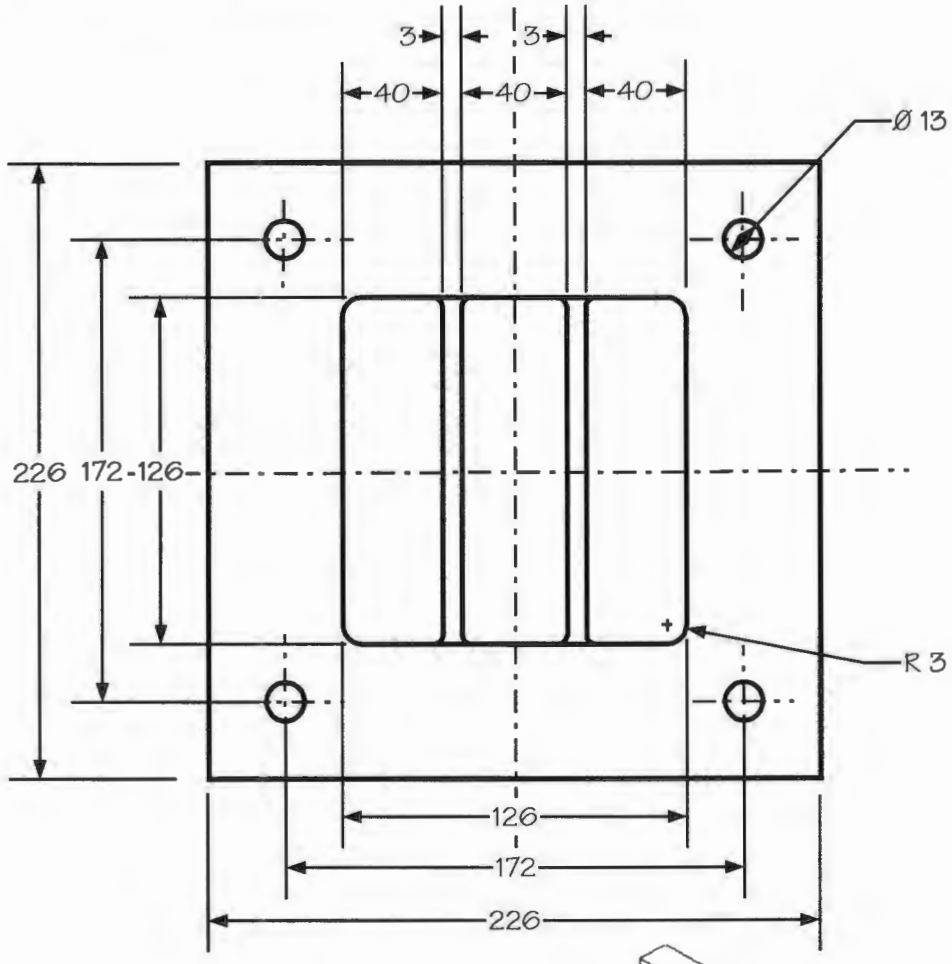

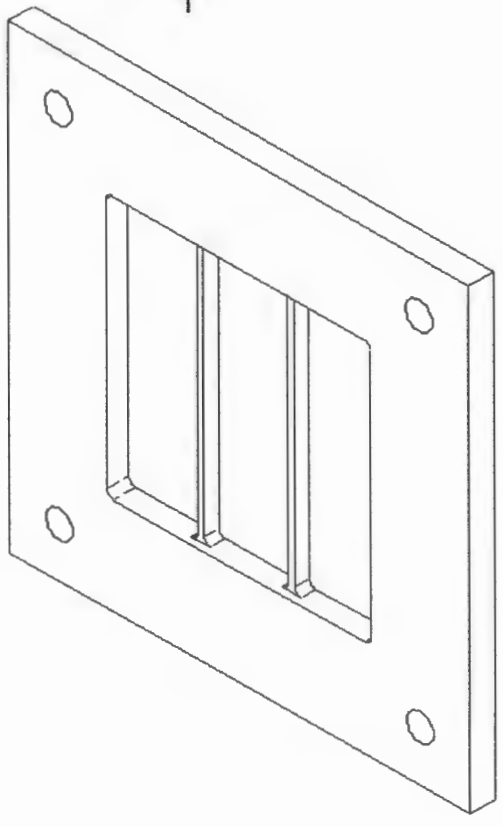

Plate thickness : 1.6mm

Stiffener width : 3mm

Stiffener height : 3, 7mm

E.4 Double cross stiffened square Plate

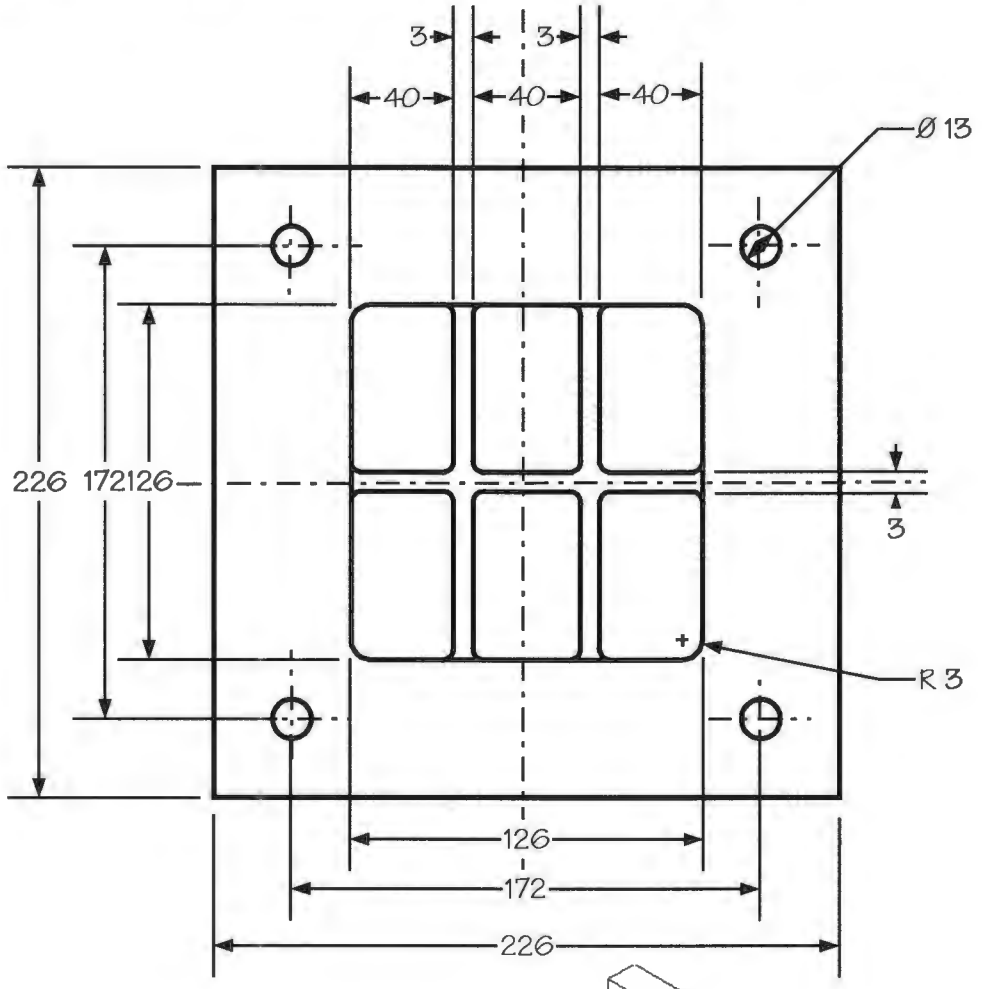

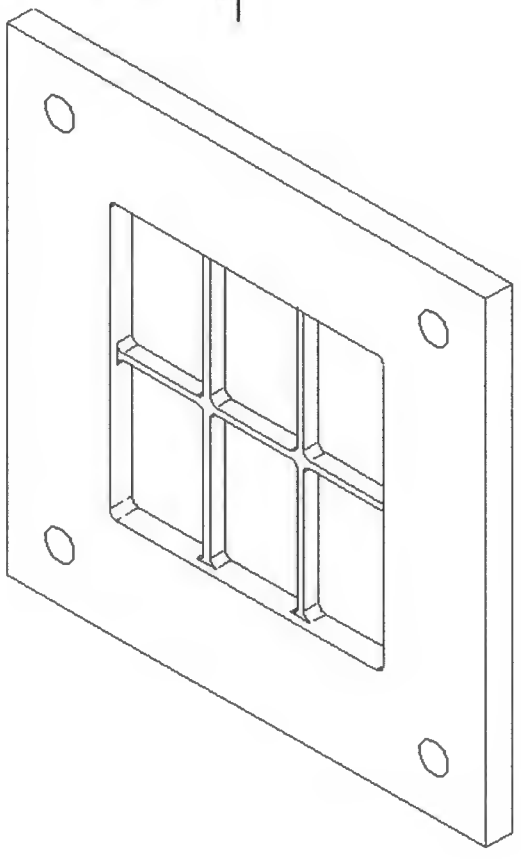

Plate thickness : 1.6mm

Stiffener width : 3mm

Stiffener height : 3, 7mm

E.5 Cross stiffened square Plate

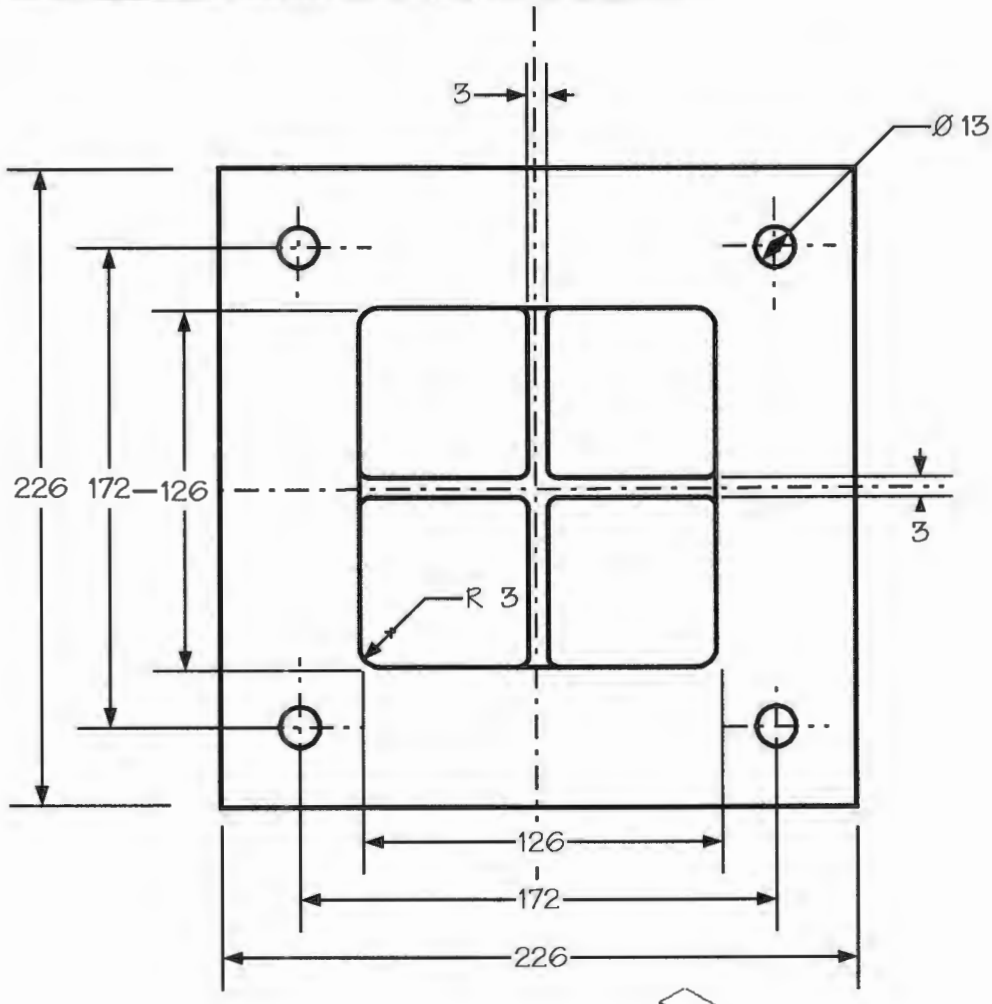

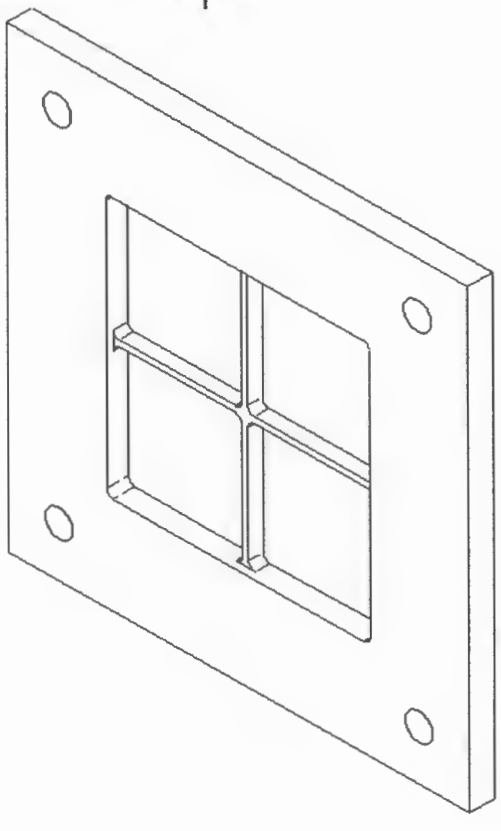

Plate thickness : 1.6mm

Stiffener width : 3mm

Stiffener height : 3, 7mm

E.6 Rectangular Plate

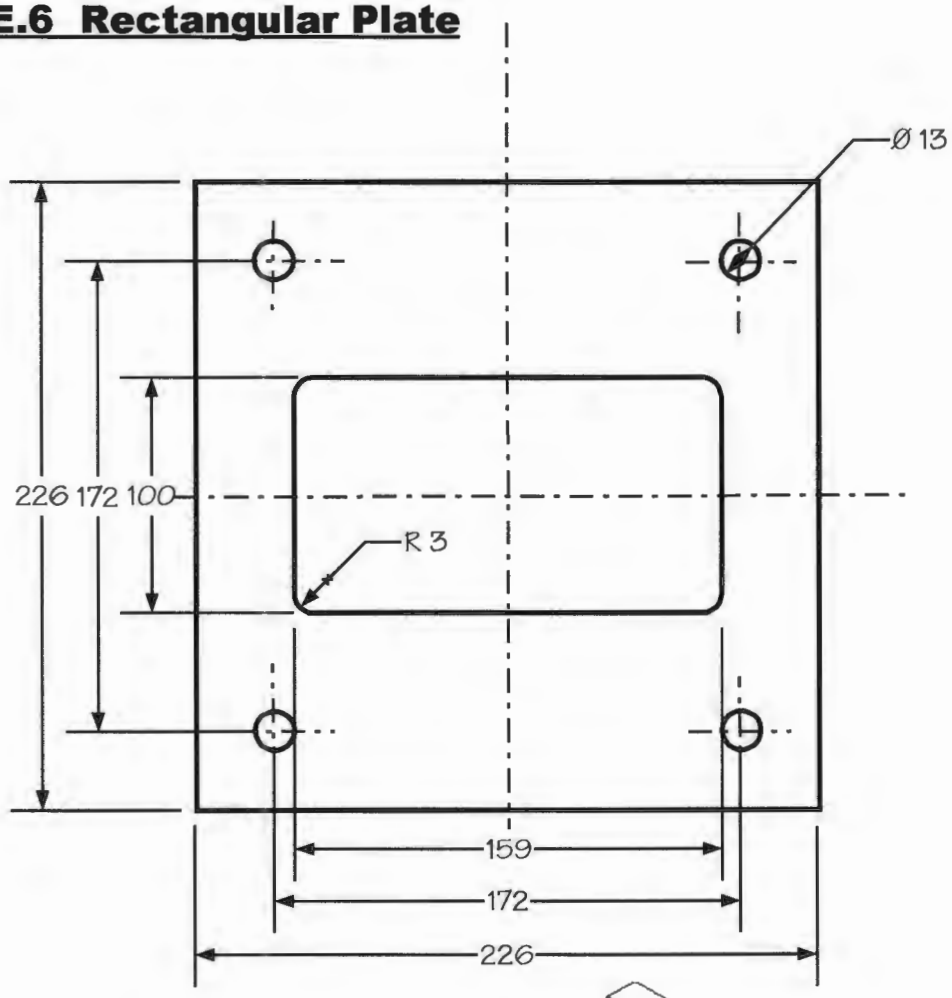

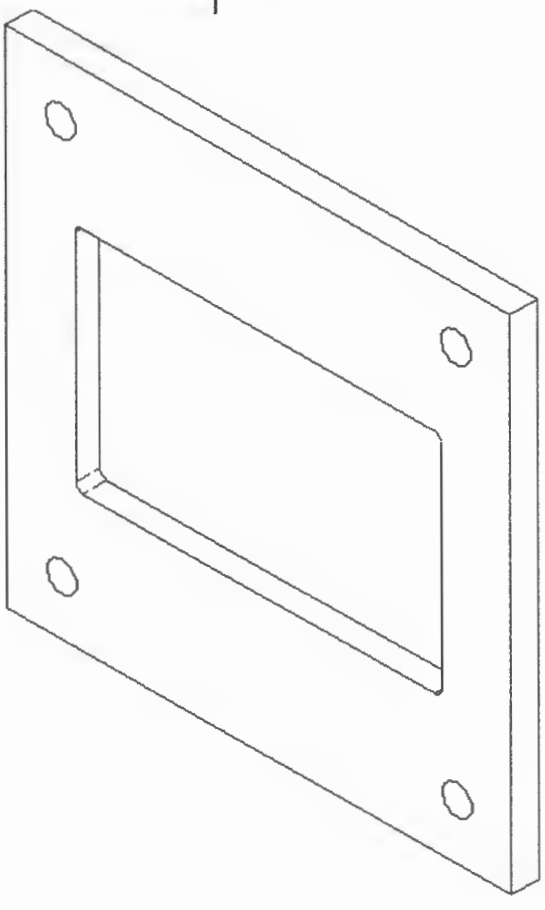

Plate thickness : 1.6mm

E.7 Double stiffened rectangular Plate

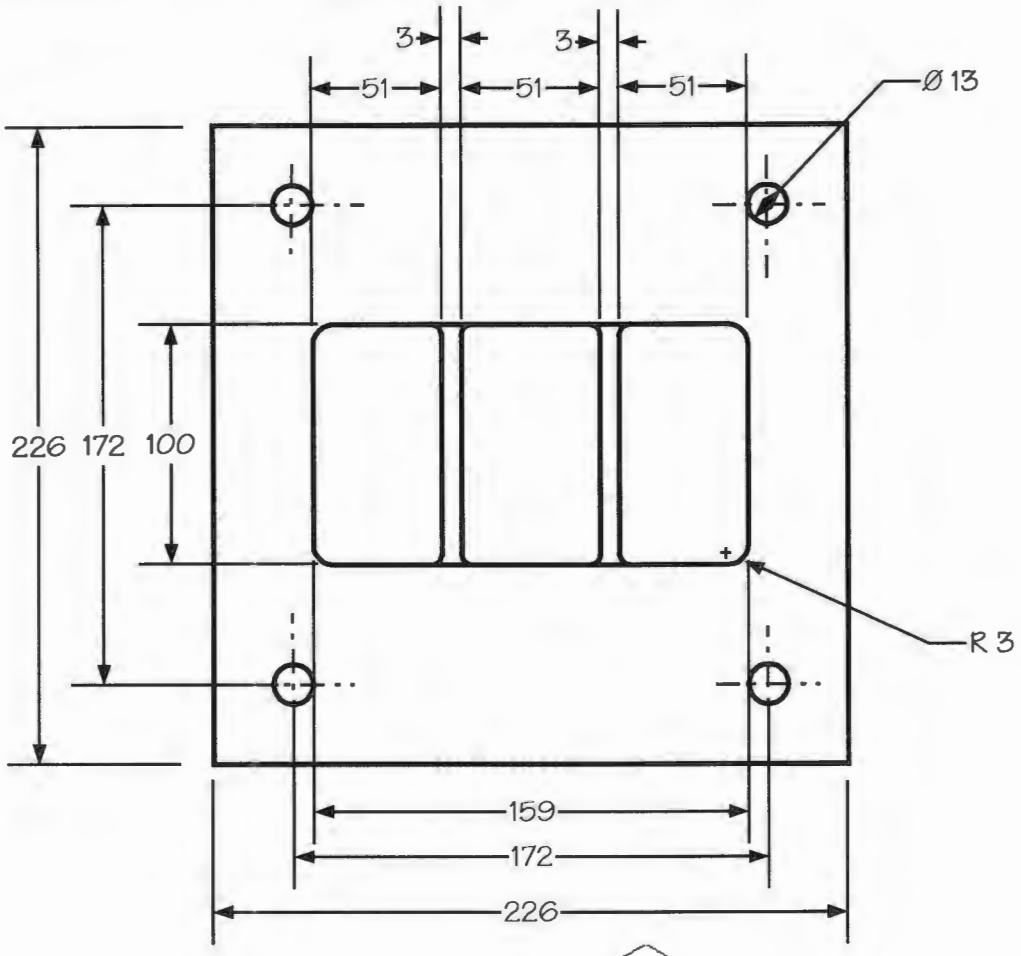

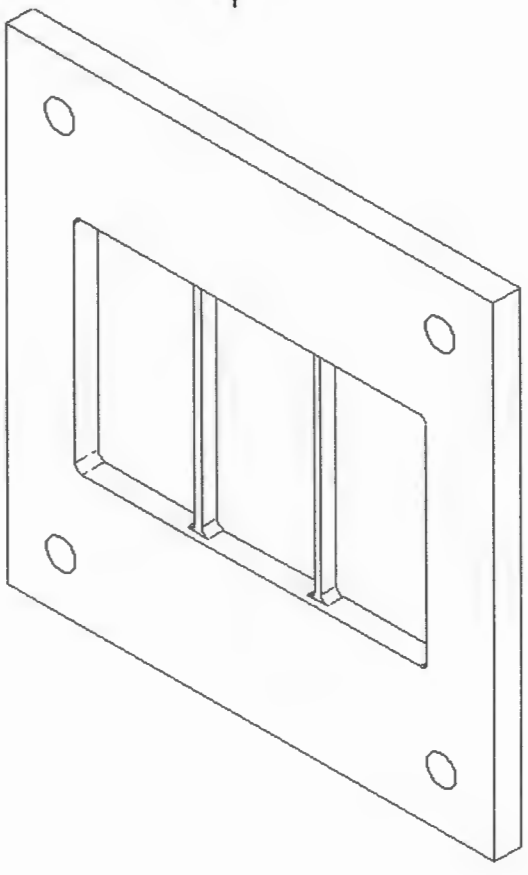

Plate thickness : 1.6mm

Stiffener width : 3mm

Stiffener height : 3, 7mm

Plate dimensions

Specimen	Type	B (mm)	L (mm)	w (mm)	h (mm)	t (mm)
S05	(R)	99.90	159.00	0.000	0.000	1.612
S11	(R)	99.90	159.90	0.000	0.000	1.608
S50	(R)	99.90	158.80	0.000	0.000	1.595
S51	(R)	99.90	159.80	0.000	0.000	1.627
S53	(R)	99.84	158.80	0.000	0.000	1.625
D32	(R-DS)	99.80	158.86	3.060	3.000	1.607
D57	(R-DS)	99.80	158.90	3.100	2.990	1.631
D55	(R-DS)	99.90	158.70	3.100	3.015	1.601
D50	(R-DS)	99.80	158.90	3.100	3.021	1.587
D31	(R-DS)	99.80	158.70	3.140	2.990	1.618
D36	(R-DS)	100.00	158.84	3.140	2.993	1.625
D52	(R-DS)	100.00	158.60	3.160	3.010	1.600
D13	(R-DS)	99.90	159.00	3.020	6.976	1.597
D05	(R-DS)	99.84	158.82	3.180	7.004	1.603
D09	(R-DS)	99.80	158.84	3.100	7.005	1.549
D01	(R-DS)	99.70	158.80	3.140	6.990	1.609
D11	(R-DS)	99.90	158.70	3.120	6.997	1.566
D07	(R-DS)	99.70	158.86	3.080	6.961	1.467
D24	(R-DS)	100.00	159.00	3.040	7.003	1.593
S01	(S)	125.80	125.80	0.000	0.000	1.632
S03	(S)	125.90	126.00	0.000	0.000	1.617
S07	(S)	125.90	126.00	0.000	0.000	1.601
S17	(S)	126.00	126.00	0.000	0.000	1.608
S56	(S)	126.00	126.00	0.000	0.000	1.595
T04	(S-CS)	125.90	125.90	3.100	3.003	1.589
S14	(S-CS)	125.90	125.90	3.000	7.028	1.590
S16	(S-CS)	125.90	125.90	3.100	6.971	1.590
S43	(S-CS)	125.90	125.90	3.100	6.979	1.589
S46	(S-CS)	125.90	125.90	3.100	6.983	1.580

Specimen	Type	B (mm)	L (mm)	w (mm)	h (mm)	t (mm)
S19	(S-CS)	125.90	125.90	3.100	7.006	1.604
S45	(S-CS)	125.90	125.90	3.100	7.015	1.609
T01	(S-DCS)	125.70	125.70	3.100	3.005	1.609
T12	(S-DCS)	125.90	125.90	3.070	7.002	1.601
T10	(S-DCS)	125.70	125.70	3.120	6.999	1.606
T02	(S-DCS)	125.90	125.90	3.140	7.008	1.604
M73	(S-DS)	125.80	125.80	3.100	3.000	1.610
M27	(S-DS)	125.80	125.80	3.140	6.995	1.481
M22	(S-DS)	125.80	125.80	3.160	6.980	1.610
M17	(S-DS)	125.80	125.80	3.180	6.990	1.610
A00	(S-S)	125.73	125.77	3.284	2.985	1.629
A01	(S-S)	125.75	125.71	2.956	3.062	1.620
A03	(S-S)	125.70	125.69	3.100	2.956	1.596
A07	(S-S)	125.67	125.69	3.120	2.986	1.596
A09	(S-S)	125.65	125.61	3.136	2.921	1.651
A11	(S-S)	125.61	125.60	3.328	3.015	1.595
A13	(S-S)	125.60	125.63	3.348	3.077	1.621
A17	(S-S)	125.63	125.52	3.364	2.992	1.596
K28	(S-S)	125.80	125.80	3.140	6.970	1.588
K10	(S-S)	125.80	125.80	3.216	6.965	1.601
C03	(S-S)	125.85	125.79	4.096	2.903	1.569
C17	(S-S)	125.92	125.91	4.120	2.991	1.549
C01	(S-S)	125.64	125.59	4.156	2.974	1.506
C07	(S-S)	125.70	125.80	4.160	2.971	1.609
C13	(S-S)	125.80	125.82	4.164	2.947	1.627
C04	(S-S)	125.57	125.58	4.176	2.972	1.532
C11	(S-S)	125.76	125.76	4.200	2.953	1.591
K03	(S-S)	125.80	125.80	4.100	6.970	1.590
K24	(S-S)	125.80	125.80	4.140	6.978	1.614

Typical input deck

Uniform blast loading on cross stiffened square plate using temperature dependent material properties

```
*HEADING
Crossed Stiffener (Square plate) 3x7mm
Units : m, Pa
Impulse 35 Ns
Continuum Element
*preprint, model=no, echo=no, history=yes
**-------------------------------------------------------
** Definition of nodes
*NODE, SYSTEM=R
      1, 5.3500000E-02,-4.4000000E-03,-8.0000000E-03
      2, 5.2330000E-02,-4.4000000E-03,-8.0000000E-03
      3, 5.1160000E-02,-4.4000000E-03,-8.0000000E-03
      4, 4.9990000E-02,-4.4000000E-03,-8.0000000E-03
      5, 4.8820000E-02,-4.4000000E-03,-8.0000000E-03
      6, 4.7650000E-02,-4.4000000E-03,-8.0000000E-03
      7, 4.6480000E-02,-4.4000000E-03,-8.0000000E-03
      8, 4.5310000E-02,-4.4000000E-03,-8.0000000E-03
       .
       .
       .
       .
  43701,-5.7500000E-03,-5.2000000E-03, 5.4500000E-02
  43702,-6.5000000E-03,-5.2000000E-03, 5.4500000E-02
  43703,-7.2500000E-03,-5.2000000E-03, 5.4500000E-02
  43706,-5.7500000E-03,-5.2000000E-03, 5.5000000E-02
  43707,-6.5000000E-03,-5.2000000E-03, 5.5000000E-02
  43708,-7.2500000E-03,-5.2000000E-03, 5.5000000E-02
  43716,-5.7500000E-03,-4.8000000E-03, 5.4000000E-02
```

**** Generation of elements**

```
*ELEMENT,TYPE=C3D6   ,ELSET=E0000001
 20255, 27648, 27649,  1224, 27693, 27694,  1275
 20253, 27646, 27647,  1224, 27691, 27692,  1275
 20252, 27645, 27646,  1224, 27690, 27691,  1275
 20251, 27644, 27645,  1224, 27689, 27690,  1275
 20250, 27643, 27644,  1224, 27688, 27689,  1275
 20249, 27021, 27643,  1224, 27276, 27688,  1275
 .
 .
 .
 20191, 27558, 27559,  1122, 27603, 27604,  1173
 20159, 27513, 27514,  1071, 27558, 27559,  1122
 20224, 27604,  918,  1173, 27649,  969,  1224
*ELEMENT,TYPE=C3D8R  ,ELSET=E0000002
   32,   32,   33,   84,   83,  287,  288,  339,  338
   33,   33,   34,   85,   84,  288,  289,  340,  339
   34,   34,   35,   86,   85,  289,  290,  341,  340
   35,   35,   36,   87,   86,  290,  291,  342,  341
   36,   36,   37,   88,   87,  291,  292,  343,  342
   37,   37,   38,   89,   88,  292,  293,  344,  343
   38,   38,   39,   90,   89,  293,  294,  345,  344
   39,   39,   40,   91,   90,  294,  295,  346,  345
 .
 .
 .
 31415, 43717, 43718, 43723, 43722, 40882, 40886, 40887, 40883
 31416, 43718, 33583, 33588, 43723, 40886, 33584, 33589, 40887
 31417, 31648, 43721, 43726, 31649, 30632, 40879, 40880, 30633
 31418, 43721, 43722, 43727, 43726, 40879, 40883, 40884, 40880
 31419, 43722, 43723, 43728, 43727, 40883, 40887, 40888, 40884
 31420, 43723, 33588, 33593, 43728, 40887, 33589, 33594, 40888
```

**Definition of material properties

**

*SOLID SECTION, ELSET=E0000001, MATERIAL=STEEL

*MATERIAL, NAME=STEEL

*SPECIFIC HEAT

660.

*DENSITY

7850.,

*INELASTIC HEAT FRACTION

*ELASTIC

2.070E+11, 0.3, 0

1.953E+11, 0.3, 200

1.720E+11, 0.3, 600

1.460E+11, 0.3, 700

1.249E+11, 0.3, 800

1.094E+11, 0.3, 900

1.001E+11, 0.3, 1000

9.700E+10, 0.3, 1100

*PLASTIC

2.59E+08, 0. ,0

2.74E+08, 0.007185 ,0

3.25E+08, 0.025556 ,0

3.85E+08, 0.051413 ,0

4.48E+08, 0.091745 ,0

4.75E+08, 0.115659 ,0

5.06E+08, 0.150734 ,0

5.23E+08, 0.174145 ,0

5.41E+08, 0.204152 ,0

5.51E+08, 0.226766 ,0

5.58E+08, 0.247764 ,0

5.48E+08, 0.280197 ,0

2.59E+08, 0. ,200

2.74E+08, 0.007185 ,200

3.25E+08, 0.025556 ,200

3.85E+08, 0.051413 ,200

4.48E+08, 0.091745 ,200

```
4.75E+08, 0.115659 ,200
5.06E+08, 0.150734 ,200
5.23E+08, 0.174145 ,200
5.41E+08, 0.204152 ,200
5.51E+08, 0.226766 ,200
5.58E+08, 0.247764 ,200
5.48E+08, 0.280197 ,200
3.44E+07, 0.       ,700
3.64E+07, 0.007185 ,700
4.32E+07, 0.025556 ,700
5.12E+07, 0.051413 ,700
5.96E+07, 0.091745 ,700
6.32E+07, 0.115659 ,700
6.73E+07, 0.150734 ,700
6.96E+07, 0.174145 ,700
7.19E+07, 0.204152 ,700
7.33E+07, 0.226766 ,700
7.42E+07, 0.247764 ,700
7.29E+07, 0.280197 ,700
4.30E+06, 0.       ,1000
4.54E+06, 0.007185 ,1000
5.40E+06, 0.025556 ,1000
6.39E+06, 0.051413 ,1000
7.44E+06, 0.091745 ,1000
7.89E+06, 0.115659 ,1000
8.40E+06, 0.150734 ,1000
8.68E+06, 0.174145 ,1000
8.98E+06, 0.204152 ,1000
9.15E+06, 0.226766 ,1000
9.26E+06, 0.247764 ,1000
9.10E+06, 0.280197 ,1000
*RATE DEPENDENT
40.4, 5.
*INITIAL CONDITIONS, TYPE=TEMPERATURE
,23.0
*SOLID SECTION, ELSET=E0000002, MATERIAL=STEEL
```

```
** Analysis Steps
** Step 1 - Blast Load
*STEP
*DYNAMIC,EXPLICIT,ADIABATIC
,14.5E-06
*RESTART,WRITE,NUMBER INTERVAL=    3
** BOUNDARY CONDITION SET 1
** RESTRAINT SET 1
*BOUNDARY,OP=NEW
BS000001,   1,,      0.00000E+00
BS000001,   4, 6,    0.00000E+00
BS000002,   3, 6,    0.00000E+00
BS000003,   1,,      0.00000E+00
BS000003,   3, 6,    0.00000E+00
BS000004,   1, 6,    0.00000E+00
** LOAD SET 1
*DLOAD,OP=NEW
BS000005,  P1, 1.5200E+08
BS000006,  P2, 1.5200E+08
BS000007,  P2, 1.5200E+08
BS000008,  P3, 1.5200E+08
BS000009,  P5, 1.5200E+08
BS000010,  P6, 1.5200E+08
*FILE OUTPUT,NUMBER INTERVAL=    100
*NODE FILE, nset=ns_out
U
*END STEP
**************************************************************
**       Step 2  - Zero Input
**
*Step
*Dynamic, Explicit, adiabatic
,550.E-6
*RESTART,WRITE,NUMBER INTERVAL=    6
**  LOAD SET 2 - No Load
*DLOAD, OP=new
```

```
*file output, number interval=1000
*node file, nset=ns_out
U
*END STEP
**********************************************************
** Definition of boundary conditions and constraints
*nset, nset=ns_out
27978
*NSET,NSET=BS000001
205,1277,1278,1279,1283,1287,1291,1295,1299,1303,1307,1311,1315,1319,1323
1327,1331,1335,1339,1343,1347,1351,1355,1359,1363,1367,1371,1375,1376,1377
1378,1379,1380,1381,1382,1383,1384,1385,1386,1387,1388,1389,1390,1391,1392
.
.
27798,27802,27814,27818,27830,27834,27846,27850,27862,27866,27878,27882
27894,27898,27968,27969,27970,27971,27973,27974,27975,27976,43576,43577
43588,43589,43600,43601,43612,43613,43624,43625,43636,43637,43648,43649
*NSET,NSET=BS000002
27707,27708,27709,27723,27724,27725,27739,27740,27741,27755,27756,27757
27771,27772,27773,27787,27788,27789,27803,27804,27805,27819,27820,27821
27835,27836,27837,27851,27852,27853,27867,27868,27869,27883,27884,27885
.
.
40784,40788,40800,40804,40808,40820,40824,40828,40840,40844,40848,40860
40864,40868,40880,40884,40888,43666,43667,43668,43686,43687,43688,43706
43707,43708,43726,43727,43728
*NSET,NSET=BS000003
27710,27726,27742,27758,27774,27790,27806,27822,27838,27854,27870,27886
27902,27978,27979,27980,27981
*NSET,NSET=BS000004
20079,20080,20081,20082,20083,20084,20085,20086,20087,20088,20089,20090
20091,20092,20093,20094,20095,20096,20097,20098,20099,20100,20101,20102
.
.
42474,42476,42477,42479,42480,42482,42483,43558,43559,43561,43562,43564
43565,
```

*ELSET,ELSET=BS000005
1449,1450,1451,1452,1453,1454,1455,1456,1457,1458,1459,1460,1461,1462,1463
1464,1465,1466,1467,1468,1469,1470,1471,1472,1473,1474,1475,1476,1477,1478
.
.
3924,3925,3926,3927,3928,3929,3930,3931,3932,3933,3934,3935,3936,3937,3938
3939,3940,3941,3942,3943,3944,3945,3946,3947,3948,31373,31374,31375,31376
31377,31378,31379,31380,31381,31382,31383,31384
*ELSET,ELSET=BS000006
20249,20250,20251,20252,20253,20254,20255,20256
*ELSET,ELSET=BS000007
19929,19930,19931,19932,19933,19934,19935,19936,19937,19938,19939,19940
19941,19942,19943,19944,19945,19946,19947,19948,19949,19950,19951,19952
19953,19954,19955,19956,19957,19958,19959,19960,19961,19962,19963,19964
20121,20122,20123,20124,20125,20126,20127,20128,20225,20226,20227,20228
20229,20230,20231,20232,20233,20234,20235,20236,20237,20238,20239,20240
20241,20242,20243,20244,20245,20246,20247,20248
*ELSET,ELSET=BS000008
801,802,803,813,814,815,825,826,827,837,838,839,22201,22202,22203,22213
.
.
.
22742,22743,22753,22754,22755,22765,22766,22767,22777,22778,22779,22789
22790,22791
*ELSET,ELSET=BS000009
151,152,153,154,155,156,157,158,159,160,161,162,163,164,165,166
167,168,169,170,171,172,173,174,175,176,177,178,179,180,181,182
761,762,763,764,765,766,767,768,769,770,771,772,773,774,775,776
777,778,779,780,781,782,783,784,785,786,787,788,789,790,791,792
793,794,795,796,797,798,799,800
*ELSET,ELSET=BS000010
849,853,857,861,865,869,873,877,881,885,889,893,897,901,905,909
913,917,921,925,929,933,937,941,945,949,953,957,961,965,969,973
1341,1345,1349,1353,1357,1361,1365,1369,1373,1377,1381,1385,1389,1393,1397
1401,1405,1409,1413,1417,1421,1425,1429,1433,1437,1441,1445,20365,20369
20373,20377,20381,20385,20389,20393,20397

Typical input deck

Uniform blast loading on rectangular plate using material properties that exclude temperature dependency

```
*HEADING
No Stiffener (Rectangular plate)
Continuum Element
Units : m, Pa
Impulse 35 Ns
*preprint, model=no, echo=no, history=yes
**-----------------------------------------------------
** Definitions of nodes
*NODE, SYSTEM=R
      1,-2.5500000E-02, 6.0000000E-03,-2.1500000E-02
      2,-2.5500000E-02, 3.9200000E-03,-2.1500000E-02
      3,-2.5500000E-02, 1.8400000E-03,-2.1500000E-02
 .
 .
 .
   31307, 5.5000000E-02, 1.8400000E-03,-2.4500000E-02
   31308, 5.5000000E-02,-2.4000000E-04,-2.4500000E-02
   31309, 5.5000000E-02,-2.3200000E-03,-2.4500000E-02
** Generation of elements
*ELEMENT,TYPE=C3D6   ,ELSET=E0000001
  7679, 10712, 10713,  8597, 10757, 10758,  8628
  7677, 10710, 10711,  8597, 10755, 10756,  8628
  7676, 10709, 10710,  8597, 10754, 10755,  8628
*ELEMENT,TYPE=C3D8R  ,ELSET=E0000002
  1432,  2168,  2169,  2175,  2174,  2594,  2595,  2601,  2600
  1433,  2169,  2170,  2176, ..... 29818, 31123, 31303,
8494,  8499, 31309
**********************************************************************
```

****Definition of material properties**

**

*SOLID SECTION, ELSET=E0000001, MATERIAL=STEEL

*MATERIAL, NAME=STEEL

*ELASTIC, TYPE=ISOTROPIC

2.07E+11, 0.285

*DENSITY

7850.,

*PLASTIC

3.08E+08, 0.

3.55E+08, 0.0085

3.90E+08, 0.017

4.25E+08, 0.029

4.60E+08, 0.042

4.85E+08, 0.055

5.15E+08, 0.072

5.40E+08, 0.094

5.50E+08, 0.106

5.65E+08, 0.14

5.69E+08, 0.1721

5.65E+08, 0.212

*SHEAR FAILURE

2.0

*RATE DEPENDENT

40.4, 5.

*SOLID SECTION, ELSET=E0000002, MATERIAL=STEEL

****

** **Analysis Steps**

** **Step 1 - Blast Load**

*STEP

*DYNAMIC,EXPLICIT

,14.5E-06

*RESTART,WRITE,NUMBER INTERVAL= 3

```
** BOUNDARY CONDITION SET 1
** RESTRAINT SET 1
*BOUNDARY,OP=NEW
BS000001,  1,,     0.00000E+00
BS000001,  4, 6,    0.00000E+00
BS000002,  3, 6,    0.00000E+00
BS000003,  1,,     0.00000E+00
BS000003,  3, 6,    0.00000E+00
BS000004,  1, 6,    0.00000E+00
** LOAD SET 1
*DLOAD,OP=NEW
BS000005,  P2, 1.5200E+08
BS000006,  P2, 1.5200E+08
BS000007,  P4, 1.5200E+08
BS000008,  P5, 1.5200E+08
*FILE OUTPUT,NUMBER INTERVAL=    100
*NODE FILE, nset=ns_out
U
*END STEP
**************************************************************
**       Step 2  -  Zero Input
**
*Step
*Dynamic, Explicit
,550.E-6
*RESTART,WRITE,NUMBER INTERVAL=    6
**  LOAD SET 2 - No Load
*DLOAD, OP=new
*file output, number interval=1000
*node file, nset=ns_out
U
*END STEP
**************************************************************
```

** **Definition of boundary conditions and constraints**

*nset, nset=ns_out

27978

*NSET,NSET=BS000001

8499,8500,8501,8502,8503,8534,8565,8596,8627,8658,8689,8720,8751,8782,8813

8844,8875,8906,8937,8968,8999,9030,9061,9092,9123,11064,11065,11066,11067

11068,11219,11220,11221,11222,11223,11374,11375,11376,11377,11378, …

30564,30565,30747,30748,30749,30750,30751,30933,30934,30935,30936,30937

31119,31120,31121,31122,31123,31305,31306,31307,31308,31309

*NSET,NSET=BS000002

2101,2102,2103,2104,2105,2106,2130,2977,2978,2979,2980,2981,2982,3403,3404

3405,3406,3407,3408,3829,3830,3831,3832,3833,3834,5586,5587,5588, …

27977,27978,27979,27980,27982,27983,27984,27985,27987,27988,27989,27990

27992,27993,27994,27995,27997,27998,27999,28000,28002,28003,28004,28005

*NSET,NSET=BS000003

21759,21760,21761,21762,21763

*NSET,NSET=BS000004

2131,2132,2133,2134,2135,2136,2137,2138,2139,2140,2141,2142,2143,2144,2145

2146,2147,2148,2149,2150,2151,2152,2153,2154,2155,2156,2157,2158,…..

29994,29995,29997,29998,29999,30000,30001,30003,30004,30005,30006,30007

*ELSET,ELSET=BS000005

7673,7674,7675,7676,7677,7678,7679,7680

*ELSET,ELSET=BS000006

7649,7650,7651,7652,7653,7654,7655,7656,7657,7658,7659,7660,7661,7662,7663

7664,7665,7666,7667,7668,7669,7670,7671,7672

*ELSET,ELSET=BS000007

7684,7688,7692,7696,7700,7704,7708,7712,7716,7720,7724,7728,7732,7736,7740

……16020,16024,16028,16032,16036,16040,16044,16048,16052,16056

16068,16072,16076,16080

*ELSET,ELSET=BS000008

6043,6044,6045,6046,6047,6048,6049,6050,6051,6052,6053,6054,6055,6056,6057

6058,6059,6060,6061,6062,6063,6064,6065,6066,6067,6068,6069,6070,6071,6072

6163,6164,6165,6166,6167,6168,6169,6170…

Finite Element models and results

H.1 Square plate

Square plate model

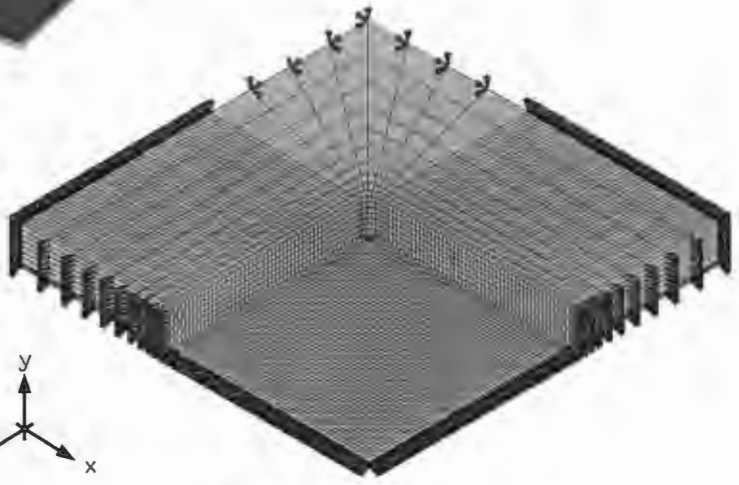

Mesh model and Boundary conditions

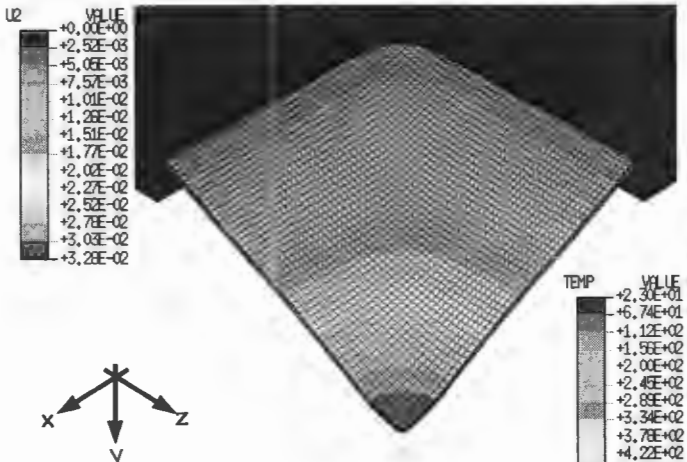

Displacement in the y-direction at impulse 38Ns

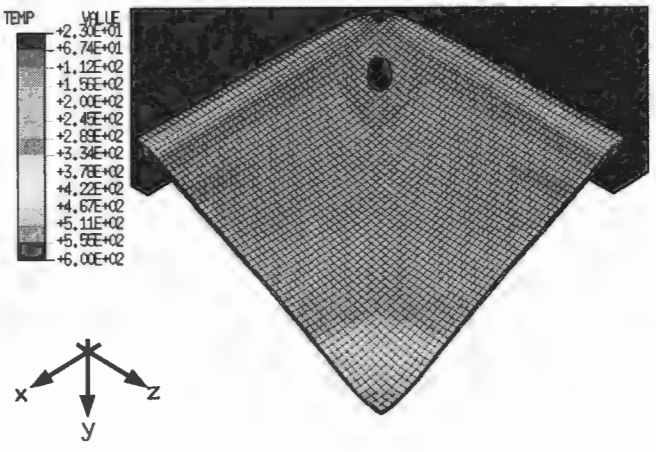

Temperature distribution at impulse 38Ns

H.2 Single stiffened square plate (3x3mm)

Single Stiffened Square plate (3x3mm) model

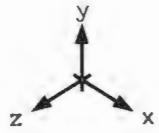

Mesh model and Boundary conditions

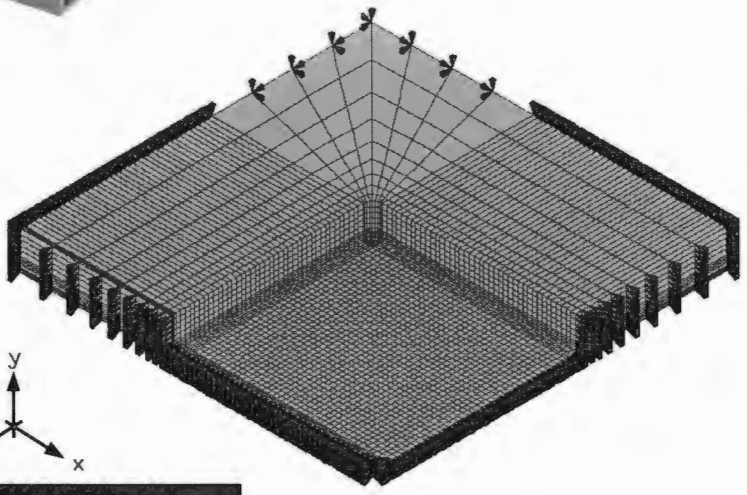

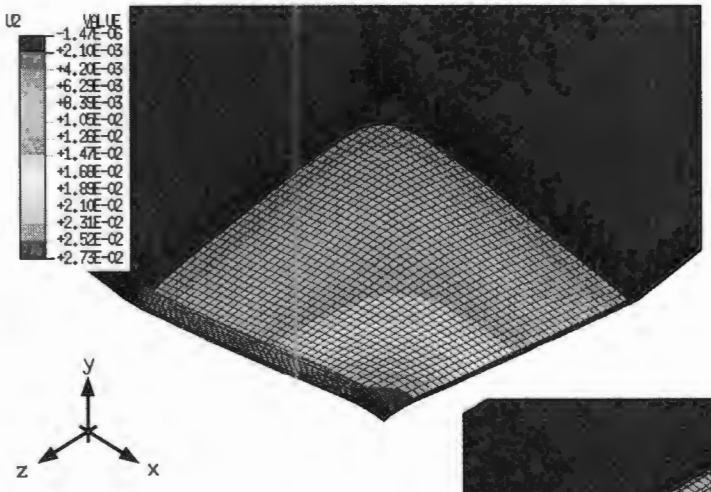

Displacement in the y-direction at impulse 35Ns

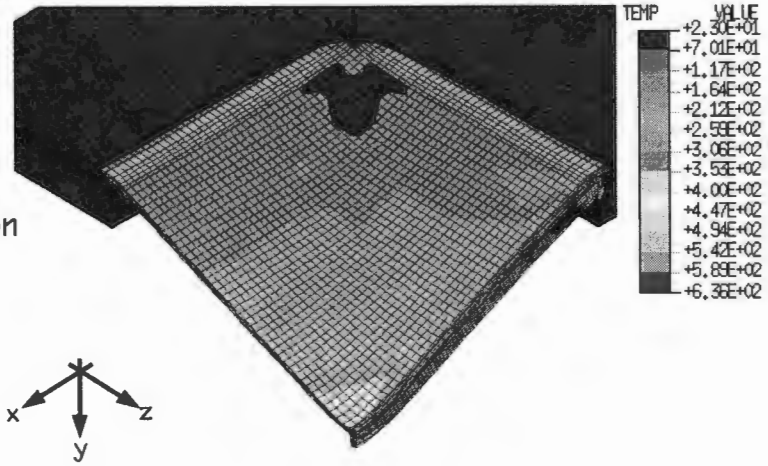

Temperature distribution at impulse 35Ns

H.3 Single stiffened square plate (3x7mm)

Single Stiffened Square plate (3x7mm) model

Mesh model

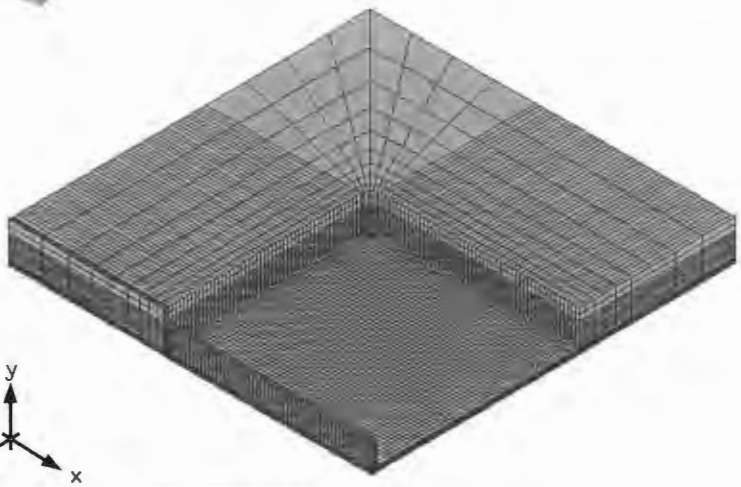

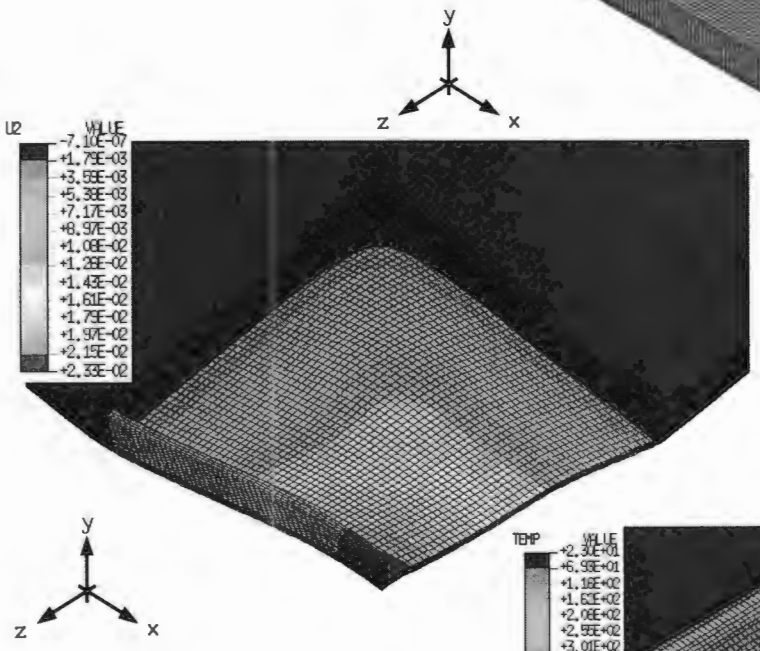

Displacement in the y-direction at impulse 34Ns

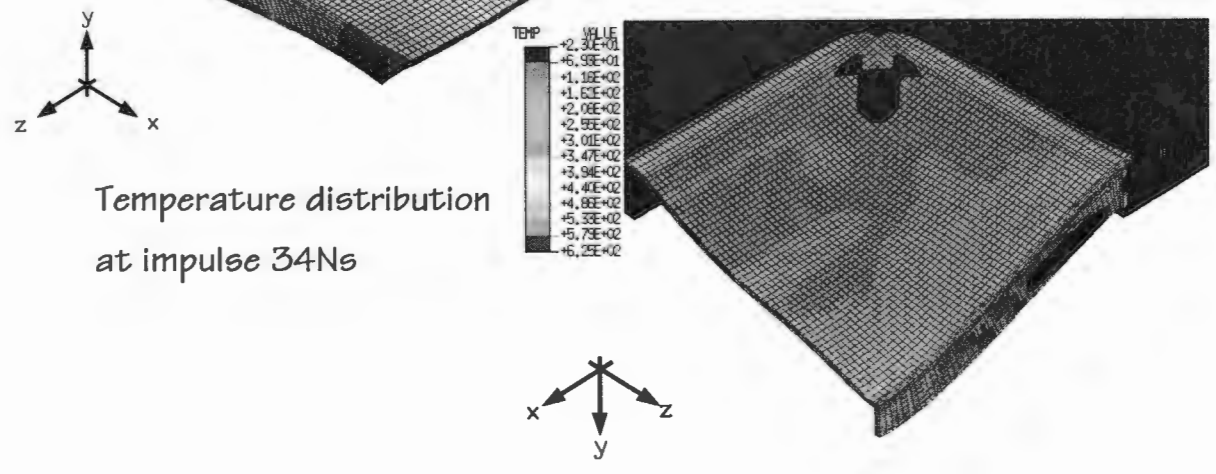

Temperature distribution at impulse 34Ns

H.4 Single stiffened square plate (4x3mm)

Single Stiffened Square plate (4x3mm) model

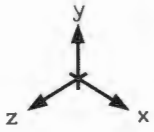

Mesh model and Boundary Conditions

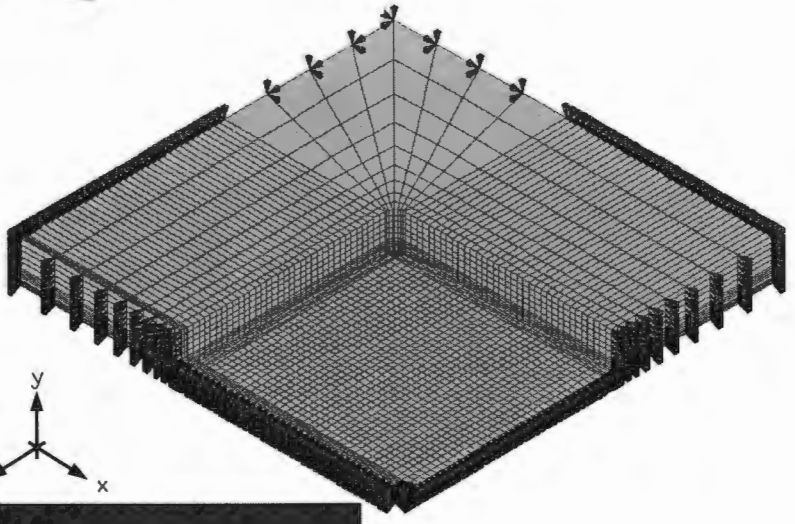

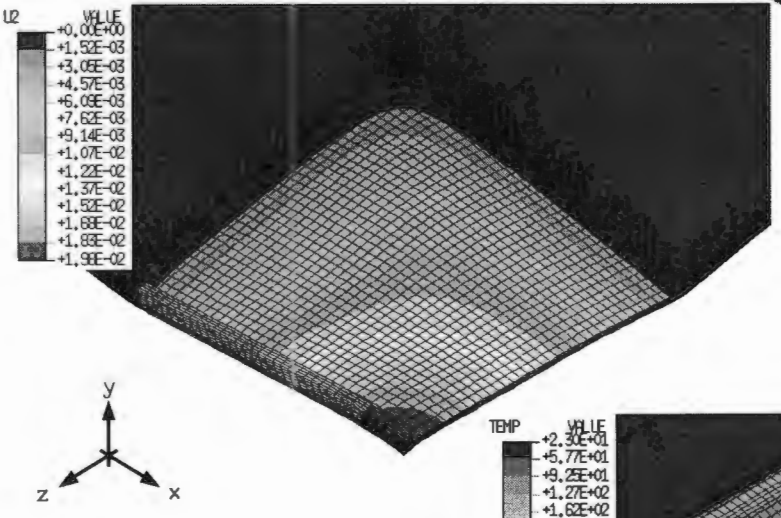

Displacement in the y-direction at impulse 27Ns

Temperature distribution at impulse 27Ns

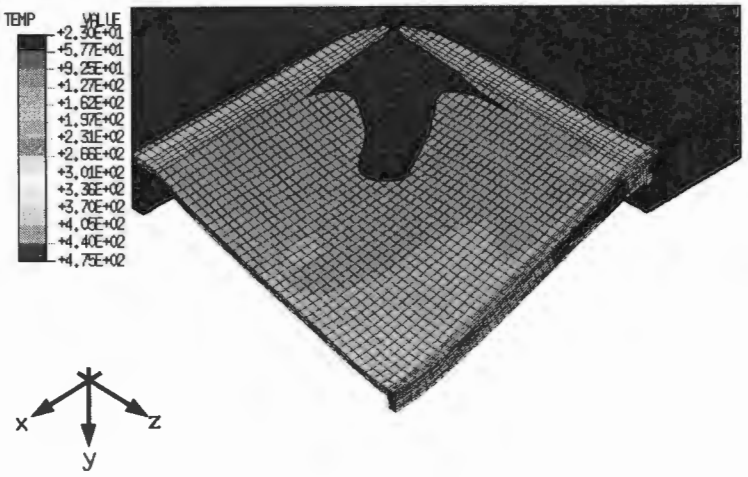

H.5 Single stiffened square plate (4x7mm)

Single Stiffened Square plate (4x7mm) model

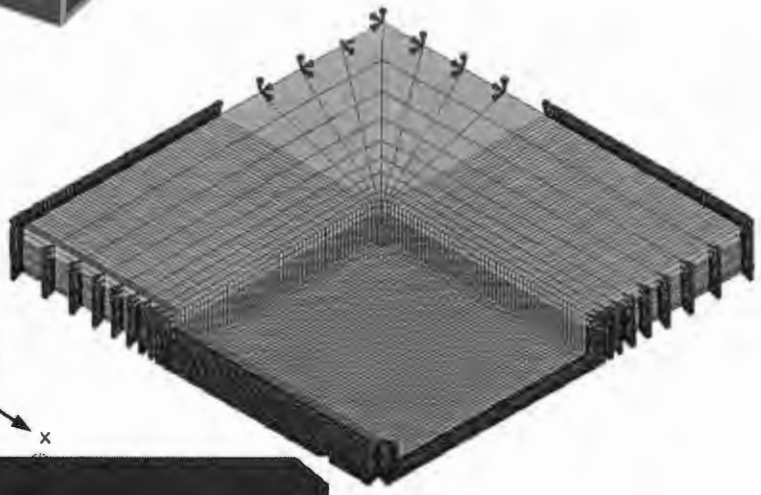

Mesh model and Boundary Conditions

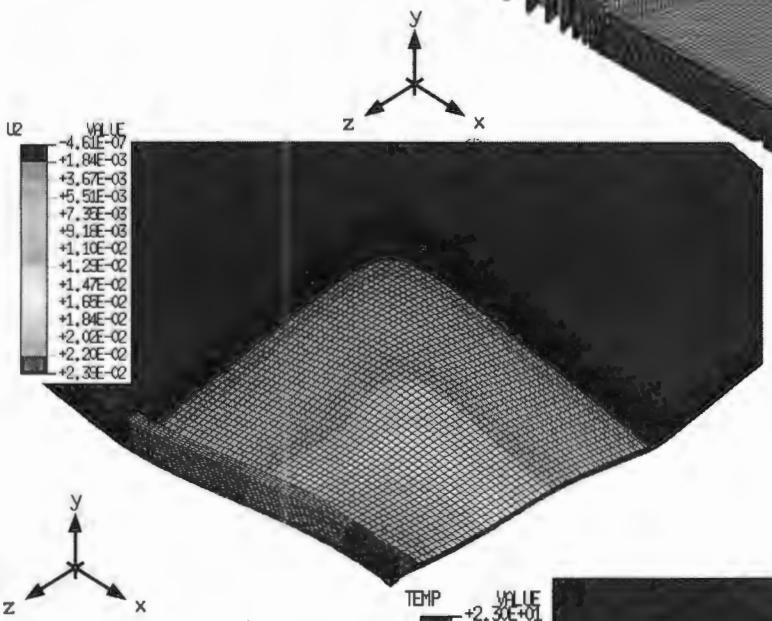

Displacement in the y-direction at impulse 37Ns

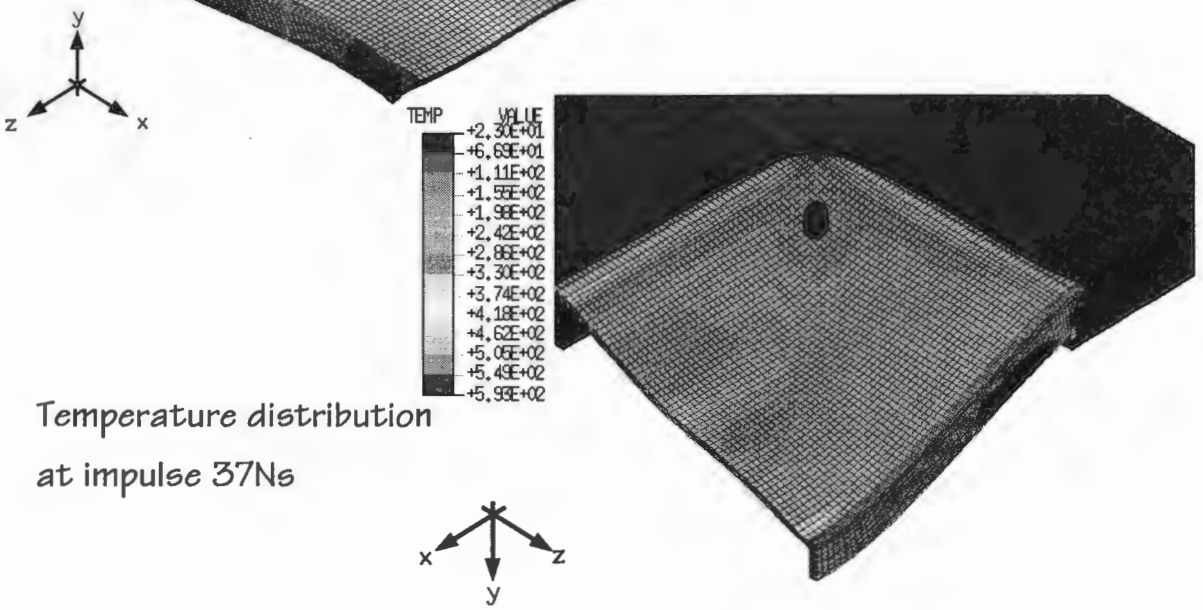

Temperature distribution at impulse 37Ns

H.6 Double stiffened square plate (3x3mm)

Double Stiffened Square plate (3x3mm) model

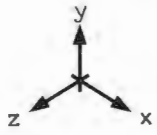

Mesh model and Boundary Conditions

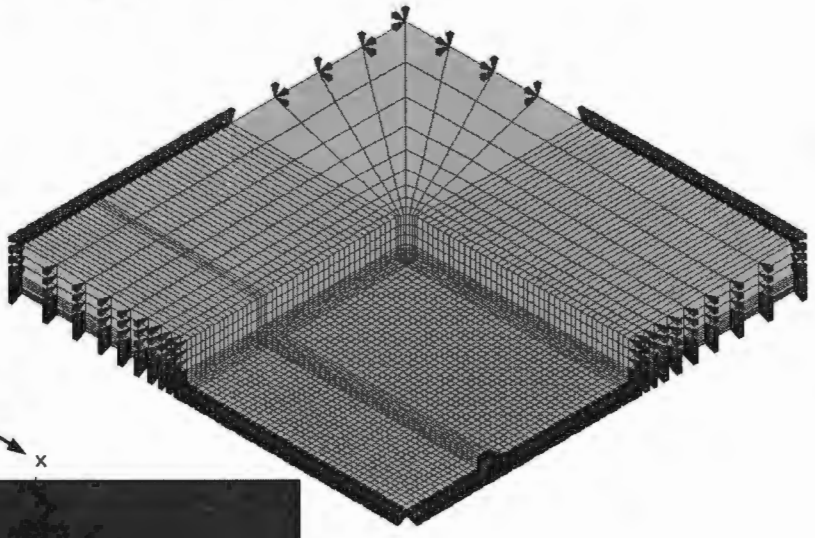

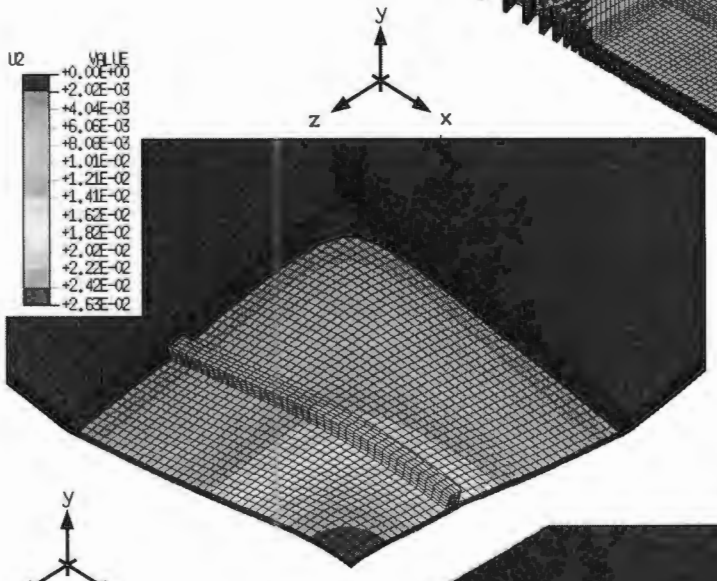

Displacement in the y-direction at impulse 35Ns

Temperature distribution at impulse 35Ns

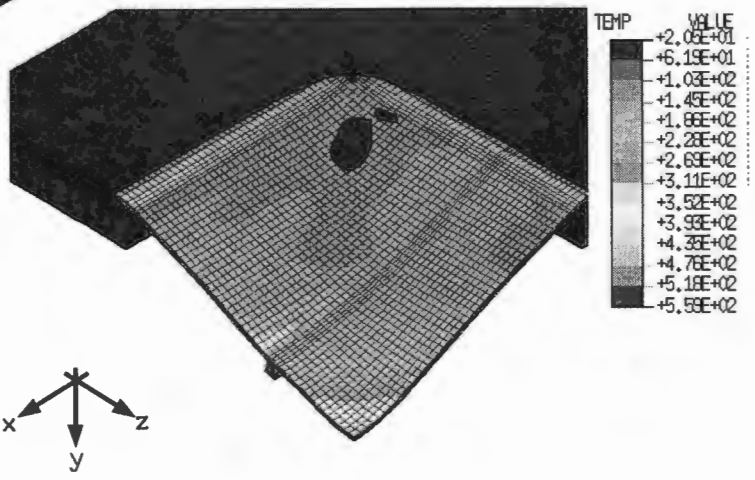

H.7 Double Stiffened square plate (3x7mm)

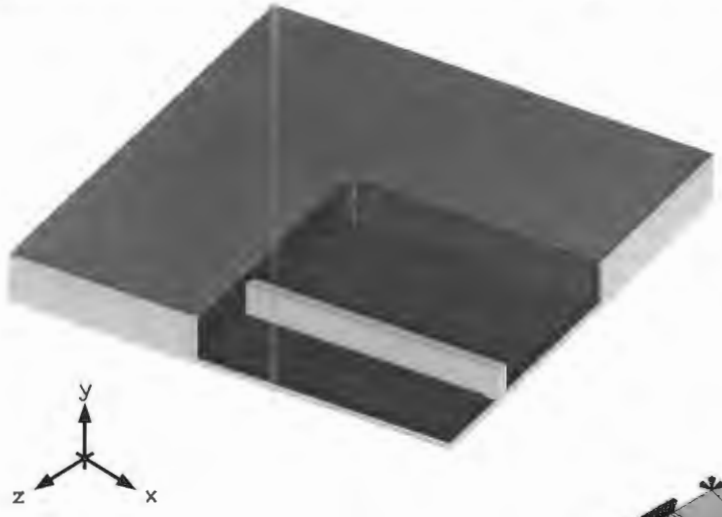

Double Stiffened Square plate (3x7mm) model

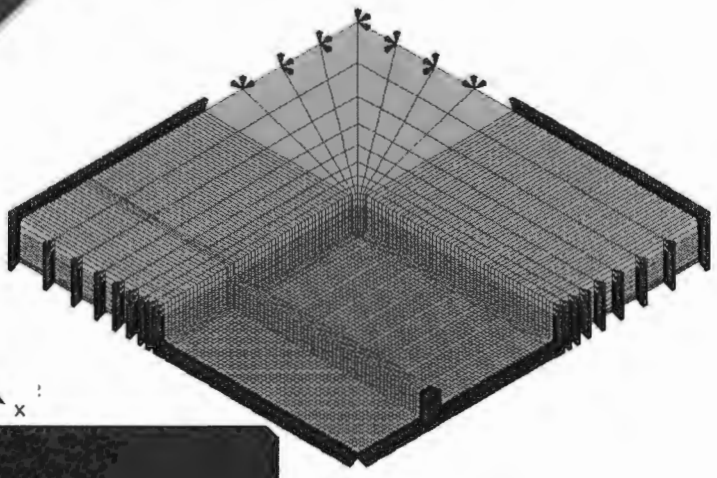

Mesh model and Boundary Conditions

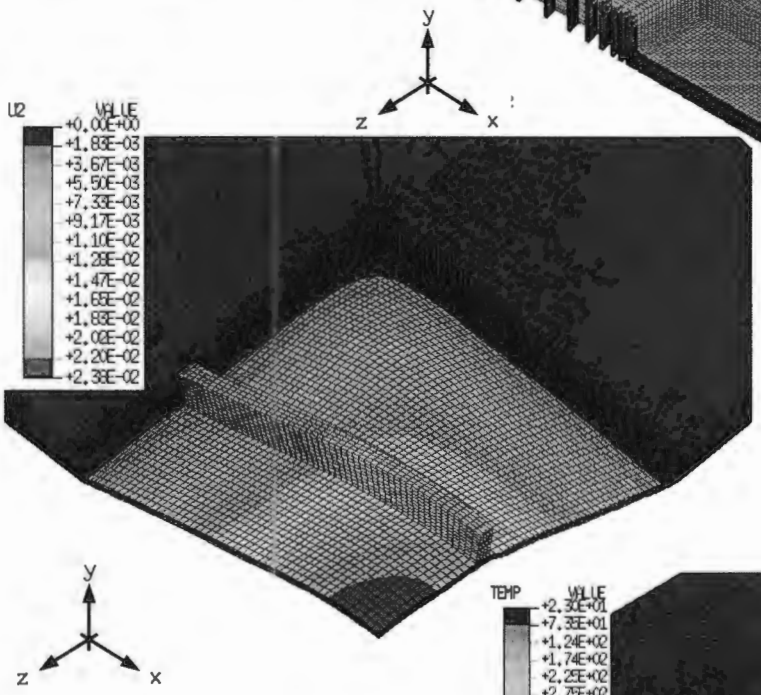

Displacement in the y-direction at impulse 39Ns

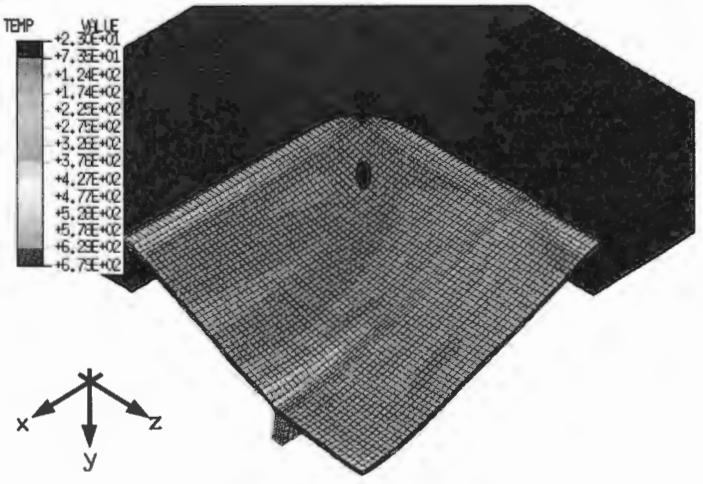

Temperature distribution at impulse 39Ns

H.8 Double cross Stiffened square plate (3x3mm)

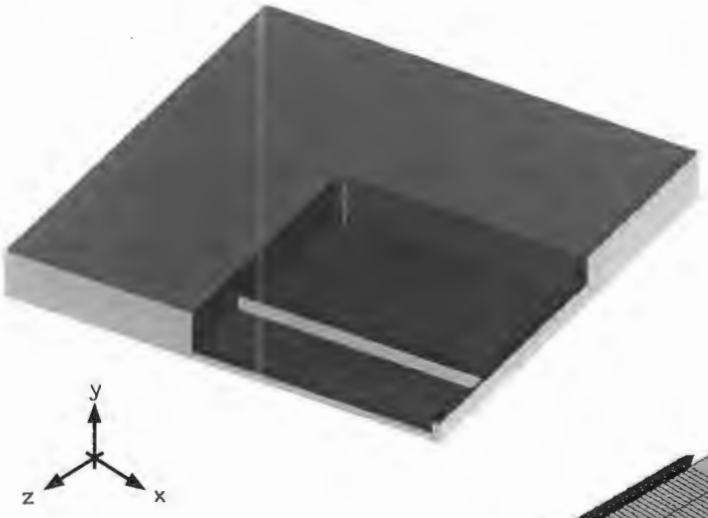

Double cross stiffened
Square plate (3x3mm) model

Mesh model and
Boundary Conditions

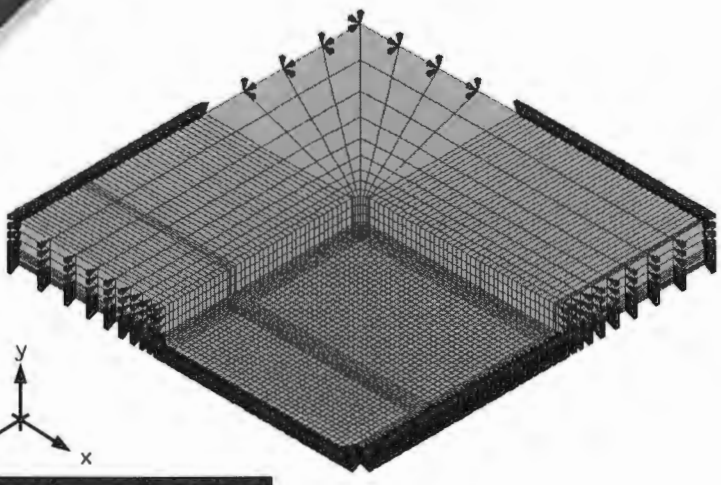

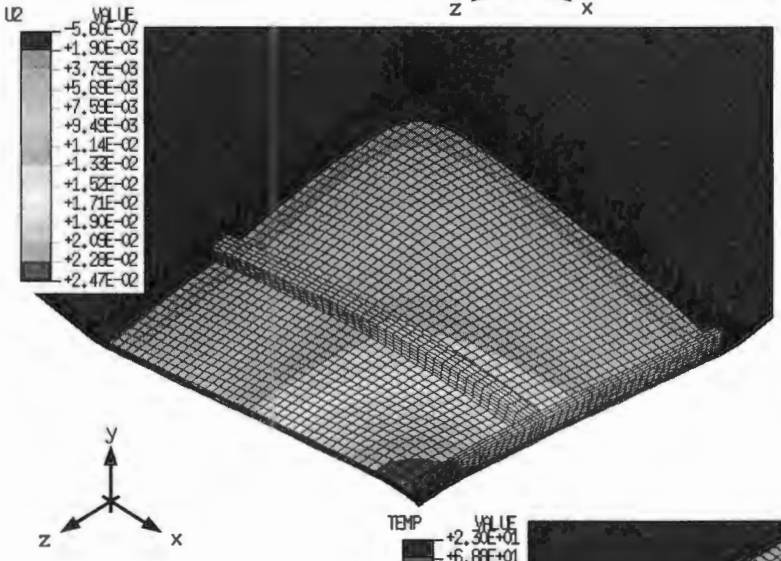

Displacement in the
y-direction at impulse 35Ns

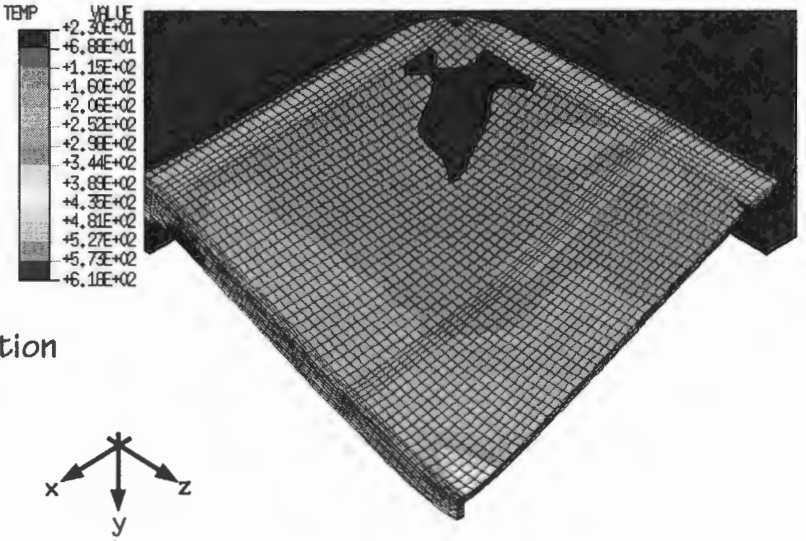

Temperature distribution
at impulse 35Ns

H.9 Double cross Stiffened square plate (3x7mm)

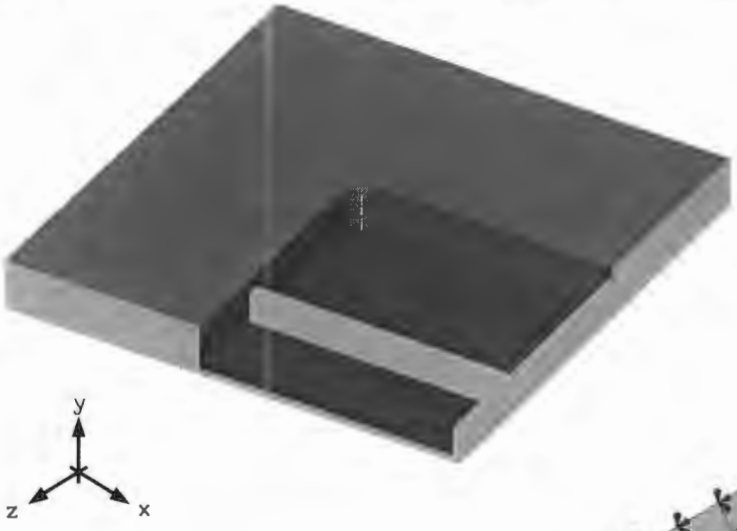

Double cross stiffened Square plate (3x7mm) model

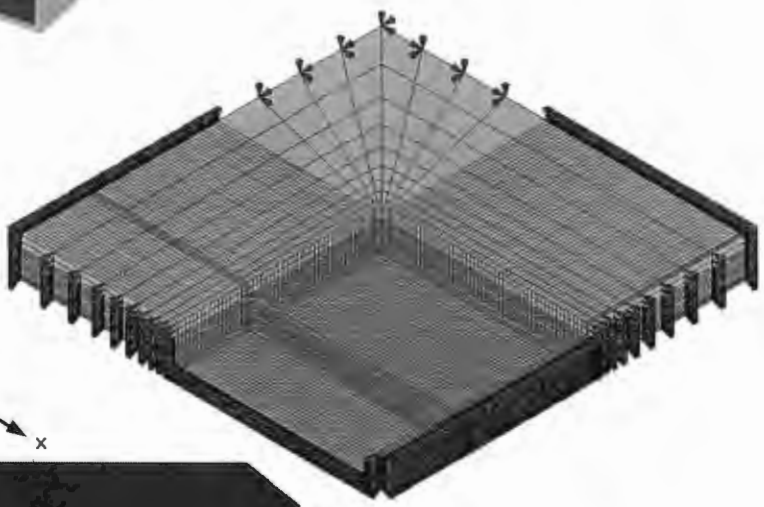

Mesh model and Boundary Conditions

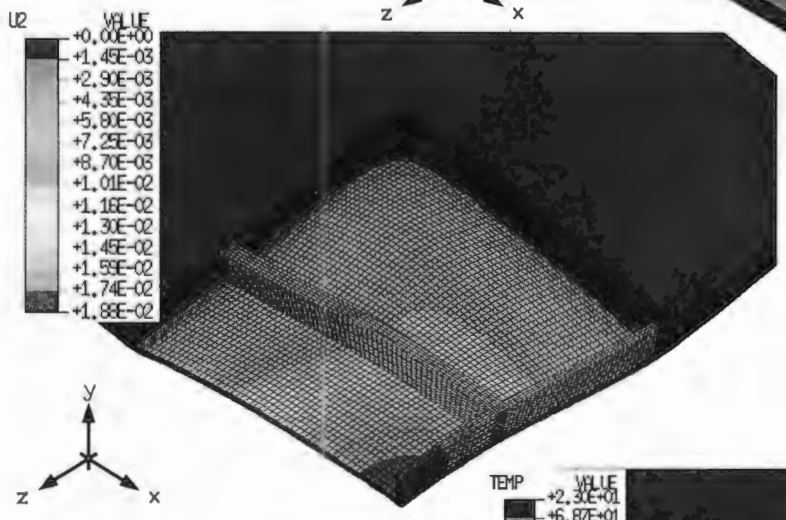

Displacement in the y-direction at impulse 35Ns

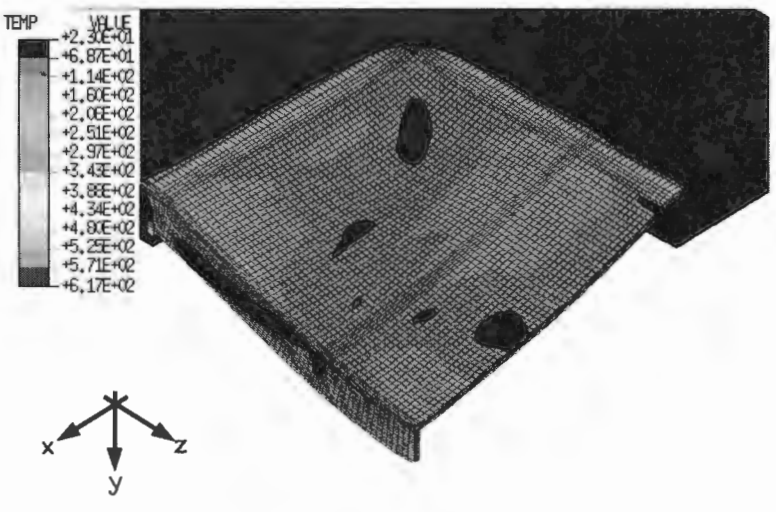

Temperature distribution at impulse 35Ns

H.10 Cross Stiffened square plate (3x3mm)

Cross stiffened
Square plate (3x3mm) model

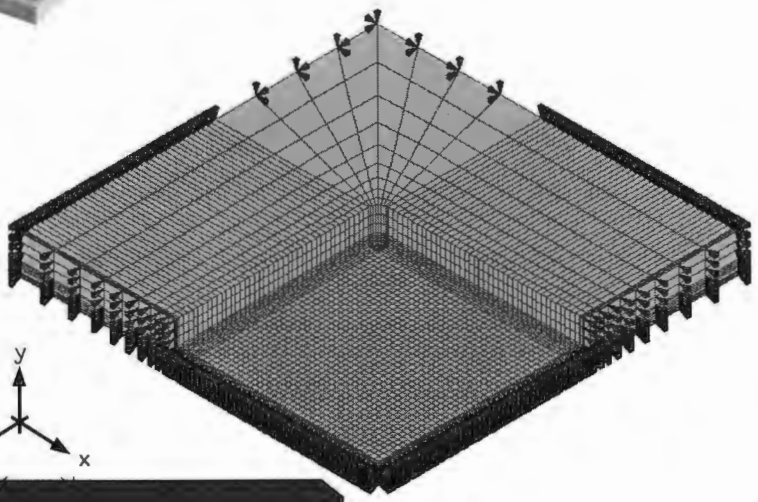

Mesh model and
Boundary Conditions

Displacement in the
y-direction at impulse 35Ns

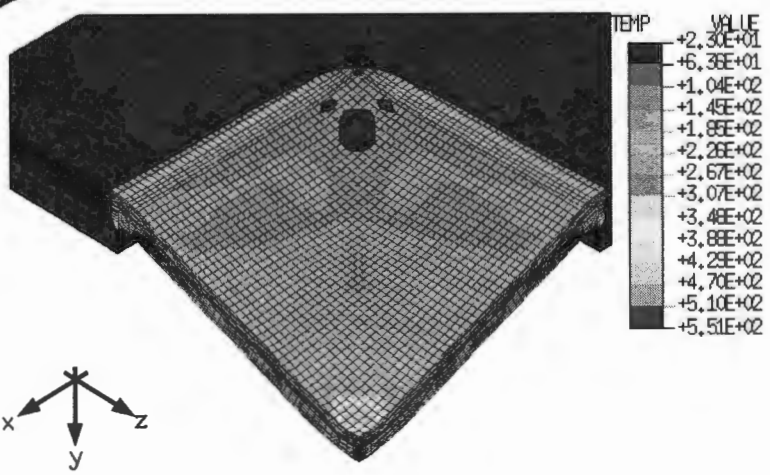

Temperature distribution
at impulse 35Ns

H.11 Cross Stiffened square plate (3x7mm)

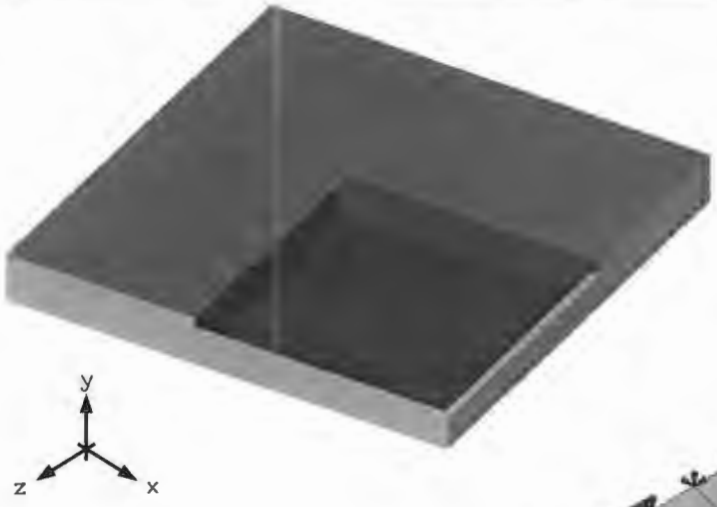

Cross stiffened
Square plate (3x7mm) model

Mesh model and
Boundary Conditions

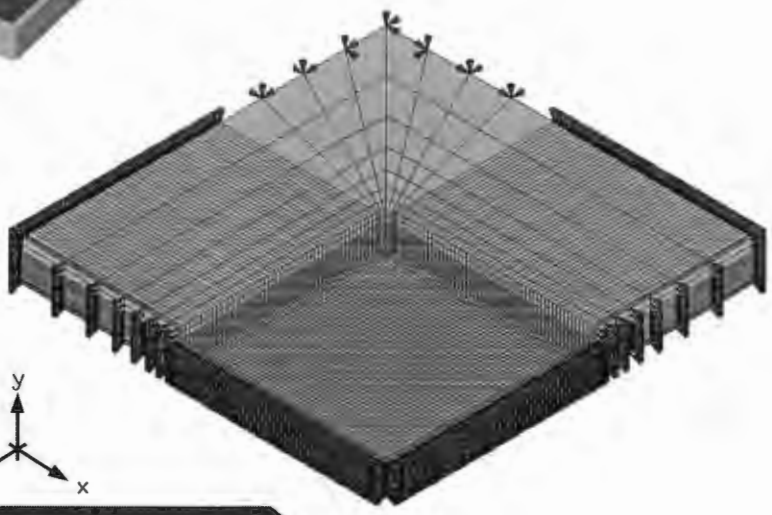

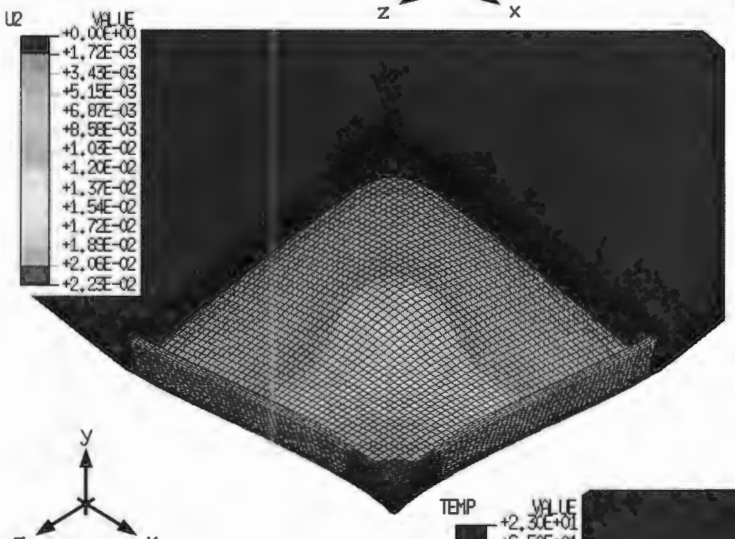

Displacement in the
y-direction at impulse 39Ns

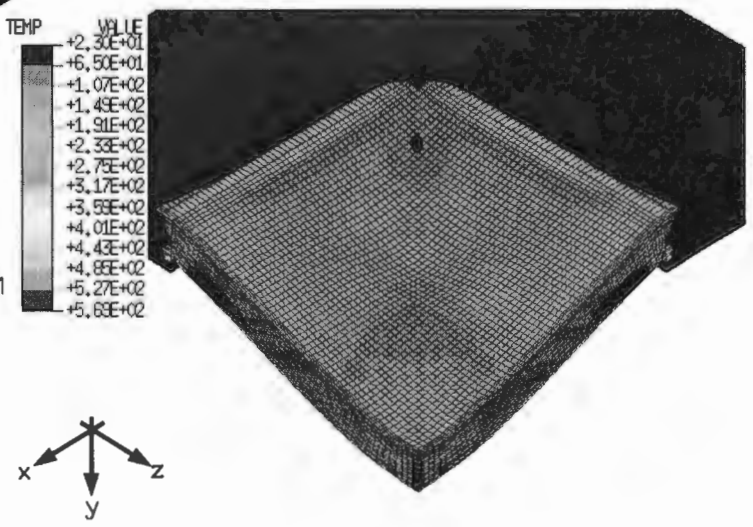

Temperature distribution
at impulse 39Ns

H.12 Rectangular plate

Rectangular plate model

Mesh model and
Boundary Conditions

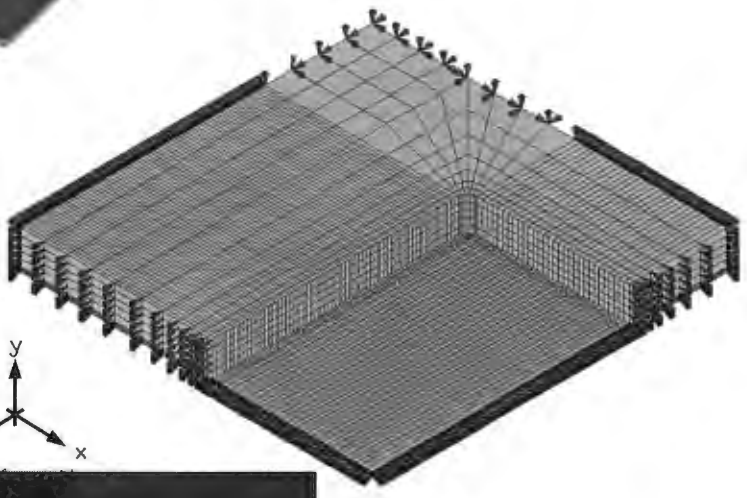

Displacement in the
y-direction at impulse 35Ns

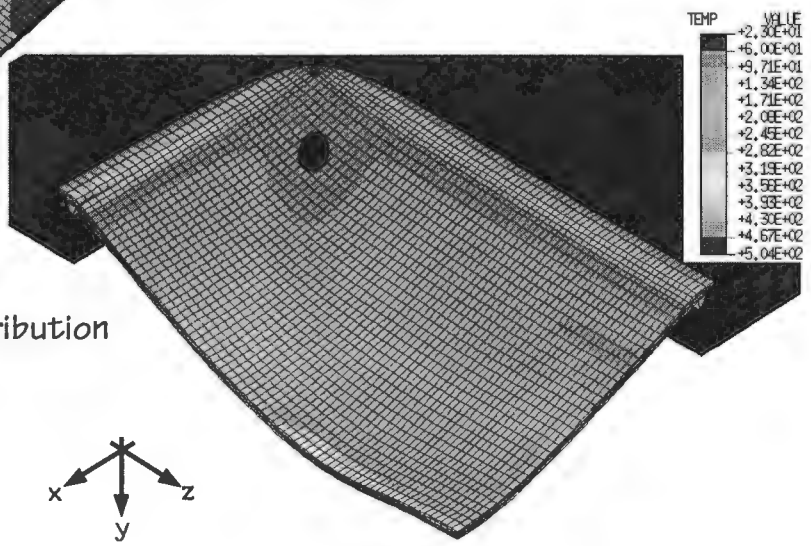

Temperature distribution
at impulse 35Ns

H.13 Double Stiffened rectangular plate (3x3mm)

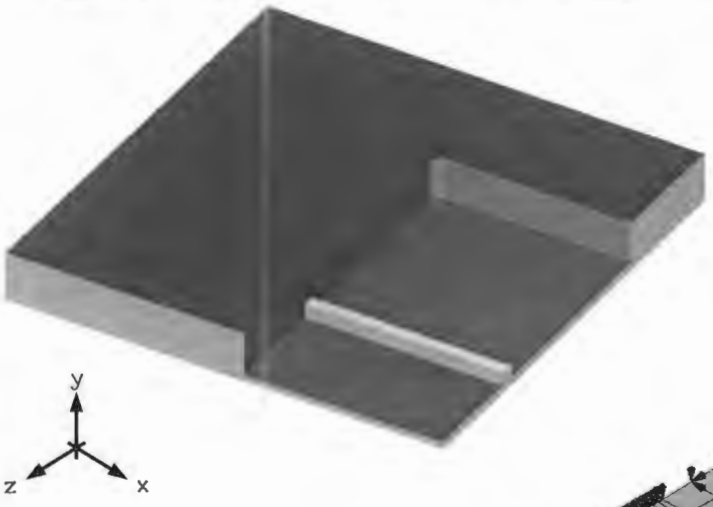

Double stiffened rectangular plate (3x3mm) model

Mesh model and Boundary Conditions

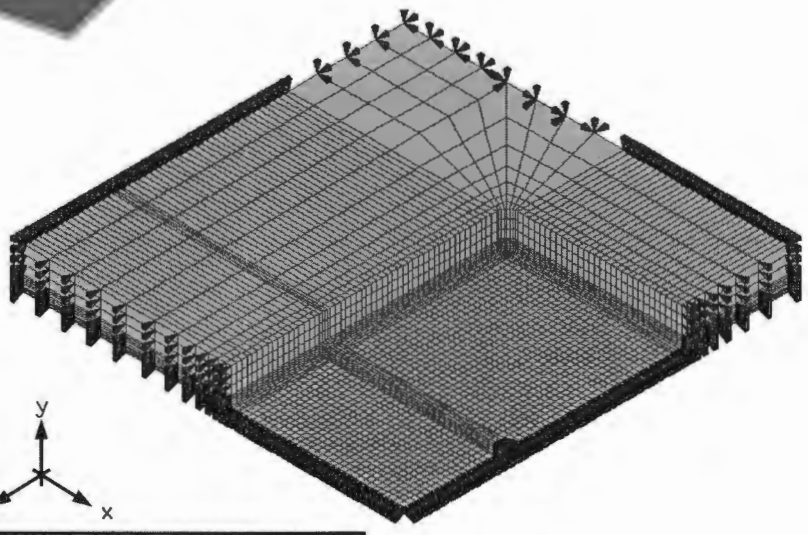

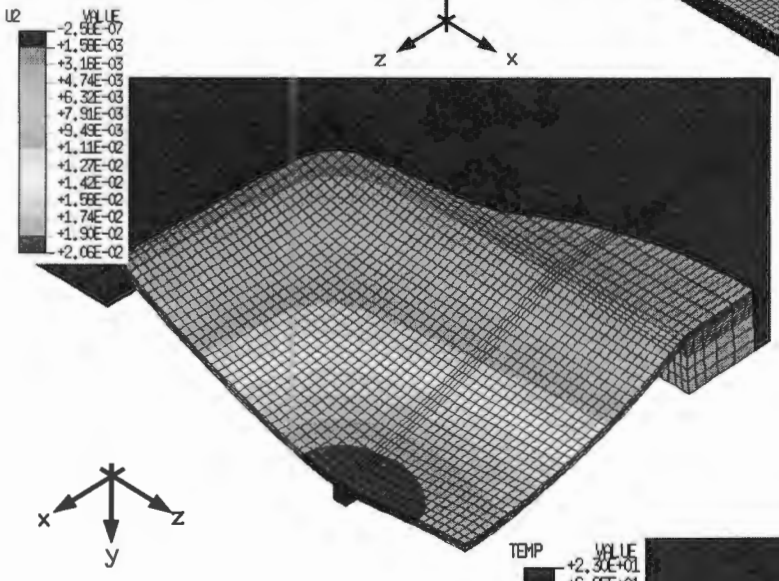

Displacement in the y-direction at impulse 35Ns

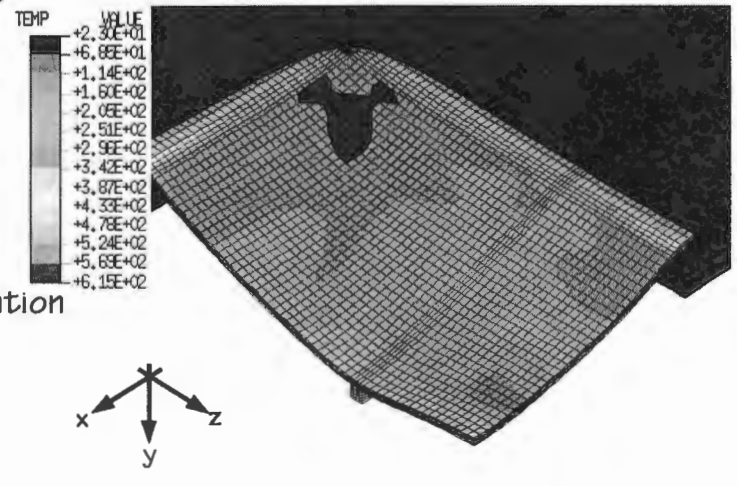

Temperature distribution at impulse 35Ns

H.14 Double Stiffened rectangular plate (3x7mm)

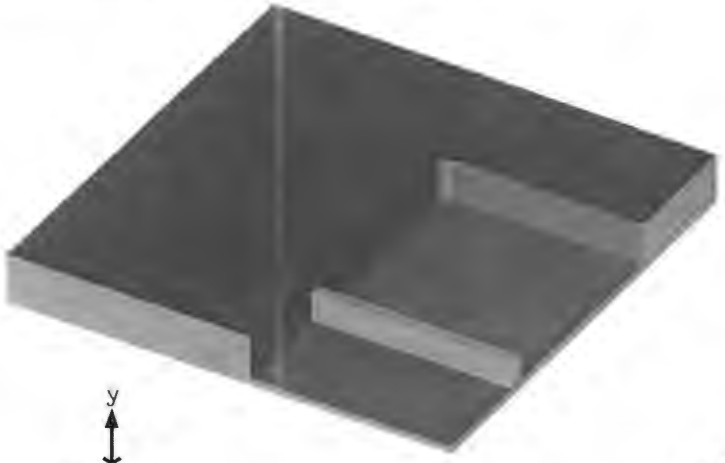

Double stiffened rectangular plate (3x7mm) model

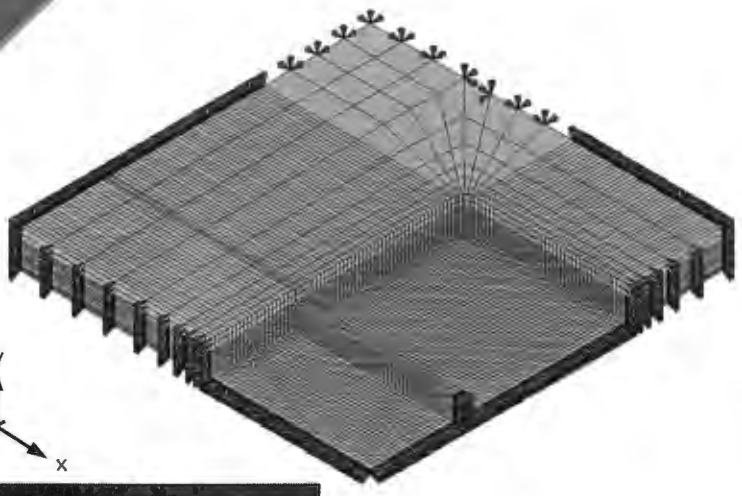

Mesh model and Boundary Conditions

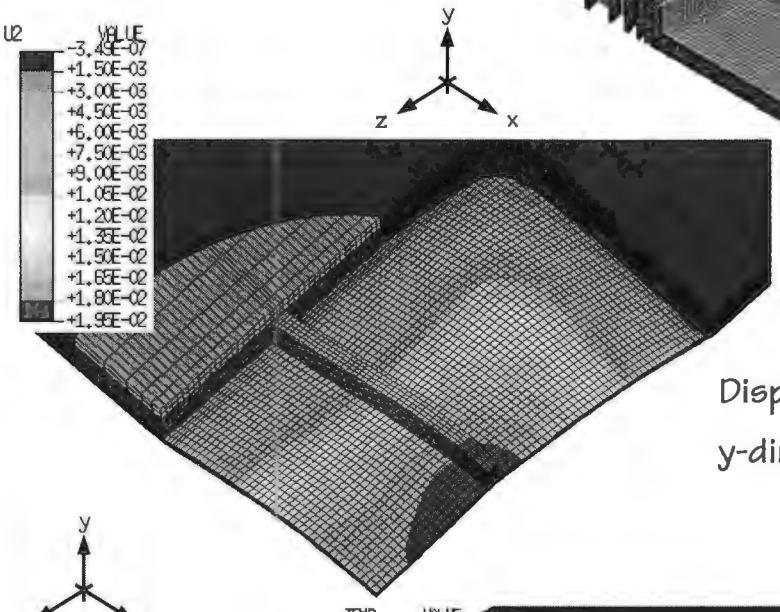

Displacement in the y-direction at impulse 37Ns

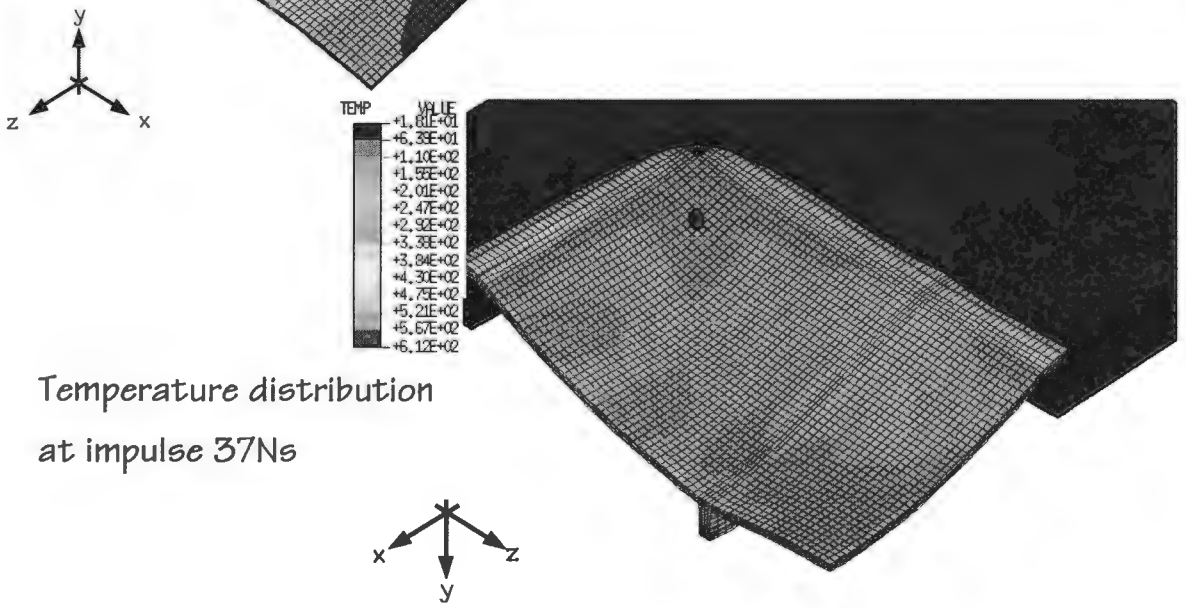

Temperature distribution at impulse 37Ns